

# Analysis of the Workspace of Tendon-based Stewart Platforms

Von der Fakultät für Ingenieurwissenschaften, Abteilung Maschinenbau der  
Universität Duisburg-Essen  
zur Erlangung des akademischen Grades

DOKTOR-INGENIEUR

genehmigte Dissertation

von

Richard Verhoeven  
aus  
Oberhausen

Referent:

Prof. Dr.-Ing. habil. Manfred Hiller

Koreferenten:

Prof. Dr.-Ing. habil. Christoph Woernle

Prof. Dr. rer. nat. Klaus Werner Wiegmann

Tag der mündlichen Prüfung: 29. Juli 2004

*There is work together  
A Church for all  
And a job for each  
Every man to his work.*

Thomas Stearns Eliot



# Preface

This thesis results from my research activity at the Institute of Mechatronics and System Dynamics at the University Duisburg-Essen, partially funded by Deutsche Forschungsgemeinschaft within the project «Seilgetriebene Stewart-Plattformen in Theorie und Anwendung»<sup>1</sup> (SEGESTA)».

First of all, I'd like to thank Prof. Dr.-Ing. habil. Manfred Hiller for providing me, originally a pure mathematician, with the unique opportunity to collaborate with engineers in a most innovative branch of robotics and for critically accompanying this work while introducing me to the engineer's point of view. I am very grateful to Prof. Dr.-Ing. habil. Christoph Woernle and Prof. Dr. rer. nat. Klaus Werner Wiegmann for accepting the charge of co-reviewing my thesis.

A very special gratitude I'd like to express to Prof. Dr. Satoshi Tadokoro who shared with me his tremendous experience in the field of tendon-based parallel robots, thus enabling me to enter this recent area of research.

Very much inspiration I owe to my colleagues at the laboratory – in particular Dipl.-Math. Sonja Mielczarek, Dr.-Ing. Martin Schneider, Dipl.-Ing. Andreas Pott and Dipl.-Ing. Daniel Germann – and to the scientific community known as «ARK people», especially Prof. Dr. Jorge Angeles, Prof. Dr. Oussama Khatib, Prof. Dr. Vincenzo Parenti-Castelli and Prof. Dr. Paul J. Zsombor-Murray. As they all work in areas related to mine but distinct from it, the discussions with them helped me a great deal in identifying and understanding my own key issues.

I am most grateful to those colleagues who took a look at drafts of my thesis, and with their questions and suggestions helped me to clarify and express my ideas: Dipl.-Ing. Ulrike Zwiers, Dr. rer. nat. Paola D'Ambros, Dr. rer. nat. Benjamin Klopsch, Dipl.-Ing. Olav Lange, Dipl.-Ing. Ya-Qing Zheng and Dipl.-Ing. Pascal Lafourcade.

I would like to extend my warmest thanks to my colleagues at WestLB, especially Dipl.-Kfm. Heinz Kramer who accepted me as a part-time employee with most flexible working hours, thus giving me the chance of embarking upon a research project when funding was not yet available.

While all of these people offered their presence beyond scientific and economic aspects, I would certainly not have completed my thesis without the personal support provided by my family and, among many of my friends, Prof. Dr. rer. phil. Tobias Hoffmann and Don Romano Christen.

Duisburg, September 2004

Richard Verhoeven

---

<sup>1</sup>tendon-based Stewart platforms in theory and applications



# Contents

<b>Index of Formula Items</b>	<b>VII</b>
<b>1. Introduction</b>	<b>1</b>
1.1. Why Tendon-based Stewart Platforms? . . . . .	1
1.2. Current State of Research . . . . .	8
1.2.1. Tendon-driven Serial Robots . . . . .	8
1.2.2. Parallel Robots . . . . .	9
1.2.3. Tendon-based Parallel Robots . . . . .	10
1.3. Objectives and Structure of this Thesis . . . . .	13
<b>2. Delimitation and Classification</b>	<b>17</b>
2.1. Duality of Serial and Parallel Systems . . . . .	17
2.1.1. Equations and Mappings . . . . .	17
2.1.2. Mobility . . . . .	20
2.1.3. Controllability . . . . .	22
2.2. Tendon-based Stewart Platforms . . . . .	23
2.2.1. Force Equilibrium . . . . .	23
2.2.2. Degree of Redundancy . . . . .	27
2.2.3. Degrees of Freedom . . . . .	28
<b>3. Aspects of Workspace</b>	<b>35</b>
3.1. Summary of the Criteria . . . . .	35
3.2. Controllable Workspace . . . . .	35
3.3. Singularities . . . . .	43
3.4. Stiffness . . . . .	48
3.5. Autocollisions . . . . .	54
<b>4. Optimal Tension Distribution</b>	<b>57</b>
4.1. Introduction . . . . .	57
4.2. Optimal Solutions for CRPMs . . . . .	58
4.3. Optimal Solutions in the General Case . . . . .	60
4.4. Discontinuity of Optimal Solutions . . . . .	64
4.4.1. Nonsingular Case . . . . .	64

4.4.2. Singular Case . . . . .	67
4.5. Approximation of Optimal Solutions . . . . .	69
4.6. Proof of Continuity . . . . .	72
4.7. Practical Computation . . . . .	77
<b>5. Workspace Optimization</b>	<b>85</b>
5.1. Introduction . . . . .	85
5.2. Measuring Workspace Quality . . . . .	87
5.3. Class 2T . . . . .	88
5.4. Class 1R2T . . . . .	90
5.5. Class 2R3T . . . . .	92
5.6. Class 3R3T . . . . .	95
<b>6. Motion Simulation Results</b>	<b>99</b>
6.1. Characteristics of Tendon Motion . . . . .	99
6.2. Planar Translational Systems . . . . .	101
6.3. Spatial Systems with six DOFs . . . . .	115
<b>7. Conclusions and Outlook</b>	<b>121</b>
7.1. Workspace Basics . . . . .	121
7.2. Optimal Tension Distribution . . . . .	121
7.3. Workspace Optimization . . . . .	121
7.4. Outlook . . . . .	122
<b>A. Mathematical Background</b>	<b>123</b>
A.1. Set Theory . . . . .	123
A.2. Vector Spaces and Linear Mappings . . . . .	125
A.3. Convex Sets and Polyhedra . . . . .	127
A.4. Normed Vector Spaces and Topology . . . . .	130
A.5. Parametric Optimization . . . . .	134
<b>B. List of Figures</b>	<b>137</b>
<b>C. List of Tables</b>	<b>141</b>
<b>D. Bibliography</b>	<b>143</b>



# Index of Formula Items

*The following index does not contain symbols which are used only in a local context (in particular most of the sets and mappings introduced in Section 4.6, p. 72 ff. and Section 4.7, p. 77 ff.). Each item is given a brief explanation and a cross-reference to a page where it is introduced.*

## Expressions

$\emptyset$	empty set	Section A.1, p. 123 ff.
$\mathcal{X} \cap \mathcal{Y}$	intersection of sets $\mathcal{X}, \mathcal{Y}$	Section A.1, p. 123 ff.
$\mathcal{X} \cup \mathcal{Y}$	union of sets $\mathcal{X}, \mathcal{Y}$	Section A.1, p. 123 ff.
$\mathcal{X} \times \mathcal{Y}$	cartesian product of sets $\mathcal{X}, \mathcal{Y}$	Section A.1, p. 123 ff.
$2^{\mathcal{X}}$	power set of a set $\mathcal{X}$	Section A.1, p. 123 ff.
$\overline{\mathcal{X}}$	closure of a set $\mathcal{X}$	Def. A.18, p. 131
$[a, b], ]a, b[, \dots$	real intervals	Section A.1, p. 123 ff.
$ \mathcal{X} $	number of elements in a set $\mathcal{X}$	Section A.1, p. 123 ff.
$\ \underline{v}\ _p$	$p$ -norm of a vector $\underline{v}$	Def. A.17, p. 130
$\ \underline{v}\ _\infty$	maximum norm of a vector $\underline{v}$	Def. A.17, p. 130
$\underline{A}_{\hat{\mu}}$	matrix $\underline{A}$ without $\mu$ th column	Theorem 3.4, p. 40
$\langle \underline{A} \rangle$	span of a matrix $\underline{A}$	Def. A.6, p. 126
$\underline{A}^+$	pseudo inverse of a matrix $\underline{A}$	Prop. A.8, p. 126
$\underline{A}^{-T}, \underline{A}^{+T}$	shorthands for $(\underline{A}^{-1})^T, (\underline{A}^+)^T$	Prop. A.8, p. 126
aff.hull $\mathcal{X}$	affine hull of a set $\mathcal{X}$	Def. A.12, p. 127
ch.ind $\Gamma(\underline{\lambda})$	characteristic index set of a set $\Gamma(\underline{\lambda})$	Def. A.29, p. 135
char.cone $\mathcal{P}$	characteristic cone of a polyhedron $\mathcal{P}$	Def. A.14, p. 129
cone $\mathcal{X}$	cone generated by a set $\mathcal{X}$	Def. A.12, p. 127
conv $\mathcal{X}$	convex hull of a set $\mathcal{X}$	Def. A.12, p. 127
$\delta \underline{x}$	infinitesimal deflection in $\underline{x}$	Eq. (3.24), p. 49
dim $\mathcal{V}$	dimension of a vector space $\mathcal{V}$	Def. A.4, p. 125
dim $\mathcal{X}$	dimension of a set $\mathcal{X}$	Def. A.12, p. 127
inf $\mathcal{X}$	infimum of a set $\mathcal{X}$	Def. A.3, p. 124
ker $\underline{A}$	kernel of a matrix $\underline{A}$	Def. A.6, p. 126
lin.space $\mathcal{P}$	lineality space of a polyhedron $\mathcal{P}$	Def. A.14, p. 129
rank $\underline{A}$	rank of a matrix $\underline{A}$	Def. A.6, p. 126

$\sup \mathcal{X}$	supremum of a set $\mathcal{X}$	Def. A.3, p. 124
$\text{trace } \underline{A}$	trace of a matrix $\underline{A}$	Prop. A.10, p. 126
$U_\epsilon(\underline{v})$	$\epsilon$ -environment of a vector $\underline{v}$	Def. A.18, p. 131

## Symbols

$\underline{0}$	null vector	Section A.2, p. 125 ff.
$\underline{1}$	vector $(1, \dots, 1)$	Section A.2, p. 125 ff.
$\underline{A}^T$	structure matrix	Eq. (2.24), p. 26
$\underline{A}_L^T$	scaled structure matrix	Eq. (3.12), p. 39
$\alpha_\mu$	angle of $\mu$ th tendon with x axis of $\mathcal{K}_B$	Fig. 3.4, p. 38
$\mathbf{b}_\mu$	$\mu$ th connection point on the base	Fig. 2.5, p. 25
$\beta_\mu$	angle of $\mu$ th tendon with x axis of $\mathcal{K}_P$	Fig. 3.4, p. 38
$d_\partial$	workspace quality index	Eq. (5.2), p. 87
$\underline{f}$	actuator forces	Section 2.1.1, p. 17 ff.
$\underline{f}_0$	arbitrary solution of tension problem	Prop. 3.2, p. 36
$\underline{f}_{\text{high}}$	highest solution of tension problem	Eq. (4.11), p. 61
$\underline{f}_{\text{high},p}$	approximation of highest solution	Section 4.5, p. 69 ff.
$\underline{f}_{\text{low}}$	lowest solution of tension problem	Eq. (4.8), p. 61
$\underline{f}_{\text{low},p}$	approximation of lowest solution	Section 4.5, p. 69 ff.
$\underline{f}_{\text{max}}$	maximum tendon force	Def. 3.5, p. 43
$\underline{f}_{\text{min}}$	minimum tendon force	Def. 3.5, p. 43
$\mathbf{f}_\mu$	force exerted by $\mu$ th tendon	Eq. (2.21), p. 26
$\underline{f}_P$	force acting on the platform	Eq. (2.21), p. 26
$\underline{H}$	matrix spanning $\ker \underline{A}^T$	Eq. (3.2), p. 36
$\underline{h}$	positive vector in $\ker \underline{A}^T$	Prop. 3.2, p. 36
$\underline{K}$	stiffness matrix	Eq. (3.24), p. 49
$\underline{k}'$	stiffness per reciprocal length	Eq. (3.28), p. 50
$\underline{k}_{\text{ev}}$	$\nu$ th stiffness eigenvalue	Eq. (3.31), p. 50
$\underline{k}_\nu$	stiffness of $\nu$ th tendon	Eq. (3.25), p. 49
$\mathcal{K}_B$	base coordinate frame	Fig. 2.5, p. 25
$\mathcal{K}_P$	platform coordinate frame	Fig. 2.5, p. 25
$\underline{L}$	diagonal matrix of tendon lengths	Eq. (3.12), p. 39
$\underline{l}_\mu$	length $\mu$ th tendon	Fig. 2.5, p. 25
$\lambda$	multiplier for $\underline{h}$	Eq. (4.2), p. 59
$\underline{\lambda}$	multiplier for $\underline{H}$	Eq. (3.2), p. 36
l. s. c.-B	lower semicontinuous according to Berge	Def. A.28, p. 134
u. s. c.-B	upper semicontinuous according to Berge	Def. A.28, p. 134
$m$	number of tendons	Eq. (2.20), p. 24
$m_P$	mass of platform	Eq. (2.30), p. 29

$\mu$	index for tendons, $\mu \in \{1, \dots, m\}$	Fig. 2.5, p. 25
$n$	number of end-effector DOFs	Section 2.2.3, p. 28 ff.
$\nu$	index for DOFs, $\nu \in \{1, \dots, n\}$	Prop. 3.7, p. 48
$\mathbb{N}$	natural numbers (1, 2, 3, ...)	Section A.1, p. 123 ff.
$\mathbb{N}_0$	nonnegative integers (0, 1, 2, 3, ...)	Section A.1, p. 123 ff.
$p$	approximation parameter	Section 4.5, p. 69 ff.
$P_+$	sum of positive actuator powers	Eq. (6.11), p. 100
$\mathbf{p}_{B,\mu}$	$\mu$ th connection point on the platform	Fig. 2.5, p. 25
$P_\mu$	power at $\mu$ th actuator	Eq. (6.9), p. 100
$\mathbf{p}_\mu$	$\mu$ th connection point on the platform	Fig. 2.5, p. 25
$P_\Sigma$	sum of actuator powers	Eq. (6.10), p. 100
$\mathcal{P}_{\text{high}}$	polyhedron of highest solutions	Eq. (4.9), p. 61
$\mathcal{P}_{\text{low}}$	polyhedron of lowest solutions	Eq. (4.5), p. 60
$\mathcal{Q}_{\text{high}}$	convex hull of the vertices of $\mathcal{P}_{\text{high}}$	Theorem 4.4, p. 64
$\mathcal{Q}_{\text{low}}$	convex hull of the vertices of $\mathcal{P}_{\text{low}}$	Theorem 4.4, p. 64
$\mathbf{r}$	position of the end-effector	Fig. 2.5, p. 25
$\mathbf{R}$	orientation of the end-effector	Fig. 2.5, p. 25
$\mathbb{R}$	real numbers	Section A.1, p. 123 ff.
$\mathbb{R}_+$	positive real numbers	Section A.1, p. 123 ff.
$\mathbb{R}_{+0}$	nonnegative real numbers	Section A.1, p. 123 ff.
$\mathbb{R}_-$	negative real numbers	Section A.1, p. 123 ff.
$\mathbb{R}_{-0}$	nonpositive real numbers	Section A.1, p. 123 ff.
$\mathbb{R}^{n \times m}$	matrices with $n$ rows and $m$ columns	Def. A.5, p. 125
$S^n$	$n$ -dimensional sphere	Def. A.11, p. 127
$\sigma$	force choice parameter	Def. 4.1, p. 62
$\text{SO}_3$	set of three-dimensional rotations	Def. A.11, p. 127
$\underline{t}$	end-effector twist	Eq. (6.1), p. 99
$t_{\text{CPU}}$	computation time	Table 6.5, p. 111
$\underline{\tau}_{\text{P}}$	torque acting on the platform	Eq. (2.21), p. 26
$\underline{\vartheta}$	actuator variables	Section 2.1.1, p. 17 ff.
$\mathbf{u}_\mu$	unit vector along $\mu$ th tendon	Eq. (2.22), p. 26
$\underline{v}$	linear velocity of the platform	Eq. (6.3), p. 99
$W$	net energy required for a trajectory	Eq. (6.13), p. 101
$\underline{w}$	end-effector wrench	Section 2.1.1, p. 17 ff.
$\underline{x}$	end-effector posture	Section 2.1.1, p. 17 ff.



# Chapter 1

## Introduction

*Section 1.1 provides a motivation why tendon-based Stewart platforms are interesting for applications and lists the main challenges for research. Section 1.2 presents a brief overview of the current state of research in relevant fields. Objectives and structure of this dissertation are summarized in Section 1.3.*

### 1.1. Why Tendon-based Stewart Platforms?

One of the fundamental issues in robotics is the design of mechanical systems to manipulate loads. While there is a large and rapidly increasing variety of applications of robotic manipulators, the key requirements are mostly the same and typically include some of the following:

- The mechanical system should have a simple structure such that it is easy to manufacture at low cost. As electronic components are becoming cheaper and cheaper, while the price of mechanical parts does not change considerably, there is a general trend towards systems which are mechanically simple but computationally demanding.
- The system's behavior should be sufficiently predictable such that it can be controlled by a computer with little or no manual user interaction.
- In the past researchers used to investigate the limits of what is technically possible, paying little attention to economic aspects. In that context high precision positioning was often a main requirement for manipulators. Due to a general paradigm shift in science, nowadays the objective is to develop solutions satisfying the needs of a specific application at the lowest possible cost. In that sense there is an increasing interest in robots of low price but with limited precision.
- The system should consume little energy, especially when employed in mobile robots or when handling very heavy loads.
- For some applications a high load capacity is required.
- The end-effector should achieve high velocities and/or high accelerations.

- The concept should be appropriate for micro-scale and/or large-scale applications.

There are many different concepts for manipulators, each of them has a specific profile with respect to these requirements. We briefly present the characteristics of some of them.

*Serial Manipulators* are currently the most common type of manipulators used in robotics. From a manufacturing point of view, they can be more or less simple, depending on how the joints are actuated. Common solutions include hydraulic/pneumatic cylinders or motors acting directly (or through gears) on the joint axis. Computation of the load's posture from the joint variables (the so-called *forward kinematics problem*) is straightforward, while the problem of *inverse kinematics* is more complicated. The most general case was resolved only after many years of research [104, 142]. The limited computational effort and the good predictability of motion have led to many applications in manufacturing.

The energy consumption is rather high because each actuated joint has to carry not only the load, but also all the subsequent links with their actuators. As heavy loads require strong links and this increases energy consumption further, the capability of handling large masses is limited. In fact, in most manufacturing applications the payload is quite small when compared to the mass of the whole manipulator. High velocities and accelerations can be achieved easily, especially when revolute joints are employed. Links act as levers and therefore the end-effector generally moves faster than the joints. High precision operation is possible, especially in small-scale applications (with workspaces up to about 1 m).



Figure 1.1: Skywash manipulator  
photo © Putzmeister AG

Large-scale operation presents a number of problems: the leverage effect of long links increases very much the torque on actuated joints and one must take into account the bending of links and vibrations of large amplitude for automa-



tized/precise motions. (Indeed, Fig. 1.1 shows an application where high precision is not required.) These problems can be managed to a certain degree [85], but they are quite demanding in terms of control technology. Energy consumption remains high anyway.

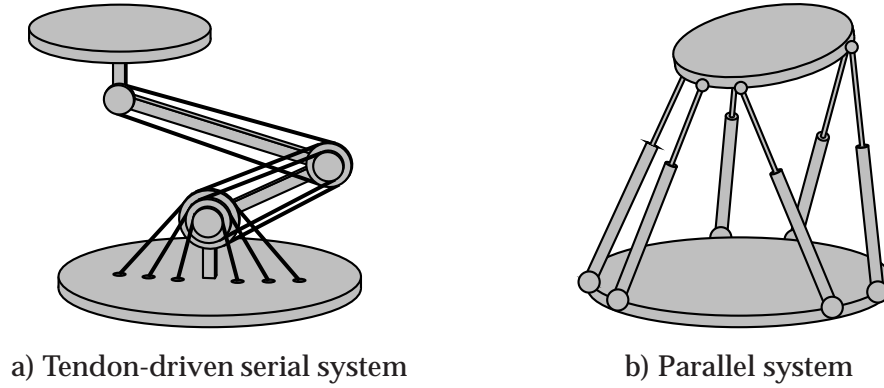


Figure 1.2: Manipulator concepts

*Tendon-driven serial manipulators* (Fig. 1.2a) are considerably more energy efficient because the actuators are fixed, i. e. they do not need to be moved.<sup>1</sup> However, in three-dimensional applications it is very difficult to guide the tendons around joints. Therefore, this concept is used in practice mainly for planar systems.



Figure 1.3: Boom crane  
photo © Kranservice Rheinberg GmbH

*Cranes* (Fig. 1.3) where a load is suspended from a single tendon were already in use millenia ago. Their mechanical system is not that simple because the pulley carrying the load must be movable at least in one or two directions of translation. Therefore it is usually combined with a serial manipulator having two degrees of freedom (DOFs). As the end-effector is kinematically underconstrained, motion prediction requires very good models of sway motion together with sophisticated

<sup>1</sup>Clearly, the advantage of fixed actuators can also be achieved in other ways, e. g. with gear-trains or tie-rod linkages. So this does not apply exclusively to tendon-driven systems.

sensor technology. Consequently, there are no crane applications which are 100% automatized.



Figure 1.4: Container crane  
photo © Kranservice Rheinberg GmbH

Energy consumption depends on the design of the serial subsystem: typically this provides a planar translation where actuators need energy to accelerate a trolley, but not to carry its weight (Fig. 1.4). Cranes are currently the only available technology that can handle very heavy loads with a reasonable amount of energy. Accelerations generate sway motions and must be limited therefore: indeed, cranes are most appropriate for quasistatic motions. This limits velocity in curved paths. Control with high precision is basically impossible, although a controller predicting/measuring sway motions can improve such capabilities. Cranes require a minimum load to hold the tendons in the pulleys, so they are not appropriate for very small loads and hence are not suitable for micro-scale applications. On the other hand, they are quite good for large-scale tasks: with serial subsystems based on trolleys, workspace diameters of about 20 m can be obtained.

*Parallel robots* (also known as Parallel Kinematic Machines, Stewart platforms or Gough platforms; Fig. 1.2b) have attracted increasing attention in the past two decades. Here each actuated leg has to carry only part of the payload: this is quite energy efficient and allows to handle heavy loads. The parallel structure typically implies that the end-effector moves slower than the actuated joints. Nevertheless, appropriate actuator technology can reach highly dynamic motions. Control is a nontrivial issue because the forward kinematics problem may have up to 40 solutions [40] and in general it cannot be computed in real time. A major problem in practice is the need for spherical joints with a very large angular range and a sufficient stiffness at the same time. This is crucial when the system is subject to large contact forces (e. g. in milling applications). Although some industrial applications exist (Fig. 1.5), it is now fair to say that much of the initial enthusiasm has given way to disappointment, because the practical problems just turned out to be more difficult than they were expected to be.





Figure 1.5: Hexabot™ 5-axis CNC machine  
photo © Hexel Corporation

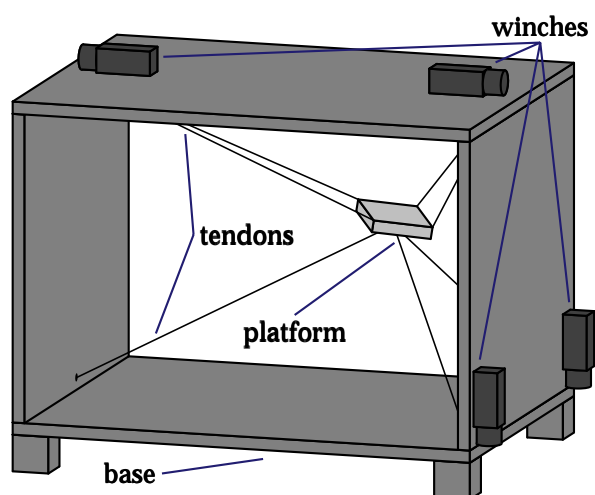


Figure 1.6: Tendon-based Stewart platform

*Tendon-based Stewart platforms*<sup>2</sup> are the subject of this dissertation: here, a movable *platform* is connected to the fixed *base* by a number of *tendons*, as in Fig. 1.6. Typically, the tendons are rolled up on winches attached to the base, hence the only moving parts are the tendons and the platform (and some mechanical parts inside the winches).



Figure 1.7: C-MISPP prototype  
photo © North Carolina State University

This approach was first proposed about fifteen years ago<sup>3</sup> [33]. Tendon-based Stewart platforms can be considered as a synthesis of the concepts explained before: they inherit some advantage from each of them. Indeed, they are very energy efficient because the actuators are fixed *and* the payload is subdivided between actuators. Therefore they are appropriate to handle very heavy loads, like cranes [105, 145] (Fig. 1.7) and can achieve very high accelerations and velocities. They can be designed in extremely large scale (up to about 100 m, e. g. the Skycam<sup>TM</sup> in Fig. 1.8 [167], or even several km as the aerostat in Fig. 1.11 [130]) as well as in micro-scale applications. Unlike in the case of cranes, motion is highly predictable and can be controlled without manual interaction. In a paper on force redundancy in parallel manipulators [35], the authors state that «the primary objective of a serial manipulator is to move an object, while that of a parallel one is to support a load». In some sense, it can be said that tendon-based Stewart platforms can serve both purposes.

Unlike conventional Stewart platforms, they do not need spherical joints, but construction of the connection points in tendon-based systems is still a challenge:

---

<sup>2</sup>The concept has various names in different geographical regions. Americans speak of «cables» while Japanese write «wires». This thesis has adopted the term «tendons» from the papers about tendon-driven serial systems. The term «tendon-based» is used instead of «tendon-driven» because the latter could be confused with Stewart platforms with rigid links having tendons for force transmission only.

<sup>3</sup>Actually, systems like that in Fig. 1.4 already implemented the idea, probably even before the term «parallel manipulator» was invented. However, the concept was never subject of systematic research.



Figure 1.8: Skycam™ tendon-suspended camera  
photo © CF InFlight

the point where a tendon leaves a winch should be well-defined and point-shaped; at the same time, the tendon should be able to take any direction with low friction. Another major problem in design concerns precise control of the tendon length. To achieve this, the tendon can be rolled up on a cylinder or screw in a regular, well-defined manner. An alternative solution is to connect the tendon to a linear direct drive. Regarding these questions, there is a strong connection between the desired precision in positioning and the necessary complexity in mechanical design. When precision is not an issue, the mechanical design can be simple.

On the other hand, tendon-based Stewart platforms lead to theoretical questions, some of which are completely new and do not apply to other concepts:

- The workspace is restricted mainly by the requirement to have positive but limited tension in all tendons. This *controllable workspace* has a complicated shape and its closed form description is extremely complex.
- A related problem is to find an *optimal distribution of tension* between tendons, especially in highly redundant systems.
- In many cases, for  $n$  end-effector-DOFs, we use at least  $n + 1$  tendons. Such systems are actuation redundant and this can be used to reduce singularities.
- As tendons are much more compliant than rigid links, *stiffness* becomes an important issue.
- Collision of tendons with each other, with the load or with the framework is an important problem in spatial redundant systems.

The present thesis deals with these questions. For completeness, we also mention some other points which are being investigated at the laboratory at Duisburg but will not be covered here:

- The *forward kinematics* problem is difficult as in all parallel systems. The actuation redundancy can be used to reduce multiplicity of solutions. But surprisingly, there exist designs where additional legs do not change kinematics at all [65, 66, 122].

- Due to the nonconvex controllable workspace, even a simple point-to-point motion requires a complex algorithm to find a *trajectory* which lies inside the controllable workspace and optimizes time or energy [57].

Research on tendon-based Stewart platforms has developed only in the last years, mainly in Japan and the USA. To the author's knowledge, the Universities of Rostock and Duisburg were the first places in Europe to study such systems (since 1996). Up to now, much work was done on experimental setups and practical questions, especially in Japan, while there is relatively little literature on theoretical aspects. One objective of the present dissertation is to help filling this gap.

## 1.2. Current State of Research

### 1.2.1. Tendon-driven Serial Robots

All tendon-driven robots, whether they are serial or parallel, share the property that tendons support tension but not compression. Thus, for  $n$  DOFs, at least  $n + 1$  tendons are required. In several publications by Tsai et al. [137, 138, 139, 168] this is examined in the context of isotropic configurations of serial systems. The authors explain that it is important to distinguish between actuator space (the tendon lengths/forces) and joint space (the angles/torques of the revolute joints). The matrix transforming actuator forces in joint torques is called «structure matrix». It turns out that isotropic configurations are obtained if either  $n + 1$  or  $2n$  tendons are used. In the  $2n$  case, each joint is then driven by two antagonistic actuators. This result is interesting because it shows us a fundamental difference between tendon-driven serial systems and tendon-based parallel ones: in the latter, joint space and actuator space *coincide*. In that sense, tendon-based parallel systems are *directly driven*.<sup>4</sup>

Several basic issues regarding tendon-driven serial systems are discussed in a paper by Kobayashi et al. from 1998 [84], summarizing almost ten years of research in this field. The authors point out that a tendon-driven system must be force redundant, and that the basic problem is to solve the redundancy so that a vector of positive tensions is obtained. A system is defined as «tendon controllable» if this is possible for any set of joint torques. This is the case if and only if the structure matrix has full rank and there is a vector of positive tendon forces that generates a zero torque in all joints. These results are exactly the same as for tendon-based parallel systems (cf. Section 2.2.1, p. 23 ff.).

Furthermore Kobayashi et al. examine whether a system is still controllable when a number of tendons is removed. They supply an irreducible description of tendons which are redundant in that sense. Then their paper describes how redundancy can be used to adjust stiffness. These results could also be applied to tendon-based parallel systems because the structure of the equations is the same.

---

<sup>4</sup>Nevertheless, the term «structure matrix» was adopted in the current thesis for the matrix transforming tendon forces into end-effector wrenches. This is appropriate because the mathematical structure of the equations is the same and the term «transpose of the Jacobian» – which could also be used – may be misunderstood (see the discussion after Eq. (2.3), p. 19).



In parallel manipulators, though, these problems are secondary due to another fundamental difference between the serial and the parallel case: the structure matrix in the serial case is constant, so a design is either always or never controllable, independently of the end-effector posture. In parallel systems, instead, the structure matrix strongly depends on the posture, so that the main problem is always to find a solution with positive tensions. Any other question is subordinate to this.

Several prototypes of tendon-driven serial manipulators were built, especially for articulated fingers or arms, see e. g. [59, 67, 73, 101, 106, 133, 146]. Here, the tendon-driven mechanisms have the main advantage of low weight and small size of the movable parts. Most of the existing systems are planar. It seems that the difficulty of tendon routing discourages researchers from extending the concept to spatial applications. However, one can build spatial parallel systems where the legs are serial tendon-driven subsystems [20].

### 1.2.2. Parallel Robots

Parallel robots were proposed for the first time in the 1950s [52] and 60s [155], but at the beginning there was little response from the scientific world. From the 1980s on, increasing attention has been paid to the idea. This might be due to the fact that investigation of certain aspects of parallel robots requires either sophisticated computer algebra systems for symbolic calculation or high-speed computers for numerical solutions. Both of them became available during that period.

One of these aspects is forward kinematics, i. e. the problem of determining the posture of the platform given the leg lengths. At the beginning, even the number of possible solutions was unknown and early works gave upper bounds of hundreds of solutions. After several years of research, Lazard proved in 1993 [100] an upper bound of at most 40 solutions, and Raghavan [141] could provide a numerical example having actually 40 (partly complex) solutions. Five years later, Dietmaier [40] supplied the first example with 40 real postures. The maximum number of real solutions for systems with planar base and planar platform is still unknown, up to now only examples with 36 real postures were found [41].

In the meantime, much work was done on special geometries where some connection points on basis or platform coincide. Faugère and Lazard [47] gave an exhaustive combinatorial classification of spatial geometries and listed the maximum number of solutions for each of them. Gosselin and Merlet [51] supplied similar results for planar systems. After several papers on special cases [69, 70, 71], Innocenti and Parenti-Castelli [72] developed a closed-form solution for the spatial 5 – 5 case (the relatively general situation where at least two platform connection points and at least two basis connection points coincide). Other particular situations were analyzed by Merlet [120]. These results are interesting in the context of tendon-based robots because such special geometries are advantageous because they tend to have larger workspaces and less problems with tendon collisions (see Section 3.5, p. 54 ff.).

The problem of forward kinematics has led scientists to rediscover the theory of kinematic mapping [156], which allows to transform the forward kinematics

problem (which in common representations involves transcendental functions) into a system of algebraic equations in a projective space [64]. The research team at Duisburg has found kinematic mapping a most useful tool to analyze forward kinematics of kinematically overconstrained systems [122], which is the normal case in tendon-based manipulators.

Another important task is the examination of singularities, which in parallel robots are of different nature than in serial ones (cf. Section 2.1, p. 17 ff.). Analytical studies [178] have clarified the connection between assembly modes, solutions of the forward kinematics problem and singularities. The study of systems which are singular in every posture has proven a complex problem of its own [76, 77, 78, 164]. Recipes to find singularities were proposed for the spatial [113, 121] and the planar case [149, 150, 151]. Other authors proposed algorithms for singularity-free path-planning [22, 34]. It turns out that singularities are both a real problem in practice because they tend to go through the center of the workspace, much more than they usually do in serial systems and a theoretical challenge because it is very difficult to give an exhaustive description of their occurrence. Therefore, the author found it worthwhile to include in this thesis a method of building singularity-free redundant manipulators, which is trivial (and maybe expensive) but efficient (Section 3.3, p. 43 ff.).

Redundant parallel robots are subject to inner forces which have to be controlled carefully in order to avoid damage. Maybe due to this difficulty, they were not considered much. Several authors [54, 89, 90, 143] provide contributions about spherical joints redundantly driven by prismatic actuators. [132] presents a detailed analysis of a particular redundant prototype. Other research was devoted to arrays of binary actuators [43, 102, 176]. A remarkable result is reported by Dasgupta and Mruthyunjaya [35]: while redundancy in serial robots can only change the location of the singularity manifold, redundancy in parallel ones can reduce its dimension and can even make it vanish completely.

Originally, parallel robots were proposed for flight simulators. Nowadays, there are applications, among others, in manipulation [114, 115] high-speed milling (Fig. 1.5). The latter suffers considerably from the above mentioned joint stiffness problem.

Several variations of the concept were proposed, e.g. the Hexaglide [63], where the legs have fixed length but the winches can be moved along a rail; manipulators where legs have more than one actuated joint [4, 152, 169]; the DELTA robot [31, 124], which is a purely translational parallel robot with three degrees of freedom. Such designs do not have a tendon-based analog.

An overall review on parallel mechanisms was published recently [36], but the included bibliography is not that useful because all references are given without title. There is also a very comprehensive web resource about parallel robots [23].

### 1.2.3. Tendon-based Parallel Robots

The idea of tendon-based parallel robots for motion with six DOFs was proposed for the first time in 1989 in the USA [33], in order to replace cranes in shipbuilding by systems that can be computerized. That was the beginning of ROBOCRANE, a prototype which was used for about ten years [3, 24, 25, 26,

27, 28, 29] and had some follow-up projects in other institutions [42, 105, 145] (Fig. 1.7). Before that, the Skycam<sup>TM</sup> (Fig. 1.8 [167]) had been developed as a parallel tendon-based system moving a camera in three DOFs of translation.

Still earlier a slightly different concept had been patented, where a platform is attached to the base by one leg containing a passive spring [97, 98, 99], with a number of actuated tendons that provide a pulling force balanced by the pushing force of the spring. There are recent works based on similar concepts [86, 87, 131], also combining tendons with rigid links [83]. From an analytical viewpoint, these mechanisms are rather different from normal tendon-based Stewart platforms, and therefore are not covered by the present thesis.



Figure 1.9: Cablev prototype at Rostock  
photo © University of Rostock

At about the same time (since 1988), similar ideas became popular in Japan [56] and prototypes with extremely high acceleration capabilities were built [79, 81]. One of the few theoretical publications on the subject was written by Ming and Higuchi [125], who provided the fundamental classification into «completely restrained positioning mechanisms» (CRPMs), which are kinematically redundant, and «incompletely restrained positioning mechanisms» (IRPMs), which require additional forces (e. g. gravity) for stabilization. (The present thesis, unlike that publication, distinguishes further between CRPMs – with exactly  $n + 1$  tendons – and «redundantly restrained positioning mechanisms» (RRPMs) with even more tendons.) The same authors also built a planar prototype [126]. Much research on workspace optimization [107, 161], prototypes and control [162] has then been done at Kobe, mainly for RRPMs.

After early works on IRPMs in Japan [8, 60, 61, 62, 134, 135, 136] which often included serial subsystems, a main center of research on IRPMs was established at Rostock, Germany. There a prototype named Cablev (Fig. 1.9) was built and much effort has been devoted to control issues [55, 108, 109, 110, 111, 112]. At

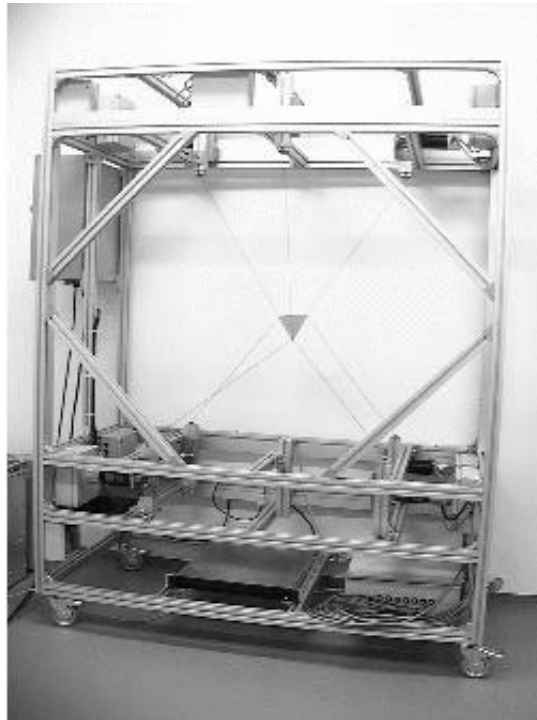


Figure 1.10: SEGESTA prototype at Duisburg

the same time, the research project SEGESTA<sup>5</sup> [44, 48, 58, 123] was established at the mechatronics laboratory at the University of Duisburg, focusing on CRPMs and RRPMS. Besides the results presented in this dissertation, the project includes research on forward kinematics and trajectory planning (cf. Section 1.1). A prototype was built recently (Fig. 1.10). In the last years, research groups developed in several countries [49, 145, 177, 180], working on various types of tendon-based parallel systems. The author has prepared a list of web links to related projects [170].

As mentioned above, tendon-based Stewart platforms have been employed for many years already in camera systems. Current and future areas of application span a wide range, also in terms of scale. Examples of small-size devices are haptic displays [9, 10, 80, 117, 118, 119, 129, 179]; at the other end of the spectrum, there are large-scale manufacturing and wind-tunnel positioning systems [92, 93, 96], as well as rescue systems in earthquake areas [157, 158, 162, 163] (here the idea is that a number of winches can be attached to some rest of building structure, providing in a very simple manner a large-scale high-capacity multi-DOF manipulator). One of the largest applications conceived up to now is a radio telescope [130] where one component is suspended from a helium aerostat and the aerostat is controlled by a number of parallel tendons (Fig. 1.11). Thus, the concept of tendon-based Stewart platforms is likely to extend the field of robotic manipulators to several new areas.

---

<sup>5</sup>Abbreviation of the German title «Seilgetriebene Stewart-Plattformen in Theorie und Anwendung» – tendon-based Stewart platforms in theory and applications. The name was inspired by a beautiful place named Segesta in western Sicily with an ancient Greek theater, because the concept might be used in theater technology in the future.



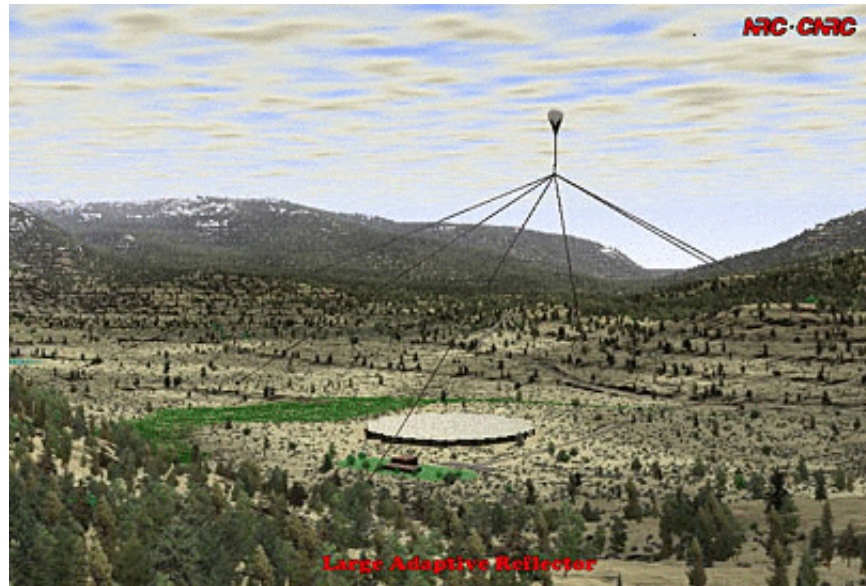


Figure 1.11: Tethered aerostat  
photo © National Research Council of Canada

### 1.3. Objectives and Structure of this Thesis

The present exposition focuses on perspectives and limits of tendon-based Stewart platforms inherent in the concept itself, giving an overall picture of what can be achieved at most. Therefore it relies on geometric, kinematic and dynamic conditions in ideal cases, disregarding further restrictions due to currently unavailable technology. For instance, Chapter 4 provides the optimal distribution of forces in the tendons that can be obtained for a given geometry, thus stating the theoretical optimum that can (and should) be sought in practical construction. Further limitations may arise, among others, from limited actuator torque (this is a subject of ongoing research at Duisburg [57]), joint limits and the geometry of the supporting frame and the load.

We limit ourselves to manipulators as in Fig. 1.6. These are kinematically equivalent to an end-effector attached to the ground by a couple of RRRPRR chains, where the (prismatic) P-joints are actuated and the (revolute) R-joints are passive. We do not consider systems where the R-joints are actuated because this is not possible in the case of tendons. Neither do we include arrangements where the winches themselves are mounted on some movable parts [111] or the tendons are guided around movable pulleys, because all this leads to completely different kinematical structures that cannot be handled by the same means.

When designing such a mechanism, there is a large number of theoretical as well as technical problems, many of which are currently under investigation at Duisburg, Kobe, Rostock and other places around the world. Here, we focus on the question:

given	geometry of platform and base, force limits and elasticity of the tendons, forces and torques acting on the platform,
what can be said about	tendon forces,

singularities,  
stiffness and  
workspace?

The objective is to present a basic theory of tendon-based Stewart platforms and their workspace, to develop an algorithm that computes optimal tension distributions, especially for highly redundant manipulators, and to provide tools for workspace analysis.

This means that we will not discuss practical issues in detail, e. g. which material should be used for base and platform, which type of tendon fits our needs, how we can build the winches, what kind of motors and controllers are appropriate etc. Neither do we ask where the forces and torques acting on the platform come from (mainly gravity, inertia, contact), we just consider them as given. Nevertheless, the simulations in Chapter 6 use realistic values for geometry and tendon properties and compute forces and torques from inertia in simulated motions.

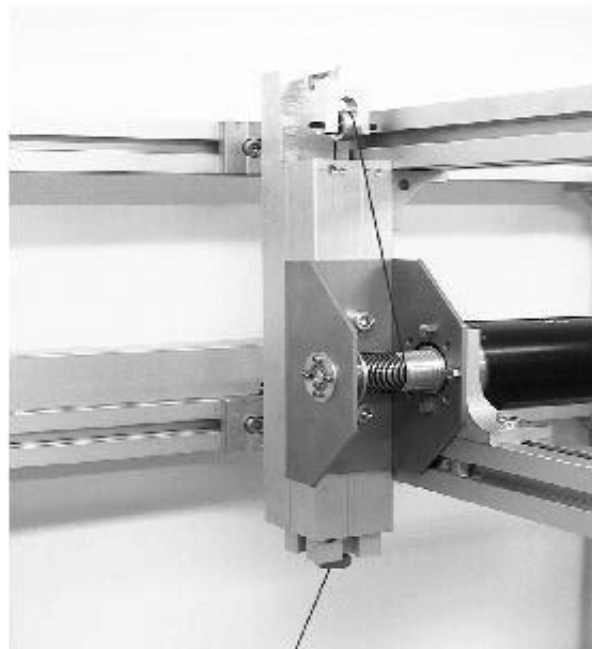


Figure 1.12: Winch design in the SEGESTA prototype

This approach implies a number of model assumptions that we briefly summarize:

- Tendons are supposed to form straight lines; therefore, we ignore deformation due to gravity. This assumption becomes quite wrong in the case of very large systems (with tendons of length 10 m – 1000 m) on earth, but it is acceptable in space applications of arbitrary size and in small-to-medium-scale robots anywhere. Furthermore we do not consider vibrations in tendons, because that is a major subject of research which requires its own mathematical tools.
- The points where tendons are connected to base and platform are fixed and behave as ideal spherical joints of infinite stiffness. This is not that easy

to achieve in practice, especially on the base (i. e. near the winches). The current prototype at Duisburg uses thin tendons of synthetic fiber coming out of a small ceramic eye (Fig. 1.12), while the Cablev prototype at Rostock [181] has steel wires in a sophisticated construction with a movable pulley (Fig. 1.13).

- Tendons behave as linear springs. This is not a strong limitation because in typical applications, changes in tendon length due to elasticity are below 1 %. So in many cases elasticity can even be neglected completely.
- Platform and base are rigid bodies. As both must bear rather large tendon forces in different points, some engineering effort may be required to ensure this. A possible solution was proposed by the ROBOCRANE team [2], with grid structures designed in such a manner that all inner forces in the structure result in longitudinal forces along metal tubes, without bending or torsion.

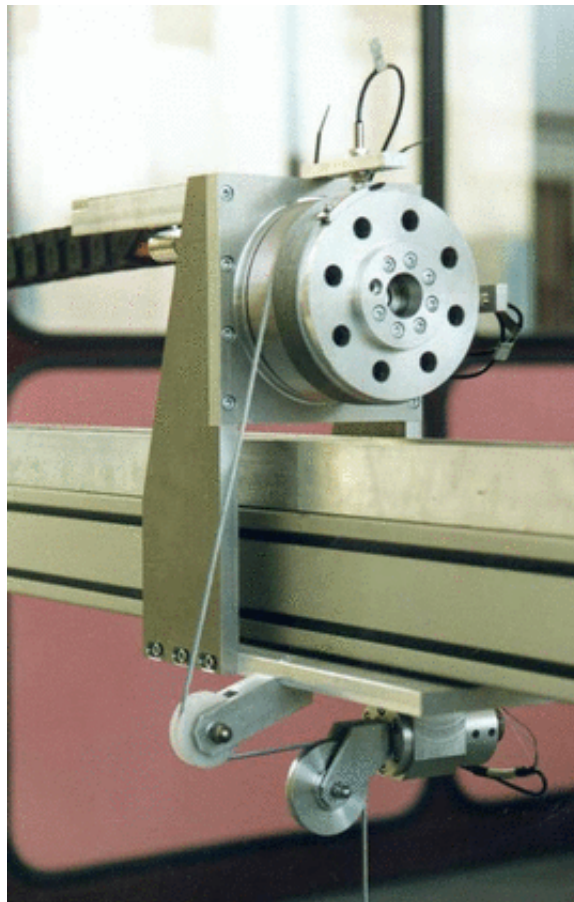


Figure 1.13: Winch design in the Cablev prototype  
photo © University of Rostock

Chapter 2 provides a short introduction to the duality between serial and parallel manipulators, focusing on the fact that serial systems can be described best in terms of mobility, whereas parallel ones are suited for a treatment in terms of controllability. Then the force equilibrium equations for tendon-based Stewart

platforms are developed. This gives rise to a two-fold classification: one related to the degree of redundancy, the other to the number and type of DOFs.

Chapter 3 develops a number of criteria for workspace of tendon-based Stewart platforms. First of all tendon forces must be positive. It is explained how this can be verified for each single posture. The region where positive tension can always be achieved is called «controllable workspace». In addition, tensions must also be limited. This is treated more in detail in Chapter 4. Then it is important to avoid singularities. It is shown that certain types of manipulators do not have singularities at all. For other types a method is presented that allows to find redundant singularity-free designs. The following section describes how to compute passive stiffness in each posture and gives an overall estimate of the stiffness near the center of the workspace. Finally the problem of autocollisions is stated and some solution strategies are shown.

Chapter 4 explains in depth how to find «acceptable» tension distributions that satisfy given bounds and how to optimize tension. The strategy is first illustrated by a simple example. Then it is shown how «optimal» solutions of the tension problem can be defined so that either each optimal solution is acceptable or no acceptable solution exists. Examples show that such optimal solutions can lead to discontinuous force paths along a trajectory. To avoid this, an approximation of the optimal solutions is proposed and is shown to be everywhere continuous except in singularities. The last section describes an algorithm that was implemented for the practical computation of such solutions.

Chapter 5 develops a quality measure which indicates, for a given posture, how far it is from the border of the workspace. This measure is used to examine a number of designs and to identify some «good» ones with large workspaces. Furthermore the chapter states some rules of thumb, obtained from a mixture of computation and experience, that help to find designs with large workspaces.

Chapter 6 uses the implementation outlined in Chapter 4 to compute example trajectories for some planar and spatial manipulators.

Chapter 7 summarizes the results and gives suggestions for further research.

This dissertation is intended for readers working in the field of engineering, therefore it focuses on questions which are relevant. On the other hand, one of its goals is to provide a sound theoretical description. Therefore, some ideas are *also* defined in mathematical terms and sometimes results are stated and proven as in a mathematical paper. As an exception, parts of Chapter 4 are written *mainly* in mathematical style because the desired result on continuity, which is important for engineering, requires complex mathematical proofs. The reader who likes to follow the details can find in Appendix A a brief survey of the mathematical background involved.

# Chapter 2

## Delimitation and Classification

*Section 2.1 provides a short introduction to the notions of singularity and redundancy of parallel manipulators in contrast to serial ones. It turns out that the key issue of serial systems is mobility, while parallel ones are described better in terms of controllability. Section 2.2 supplies the basic force equations for tendon-based Stewart platforms and develops two classifications based on the number of tendons and on the type of end-effector DOFs, respectively.*

### 2.1. Duality of Serial and Parallel Systems

#### 2.1.1. Equations and Mappings

Although parallel robots have become more and more popular in the past two decades, people working in the field of serial robotics might not be familiar with the nature of singularity and redundancy in parallel systems. In addition, there is not yet a unified terminology in literature. In particular, the term «singularity» is used with a wide range of meanings. As the workspace boundary of serial robots typically consists of kinematic singularities, some authors identify the terms «singularity» and «workspace boundary».<sup>1</sup> This is not at all appropriate for parallel systems and even less for tendon-based ones. Therefore it appears useful to give a short introduction to the theory of parallel manipulators and the duality between serial and parallel systems [171, 172, 175], defining precisely the concepts of singularity and redundancy as needed in subsequent chapters.

On an abstract level any manipulator can be seen as a mechanical system transforming  $m$  actuator variables  $\vartheta_1, \dots, \vartheta_m$  and forces  $f_1, \dots, f_m$  into  $n$  end-effector variables  $x_1, \dots, x_n$ , which describe the end-effector position and/or orientation, and forces  $w_1, \dots, w_n$ . The end-effector variables are assumed to be independent,<sup>2</sup> so  $n$  cannot be greater than six. As pointed out by Ou and Tsai

---

<sup>1</sup>Therefore some of them even use the term «singularity» to denote postures where joint limits are reached.

<sup>2</sup>Mathematically speaking, this means that the set of possible end-effector postures forms an  $n$ -dimensional manifold and the end-effector variables are coordinates for this manifold with respect to some chart. It may happen that we need a couple of maps to describe the manifold.



[139], there may be a difference between «joint» variables and «actuator» variables: for example, for a revolute joint driven by a linear hydraulic actuator, there is a nontrivial transformation of the actuator variable (position of the piston) to the joint variable (rotation angle). This example shows that the choice of actuator variables is to some extent a matter of taste, or it depends on the objective of the investigation. The number  $m$  of actuator variables can be arbitrarily large, but must be greater than or equal to  $n$ . In general, neither  $\vartheta_1, \dots, \vartheta_m$  nor  $x_1, \dots, x_n$  needs to be a set of minimal coordinates for the given system: if the forward kinematics problem has multiple solutions, the variables  $\vartheta_1, \dots, \vartheta_m$  do not completely determine the end-effector posture; on the other hand, if the inverse kinematics problem has multiple solutions, then  $x_1, \dots, x_n$  do not completely determine the joint parameters.

Restricting the following discussion to holonomic systems, the relation between joint variables and end-effector variables can always be expressed in a constraint equation

$$(2.1) \quad \Phi(\underline{\vartheta}, \underline{x}) = \underline{0}$$

where  $\Phi$  is a function with values in the «constraint space»  $\mathbb{R}^g$ . Sometimes the values in  $\mathbb{R}^g$  have an intuitive meaning: for instance, they may represent the distance between the axis and the slider of a revolute joint and the meaning of the constraint is that the slider is on the axis.

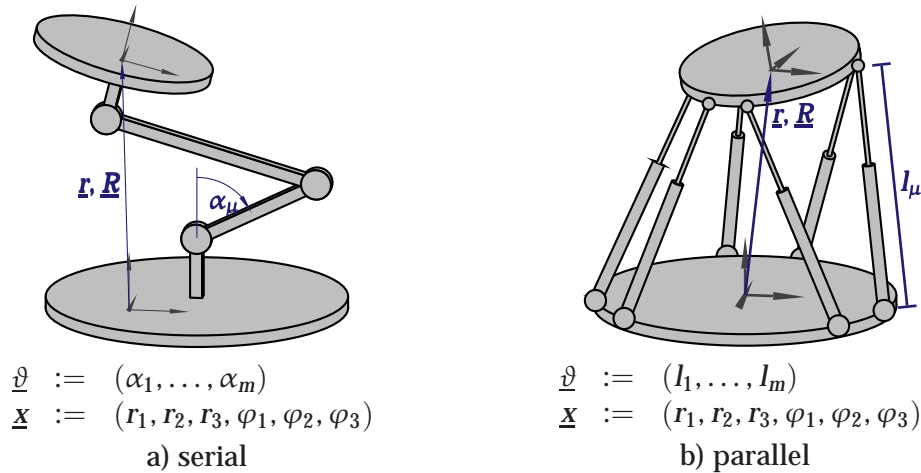


Figure 2.1: Examples of serial and parallel manipulators

For typical serial systems (such as Fig. 2.1a), with an appropriate choice of actuator and end-effector variables, the constraint equation can be written in the form

$$(2.2) \quad \Phi_{\text{act}}(\underline{\vartheta}) - \underline{x} = \underline{0},$$

and the derivative of  $\Phi_{\text{act}}$  with respect to  $\underline{\vartheta}$  – the so-called *Jacobian* – transforms infinitesimal actuator motions  $\delta \underline{\vartheta} \in \mathbb{R}^m$  (or actuator velocities  $\dot{\underline{\vartheta}}$ ) into infinitesimal motions  $\delta \underline{x} \in \mathbb{R}^n$  (or velocities  $\dot{\underline{x}}$ ) of the end-effector. Furthermore the transpose of the Jacobian transforms forces/torques in the opposite sense, i. e. (generalized) end-effector forces  $\underline{w} \in \mathbb{R}^n$  into (generalized) actuator forces  $\underline{f} \in \mathbb{R}^m$ .

For instance, when an end-effector is capable of performing all possible rotations, this cannot be described by a single global map. The discussion in this section refers to local properties, so it does not matter how many maps we need for a global description.

On the other hand, typical<sup>3</sup> parallel systems (as in Fig. 2.1b) with appropriately chosen coordinates have an equation of type

$$(2.3) \quad \underline{\vartheta} - \Phi_{ee}(\underline{x}) = \underline{0}.$$

Then the derivative of  $\Phi_{ee}$  with respect to  $\underline{x}$  transforms end-effector motions into actuator motions and its transpose transforms actuator forces into end-effector wrenches. Some authors call this derivative Jacobian, too. Such terminology may be misunderstood because this matrix transforms in the opposite direction when compared to the Jacobian of serial systems. On the other hand, one cannot call it «inverse Jacobian» because in general it is not quadratic and hence cannot be the inverse of a matrix.

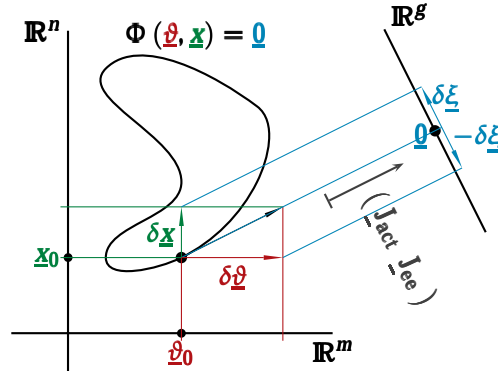


Figure 2.2: Constraint as a relation between actuator and end-effector

In the general case of Eq. (2.1), we have to consider two partial derivatives

$$(2.4) \quad \underline{J}_{act} := \frac{\partial \Phi}{\partial \underline{\vartheta}}(\underline{\vartheta}_0, \underline{x}_0) \in \mathbb{R}^{g \times m} \quad \text{and} \quad \underline{J}_{ee} := -\frac{\partial \Phi}{\partial \underline{x}}(\underline{\vartheta}_0, \underline{x}_0) \in \mathbb{R}^{g \times n}.$$

Both matrices  $\underline{J}_{act}$  and  $\underline{J}_{ee}$  transform motions from the actuator space and the end-effector space, respectively, into the constraint space. This idea is illustrated in Fig. 2.2: the constraint equation Eq. (2.1) defines a relation between actuator variables  $\underline{\vartheta}$  and end-effector variables  $\underline{x}$ , shown as a curve. For a given pair  $(\underline{\vartheta}_0, \underline{x}_0)$  that belongs to this relation, there are the Jacobians  $\underline{J}_{act}$  and  $\underline{J}_{ee}$  (both dependent on  $\underline{\vartheta}$  as well as on  $\underline{x}$ ) which map infinitesimal motions  $\delta \underline{\vartheta}$ ,  $\delta \underline{x}$  to motions  $\delta \underline{\xi}$  in the space of constraint variables. Now a pair  $(\delta \underline{\vartheta}, \delta \underline{x})$  belongs to the tangent space if and only if the images of both contributions cancel each other in the constraint space, i. e.

$$(2.5) \quad \underline{J}_{act} \delta \underline{\vartheta} - \underline{J}_{ee} \delta \underline{x} = \underline{0}.$$

<sup>3</sup>From the point of view of transformation behavior, it seems logical to consider a system as «serial» if it can be described as in Eq. (2.2), «parallel» if it obeys an equation like Eq. (2.3), and «hybrid» if neither one applies. However, this differs from the definition in terms of multibody systems: for instance, the Hexaglide [63] is purely parallel in the sense that it has only closed loops and no open chains; but it cannot be globally described by Eq. (2.3) because its inverse kinematics have multiple solutions. Therefore, in this chapter we speak of «typical» serial/parallel manipulators. For the purposes of this dissertation it does not matter which kind of definition is adopted; tendon-based Stewart platforms are purely parallel in both the multibody sense and the transformation behavior sense.

For typical serial manipulators, the latter equation can always be solved for  $\delta \underline{x}$ . This means that locally, any actuator motion is possible and each actuator motion achieves exactly one end-effector motion. For typical parallel systems, instead, Eq. (2.5) can always be solved for  $\delta \underline{\vartheta}$ , i. e. any end-effector motion is possible and each end-effector motion determines a unique actuator motion. There are hybrid systems where the equation can be solved neither for  $\delta \underline{x}$  nor for  $\delta \underline{\vartheta}$ .

Let us take a look at the relation between the dimensions  $m, n$  and  $g$ . We assume that we have a minimal set of constraints, in other words, the constraints are linearly independent in the tangent space:

$$(2.6) \quad \text{rank} \left( \begin{array}{cc} \underline{J}_{\text{act}} & -\underline{J}_{\text{ee}} \end{array} \right) = g.$$

Then there are in total  $m + n$  variables and  $g$  independent constraints. If we had  $g > m$ , then the total number of DOFs in the system would be less than  $n$  – this is not possible because we said before that we have  $n$  independent end-effector-DOFs. Furthermore if we had  $g < n$ , then we would have more system DOFs than actuator variables, so the system could not be completely controlled with the actuators. Thus, we find that

$$(2.7) \quad n \leq g \leq m.$$

In typical serial systems the first inequality is an equality, while in typical parallel ones the second one is an equality. In hybrid systems both inequalities may be strict.

The transposed matrices  $\underline{J}_{\text{act}}^T$  and  $\underline{J}_{\text{ee}}^T$  convey the transformation of forces, in the opposite directions. If  $\underline{f}$  are the actuator forces,  $\underline{\tau}$  the forces belonging to the constraints and  $\underline{w}$  the end-effector forces/torques, then we can summarize the mapping of motions and forces as follows.

$$(2.8) \quad \begin{array}{lcl} \text{deflection:} & \delta \underline{\vartheta} & \xrightarrow{\underline{J}_{\text{act}}} \delta \underline{\xi} \xleftarrow{\underline{J}_{\text{ee}}} \delta \underline{x} \\ \text{force:} & \underline{f} & \xleftarrow{\underline{J}_{\text{act}}^T} \underline{\tau} \xrightarrow{\underline{J}_{\text{ee}}^T} \underline{w} \\ & \in \mathbb{R}^m & \in \mathbb{R}^g \in \mathbb{R}^n \end{array}.$$

### 2.1.2. Mobility

If the rank of the matrix  $\underline{J}_{\text{act}} \in \mathbb{R}^{g \times m}$  is inferior to the number of actuators, i. e. if

$$(2.9) \quad \text{rank } \underline{J}_{\text{act}} < m,$$

then  $\underline{J}_{\text{act}}$  is not one-to-one, i. e. there are actuator motions  $\delta \underline{\vartheta} \neq \underline{0}$  with  $\underline{J}_{\text{act}} \delta \underline{\vartheta} = \underline{0}$ . It follows that for these motions

$$(2.10) \quad \underline{J}_{\text{act}} \delta \underline{\vartheta} - \underline{J}_{\text{ee}} \underline{0} = \underline{0}.$$

In other words, these so-called *self-motions*  $\delta \underline{\vartheta}$  can occur in the actuators without provoking any motion of the end-effector: the system is *velocity redundant*. If we



have  $g < m$ , i. e. less constraints than actuators, then this is always the case: the manipulator has a redundant architecture.

If in addition the rank of  $\underline{J}_{\text{act}}$  is inferior to the number of constraints, i. e. if

$$(2.11) \quad \text{rank } \underline{J}_{\text{act}} < g,$$

then the mapping  $\underline{J}_{\text{act}}$  is not surjective, i. e. there are motions  $\delta \underline{\xi}$  in the constraint space that cannot be reached with any actuator motion. Now, the image of  $\underline{J}_{\text{ee}}$  is a  $(\text{rank } \underline{J}_{\text{ee}})$ -dimensional subspace of  $\mathbb{R}^g$ . It may still be contained<sup>4</sup> in the  $(\text{rank } \underline{J}_{\text{act}})$ -dimensional image of  $\underline{J}_{\text{act}}$ . If this is not the case, then there are end-effector motions  $\delta \underline{x}$  with<sup>5</sup>

$$(2.12) \quad \underline{J}_{\text{ee}} \delta \underline{x} \notin \langle \underline{J}_{\text{act}} \rangle.$$

This means that such end-effector motions cannot be achieved with any actuator motion. This situation is called a *singularity with undermobility*.



Figure 2.3: Redundancy and singularity in serial systems

Summarizing, there are three situations:

1. If  $\text{rank } \underline{J}_{\text{act}} = m$  (which implies  $g = m$ ), then there is a one-to-one-relation between actuator motions and constraint space motions. Hence, for a given end-effector motion  $\delta \underline{x}$  there is exactly one corresponding actuator motion  $\delta \underline{\vartheta}$ :

$$(2.13) \quad \delta \underline{\vartheta} = \underline{J}_{\text{act}}^{-1} \underline{J}_{\text{ee}} \delta \underline{x}.$$

2. If  $\text{rank } \underline{J}_{\text{act}} < m$  but there is no singularity<sup>6</sup>, then for any end-effector motion  $\delta \underline{x}$  there is an infinite number of possible actuator motions  $\delta \underline{\vartheta}$ :<sup>7</sup>

$$(2.14) \quad \delta \underline{\vartheta} \in \underline{J}_{\text{act}}^+ \underline{J}_{\text{ee}} \delta \underline{x} + \ker \underline{J}_{\text{act}}.$$

For  $\delta \underline{x} = \underline{0}$  we obtain the self-motions, as in Fig. 2.3a: the arrows indicate infinitesimal actuator motions that do not change the end-effector posture. The system is velocity redundant.

<sup>4</sup>If  $\text{rank } \underline{J}_{\text{act}} < n$  and  $\text{rank } \underline{J}_{\text{ee}} = n$ , then this is not possible. In all other cases, this depends on the location of the spaces.

<sup>5</sup> $\langle \underline{J}_{\text{act}} \rangle$  denotes the subspace generated by the columns of  $\underline{J}_{\text{act}}$ , cf. Def. A.6, p. 126.

<sup>6</sup>i. e. either  $g = \text{rank } \underline{J}_{\text{act}}$  or  $\text{rank } \underline{J}_{\text{act}} < g$  and  $\text{rank } \underline{J}_{\text{ee}} < g$  such that  $\langle \underline{J}_{\text{ee}} \rangle \subset \langle \underline{J}_{\text{act}} \rangle$

<sup>7</sup>The term  $\underline{J}_{\text{act}}^+$  denotes the Moore-Penrose pseudo inverse, cf. Prop. A.8, p. 126, while  $\ker \underline{J}_{\text{act}}$  is the kernel (null space) of  $\underline{J}_{\text{act}}$ , cf. Def. A.6, p. 126.

3. If we have  $\text{rank } \underline{J}_{\text{act}} < g$  and there is a singularity, then for some end-effector motions there is an infinite number of corresponding actuator motions (and in particular, self-motions exist), but for some others there is no solution. Thus, the system is velocity redundant for certain end-effector motions and at the same time the end-effector mobility is restricted, excluding certain other motions. (For instance, the end-effector in Fig. 2.3b cannot rotate about its axis as indicated by the arrows.)

Hence, both actuator redundancy and end-effector restrictedness refer to mobility. This is the typical well-known situation for serial manipulators. In fact, traditionally the behavior of serial robots is described in terms of mobility, because the main problem of a serial manipulator is the ability of the end-effector to move in a desired direction. This remains true even when disregarding joint limits, because the geometry itself of such systems often limits the workspace. For instance, the workspace of a planar manipulator with a number of revolute joints is a circle around the first joint.

### 2.1.3. Controllability

We could proceed in a very similar way for the matrix  $\underline{J}_{\text{ee}}$ , but here it is more appropriate to consider the forces. If the rank of this matrix (which is always equal to the rank of  $\underline{J}_{\text{ee}}^T$ ) is less than the number of constraints, i. e. if

$$(2.15) \quad \text{rank } \underline{J}_{\text{ee}} < g,$$

then  $\underline{J}_{\text{ee}}^T$  is not one-to-one, i. e. there are forces  $\underline{\tau} \neq \underline{0}$  in the constraint space with<sup>8</sup>

$$(2.16) \quad \underline{J}_{\text{ee}}^T \underline{\tau} = \underline{0} \quad \text{and} \quad \underline{J}_{\text{act}}^T \underline{\tau} \neq \underline{0}.$$

Thus, we have *inner forces*  $\underline{J}_{\text{act}}^T \underline{\tau}$  in the actuators that do not lead to forces at the end-effector, as in Fig. 2.4a where the arrows indicate inner forces: the system is *force redundant*. If  $g > n$ , i. e. there are more constraints than end-effector DOFs, then this is always the case and the system is architecturally redundant.

If the rank of  $\underline{J}_{\text{ee}}^T$  is even less than the number of end-effector DOFs, i. e. if

$$(2.17) \quad \text{rank } \underline{J}_{\text{ee}} < n,$$

then the mapping  $\underline{J}_{\text{ee}}$  it is not surjective, i. e. there are end-effector wrenches  $\underline{w}$  that cannot be obtained with any actuator force (e. g. in Fig. 2.4b the indicated force in y direction cannot be achieved with the actuators). This is called a *singularity with overmobility*.<sup>9</sup>

Thus, similarly to the discussion of mobility, we have again three situations.

---

<sup>8</sup> To be precise,  $\underline{\tau}$  fulfilling the inequality in the second part may not exist if  $\text{rank } \underline{J}_{\text{act}} < g$ , i. e. in the case that both matrices are singular at the same time and the space of undermobility of the end-effector coincides with the space of its overmobility. However, it is rather difficult to imagine a manipulator having such configurations.

<sup>9</sup> As explained in footnote 4, typical serial systems can have special situations of *singularity* where the comparison of ranks of both matrices is not sufficient to characterize the manipulator's behavior, while redundancy only depends on the ranks. It is interesting to observe that the opposite happens in the parallel case: here *redundancy* is subject to special cases (footnote 8), while singularity is given by the rank comparison only.



Figure 2.4: Redundancy and singularity in parallel systems

1. If  $\text{rank } \underline{J}_{ee} = g$  (which implies  $g = n$ ), then there is a one-to-one-relation between end-effector forces and constraint space forces. Thus, for a given end-effector force/torque  $\underline{w}$  there is exactly one corresponding actuator force:<sup>10</sup>

$$(2.18) \quad \underline{f} = \underline{J}_{act}^T \underline{J}_{ee}^{-T} \underline{w}.$$

2. If  $n \leq \text{rank } \underline{J}_{ee} < g$  and the matrix  $\underline{J}_{act}$  has full rank, then for any end-effector wrench  $\underline{w}$  there is an infinite number of possible actuator forces:<sup>11</sup>

$$(2.19) \quad \underline{f} \in \underline{J}_{act}^T \left( \underline{J}_{ee}^{+T} \underline{w} + \ker \underline{J}_{ee}^T \right);$$

for  $\underline{w} = \underline{0}$  we obtain the inner forces. The system is force redundant.

3. If we have  $\text{rank } \underline{J}_{act} < n$ , then for some end-effector wrenches there is an infinite number of corresponding actuator forces (and in particular, inner forces exist), but for some others there is no solution. Hence, the system is force redundant and at the same time the end-effector controllability is restricted.

Here both actuator redundancy and end-effector restrictedness refer to controllability. This is typical for parallel manipulators. Therefore it is natural to express the properties of parallel systems in terms of controllability rather than mobility: *the theoretical key problem of parallel robots is the ability to exert a wrench in a desired direction*. This holds under the assumption that joint limits are not an essential restriction. In reality this assumption is often perfectly wrong because one of the main practical problems in building parallel systems is the unavailability of spherical joints with large angular ranges (and a high stiffness at the same time).

## 2.2. Tendon-based Stewart Platforms

### 2.2.1. Force Equilibrium

Fig. 2.5 explains most of the symbols needed in this section. We have a coordinate frame  $\mathcal{K}_B$  fixed on the base and another frame  $\mathcal{K}_P$  attached to the movable platform. In all our three-dimensional sketches,  $\mathcal{K}_B$  is aligned with the supporting frame so that the x axis points to the right, the y axis into drawing plane and

<sup>10</sup>  $\underline{J}_{ee}^{-T}$  is a shorthand for  $(\underline{J}_{ee}^{-1})^T$ .

<sup>11</sup>  $\underline{J}_{ee}^{+T}$  is a shorthand for  $(\underline{J}_{ee}^{+})^T$ .

the  $z$  axis upwards. We assume that gravity (if taken into account) acts in negative  $z$  direction of  $\mathcal{K}_B$ .

There are no special requirements on the choice of origin and orientation of  $\mathcal{K}_P$ . In particular, its origin does not need to coincide with the center of gravity of the platform (although this is the case in many examples because usually this leads to the simplest descriptions). The position of  $\mathcal{K}_P$  with respect to  $\mathcal{K}_B$  is written as  $\mathbf{r} \in \mathbb{R}^3$  and its orientation is expressed by a rotation<sup>12</sup>  $\mathbf{R} \in \text{SO}_3$ .

The vectors  $\mathbf{b}_1, \dots, \mathbf{b}_m$  denote the positions of the base points, i. e. the points where tendons leave the winches. Similarly,  $\mathbf{p}_1, \dots, \mathbf{p}_m$  are the connection points on the platform, but measured from the origin of  $\mathcal{K}_P$ . Their positions with respect to  $\mathcal{K}_B$  are written as  $\mathbf{p}_{B,1}, \dots, \mathbf{p}_{B,m}$ , which means that  $\mathbf{p}_{B,\mu} = \mathbf{r} + \mathbf{p}_\mu$ . The tendon length vectors  $\mathbf{l}_1, \dots, \mathbf{l}_m$  point from the platform to the base. This convention is mostly adopted in literature because then possible (i. e. pulling) tendon forces are positive with respect to the tendon lengths. However, one must pay attention when simulating motions because this means that when the length of the  $\mu$ th tendon increases, the vector  $\dot{\mathbf{l}}_\mu$  has negative orientation with respect to  $\mathbf{l}_\mu$ .

For the purposes of this dissertation we consider the tendon lengths  $\underline{\mathbf{l}} = (l_1, \dots, l_m)$  as the actuator variables. Another possible choice would have been the rotation angles of the shafts of the winches or the motors, but this would involve technical details of winch construction which are outside our focus. The systems considered are purely parallel in the sense that they obey the system of constraint equations<sup>13</sup>

$$(2.20) \quad \underline{\mathbf{l}} - \begin{pmatrix} |\underline{\mathbf{b}}_1 - \underline{\mathbf{r}} - \underline{\mathbf{R}} \underline{\mathbf{p}}_1| \\ \vdots \\ |\underline{\mathbf{b}}_m - \underline{\mathbf{r}} - \underline{\mathbf{R}} \underline{\mathbf{p}}_m| \end{pmatrix} = \underline{\mathbf{0}}$$

which has the form of Eq. (2.3). Hence, the only possible type of redundancy is force redundancy and the only possible type of singularity is overmobility.

As pointed out in Section 2.1.3, in theory it is a good idea to describe parallel robots in terms of controllability, but for systems with rigid links this is often secondary because the main problem are the joint limits. The picture is quite different when dealing with tendon-based systems: assuming the tendons are long enough, the space of postures that can be reached is arbitrarily large and motion in any desired direction is possible. But a sophisticated arrangement is necessary to enable the system of exerting forces and torques on the platform. Here the key issue really is controllability [161] and therefore the following treatment is based on forces instead of velocities.

As shown in Fig. 2.5,  $\mathbf{f}_1, \dots, \mathbf{f}_m$  denote the forces in the tendons, while  $\mathbf{f}_P$  and  $\boldsymbol{\tau}_P$  summarize all other forces and torques acting on the platform, including e. g. gravity, inertia, or contact forces/torques. We refer to them as «platform

<sup>12</sup>The term  $\text{SO}_3$  denotes the special orthogonal group in three dimensions, i. e. the set of rotations in  $\mathbb{R}^3$ .

<sup>13</sup>As explained in Section A.2, p. 125 ff., the bold letters in the previous paragraph refer to physical vectors, while the underlined letters in the following equation denote tuples of coordinates. Throughout this thesis it does not matter which coordinate system is used for decomposition.

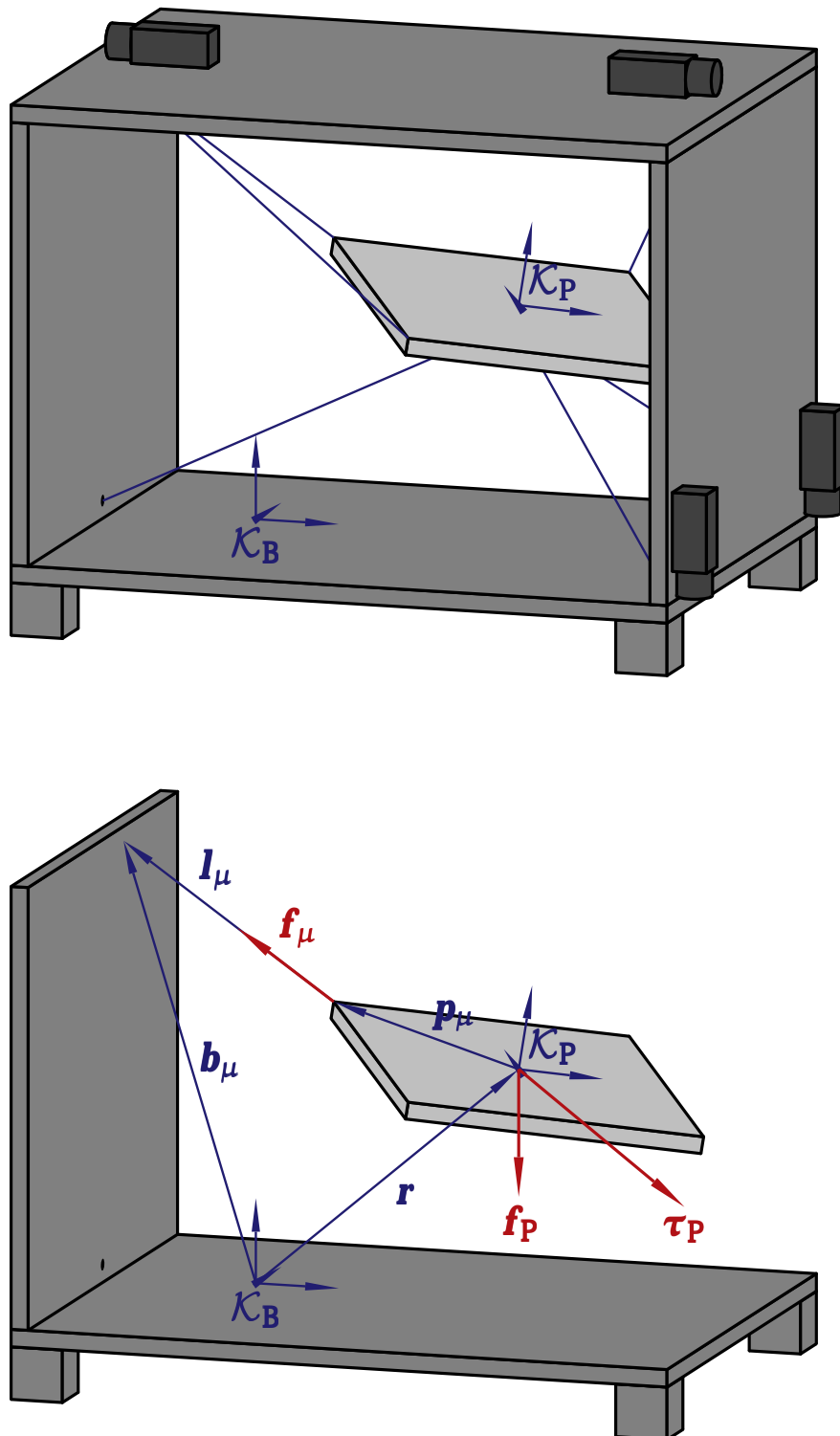


Figure 2.5: Symbols used to describe tendon-based Stewart platforms

wrenches». The force and torque equilibrium supplies

$$(2.21) \quad \sum_{\mu=1}^m \mathbf{f}_{\mu} + \mathbf{f}_P = \mathbf{0} \quad \text{and} \quad \sum_{\mu=1}^m \mathbf{p}_{\mu} \times \mathbf{f}_{\mu} + \boldsymbol{\tau}_P = \mathbf{0} .$$

The tendon forces act along the tendons, hence

$$(2.22) \quad \mathbf{f}_{\mu} = f_{\mu} \frac{\mathbf{l}_{\mu}}{l_{\mu}} = f_{\mu} \mathbf{u}_{\mu}$$

where  $\mathbf{u}_{\mu}$  denotes the unit vector along the  $\mu$ th tendon. Decomposing the vectors in an arbitrary coordinate system, Eq. (2.21), (2.22) yield

$$(2.23) \quad \begin{pmatrix} \underline{p}_1 \times \underline{u}_1 & \cdots & \underline{p}_m \times \underline{u}_m \end{pmatrix} \begin{pmatrix} f_1 \\ \vdots \\ f_m \end{pmatrix} + \begin{pmatrix} f_P \\ \tau_P \end{pmatrix} = \underline{0}$$

which can be abbreviated as

$$(2.24) \quad \underline{A}^T(\underline{r}, \underline{R}) \underline{f} + \underline{w} = \underline{0} .$$

The posture-dependent matrix  $\underline{A}^T$  is called *structure matrix* [139]. It transforms actuator forces into end-effector wrenches and is the transpose of the Jacobian, which transforms end-effector twists into actuator velocities.<sup>14</sup> In fact, we could have derived the same result by computing the velocity transformation, but in this context, the force approach is simpler and more intuitive.

The above writing for  $\underline{A}^T$  represents the most general case with six DOFs in the end-effector. There are several cases where the number of DOFs is restricted a priori: for instance, when moving an object that slides horizontally on a plane three rows of the above matrix (and of the vector  $\underline{w}$ ) constantly vanish. Then it is sufficient to work with a matrix consisting in the other three rows. In general, for  $n$  end-effector-DOFs and  $m$  tendons, we obtain an  $n \times m$  matrix. We denote such matrices with  $\underline{A}^T$ , too.

Now, if we want to use the platform in a given posture with given platform wrench  $\underline{w}$ , the minimum requirement is that all tendons are under tension, i. e.<sup>15</sup>

$$(2.25) \quad \underline{f} > \underline{0} .$$

Hence, the most basic problem for the workspace of tendon-based Stewart platforms is: *are there positive solutions of the structure matrix equation and how can we find them?*

<sup>14</sup>This is not  $J_{ee}$  in terms of Section 2.1, because  $J_{ee}$  applies to derivatives of angle coordinates whereas  $\underline{A}$  applies to angular velocities. Bruno Siciliano [148] has proposed to speak of  $\underline{J}_{ee}$  as an «analytic Jacobian» and  $\underline{A}$  as a «geometric Jacobian». In our context, we do not need the analytic Jacobian because the treatment is entirely based on a discussion of (generalized) forces, without any reference to the coordinate transformation behind it.

<sup>15</sup>The notation means that each entry of the left hand side satisfies the inequality with the corresponding entry on the right hand side.

### 2.2.2. Degree of Redundancy

The problem of solvability of the structure matrix equation gives rise to a classification based on the dimension of  $\underline{A}^T$ . This was first proposed by Ming and Higuchi in 1994 [125]; we extend it to a more detailed<sup>16</sup> classification as follows.

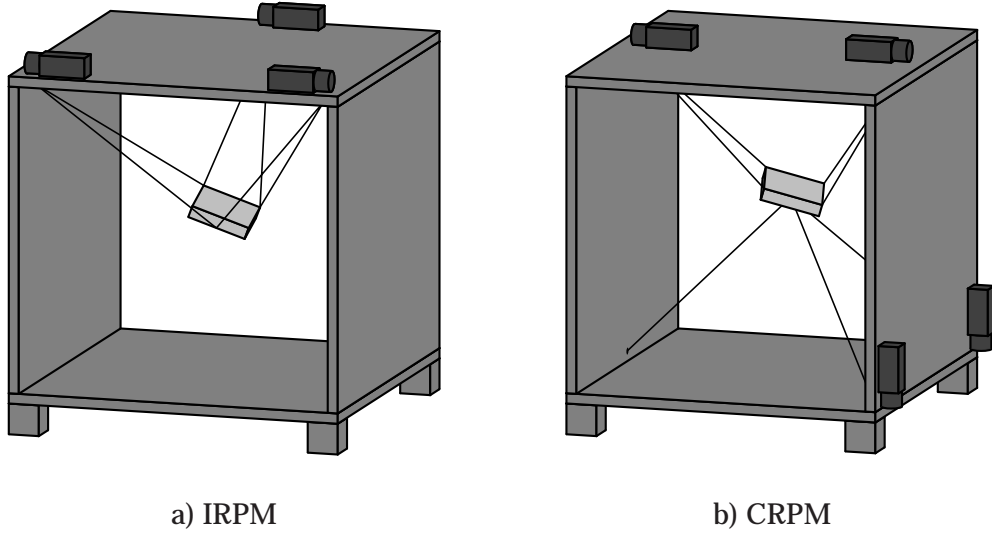


Figure 2.6: Incompletely / completely restrained positioning mechanism

If the number of tendons is less than or equal to the number of DOFs (Fig. 2.6a), i. e. if

$$(2.26) \quad m \leq n ,$$

then Eq. (2.24) always has at most one solution (except in singular postures). In particular, in the homogeneous case with  $\underline{w} = \underline{0}$ , the solution is  $\underline{f} = \underline{0}$ , so there are no positive solutions. This implies that the manipulator can be used only if there are platform wrenches involved, for instance gravity. Such systems are called *Incompletely Restrained Positioning Mechanisms* (IRPMs). They can even have less than  $n$  tendons, although this restricts the possible directions of motion. Such systems are currently being studied in particular at laboratories at Rostock [55] and Kobe.

So the minimum requirement for a manipulator that can work without platform wrenches (e. g. for quasistatic motions in space or in applications with negligible mass) is to have one extra tendon (Fig. 2.6b), i. e.

$$(2.27) \quad m = n + 1 .$$

We speak then of *Completely Restrained Positioning Mechanisms* (CRPMs). Except in cases of singularity, this means that the space of solutions of Eq. (2.24) is a one-dimensional affine subspace of  $\mathbb{R}^m$ . Dependent on the properties of  $\underline{A}^T$ , positive solutions can exist and it is easy to check if they do.

If we have even more tendons (Fig. 2.7), i. e.

$$(2.28) \quad m > n + 1 ,$$

<sup>16</sup>Indeed, Ming and Higuchi do not distinguish between CRPMs and RRPMS.



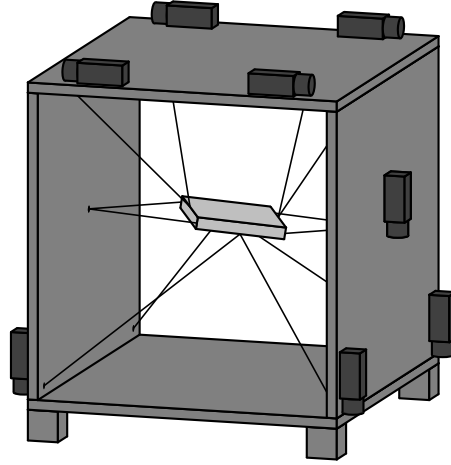


Figure 2.7: Redundantly restrained positioning mechanism

the situation is similar, but the space of solutions is multidimensional. Thus, more sophisticated algorithms are needed to check if positive solutions exist and eventually to find them. In addition, normally there are infinitely many positive solutions with very different properties. So the problem of optimal tension distribution (which is present also in CRPMs, but on a trivial level) becomes an interesting topic. Hence, it is worthwhile to distinguish these *Redundantly Restrained Positioning Mechanisms* (RRPMs) from the CRPMs. Usage of redundant winches tends to be more expensive, but it has a number of advantages.

- First of all, workspace can be extended considerably and singularities can be reduced. Furthermore passive stiffness increases.
- Less powerful actuators can be employed, not only because the load is redistributed, but also because more advantageous geometries can be achieved.
- When transporting persons e. g. in rescue applications [162], safety is an important issue. Then the operational risk is reduced when employing many redundant tendons.

### 2.2.3. Degrees of Freedom

Another classification derives from the number and type of end-effector DOFs that can be achieved. Unlike the classical approach in robotics (which refers to the dimension of the manifold of possible motions and is particularly suited for serial manipulators), here the notion of DOF must be defined in terms of controllability rather than mobility. Hence, we look at the wrenches that the end-effector can apply in a given posture.<sup>17</sup> They are given by the set  $\underline{A}^T(\mathbb{R}_+^m)$ , i. e. the image of all vectors  $\underline{f} > \underline{0}$  under the mapping  $\underline{A}^T$ . The closure<sup>18</sup> of this set is a convex

<sup>17</sup>In practice, wrenches in other directions may occur as perturbations which need to be captured by appropriate means, for instance a guiding plane for planar systems.

<sup>18</sup>The set itself is open or (if  $\underline{A}^T$  is rank deficient) an open subset of a lower dimensional subspace because its border is the image of vectors  $\underline{f} \geq \underline{0}$  having some components equal to zero.



cone (Def. A.12, p. 127) and for the discussion of DOFs, we have to look at its lineality space (Def. A.14, p. 129)

$$(2.29) \quad \text{lin.space } \overline{\underline{A}^T}(\mathbb{R}_{+0}^m) = \text{lin.space } \underline{A}^T(\mathbb{R}_{+0}^m) .$$

In particular, the number of DOFs is the dimension of this space.

For IRPMs, the dimension resulting from this definition is always zero because of the uniqueness of solutions: if a wrench  $\underline{w}_0$  can be balanced with tendon forces  $\underline{f}_0 > \underline{0}$ , then the only way to balance  $-\underline{w}_0$  would be  $-\underline{f}_0 \not> \underline{0}$  which cannot be achieved with tendons. But the most important application of IRPMs are crane-like manipulators for rather heavy loads on earth, where gravity always plays an important role. In that case, we can handle gravity like an additional tendon. Given a platform of mass  $m_P$  with the origin of  $\mathcal{K}_P$  in its center of gravity, we have an equation

$$(2.30) \quad \underline{A}^T \underline{f} + m_P \underline{g} + \underline{w} = \underline{0}$$

where  $\underline{w}$  represents all other forces/torques except gravity. We write now

$$(2.31) \quad \underbrace{\begin{pmatrix} 0 \\ 0 \\ \underline{A}^T & 1 \\ 0 \\ 0 \\ 0 \end{pmatrix}}_{=: \underline{A}'^T} \underbrace{\begin{pmatrix} \underline{f} \\ \underline{f}_{m+1} \end{pmatrix}}_{=: \underline{f}'} + \underline{w} = \underline{0}$$

which is equivalent to the previous equation if we define

$$(2.32) \quad \underline{f}_{m+1} = m_P \underline{g} .$$

In other words, gravity is like an additional tendon attached to the origin of  $\mathcal{K}_P$ , with a winch at infinite distance that can only create a constant force of amount  $m_P \underline{g}$ . Any positive solution  $(\underline{f}^T, \underline{f}_{m+1})^T$  of the structure matrix equation can be scaled such that Eq. (2.32) is fulfilled. Hence, when working with IRPMs,  $\underline{A}'^T$  should be substituted for  $\underline{A}^T$ .

Now we ask if it is possible to build a tendon-based Stewart platform such that in all postures, the space  $\text{lin.space } \underline{A}^T(\mathbb{R}_{+0}^m)$  is precisely the set of all forces in a plane, for instance. (While the dimension of this space is constant except for singularities, its location may depend on the posture.) The result is summarized by the following theorem.

**2.1 Theorem (DOF Classes)** *The combinations of end-effector DOFs which a tendon-based Stewart platform can have in all postures are precisely those listed in Table 2.1.  $\diamond$*

**Proof.** The existence is shown by the examples in Fig. 2.8. We argue that the combinations not listed in the table cannot exist.

DOFs	$n$	Type of Motion
1T	1	linear motion of a body
2T	2	planar motion of a point
1R2T	3	planar motion of a body
3T	3	spatial motion of a point
2R3T	5	spatial motion of a beam
3R3T	6	spatial motion of a body

Table 2.1: Possible DOF classes  
(R stands for rotational, T for translational DOFs)

If the manipulator could produce only torques, then Eq. (2.23) would imply that all vectors  $\mathbf{u}_\mu$  vanish, and then all torques would be zero, too. Hence, there are no designs with rotational DOFs only.

If the projection of  $\text{lin.space } \underline{A}^T(\mathbb{R}_{+0}^m)$  onto the space of forces is one-dimensional, then Eq. (2.23) implies that all the vectors  $\mathbf{u}_\mu$  are parallel and that their direction is constant. The latter implies that translation takes place in this direction only. Then all connection points on the platform, as well as all winches, must lie on a common axis in this direction and hence no torque can be applied at all. Hence, 1T is the only system with exactly 1 DOF in translation.

If the force component of  $\text{lin.space } \underline{A}^T(\mathbb{R}_{+0}^m)$  is two-dimensional, then all  $\mathbf{u}_\mu$  must be coplanar. Hence, torque can be applied about an axis orthogonal to this plane (case 1R2T), or no torque is applied (case 2T).

Finally, we show that a 1R3T manipulator cannot be built. Without loss of generality, let the torque be applied about the z axis. Then Eq. (2.23) yields

$$(2.33) \quad \underline{p}_\mu \times \underline{u}_\mu = (0, 0, p_{\mu 1} u_{\mu 2} - p_{\mu 2} u_{\mu 1})^T$$

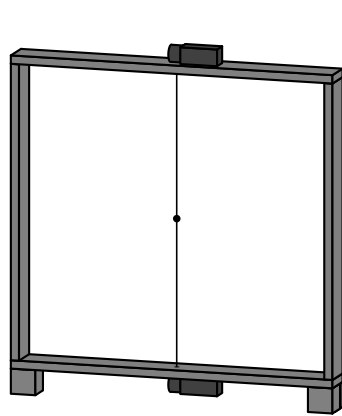
As we assume that we can apply a nonzero torque, in all postures of the workspace there is some  $\mu$  with  $\underline{p}_\mu \times \underline{u}_\mu \neq 0$ . Then  $\underline{p}_\mu, \underline{u}_\mu$  must lie in the xy plane, hence the platform cannot move in z direction, in contradiction to the assumption of 3 DOFs in translation.  $\square$

In the following, we give a brief survey of the classes of Table 2.1. The 1T manipulator (Fig. 2.8a) is just a point-shaped load moved by antagonistic tendons along a line. The only reasonable construction employs two tendons, as any further tendon would coincide with one of the two. The set of postures can be described by real numbers  $r \in \mathbb{R}$  and the structure matrix is simply

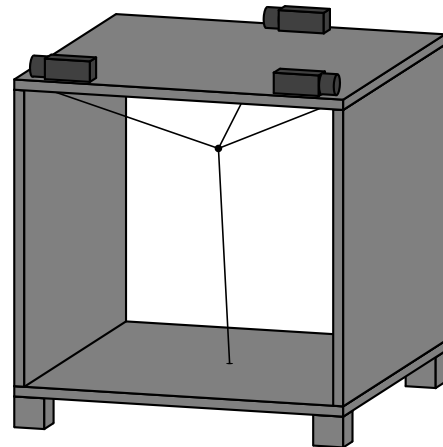
$$(2.34) \quad \underline{A}^T = \begin{pmatrix} -1 & 1 \end{pmatrix} \in \mathbb{R}^{1 \times 2}$$

which is the only case where the structure matrix is constant. So this class is not only trivial but also untypical and we will not consider it any more.

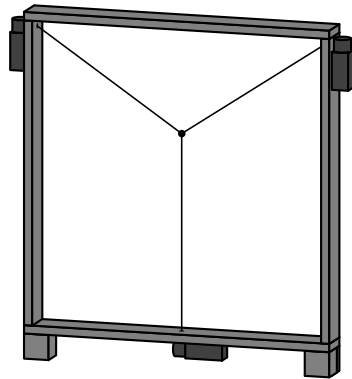
In a system of class 2T a still point-shaped load is moved in a plane. Here the number of tendons can be three as in Fig. 2.8b, or just two together with gravity (eliminating the tendon below the load in the figure), or also any higher number.



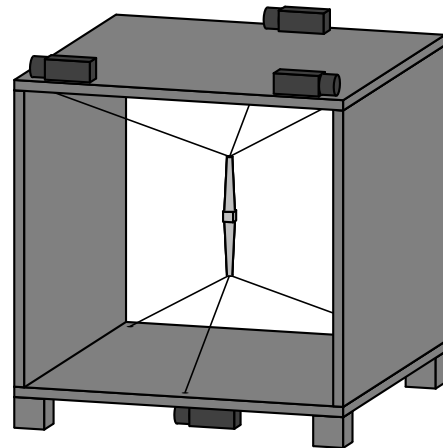
a) class 1T



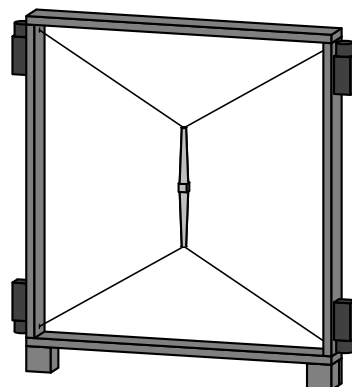
d) class 3T



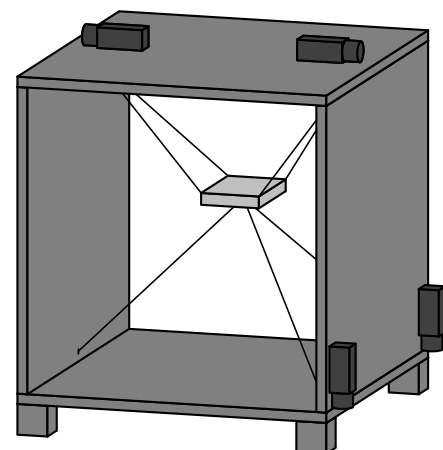
b) class 2T



e) class 2R3T



c) class 1R2T



f) class 3R3T

Figure 2.8: The classes of Theorem 2.1

(Indeed, in this and all the following classes, a arbitrarily high number of tendons can be employed.) The postures are given as points  $\underline{r} \in \mathbb{R}^2$  in the plane and the structure matrix consists in the unit vectors indicating the tendon directions in this plane:

$$(2.35) \quad \underline{A}^T = ( \underline{u}_1 \quad \cdots \quad \underline{u}_m ) \in \mathbb{R}^{2 \times m}.$$

There are no point-shaped loads in the real world, so the main application of this class are mechanisms where a load is *suspended* from a point that has to be controlled in two DOFs. Then the load itself still is subject to sway motions, hence this is neither appropriate for precision engineering tasks, nor for motions with high acceleration.

More interesting in applications are manipulators of class 1R2T which allow for complete control of the load in a plane. Here the postures can be described by a pair  $(r, \varphi) \in \mathbb{R}^2 \times S^1$  consisting of two Cartesian coordinates and an angle<sup>19</sup> and the respective wrenches  $\underline{w} = (\underline{f}_p, \tau_p)$  include two force components and one torque component. The structure matrix contains tendon unit vectors and torques applied by the tendons:

$$(2.36) \quad \underline{A}^T = \begin{pmatrix} \underline{u}_1 & \cdots & \underline{u}_m \\ \det(\underline{p}_1 \ \underline{u}_1) & \cdots & \det(\underline{p}_m \ \underline{u}_m) \end{pmatrix} \in \mathbb{R}^{3 \times m}$$

where the entries of the last row denote determinants. Such systems can perform any positioning task in the plane, also with high acceleration. A prototype was described in 1994 [126].

Moving on from planar to spatial systems, we find that the class 3T moving a point in space is perfectly analogous to the 2T type described above. The structure matrix is identical to that of Eq. (2.35), the only difference is that the unit vectors  $\underline{u}_\mu$  (as well as the posture vector  $\underline{r}$ ) have three instead of two components. Furthermore the limits in applications (considering that really point-shaped loads do not exist) apply in a similar way.

More complicated to handle are the 2R3T systems which move a bar-shaped load in space [82]. All force/torque components except rotation about the bar's axis can be controlled with the tendons. To describe the posture, we need three Cartesian coordinates for the position and something to describe the bar's direction. For the latter, one could employ an equivalence class of spatial rotations (considering two rotations as equivalent if they differ only by a rotation about the bar's axis), but an easier way is to use unit vectors along the bar's axis, i. e. elements  $d$  of the two-dimensional unit sphere  $S^2 \subset \mathbb{R}^3$ . Hence, the posture is described by a pair  $(\underline{r}, \underline{d}) \in \mathbb{R}^3 \times S^2$ . On the other hand, the space of forces/torques that can be controlled consists of the forces  $\underline{f}_p \in \mathbb{R}^3$  and the two-dimensional space of those torques  $\underline{\tau}_p$  that are orthogonal to the bar's axis. This space varies with the axis direction.

If we want to express these torques with a two-dimensional vector, we could think of using a matrix  $\underline{T}_d^T(\underline{d}) \in \mathbb{R}^{2 \times 3}$  depending on the direction  $\underline{d}$  that maps the set of such torques one-to-one onto  $\mathbb{R}^2$ . This is possible, but there is a drawback:

---

<sup>19</sup>There are various possible ways to write down the set of angles, e. g. as the half-open interval  $[0, 2\pi[$ . Here we identify the set with the points on a unit circle  $S^1$  which is mathematically easier to handle.

**2.2 Proposition (Mapping for 2R3T)** For each direction  $\underline{d} \in S^2$ , let  $\underline{T}_d^T(\underline{d}) \in \mathbb{R}^{2 \times 3}$  be a matrix such that

$$(2.37) \quad \begin{pmatrix} \underline{d} & \underline{T}_d(\underline{d}) \end{pmatrix} \in \text{SO}_3,$$

i. e. the rows of  $\underline{T}_d^T(\underline{d})$  are unit vectors orthogonal to each other and to the vector  $\underline{d}$  such that these three vectors form a right-handed system. Then the mapping

$$(2.38) \quad S^2 \rightarrow \mathbb{R}^{2 \times 3}, \quad \underline{d} \mapsto \underline{T}_d^T(\underline{d})$$

cannot be continuous.  $\diamond$

**Proof.** Let  $\underline{t}_1(\underline{d})$  be the first column of  $\underline{T}_d^T(\underline{d})$ . Then the mapping of  $\underline{d}$  to  $\underline{t}_1(\underline{d})$  is a vector field on the sphere, i. e. it maps each element of the sphere to a vector in the respective tangent space. Now, a continuous vector field on the sphere vanishes in at least one point [14, Theorem 9.6], but this is not possible here because  $\underline{t}_1(\underline{d})$  must be a unit vector.  $\square$

Thus, we always have to switch at least between some transformations; depending on what the transformation is used for, this might lead to discontinuities during a trajectory. An example of a good<sup>20</sup> choice of transformations that works for all directions is

$$(2.39) \quad \underline{T}_d(\underline{d}) := \begin{cases} \frac{1}{1-d_3^2} \begin{pmatrix} \begin{pmatrix} -d_2 \\ d_1 \\ 0 \end{pmatrix} & \underline{d} \times \begin{pmatrix} -d_2 \\ d_1 \\ 0 \end{pmatrix} \end{pmatrix} & \text{if } |d_3| \leq |d_1| \wedge |d_3| \leq |d_2| \\ \frac{1}{1-d_2^2} \begin{pmatrix} \begin{pmatrix} d_3 \\ 0 \\ -d_1 \end{pmatrix} & \underline{d} \times \begin{pmatrix} -d_3 \\ 0 \\ d_1 \end{pmatrix} \end{pmatrix} & \text{if } |d_2| \leq |d_1| < |d_3| \\ \frac{1}{1-d_1^2} \begin{pmatrix} \begin{pmatrix} 0 \\ -d_3 \\ d_2 \end{pmatrix} & \underline{d} \times \begin{pmatrix} 0 \\ -d_3 \\ d_2 \end{pmatrix} \end{pmatrix} & \text{if } |d_1| < |d_2| < |d_3|. \end{cases}$$

But usually the set of directions that the robot can actually achieve is not that large, so with a good choice of the coordinate system  $\mathcal{K}_P$  one can ensure that at least one component of  $\underline{d}$  is sufficiently far from zero and use always one of the three alternatives.

With any such transformation  $\underline{T}_d^T$ , we can write the structure matrix as

$$(2.40) \quad \underline{A}^T = \begin{pmatrix} \underline{I}_3 \\ \underline{T}_d^T \end{pmatrix} \begin{pmatrix} \underline{u}_1 & \cdots & \underline{u}_m \\ \underline{p}_1 \times \underline{u}_1 & \cdots & \underline{p}_m \times \underline{u}_m \end{pmatrix} \in \mathbb{R}^{5 \times m}.$$

In many cases we do not need such a «minimal» representation of the structure matrix because the torques are naturally given as elements of  $\mathbb{R}^3$  orthogonal to the axis of the bar, e. g. if the torques represent inertia while rotating the bar (about some axis different from the bar's axis). Then it is convenient just to use the general form in Eq. (2.41) below.

While applications appropriate for the 2R3T class are rather seldom, the most general class 3R3T has the largest variety of applications, including among others

<sup>20</sup>in the sense that the denominator is as large as possible – obviously this is just one of several ways to obtain this

shipbuilding [33], rescue [162] and motions with high acceleration [80]. Here the posture can be written as a pair  $(\underline{r}, \underline{R}) \in \mathbb{R}^3 \times \text{SO}_3$  of a translation and a spatial rotation and the wrench is simply a pair  $\underline{w} = (\underline{f}_P, \underline{\tau}_P) \in \mathbb{R}^6$  consisting of arbitrary forces and torques. The structure matrix is

$$(2.41) \quad \underline{A}^T = \begin{pmatrix} \underline{u}_1 & \cdots & \underline{u}_m \\ \underline{p}_1 \times \underline{u}_1 & \cdots & \underline{p}_m \times \underline{u}_m \end{pmatrix} \in \mathbb{R}^{6 \times m}.$$



# Chapter 3

## Aspects of Workspace

*Relevant aspects for the problem of the technically usable workspace are summarized and then treated in detail: conditions on tensions in Section 3.2, the question of singularities in Section 3.3, requirements on stiffness in Section 3.4. The problem of autocollisions is shortly addressed in Section 3.5.*

### 3.1. Summary of the Criteria

One of the major problems of tendon-based Stewart platforms is the rather small workspace, compared to serial manipulators. The technically interesting part of workspace is the set of those postures which satisfy the following conditions:

- the platform is controllable;
- tendon forces are positive;
- tendon forces lie between minimum and maximum tension;
- the end-effector is far from singularities;
- the structure is sufficiently stiff;
- tendons do not intersect with each other.

Neither joint limits nor collisions of tendons with the support structure, the platform, or obstacles appear in the list because they depend on the technical realization or environment of the system, rather than theoretical limits. The same applies to limits in actuator power or controller capabilities.

### 3.2. Controllable Workspace

With the term *controllable workspace*<sup>1</sup> we denote the set of all postures where the platform can be controlled with positive tensions.

---

<sup>1</sup>This expression was proposed by Oussama Khatib when the author presented his first paper [174] on the 6th Int. Symposium on Advances in Robot Kinematics.

**3.1 Definition (controllable workspace)** A posture<sup>2</sup>  $\underline{x}$  is said to belong to the controllable workspace if for each wrench vector  $\underline{w} \in \mathbb{R}^n$  there is a distribution of tendon forces  $\underline{f} \in \mathbb{R}^m$  such that

$$(3.1) \quad \underline{A}^T(\underline{x}) \underline{f} + \underline{w} = \underline{0} \quad \text{and} \quad \underline{f} > \underline{0}.$$

Such a vector  $\underline{f} \in \mathbb{R}_+^m$  is called a positive solution.  $\diamond$

As pointed out in Section 2.2.3, p. 28 ff., gravity can be considered as an additional tendon for systems operating on earth with heavy loads, hence in such cases the matrix  $\underline{A}'^T$  can be substituted for  $\underline{A}^T$ .

Def. 3.1 actually can be split into two conditions:

- For each  $\underline{w} \in \mathbb{R}^n$  there is a solution of the matrix equation. Thus, the image space of  $\underline{A}^T$  is  $n$ -dimensional. In other words, the structure matrix has full rank. This is the condition needed in any parallel or hybrid system, whether tendon-driven or not.
- Assuming that this condition is satisfied, each element in the image space can be obtained in particular as the image of a vector with positive components.

Given the first condition, the matrix  $\underline{A}^T$  has a Moore-Penrose pseudo inverse<sup>3</sup>  $\underline{A}^{+T}$  and all the solutions  $\underline{f} \in \mathbb{R}^m$  (positive or not) can be represented as

$$(3.2) \quad \underline{f} = -\underline{A}^{+T} \underline{w} + \underline{H} \underline{\lambda} \quad \text{with} \quad \underline{\lambda} \in \mathbb{R}^{m-n}$$

where  $\underline{H} \in \mathbb{R}^{m \times (m-n)}$  is a matrix whose columns span the kernel of  $\underline{A}^T$ . This provides a handy criterion for the controllable workspace.

**3.2 Proposition (controllable workspace condition)** A posture  $\underline{x}$  belongs to the controllable workspace if and only if

$$(3.3) \quad \text{rank } \underline{A}^T(\underline{x}) = n \quad \text{and} \quad \ker \underline{A}^T(\underline{x}) \cap \mathbb{R}_+^m \neq \emptyset. \quad \diamond$$

**Proof.** a) Assume that a posture belongs to the controllable workspace. Then there is, in particular, a positive solution if no platform wrenches apply, i. e. there is  $\underline{h} \in \mathbb{R}^m$  with

$$(3.4) \quad \underline{A}^T(\underline{x}) \underline{h} = \underline{0} \quad \text{and} \quad \underline{h} > \underline{0}.$$

So this  $\underline{h}$  is an element of the kernel of  $\underline{A}^T$  and of the positive quadrant  $\mathbb{R}_+^m$ , hence the intersection is not empty.

<sup>2</sup>As explained in Section 2.2.3, p. 28 ff., the posture of a platform is described in different ways for different types of controlled DOFs (e. g.  $\underline{r}$  for 2T and 3T,  $(\underline{r}, \underline{R})$  for 3R3T etc.). So we use the symbol  $\underline{x}$  as a shorthand for the general case.

<sup>3</sup> $\underline{A}^{+T}$  is a shorthand for  $(\underline{A}^+)^T = (\underline{A}^T)^+$ , see Prop. A.8, p. 126.

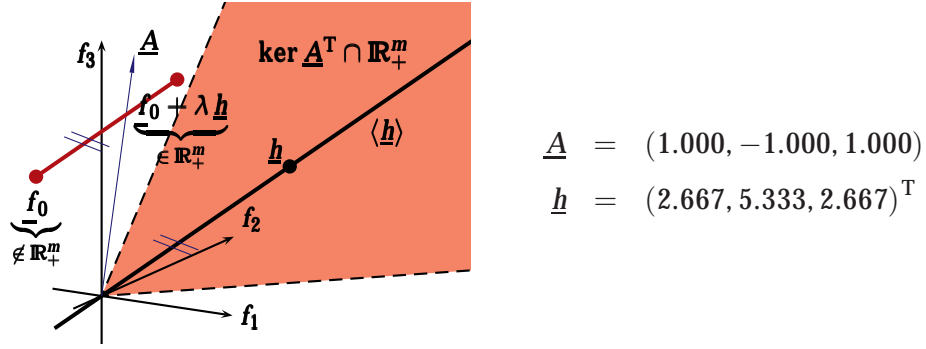


Figure 3.1: The proof of Prop. 3.2

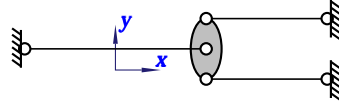


Figure 3.2: The manipulator corresponding to Fig. 3.1

b) Conversely, assume that such  $\underline{h}$  exists. As  $\text{rank } \underline{A}^T = n$ , for any wrench  $\underline{w} \in \mathbb{R}^n$  acting on the platform, the matrix equation in Eq. (3.1) has a solution

$$(3.5) \quad \underline{f}_0 := -\underline{A}^{+T} \underline{w}.$$

If this is positive, we are finished, otherwise let  $1 \leq \mu_0 \leq m$  be such that

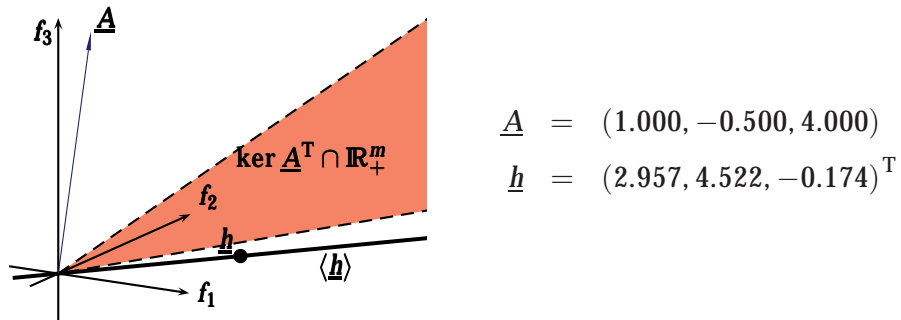
$$(3.6) \quad \frac{|f_{0,\mu_0}|}{h_{\mu_0}} = \max \left\{ \frac{|f_{0,\mu}|}{h_{\mu}} : 1 \leq \mu \leq m \wedge f_{0,\mu} < 0 \right\}.$$

Then

$$(3.7) \quad \underline{f} := \underline{f}_0 + 2 \frac{|f_{0,\mu_0}|}{h_{\mu_0}} \underline{h}$$

is a positive solution.  $\square$

The idea of the second part of the proof is illustrated in Fig. 3.1 (for the very simple 1T manipulator shown in Fig. 3.2): given a solution  $\underline{f}_0$  anywhere in  $\mathbb{R}^m$ , we can «transport» it into the positive quadrant by adding some multiple of the positive vector  $\underline{h}$ .

Figure 3.3: Counterexample for the projection of  $\underline{1}$  onto  $\ker \underline{A}^T$

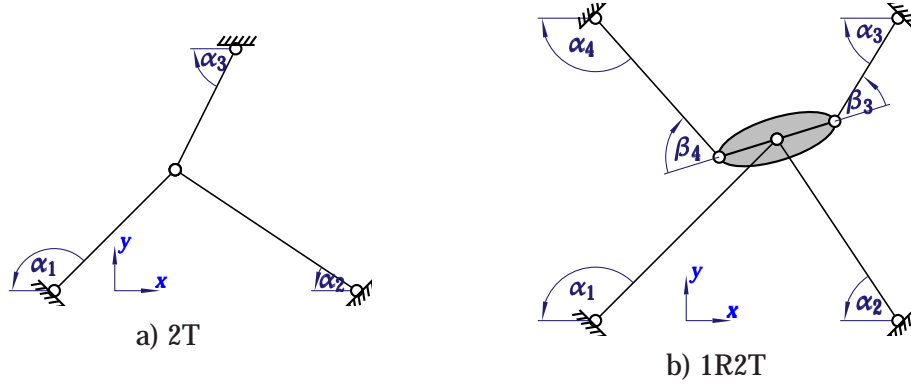


Figure 3.4: Example CRPMs

For RRPMS it is not easy to find such an  $\underline{h}$ . Intuitively one might try projecting the vector  $\underline{1} := (1, \dots, 1)$  orthogonally into the kernel of  $\underline{A}^T$ . This supplies an element of  $\ker \underline{A}^T$  whose components are all close to 1 and it seems clear that the result has all components positive whenever  $\underline{h} \in \ker \underline{A}^T \cap \mathbb{R}_+^m$  exists at all. *This intuition is wrong*, as shown by the example<sup>4</sup> in Fig. 3.3: here,  $\underline{h}$  was determined that way, but it is slightly outside  $\mathbb{R}_+^m$ .

**3.3 Proposition (projection counterexample)** *Orthogonal projection of a vector of positive forces into the kernel of the structure matrix does not always provide a positive distribution of tendon forces even if such a distribution exists.*  $\diamond$

Nevertheless, this happens rather near the border of the controllable workspace. So this projection can still be used as a very simple (and hence fast) algorithm when only the central region of the controllable workspace is needed. Furthermore it is a good initial guess when looking for positive solutions via iteration.

For CRPMs instead, such  $\underline{h}$  is easy to find: then  $\underline{A}^T$  has a one-dimensional kernel and we can look at an arbitrary (nonzero) element  $\underline{h} \in \ker \underline{A}^T$ : if  $\underline{h} > \underline{0}$  or  $\underline{h} < \underline{0}$ , then the posture is inside the controllable workspace; if instead there are components with different signs (or zeros) in  $\underline{h}$ , it is outside. For example let us consider a CRPM of class 2T, i.e. a system of three tendons<sup>5</sup> carrying a point-shaped load (Fig. 3.4a). Then the structure matrix is

$$(3.8) \quad \underline{A}^T = \begin{pmatrix} \cos \alpha_1 & \cos \alpha_2 & \cos \alpha_3 \\ \sin \alpha_1 & \sin \alpha_2 & \sin \alpha_3 \end{pmatrix}$$

and an element of the kernel is

$$(3.9) \quad \underline{h} = (\sin \alpha_{23}, \sin \alpha_{31}, \sin \alpha_{12})^T \quad \text{with} \quad \alpha_{ij} := \alpha_j - \alpha_i.$$

Thus, the force in each tendon is proportional to the sine of the angle between the other two tendons. A solution with positive forces exists as long as each of these

<sup>4</sup>Note that the figure does not correspond to a real mechanism because a system with three tendons and a two-dimensional null space would have to be of type 1T, and hence all entries in  $\underline{A}^T$  would be either  $-1$  or  $1$ . Examples derived from real mechanisms exist but require more than three dimensions and hence cannot be illustrated this way.

<sup>5</sup>In the figures, the tendons are drawn as prismatic joints in order to distinguish them easily, but one should keep in mind that unlike prismatic links, they represent unilateral constraints.

angles is less than  $\pi$ , hence the controllable workspace coincides with the area of the triangle formed by the winches, which is clearly not surprising. This also results from a numerical computation, as shown in Fig. 3.5a: here each dot means that the position of the dot belongs to the controllable workspace. For CRPMs of class 1R2T (Fig. 3.4b), we obtain

$$(3.10) \quad \underline{A}^T = \begin{pmatrix} \cos \alpha_1 & \cos \alpha_2 & \cos \alpha_3 & \cos \alpha_4 \\ \sin \alpha_1 & \sin \alpha_2 & \sin \alpha_3 & \sin \alpha_4 \\ p_1 \sin \beta_1 & p_2 \sin \beta_2 & p_3 \sin \beta_3 & p_4 \sin \beta_4 \end{pmatrix},$$

$$(3.11) \quad \underline{h} = \begin{pmatrix} + p_2 \sin \beta_2 \sin \alpha_{34} + p_3 \sin \beta_3 \sin \alpha_{42} + p_4 \sin \beta_4 \sin \alpha_{23} \\ - p_1 \sin \beta_1 \sin \alpha_{34} - p_3 \sin \beta_3 \sin \alpha_{41} - p_4 \sin \beta_4 \sin \alpha_{13} \\ + p_1 \sin \beta_1 \sin \alpha_{24} + p_2 \sin \beta_2 \sin \alpha_{41} + p_4 \sin \beta_4 \sin \alpha_{12} \\ - p_1 \sin \beta_1 \sin \alpha_{23} - p_2 \sin \beta_2 \sin \alpha_{31} - p_3 \sin \beta_3 \sin \alpha_{12} \end{pmatrix}.$$

Examples are shown in Fig. 3.6a, b: here a dot indicates that a position together with the indicated platform orientation is inside the controllable workspace.

Similar formulas can be written down for CRPMs of any type, because then, an element of the kernel of  $\underline{A}^T$  can always be expressed in terms of determinants of square-shaped submatrices of  $\underline{A}^T$ .<sup>6</sup> When seeking a closed-form expression of the controllable workspace, we can consider the matrix

$$(3.12) \quad \underline{A}_L^T := \underline{A}^T \underline{L} \quad \text{with} \quad \underline{L} := \text{diag}(l_1, \dots, l_m)$$

instead of  $\underline{A}^T$ . This is like rescaling each tendon force with a positive length and therefore Prop. 3.2 applies to  $\underline{A}_L^T$  as well as to  $\underline{A}^T$ . Determinants of submatrices of  $\underline{A}_L^T$  are polynomials in the end-effector position coordinates and in sines/cosines of its orientation angles. Thus, the workspace can be expressed in terms of unions of sets defined by systems of algebraic inequalities (so-called *semi-algebraic sets*) in the end-effector posture. The number of inequalities as well as the degree of the polynomials increases considerably with the number of DOFs. We will not go into further details on CRPMs, but present directly a general approach also suitable for RRPMS.

The basic idea is that force equilibrium with nonnegative tensions can be obtained if and only if it can be obtained with at most  $n + 1$  tendons and zero tension in the others. This is an extension of an idea proposed by Barrette and Gosselin [19]. We cannot obtain precisely the controllable workspace because in Prop. 3.2 it is essential that we have a kernel element with strictly positive components, while the below theorem supplies a region where certain components can also be zero. The latter set contains part of the border of the controllable workspace which is not included in the controllable workspace itself. This difference is a lower dimensional set. If we remember that the current discussion completely disregards lower and upper limits that might be required on tendon forces and therefore only supplies a superset of the region that can really be used in practice, this little difference is certainly negligible.

<sup>6</sup>Indeed, for CRPMs, a posture belongs to the controllable workspace if and only if each  $(n \times n)$ -submatrix of  $\underline{A}^T$  has full rank and the column of  $\underline{A}^T$  which is not part of the submatrix can be expressed as a linear combination of the other columns with coefficients that are less than or equal to zero. This fact can be used to derive a force transmission index [165, 166, 183]; however, such an approach is limited to CRPMs.

**3.4 Theorem (controllable workspace in closed form)** *The set of all those postures where nonnegative solutions with positive force in tendon number  $m$  exist is a semi-algebraic set in terms<sup>7</sup> of the entries of  $\underline{A}_L^T$ :*

$$(3.13) \quad \left\{ \underline{x} : \text{rank } \underline{A}_L^T = n \wedge \bigvee_{\underline{h} \in \ker \underline{A}_L^T} \underline{h} \geq \underline{0} \wedge h_m > 0 \right\} \\ = \bigcup_{\substack{\mathcal{I} \subset \{1, \dots, m-1\} \\ |\mathcal{I}|=n}} \left( \left\{ \underline{x} : \det \underline{A}_{L, \mathcal{I}}^T > 0 \wedge \left( \det \underline{A}_{L, \mathcal{I}}^T \right) \underline{A}_{L, \mathcal{I}}^{-T} \underline{a}_{L, m} < \underline{0} \right\} \right. \\ \left. \cup \left\{ \underline{x} : \det \underline{A}_{L, \mathcal{I}}^T < 0 \wedge \left( \det \underline{A}_{L, \mathcal{I}}^T \right) \underline{A}_{L, \mathcal{I}}^{-T} \underline{a}_{L, m} > \underline{0} \right\} \right),$$

where  $\underline{A}_{L, \mathcal{I}}^T$  denotes the  $n \times n$  matrix consisting of the columns of  $\underline{A}_L^T$  numbered by the elements of  $\mathcal{I}$  and  $\underline{a}_{L, m}$  is the  $m$ th column of  $\underline{A}_L^T$ .

The right-hand side is a union of  $2 \binom{m-1}{n}$  sets given respectively by  $(n+1)$  algebraic inequalities of degree  $n$ .  $\diamond$

**Proof.** A posture belongs to the set of the left-hand side if and only if

$$(3.14) \quad \text{rank } \underline{A}_L^T = n \wedge \bigvee_{\underline{h} \geq \underline{0} \wedge h_m > 0} \underline{A}_L^T \underline{h} = \underline{0}, \quad \text{i. e. if and only if}$$

$$(3.15) \quad \text{rank } \underline{A}_L^T = n \wedge \bigvee_{\underline{h} \geq \underline{0} \wedge h_m > 0} -h_m \underline{a}_{L, m} = \underline{A}_{L, \hat{m}}^T \underline{h}_{\hat{m}}$$

where the subscript  $\hat{m}$  means that the  $m$ th column or component was dropped. We can divide the equation by  $h_m$  which is positive by assumption and obtain the equivalent condition that  $-\underline{a}_{L, m}$  is a nonnegative linear combination of the columns of  $\underline{A}_{L, \hat{m}}^T$ , i. e. it belongs to the cone (Def. A.12, p. 127) generated by this matrix:

$$(3.16) \quad \text{rank } \underline{A}_L^T = n \wedge -\underline{a}_{L, m} \in \text{cone } \underline{A}_{L, \hat{m}}^T.$$

Now Carathéodory's theorem (Theorem A.13, p. 129) states that a vector is an element of an  $n$ -dimensional cone if and only if it is a nonnegative linear combination of finitely many linear independent vectors among those which generate the cone. As the cone is contained in  $\mathbb{R}^n$ , these can be at most  $n$  and if fewer than  $n$  are needed, one can add zero multiples of some other linear independent columns of  $\underline{A}_{L, \hat{m}}^T$  (which can be found due to the rank condition). Thus, the last condition is equivalent to

$$(3.17) \quad \bigvee_{\substack{\mathcal{I} \subset \{1, \dots, m-1\} \\ |\mathcal{I}|=n}} \text{rank } \underline{A}_{L, \mathcal{I}}^T = n \wedge \bigvee_{\underline{\lambda} \geq \underline{0}} -\underline{a}_{L, m} = \underline{A}_{L, \mathcal{I}}^T \underline{\lambda}.$$

As  $\underline{A}_{L, \mathcal{I}}^T$  is now a full-rank square matrix, the vector  $\underline{\lambda}$  is unique and we can invert the matrix, obtaining the equivalent condition

$$(3.18) \quad \bigvee_{\substack{\mathcal{I} \subset \{1, \dots, m-1\} \\ |\mathcal{I}|=n}} \det \underline{A}_{L, \mathcal{I}}^T \neq 0 \wedge \underline{A}_{L, \mathcal{I}}^{-T} \underline{a}_{L, m} \leq \underline{0}.$$

---

<sup>7</sup>  $\underline{A}^{-T}$  is a shorthand for  $(\underline{A}^{-1})^T = (\underline{A}^T)^{-1}$ .



This corresponds to the right-hand side in the theorem if we split it up into the two cases that the determinant of  $\underline{A}_{L,\mathcal{I}}^T$  is either positive or negative.

Now the determinant of  $\underline{A}_{L,\mathcal{I}}^T$  is an  $n$ th order polynomial of its coefficients and the entries of  $\left(\det \underline{A}_{L,\mathcal{I}}^T\right) \underline{A}_{L,\mathcal{I}}^{-T}$  are  $(n-1)$ th order polynomials in these coefficients, hence we have systems of  $(n+1)$  algebraic inequalities of degree  $n$ .  $\square$

Class	$n$	$m$	Sets	Inequalities	Degree
general	$n$	$m$	$2 \binom{m-1}{n}$	$n+1$	$n$
1R2T	3	4	2	4	3
		5	8		
		6	20		
2R3T	5	6	2	6	5
		7	12		
		8	42		
		9	112		
		10	252		
3R3T	6	7	2	7	6
		8	14		
		9	56		
		10	168		
		11	420		
		12	924		

Table 3.1: Size of the closed-form expression for workspace

Thus, a closed form expression for the controllable workspace was found, but we have to ask whether this can be computed with reasonable effort. Table 3.1 shows the number of sets, the number of inequalities per set and the degree of the polynomials, for a number of examples. Only the classes with rotational DOFs were considered, as for the purely translational classes the workspace is obviously the convex hull of the base points. It turns out that the number of sets to consider increases very fast with the degree of redundancy. To a certain degree, the closed form can be useful for planar systems with low redundancy and in fact, some studies were conducted on this topic [19, 45, 46]. In spatial and/or highly redundant situations instead, the closed-form expression may be of some theoretical value, but it is not an appropriate tool to actually compute the workspace.

The notion of controllable workspace discussed up to now completely disregards the *amount* of tension in the tendons. In reality, tendon load must be limited to a maximum force  $f_{\max}$  depending on the material and the type of tendon. (Actually  $f_{\max}$  is also limited by the power of the motors. This problem is currently being investigated at Duisburg, but we do not consider it here because it relates

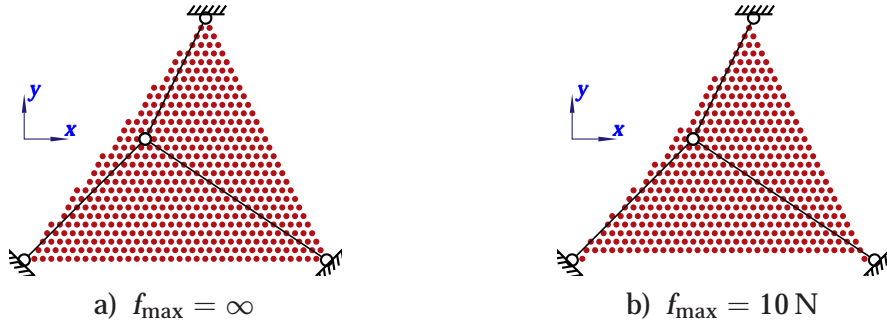


Figure 3.5: Acceptably controllable workspace of a 2T manipulator ( $f_{\min} = 1 \text{ N}$ ;  $\varphi$  denotes the rotation angle of the platform)

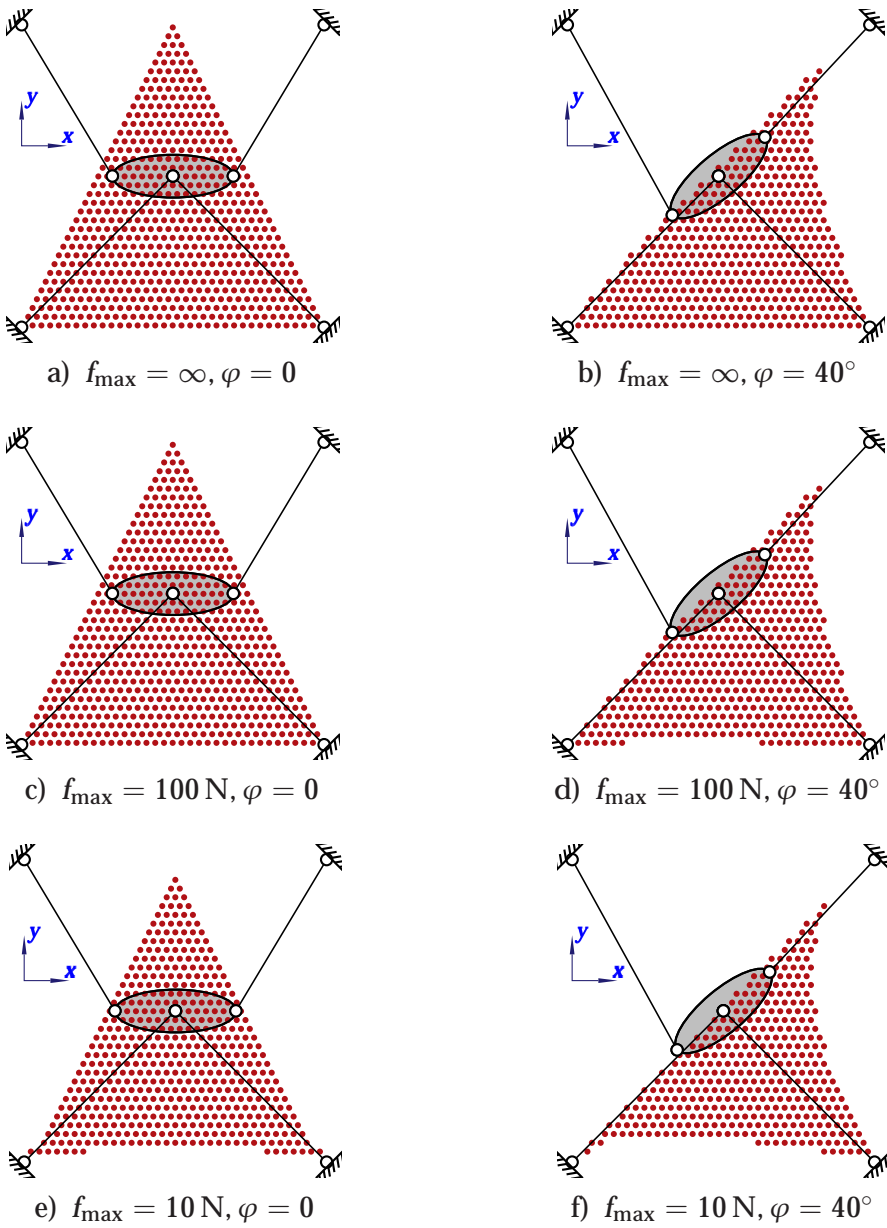


Figure 3.6: Acceptably controllable workspace of a 1R2T manipulator ( $f_{\min} = 1 \text{ N}$ )

to technical details of construction.) Furthermore real tendons have a certain stiffness against bending. So a pretension  $0 < f_{\min} \leq f_{\max}$  is also required to keep them in the right position around pulleys and other guiding devices. Solutions respecting these bounds will be called *acceptable* solutions.<sup>8</sup>

**3.5 Definition (acceptable solution)** A positive solution  $\underline{f} \in \mathbb{R}_+^m$  is called *acceptable solution* if it respects the given bounds on tension:

$$(3.19) \quad \underline{f} \in [f_{\min}, f_{\max}]^m .$$

A posture where an acceptable solution exists for a given platform wrench  $\underline{w}$  is said to belong to the *acceptably controllable workspace*<sup>9</sup> for that  $\underline{w}$ .  $\diamond$

The idea of controllable workspace is just about existence of a solution and is independent of the platform forces/torques  $\underline{w}$ . It is even possible to consider gravity as an additional tendon without any extra effort. In contrast, the notion of acceptable solution is of quantitative nature and depends on  $\underline{w}$ . For some cases, it is useful to look at the acceptably controllable workspace for  $\underline{w} = \underline{0}$ , which gives a rough estimate of the workspace that can be exploited with real tendons, independently of a particular task. This estimate is quite precise if platform wrenches play a minor role, e. g. for loads of small mass or quasistatic motions in space applications.

The controllable workspace itself is equal to the acceptably controllable workspace for  $f_{\min} = 1$  (arbitrary unit of force),  $f_{\max} = \infty$ ,  $\underline{w} = \underline{0}$ . In subsequent chapters we will just speak of «workspace» to denote the «acceptably controllable workspace».

Fig. 3.5b and Fig. 3.6c–f) show acceptably controllable workspaces: it turns out that the influence of  $f_{\max}$  is relatively limited in these cases. Fig. 3.7 shows the corresponding acceptably controllable workspaces<sup>10</sup> of the 1R2T manipulator with gravity, for a particular load and force bound.

### 3.3. Singularities

As pointed out in Section 2.2.1, p. 23 ff., we are dealing with purely parallel systems, hence the only type of singularity that can occur is overmobility. According to Section 2.1.3, p. 22 ff., a system is singular in a posture  $\underline{x}$  if and only if the structure matrix (which is the transpose of the Jacobian) is rank deficient, i. e.

$$(3.20) \quad \text{rank } \underline{A}^T(\underline{x}) < n .$$

<sup>8</sup>For simplicity of writing, within this thesis we always assume that the force limits are the same for all tendons. But the description can easily be extended to cases where tendons have individual limits, and all our results hold for that general case, too.

<sup>9</sup>That way, the acceptably controllable workspace for a particular  $\underline{w}$  is *not necessarily* a subset of the controllable workspace in the sense of Def. 3.1 because it is not guaranteed that solutions exist for other wrenches  $\underline{w}$ . However, it is a superset of the controllable workspace when considering the given  $\underline{w}$  as an additional tendon as explained in Section 2.2.3, p. 28 ff.

<sup>10</sup>The solid dots indicate postures where an acceptable solution is found immediately with the projection method of Prop. 3.3, while the empty dots denote postures inside the workspace which require iteration, see Section 4.7, p. 77 ff.

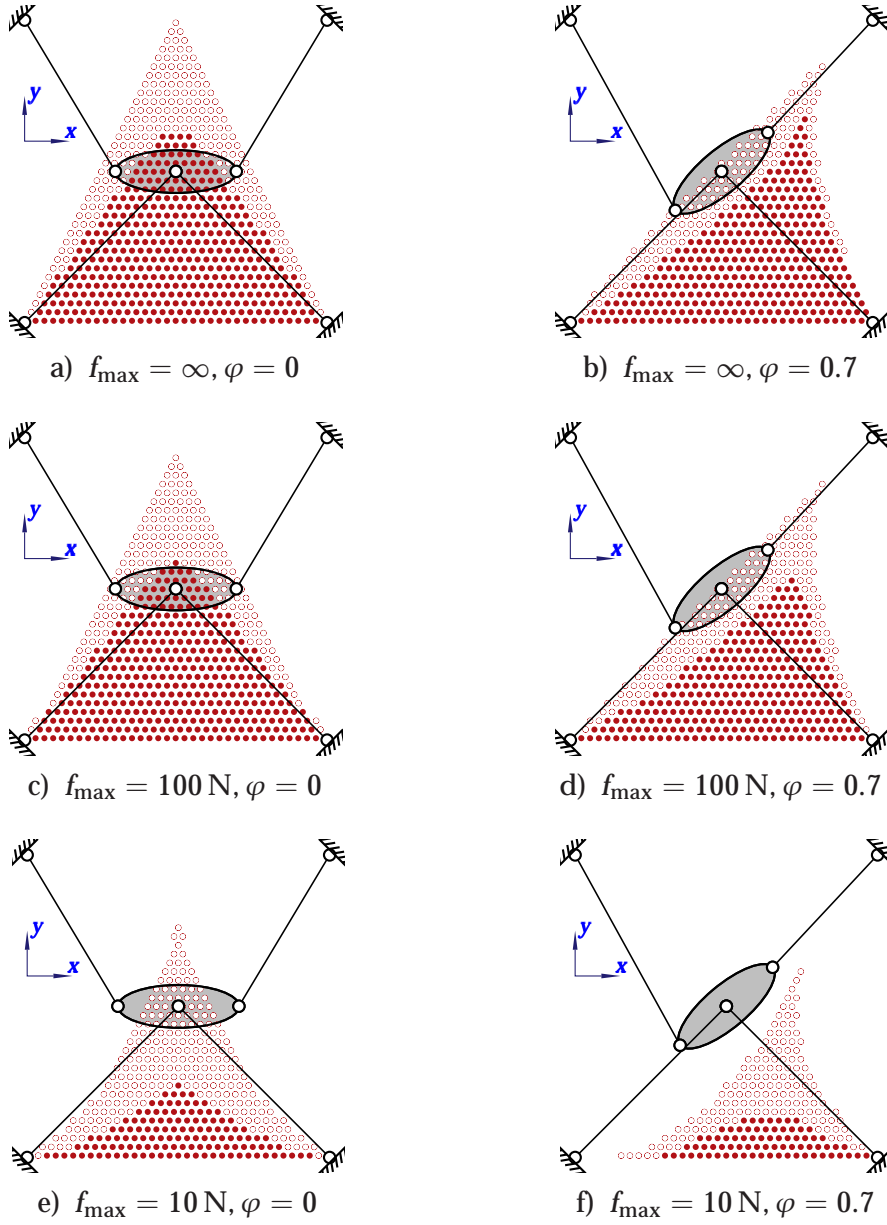


Figure 3.7: Acceptably controllable workspace with gravity  
( $m_p = 1 \text{ kg}$ ,  $f_{\min} = 1 \text{ N}$ )

According to Prop. 3.2 the singular postures themselves are not part of the controllable workspace.

We briefly go through the various classes. If a system of class 2T is singular, this means that the structure matrix has rank 1. Therefore, the column vectors – which are the unit vectors in the tendon directions – are all parallel. This is impossible except in the case that all winches are located on a common line: this makes no sense because such a system is always singular and hence the controllable workspace is empty. In a similar way, a 3T manipulator has no singularities except when all the winches lie in a plane, which is again a useless design with empty workspace. Thus, *all systems with purely translational DOFs are singularity-free*.

A 1R2T manipulator can have singularities in a lot of different circumstances.

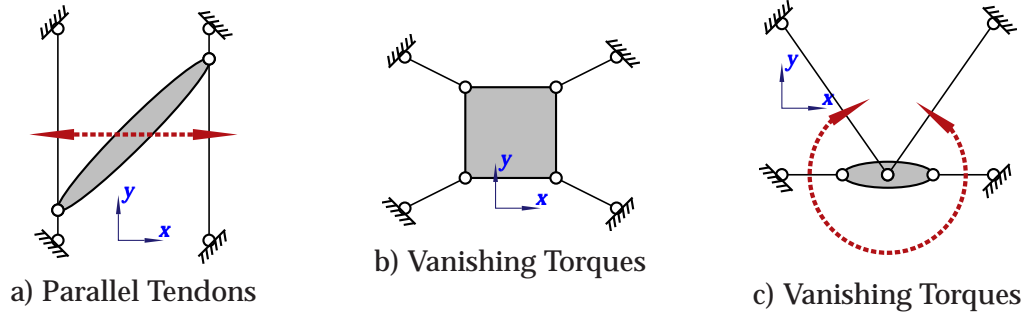


Figure 3.8: Singularities in 1R2T systems

We will not give an exhaustive classification, but just mention two typical cases: all tendons may be parallel (Fig. 3.8a), or all torques may vanish (Fig. 3.8b and c). In the first example, the platform is free to perform infinitesimal translations in  $x$  direction; in the second and third, infinitesimal rotations are possible. (Actually the singularity in the third example is also on the border of the workspace, except when gravity is involved).

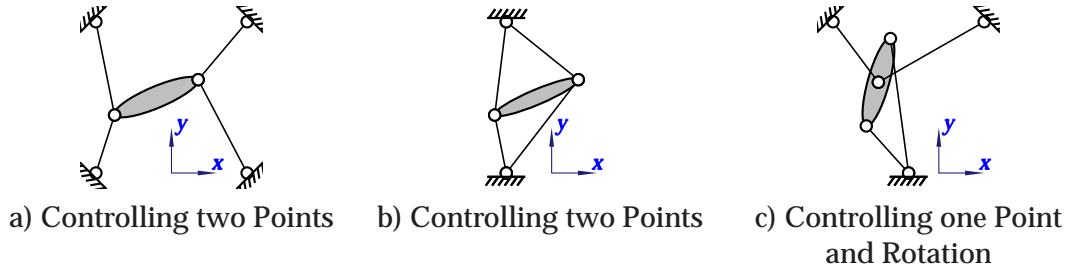


Figure 3.9: Almost singularity-free 1R2T systems

There is a simple strategy to build singularity-free parallel manipulators which is particularly relevant for tendon-based systems and can easily be demonstrated with 1R2T examples. The idea is based on the duality of serial and parallel systems. The development of *serial* robots can be thought of as a process where some joints are added up because each joint *adds* a DOF of mobility to the end-effector. In contrast, a *parallel* system can be assembled by adding links because each link *takes away* one DOF of uncontrollability. Now, overmobility arises in parallel manipulators if there are uncontrolled DOFs.

**3.6 Proposition** *A way to build up (almost) singularity-free parallel robots is to partition the set of end-effector DOFs into subsets and to ensure that each subset is completely controlled in all (desired) postures.  $\diamond$*

For instance, in Fig. 3.9a the positions of the two connection points on the platform are given as vertices of triangles (formed by two winches and a point on the platform) as long as they stay inside the square formed by the four winches. As a triangle is completely defined when the lengths of its edges are known, the positions of these points then are always under control. As the posture of a body in the plane is completely defined by the position of two points, this implies that the posture of the platform is always controlled.<sup>11</sup> The example in Fig. 3.9b

<sup>11</sup>To be precise, the system is singular if and only if both platform connection points lie on the

works in a similar way: the only singular postures are those where the platform is in a vertical orientation such that all platform connection points and winches are collinear.

A slightly different approach leads to designs such as Fig. 3.9c: here two tendons control the center point of the platform and the other two control the rotation about this point. There is no singularity except when the two rotating tendons and the two platform points lie on a common line, which is again a posture on the border of the workspace.

This technique of singularity avoidance tends to require more actuators than would be necessary for control in normal postures. In fact, in the examples a and b we need four winches in order to have two points controlled by respectively two tendons, whereas in normal circumstances three actuators would be sufficient for three end-effector DOFs. But when building tendon-based systems, we have to use at least  $n + 1$  winches anyway (except for IRPMs). So we can take advantage of the extra tendons to avoid singularities this way.

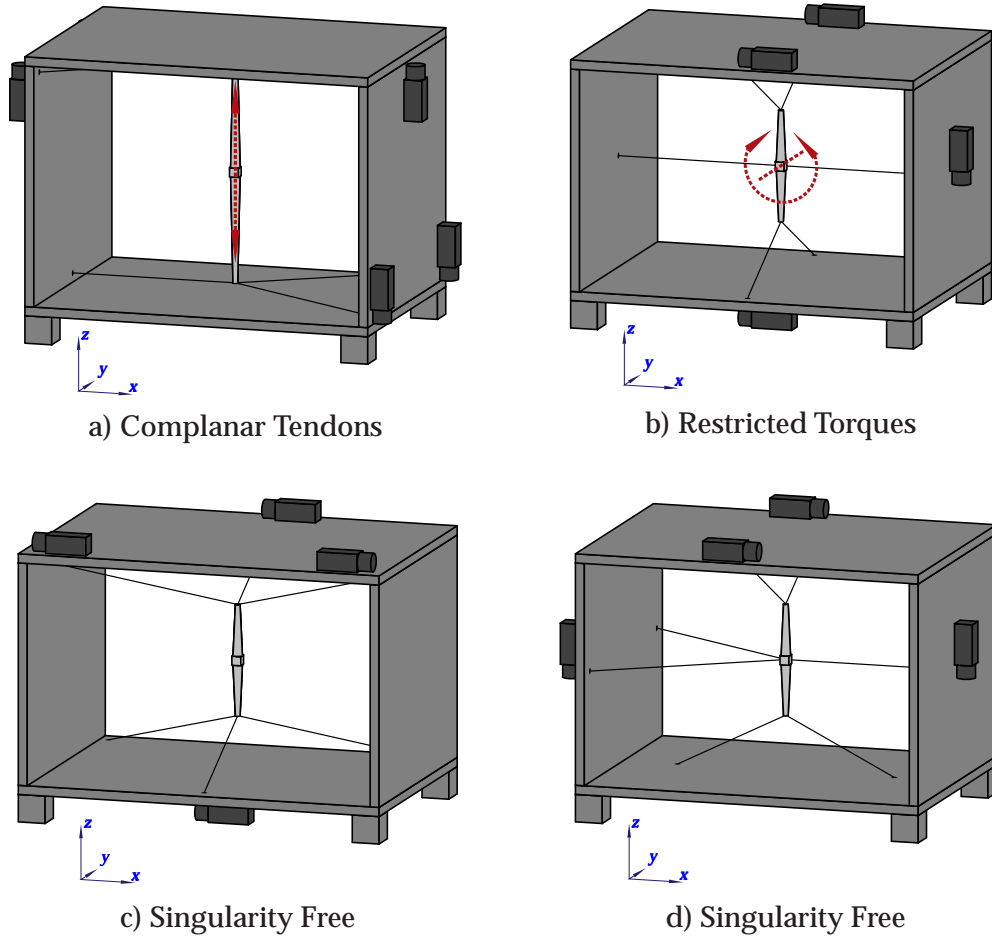


Figure 3.10: Singularities in 2R3T systems

Systems of class 2R3T can also have singularities in various situations. In Fig. 3.10a, all tendons are complanar and the platform can move infinitesimally in  $z$  direction. Fig. 3.10b shows an example where rotation about the indicated

---

line through, for instance, the two left base points. Clearly, such a posture is far away from the controllable workspace.



axis is not controllable. Obviously both of these designs are nonsense, because again it is easy to build a singularity-free system by controlling groups of DOFs separately: in Fig. 3.10c, each of the two points on the platform is completely controlled by three tendons, while in Fig. 3.10d, one point is controlled by the three horizontal tendons, the two lower tendons control rotation about the y axis and the two upper ones control rotation about the x axis.

In this last example, seven tendons are employed while normally six would be sufficient for five DOFs. So the singularity avoidance generates additional cost here. But the design has the advantage of decoupling translation from rotation, which simplifies forward kinematics: three tendons provide straightforward two possible positions of the center point and this together with the other tendons allows for easy computation of the postures.

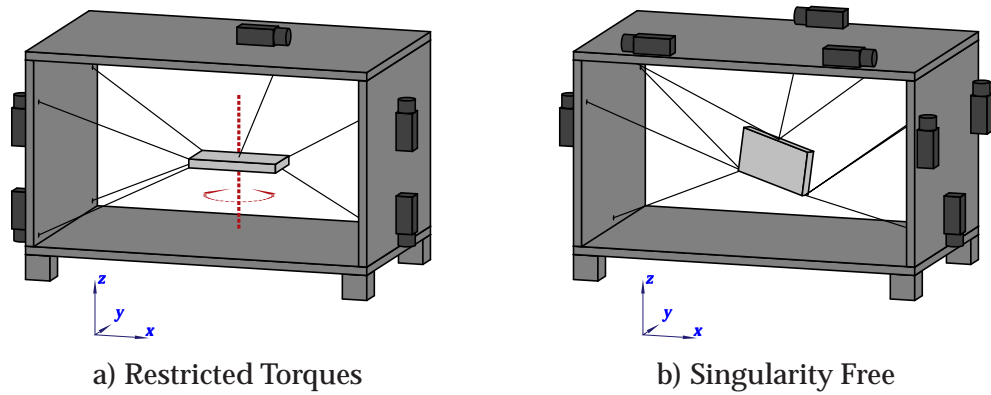


Figure 3.11: Singularities in 3R3T systems

Singularities of 3R3T manipulators are an area of research of its own, already for classical parallel systems with rigid legs [121, 178]. Fig. 3.11a shows an example where torque about the z axis is not controllable; there is a wide variety of other possibilities. Once more we can use the technique of DOF partitioning: in the RRPM in Fig. 3.11b, each of three three points on the platform is completely controlled by three tendons, so the entire platform is always under control.

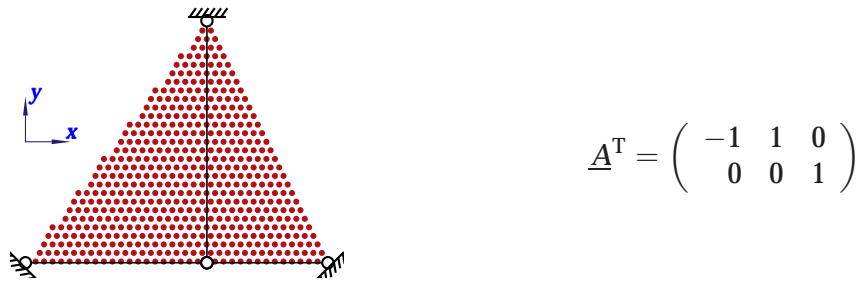


Figure 3.12: Nonsingular posture with singular submatrix

An interesting question in the context of singularities deals with the rank of submatrices of the structure matrix. Indeed, if we have a CRPM and we know that some  $n$  columns of  $\underline{A}^T$  are linearly independent, then we can fix one of the

tendon forces, say  $f_m$ , and obtain the other forces as

$$(3.21) \quad \begin{pmatrix} f_1 \\ \vdots \\ f_n \end{pmatrix} = -f_m \underline{A}_{\hat{m}}^{-T} \underline{a}_m - \underline{A}_{\hat{m}}^{-T} \underline{w} \quad \text{with} \quad \underline{A}^T = \begin{pmatrix} \underline{A}_{\hat{m}}^T & \underline{a}_m \end{pmatrix}.$$

(Note that in this case we have  $n = m - 1$ .) This can be useful for dynamic optimization of CRPMs [57]. But it requires that  $\text{rank } \underline{A}_{\hat{m}}^T = n$  and this might fail to be the case even if the system is in a nonsingular posture (i. e.  $\text{rank } \underline{A}^T = n$ ). An example is shown in Fig. 3.12, where the structure matrix is nonsingular, but the submatrix consisting of its first  $n$  columns is singular. One would expect this to be a considerable limitation to the approach of Eq. (3.21). But surprisingly it turns out that for CRPMs this condition is no limitation at all. Indeed, the posture in the example lies on the border of the controllable workspace, hence outside of it, and this is always the case under such conditions.

**3.7 Proposition (rank of submatrices)** *Inside the controllable workspace any set of  $n$  columns of the structure matrix of a CRPM has full rank  $n$ .  $\diamond$*

**Proof.** Denote with  $\underline{A}_{\hat{\mu}}^T$  the matrix of all column vectors of  $\underline{A}^T$  except the  $\mu$ th one. Then the vector  $\underline{h} = (h_1, \dots, h_m)$  with

$$(3.22) \quad \underline{h}_{\mu} := (-1)^{\mu-1} \det \underline{A}_{\hat{\mu}}^T$$

is orthogonal to all rows of  $\underline{A}^T$  because for each row  $(a_{\nu,1}, \dots, a_{\nu,m})$ , we have

$$(3.23) \quad 0 = \det \begin{pmatrix} a_{\nu,1} & \cdots & a_{\nu,m} \\ \vdots & \ddots & \vdots \\ \underline{A}^T \end{pmatrix} = (a_{\nu,1}, \dots, a_{\nu,m}) \underline{h}$$

where the first equality holds because the  $\nu$ th row appears twice in the determinant and the second one is obtained by Lagrange development. Thus, the kernel of  $\underline{A}^T$  is generated by  $\underline{h}$  as long as the system is not in a singular posture. (And by Prop. 3.2, singularities do not belong to the controllable workspace.) If a posture is inside the controllable workspace, it follows from Prop. 3.2 that each  $h_{\mu}$  is nonzero, hence all the submatrices  $\underline{A}_{\hat{\mu}}^T$  have full rank.  $\square$

The proof implies that a posture is on the border of the workspace if some  $n \times n$  submatrix is singular. The converse is not true because such a submatrix may be singular also somewhere far away from the workspace border. Clearly, the proposition applies to CRPMs only, because for RRPMS there is no such simple expression for the kernel of the structure matrix.

### 3.4. Stiffness

Tendon-based systems are much more compliant than classical robots with rigid links, so that the requirement of a minimum stiffness is a real problem in this case. While the stiffness of manipulators with rigid links is primarily limited

by actuator and joint compliance (the latter applies in particular to parallel designs), the main issue in the case of tendon-based Stewart platforms is the tendon compliance. The following analysis deals only with this aspect. It is not intended as a basis for precise computations in control strategies, but rather as an approximation that gives some overall insight.

We consider the *passive stiffness* which describes the behavior of a mechanical system under small perturbations when no active response is generated by the actuators. This can be a basis for active stiffness control strategies. When an infinitesimal wrench  $\delta \underline{w} \in \mathbb{R}^n$  is applied to the end-effector of a manipulator, the posture changes by an infinitesimal deflection  $\delta \underline{x}$  according to a linear relation

$$(3.24) \quad \delta \underline{w} = \underline{K}(\underline{x}) \delta \underline{x}.$$

The posture-dependent matrix  $\underline{K}$  is called *stiffness matrix*; its inverse (if it exists) is the *compliance matrix*. Under the assumption that links are rigid bodies, singularities with under-mobility correspond to infinite stiffness (or zero compliance), while over-mobility means zero stiffness (or infinite compliance). For typical parallel systems, the stiffness matrix always exists, while it can happen that a compliance matrix does not exist. The converse holds for typical serial systems.

The stiffness matrix of tendon-based Stewart platforms is obtained as follows. Let  $k_\mu$  be the stiffness of the  $\mu$ th tendon, then the stiffness equation in the actuator space is

$$(3.25) \quad \delta \underline{f} = \begin{pmatrix} k_1 & & \\ & \ddots & \\ & & k_m \end{pmatrix} \delta \underline{l};$$

transforming both sides to the end-effector space using the structure matrix and its transpose, respectively, we find<sup>12</sup>

$$(3.26) \quad \delta \underline{w} = \underline{A}^T \begin{pmatrix} k_1 & & \\ & \ddots & \\ & & k_m \end{pmatrix} \underline{A} \delta \underline{x},$$

where the rotational part of  $\delta \underline{x}$  is expressed in infinitesimal angles about the coordinate axes (a description which corresponds to the components of the angular velocity and cannot be used for finite rotations). The stiffness of a single tendon is reciprocally proportional to its original length  $l_{0,\mu}$ , which differs from the currently measured length  $l_\mu$  by the elongation

$$(3.27) \quad l_\mu - l_{0,\mu} = \frac{1}{k_\mu} f_\mu.$$

As we assume that tendons behave as linear springs, the proportionality factor  $k'$  (which can be interpreted as a stiffness per reciprocal length or as a force per

---

<sup>12</sup>This approach leads to the stiffness matrix. Interestingly, a similar approach for typical serial manipulators is possible, but as the Jacobian of serial systems transforms in the opposite direction, one must start from the *compliance* in the joint space and obtains therefore a *compliance* matrix.

relative elongation; it is measured in force units) is constant. The stiffness of a single tendon is then

$$(3.28) \quad k_\mu = k' I_{0,\mu}^{-1} = k' \left( 1 + \frac{1}{k'} f_\mu \right) I_\mu^{-1} = (k' + f_\mu) I_\mu^{-1}.$$

In typical applications, we have  $\frac{1}{k'} f_\mu < 0.5\%$  [96]. This can be neglected almost always because in reality, the contribution of actuator and joint compliance (not included in this model) is much higher than that. Thus, we can just use the currently measured lengths; this has the advantage that the result depends on the posture only, not on the force state.<sup>13</sup> If we denote the diagonal matrix of the lengths  $I_\mu(\underline{x})$  with  $\underline{L}(\underline{x})$ , we obtain now the stiffness matrix

$$(3.29) \quad \underline{K}(\underline{x}) = k' \underline{A}^T(\underline{x}) \underline{L}^{-1}(\underline{x}) \underline{A}(\underline{x})$$

which is related to the posture in two ways: the factor  $\underline{L}(\underline{x})$  depends on the lengths of the tendons only, while the factor  $\underline{A}(\underline{x})$  expresses the way tendon force is translated to end-effector wrench and is mainly influenced by the angles between tendons or between a tendon  $I_\mu$  and the corresponding lever  $\underline{p}_\mu$ .

In systems with only translational DOFs (i. e. 1T, 2T, 3T), Eq. (2.35), p. 32 implies that the stiffness matrix has the form<sup>14</sup>

$$(3.30) \quad \underline{K} = k' \begin{pmatrix} \underline{u}_1 & \cdots & \underline{u}_m \end{pmatrix} \underline{L}^{-1} \begin{pmatrix} \underline{u}_1^T \\ \vdots \\ \underline{u}_m^T \end{pmatrix} = k' \sum_{\mu=1}^m \frac{1}{I_\mu} \underline{u}_\mu \underline{u}_\mu^T$$

The stiffness matrix is symmetric by Eq. (3.29), hence it is positive semidefinite, i. e. it has nonnegative eigenvalues  $0 \leq k_{e1} \leq \dots \leq k_{en}$ . Stiffness in any direction is then bounded by these values in the sense that

$$(3.31) \quad k_{e1} \leq \frac{|\delta \underline{W}|}{|\delta \underline{X}|} \leq k_{en}.$$

This means that the quotient of the norms of an infinitesimal perturbation and the infinitesimal deflection resulting from the perturbation is always in the range between the smallest and the largest eigenvalue. Extreme values for the quotient are reached for the respective eigenvectors.

The smallest eigenvalue  $k_{e1}$  is particularly interesting because it indicates if a system is near to a singularity. The problem of finding such measures («dexterity indices») has been widely discussed [5, 15, 39, 50], and the result seems to be that there is not a single, natural, general-purpose measure with reasonable properties [154] and appropriate for any kind of mechanism. Now, for tendon-based Stewart platforms, the value  $k_{e1}$  vanishes at a singularity and becomes small in its neighborhood. Furthermore singularity in parallel systems means «looseness» and this is precisely represented by Eq. (3.31). In this sense,  $k_{e1}$  is a natural measure for vicinity to singularities, although it depends on the type of tendons and the absolute size of the system.<sup>15</sup>

<sup>13</sup>Here it is essential that we model tendons as linear springs, otherwise the non-linearity can imply a significant influence of tension on the stiffness.

<sup>14</sup>The formula looks similar to a spectral decomposition, but it has nothing to do with that

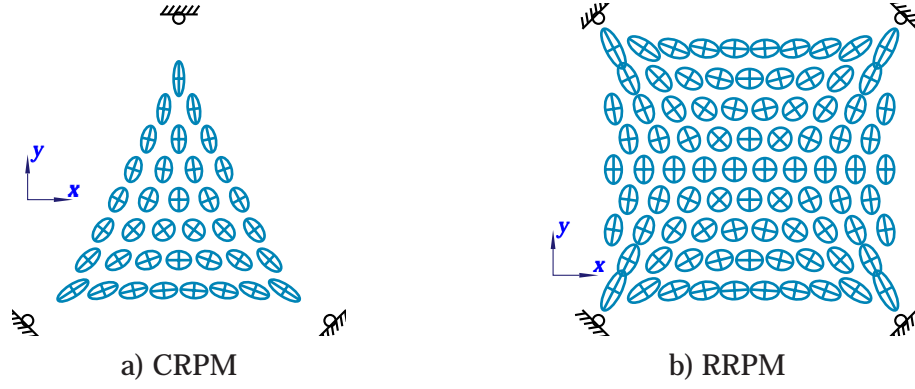


Figure 3.13: Stiffness of some 2T systems

For a 2T manipulator it is easy to write down the stiffness matrix and the resulting eigenvalues explicitly. With  $\underline{u}_\mu = (\cos \alpha_\mu, \sin \alpha_\mu)^T$  as in Eq. (3.8), one obtains the stiffness matrix

$$(3.32) \quad \underline{K} = k' \begin{pmatrix} \sum_{\mu=1}^m l_\mu^{-1} \cos^2 \alpha_\mu & \sum_{\mu=1}^m l_\mu^{-1} \sin \alpha_\mu \cos \alpha_\mu \\ \sum_{\mu=1}^m l_\mu^{-1} \sin \alpha_\mu \cos \alpha_\mu & \sum_{\mu=1}^m l_\mu^{-1} \sin^2 \alpha_\mu \end{pmatrix}$$

and the eigenvalues

$$(3.33) \quad k_{e1/e2} = \frac{1}{2} k' s_{\text{Len}} \left( 1 \pm \sqrt{1 - s_{\text{Ang}}} \right) \quad \text{with}$$

$$(3.34) \quad s_{\text{Len}} = \sum_{\mu=1}^m \frac{1}{l_\mu} \quad \text{and}$$

$$(3.35) \quad s_{\text{Ang}} = \frac{1}{s_{\text{Len}}^2} \sum_{1 \leq \mu < \mu' \leq m} \frac{1}{l_\mu l_{\mu'}} \sin^2 (\alpha_\mu - \alpha_{\mu'}) .$$

Thus we have a representation with two factors: one which depends only on the lengths and one which is mainly a function of the angles between tendons.

Fig. 3.13 shows two example manipulators with their generalized stiffness ellipses. The directions of the ellipse axes indicate the direction of stiffness eigenvectors: this means that a perturbation in such a direction generates a motion in the same direction. The length of the half axes is proportional to the square root of the respective eigenvalues. We find that there is a region close to the center where both eigenvalues are almost equal: this means that the term  $s_{\text{Ang}}$  almost vanishes. By contrast, close to the winches both values are quite different from each other: here the term  $s_{\text{Len}}$  is large because one tendon is very short, but only one of the eigenvalues takes advantage of this, while the other one almost vanishes – clearly, the stiffness along the short tendon is high, while the system is rather compliant for motions orthogonal to this because the angles of the other

---

because the number of terms is higher than  $n$  and thus the vectors  $\underline{u}_\mu$  cannot be all orthogonal to each other. Hence, this does not provide much insight into the eigenvalues of  $\underline{K}$ .

<sup>15</sup>It is made independent of the tendon type when dividing by  $k'$  and it can even be made dimensionless when dividing by some characteristic length. However, there is no easy way to transform it into a dimensionless number filling the interval  $[0, 1]$ , which is one of the properties usually desired for measures of singularity.

tendons are disadvantageous. Furthermore we observe that the manipulator with four tendons has a generally higher stiffness than that with three.

In manipulators with translational and rotational DOFs, Eq. (3.31) cannot be directly applied because then,  $\delta \underline{x}$  contains lengths as well as angles and  $\delta \underline{w}$  contains forces and torques. So the absolute values of the vectors as such are meaningless. This can be overcome by introducing a characteristic length  $p_c$  that transforms the angles to lengths and the torques to forces [6].<sup>16</sup> We obtain new generalized coordinates and forces which for the 1R2T case can be defined as follows:

$$(3.36) \quad \delta \underline{x} = \underline{S} \begin{pmatrix} \delta \underline{r} \\ \delta \varphi \end{pmatrix} \quad \text{and} \quad \delta \underline{w} = \underline{S}^{-1} \begin{pmatrix} \delta \underline{f}_P \\ \delta \tau_P \end{pmatrix} \quad \text{with} \quad \underline{S} = \begin{pmatrix} \mathbf{I}_2 & \\ & p_c \end{pmatrix}.$$

The transformations of deflection and wrench are consistent in the sense that they preserve the scalar product which represents the work performed by the motion:

$$(3.37) \quad \delta \underline{w}^T \delta \underline{x} = \begin{pmatrix} \delta \underline{f}_P^T & \delta \tau_P \end{pmatrix} \begin{pmatrix} \delta \underline{r} \\ \delta \varphi \end{pmatrix}.$$

Using these new coordinates, we obtain the corresponding stiffness matrix

$$(3.38) \quad \underline{K}(\underline{x}) = \underline{k}' \underline{S} \underline{A}^T(\underline{x}) \underline{L}^{-1}(\underline{x}) \underline{A}(\underline{x}) \underline{S}$$

$$(3.39) \quad = \underline{k}' \sum_{\mu=1}^m \frac{1}{l_\mu} \begin{pmatrix} \underline{u}_\mu \\ \det \begin{pmatrix} \frac{p_\mu}{p_c} & \underline{u}_\mu \end{pmatrix} \end{pmatrix} \begin{pmatrix} \underline{u}_\mu^T & \det \begin{pmatrix} \frac{p_\mu}{p_c} & \underline{u}_\mu \end{pmatrix} \end{pmatrix}.$$

Now Eq. (3.31) holds for the eigenvalues of this matrix.

A convenient choice for  $p_c$  is the average value of the platform link lengths  $p_1, \dots, p_m$ : then an angle is translated into the deflection of the points at average distance from the origin of  $\mathcal{K}_P$  and a torque is translated to the corresponding force applied at such a point. This is particularly useful when all the links are of equal length as in Table 3.2. The stiffness matrix of the first posture shows that any force in  $x$  direction acting on the center of the platform results in a pure translation in  $x$  direction. The same holds for such a force in  $y$  direction and also for a tangential force applied to one of the connection points.<sup>17</sup> In the second posture, translational and rotational stiffness are still independent. The remaining examples show other types of decoupling and it can be seen that in general the stiffness values in various directions are strongly coupled with each other. Note that the lists of eigenvalues in the table are just a partial information because they do not tell which type of translation/rotation they apply to. (It is difficult to include such an information in the drawing in an intuitive way.)

Similar considerations are possible for 2R3T and 3R3T manipulators. We have then a transformation matrix  $\underline{S}$  with

$$(3.40) \quad \underline{S} = \begin{pmatrix} \mathbf{I}_3 & \\ & p_c \mathbf{I}_{n_{\text{Rot}}} \end{pmatrix}$$

<sup>16</sup>This approach, widely used by Jorge Angeles, was criticized by Joseph Duffy arguing that the choice of the characteristic length is somewhat arbitrary. This may be true for the general case; however, when choosing a meaningful length appearing in the mechanism, also the resulting linear deflections and forces get a physical meaning.

<sup>17</sup>To be precise, two forces of half this amount must be applied at opposite connection points in order to achieve a pure torque on the body.



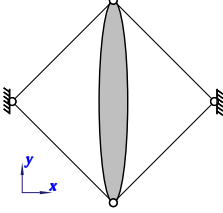
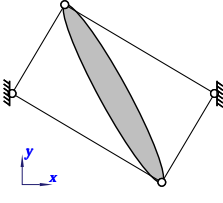
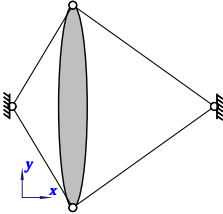
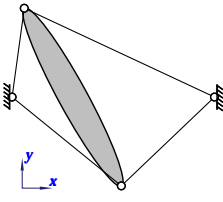
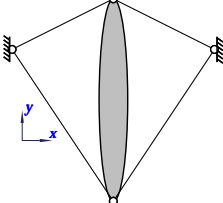
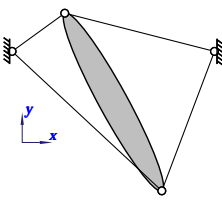
Posture	Structure Matrix $\underline{S} \underline{A}^T$	Stiffness Matrix $\underline{K}$ Eigenvalues $\underline{k}$
	$\begin{pmatrix} -0.707 & 0.707 & 0.707 & -0.707 \\ 0.707 & 0.707 & -0.707 & -0.707 \\ -0.707 & 0.707 & -0.707 & 0.707 \end{pmatrix}$	$\begin{pmatrix} 2.828 & 0.000 & -0.000 \\ 0.000 & 2.828 & -0.000 \\ -0.000 & -0.000 & 2.828 \end{pmatrix}$ (2.828, 2.828, 2.828)
	$\begin{pmatrix} -0.860 & 0.510 & 0.860 & -0.510 \\ 0.510 & 0.860 & -0.510 & -0.860 \\ -0.510 & 0.860 & -0.510 & 0.860 \end{pmatrix}$	$\begin{pmatrix} 2.740 & 0.700 & 0.000 \\ 0.700 & 3.505 & -0.000 \\ -0.000 & -0.000 & 3.505 \end{pmatrix}$ (2.325, 3.505, 3.920)
	$\begin{pmatrix} -0.514 & 0.814 & 0.814 & -0.514 \\ 0.857 & 0.581 & -0.581 & -0.857 \\ -0.514 & 0.814 & -0.814 & 0.514 \end{pmatrix}$	$\begin{pmatrix} 2.447 & 0.000 & -0.000 \\ -0.000 & 3.307 & -0.414 \\ -0.000 & -0.414 & 2.447 \end{pmatrix}$ (2.281, 2.447, 3.474)
	$\begin{pmatrix} -0.776 & 0.724 & 0.906 & -0.136 \\ 0.631 & 0.690 & -0.423 & -0.991 \\ -0.378 & 0.966 & -0.592 & 0.594 \end{pmatrix}$	$\begin{pmatrix} 2.523 & 0.016 & 0.822 \\ 0.016 & 3.709 & -0.383 \\ 0.822 & -0.383 & 2.809 \end{pmatrix}$ (1.796, 3.317, 3.928)
	$\begin{pmatrix} -0.555 & 0.555 & 0.894 & -0.894 \\ 0.832 & 0.832 & -0.447 & -0.447 \\ -0.555 & 0.555 & -0.894 & 0.894 \end{pmatrix}$	$\begin{pmatrix} 3.545 & -0.000 & -2.179 \\ -0.000 & 2.252 & -0.000 \\ -2.179 & -0.000 & 3.545 \end{pmatrix}$ (1.365, 2.252, 5.724)
	$\begin{pmatrix} -0.732 & 0.353 & 0.969 & -0.809 \\ 0.681 & 0.935 & -0.247 & -0.587 \\ -0.316 & 0.759 & -0.732 & 0.992 \end{pmatrix}$	$\begin{pmatrix} 3.967 & 1.120 & -2.833 \\ 1.120 & 2.800 & -0.823 \\ -2.833 & -0.823 & 4.641 \end{pmatrix}$ (1.375, 2.486, 7.548)

Table 3.2: Stiffness in some postures of a 1R2T manipulator  
(with  $k' = 10.0$  kN and a size of base and platform of 10 m, respectively)

where  $n_{\text{Rot}}$  equals 2 or 3, respectively. Detailed case studies for 3R3T were conducted by Lafourcade and Zheng [96, 182].

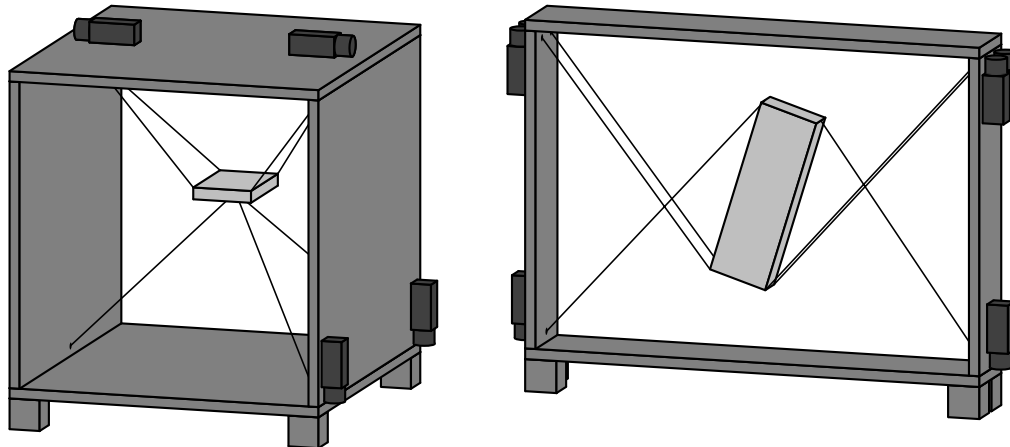
### 3.5. Autocollisions

As a last aspect of workspace, we look at the problem of autocollisions, i. e. collisions of tendons with each other. This is mentioned here for the sake of completeness because it is a question of design geometry independent of technical details and therefore it belongs to the focus of this work.<sup>18</sup> Nevertheless, we will not go into much detail because there is a theory of its own and it does not share much mathematical framework with the other aspects discussed so far.

Two tendons can cross each other in at most one point, because otherwise they would coincide completely for all postures and that would not be a reasonable design. This has an important consequence:

**3.8 Proposition** *If two tendons are connected to the same point on the base or on the platform, they will never cross each other elsewhere.  $\diamond$*

It follows immediately that autocollisions never occur in systems with pure translation (1T, 2T, 3T). For 2R3T systems, designs as in Fig. 3.10 suggest that tendons could cross each other only for very large rotations which are certainly outside the controllable workspace. It would be difficult to prove this formally, but it is clear that in normal cases, autocollisions do not play any role in 2R3T systems.



a) connection points that coincide

b) tendons in different planes

Figure 3.14: Techniques to avoid autocollisions

Thus, the only systems where the problem has to be considered are those of class 1R2T and 3R3T. Now, considering the above proposition, it is a good strategy to make coincide as many connection points as possible, as in Fig. 3.14a.

<sup>18</sup>Collisions between tendons and platform, load or obstacles also play an important role, but they depend on the shape of the involved bodies. So they cannot be discussed when only the positions of winches and connection points are given.

While it is practically impossible to do this with the spherical joints on rigid links, it is rather easy with tendons [127, 128], for instance by guiding multiple tendons through a common tube. (Clearly, the drawback of this is a limited precision, but tendon-based systems are not particular candidates for highest-precision positioning anyway.) This also has advantages for the controllable workspace because it leads to relatively large values of  $\sin \beta_\mu$  in Eq. (3.10) (Fig. 3.4b) for the 1R2T case and it has similar effects on 3R3T systems. In addition, it often simplifies the computation of forward kinematics [47, 72].

Typical solutions arrange points such that each tendon shares the base connection point with one neighboring tendon and the platform connection point with another one, as in Table 3.2 for the 1R2T class and in Fig. 2.6a, p. 27 (the classical Stewart platform) for 3R3T. Then the other tendons are so far away that autocollisions can rarely occur.

An alternative approach for 1R2T systems is to replace some tendons by a pair of tendons actuated simultaneously and arranged on parallel planes on opposite sides of the plane of motion, if the type of application and the environment allows that. Then various tendons can be put on different planes, as in Fig. 3.14b. However, this solution may be significantly more expensive and is normally not necessary because in the 1R2T class, the strategy of connection point coincidence usually works well.

Autocollisions may remain a real problem in 3R3T systems because they are so complex that usually one cannot see at a glance all possible collision problems and appropriate solutions. This applies in particular to redundant systems. Tadokoro et al. [160, 161] proposed a numerical method to check tendon distances during a trajectory. However, a comprehensive analysis of collision problems and solutions remains an open topic of research.



# Chapter 4

## Optimal Tension Distribution

*Section 4.1 explains the problem of finding acceptable and optimal solutions and briefly outlines the results of this chapter. The special case of CRPMs (Section 4.2) suggests a general strategy, which is presented in Section 4.3. Optimal solutions may be discontinuous along a trajectory, as shown by examples in Section 4.4. Therefore, Section 4.5 explains how to find almost optimal solutions and Section 4.6 proves that they are continuous. Section 4.7 explains the practical computation of such solutions.*

### 4.1. Introduction

This chapter addresses the problem of finding acceptable solutions to the tension problem as defined in Def. 3.5, p. 43, in particular for the nontrivial case of RRPMS. Related questions include:

- How can we check if an acceptable solution exists?
- If an acceptable solution exists, how can we find it?
- What is an «optimal» solution and how can we find it?
- Is that optimal solution continuous along a trajectory?

We shall obtain the following main results:

- The tension problem can be transformed into a nonlinear optimization problem on a convex polyhedron.
- Then acceptable solutions exist if and only if there are optimal solutions which are acceptable.
- The solution of the optimization problem is unique in most cases.
- In the domain of uniqueness, the solution is also continuous.
- When crossing a region of non-uniqueness, it may be impossible to follow a continuous solution path. Unfortunately, such regions may appear close to the center of the workspace.

- One can consider slightly different optimization problems that always have a unique solution which is close to the original solution. However, in this case one can fail to find an acceptable solution although it exists.
- In singularities, even these solutions fail to be continuous. But this is the case for any solution based on reasonable requirements.

These results are general in the sense that they apply to any number of tendons and DOFs. As most of the complicated cases arise in dimensions greater than three and thus are difficult to illustrate, formal proofs are required in order to be sure that all possible complications are included. For that reason, this chapter was given a structure much like a mathematical paper, with definitions, propositions and proofs. Examples demonstrate that certain complications really appear in manipulators; although, for sake of simplicity, the examples are special and not well-designed from a practical point of view.

## 4.2. Optimal Solutions for CRPMs

In general, it is not straightforward to check if an acceptable solution exists and if so to compute it. As the set of vectors  $\underline{f}$  satisfying  $\underline{A}^T \underline{f} + \underline{w} = \underline{0}$  is a  $k$ -dimensional affine space, one might try fixing  $\bar{k}$  components of  $\underline{f}$  to acceptable values and then compute the others, but this does not necessarily lead to a positive solution and in particular not to an acceptable one. A very simple case<sup>1</sup> is illustrated in Fig. 4.1: although a segment of acceptable solutions exists, one might happen to choose acceptable values  $f_1 = f_{1,0}$  or  $f_2 = f_{2,0}$  such that the other force components computed from them are not acceptable.

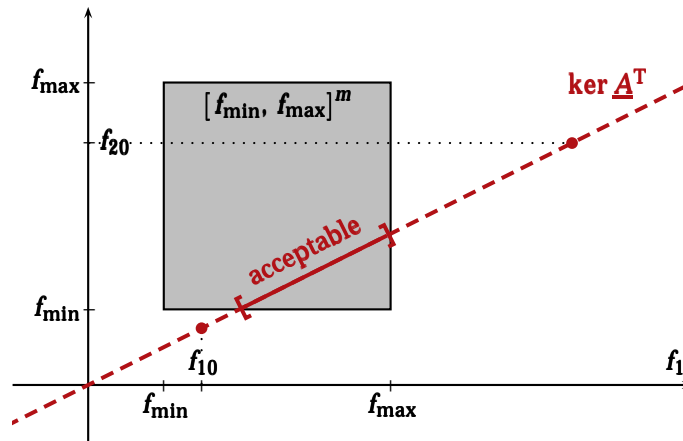


Figure 4.1: Fixing some forces does not always yield acceptable solutions

For CRPMs, it is easy to check for acceptable solutions. Given the tension problem

$$(4.1) \quad \underline{A}^T \underline{f} + \underline{w} = \underline{0} \quad \text{and} \quad \underline{f} \in [f_{\min}, f_{\max}]^m,$$

<sup>1</sup>An illustration with  $m = 2$  has been chosen because this is the most obvious case, even though there is no 2-DOF tendon-based Stewart platform corresponding to this figure. For a real example, at least  $m = 3$  would be necessary.

the solutions for CRPMs (i. e. manipulators where  $\underline{A}^T \in \mathbb{R}^{n \times (n+1)}$ ) in nonsingular postures can be written as

$$(4.2) \quad \underline{f} = \underbrace{-\underline{A}^{+T} \underline{w}}_{=: \underline{f}_0} + \lambda \underline{h} \quad \text{with} \quad \underline{h} \in \ker \underline{A}^T.$$

By Prop. 3.2, p. 36, a solution for each  $\underline{w}$  exists if and only if there is such an  $\underline{h}$  where all components are positive.<sup>2</sup> As the kernel of the structure matrix is one-dimensional for CRPMs, this is easy to check: just compute an arbitrary element of  $\ker \underline{A}^T$ ; if all components are nonzero and of equal sign, then there is such an  $\underline{h} > \underline{0}$ , otherwise not. If it exists, then the acceptability condition is

$$(4.3) \quad \forall_{1 \leq \mu \leq m} \quad f_{\min} \leq f_{0,\mu} + \lambda h_\mu \leq f_{\max}$$

and as  $\underline{h} > \underline{0}$ , this can be transformed to<sup>3</sup>

$$(4.4) \quad \max_{1 \leq \mu \leq m} \frac{f_{\min} - f_{0,\mu}}{h_\mu} \leq \lambda \leq \min_{1 \leq \mu \leq m} \frac{f_{\max} - f_{0,\mu}}{h_\mu}.$$

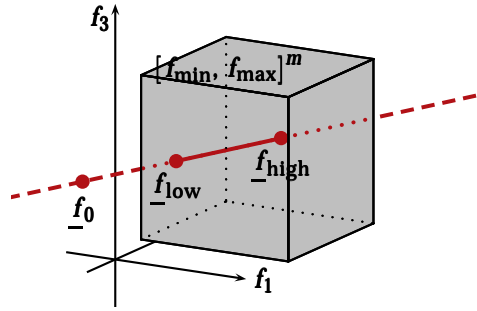


Figure 4.2: In CRPMs, acceptable solutions form a line segment

This defines a range for  $\lambda$  that provides acceptable solutions. It may be empty: in that case, no acceptable solutions exist. We observe two important points:

- The acceptable solutions form a polyhedral set. For CRPMs, the set has the simple structure of a line segment (Fig. 4.2).
- It is a matter of respective purpose which element in this segment is optimal:
  - If we want to save energy as much as possible, we will choose the minimum value of  $\lambda$ .
  - If we are seeking high eigenfrequencies in the tendons, we can take the maximum value.

<sup>2</sup>Of course, for a particular  $\underline{w}$  solutions can exist even when there is no such  $\underline{h} > \underline{0}$ . Therefore, the approach presented here is useful for explanation, but it does not actually provide a suitable algorithm. Section 4.3 presents a general algorithm, which can be applied to CRPMs as well.

<sup>3</sup>The same idea for the lower bound only was proposed by Kawamura et al. [80].



- If the key requirement is safety (e. g. when transporting people in rescue systems), we may choose the middle between both, to be sure that we remain inside the acceptable range under all circumstances, even when large control errors occur.
- Any mixture of these criteria is possible.

### 4.3. Optimal Solutions in the General Case

In the general case, the set of acceptable solutions is a polyhedron (Fig. 4.3) of generally complicated structure. Our goal is to identify in this set a «lowest» and a «highest» solution (Fig. 4.3). Then the line segment delimited by them provides a set of «optimal» solutions in a certain sense and we can choose a particular solution out of the line segment, the same way as presented above.

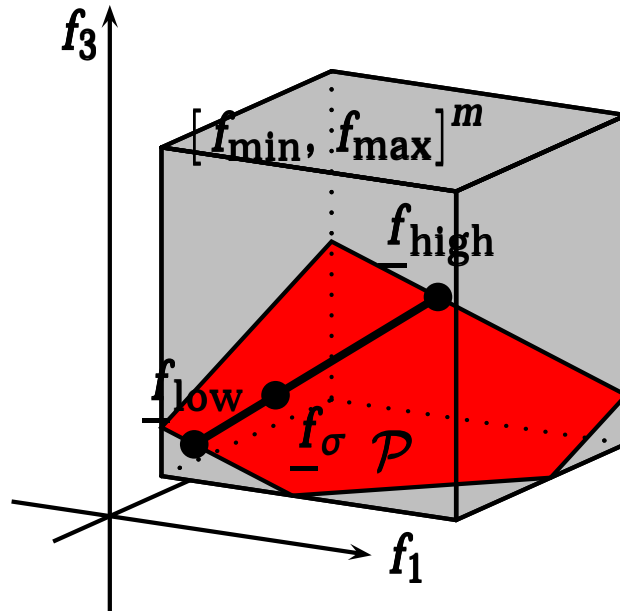


Figure 4.3: Optimal solutions as a range: basic idea

When seeking a «lowest» solution of the tension problem, we consider all the solutions of the structure matrix equation that respect the lower bound on tendon force (Fig. 4.4a). This is the unbounded polyhedron

$$(4.5) \quad \mathcal{P}_{\text{low}} := \left\{ \underline{f} \in \mathbb{R}^m : \underline{A}^T \underline{f} + \underline{w} = \underline{0} \wedge \underline{f} \geq \underline{f}_{\min} \right\} .$$

Now a solution  $\underline{f} \in \mathcal{P}_{\text{low}}$  is acceptable if it also satisfies the upper bound condition, i. e. if the maximum of the components of  $\underline{f}$  is less than or equal to  $f_{\max}$ . As all these components are positive, that condition can be formulated as

$$(4.6) \quad \|\underline{f}\|_{\infty} \leq f_{\max}$$

where  $\|f\|_\infty$  represents the maximum absolute value of the components of  $\underline{f}$  (Def. A.17, p. 130). Thus, acceptable solutions exist if and only if<sup>4</sup>

$$(4.7) \quad \min_{\underline{f} \in \mathcal{P}_{\text{low}}} \|\underline{f}\|_\infty \leq f_{\max}.$$

Elements  $\underline{f}_{\text{low}} \in \mathcal{P}_{\text{low}}$  having minimal  $\|\cdot\|_\infty$ -norm among  $\mathcal{P}_{\text{low}}$  will be called *lowest*. They satisfy

$$(4.8) \quad \|\underline{f}_{\text{low}}\|_\infty = \min_{\underline{f} \in \mathcal{P}_{\text{low}}} \|\underline{f}\|_\infty.$$

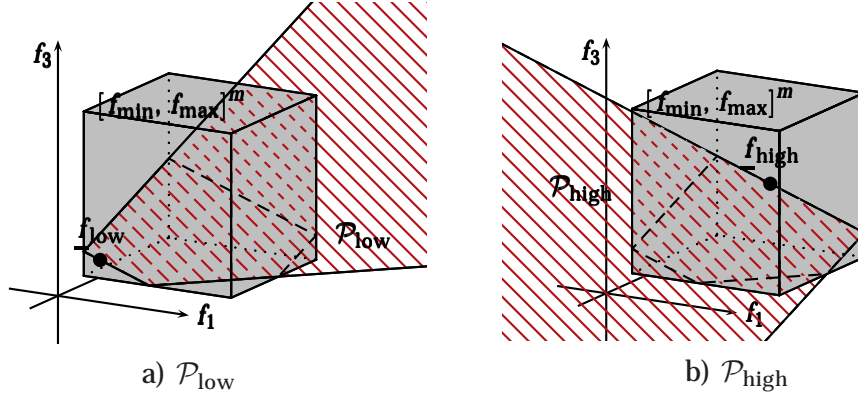


Figure 4.4: Polyhedra of solutions

Conversely, highest solutions are sought in the polyhedron (Fig. 4.4b)

$$(4.9) \quad \mathcal{P}_{\text{high}} := \left\{ \underline{f} \in \mathbb{R}^m : \underline{A}^T \underline{f} + \underline{w} = \underline{0} \wedge \underline{f} \leq f_{\max} \right\};$$

then an element of  $\mathcal{P}_{\text{high}}$  is acceptable if the minimum of its components is greater than or equal  $f_{\min}$ . This formulation is not convenient to work with because the minimum of the components of a vector is not a norm. But we can introduce again the  $\|\cdot\|_\infty$ -norm by saying, equivalently, that a solution  $\underline{f} \in \mathcal{P}_{\text{high}}$  is acceptable if and only if

$$(4.10) \quad \|f_{\max} \underline{1} - \underline{f}\|_\infty \leq f_{\max} - f_{\min}.$$

Elements  $\underline{f}_{\text{high}} \in \mathcal{P}_{\text{high}}$  where the left-hand side reaches its minimum will be called *highest* solutions. They fulfill

$$(4.11) \quad \|f_{\max} \underline{1} - \underline{f}_{\text{high}}\|_\infty = \min_{\underline{f} \in \mathcal{P}_{\text{high}}} \|f_{\max} \underline{1} - \underline{f}\|_\infty.$$

Elements on the line segment joining a lowest and a highest solution (Fig. 4.3) will be called *optimal*.<sup>5</sup> As an example, Fig. 4.5 shows two postures of a highly redundant manipulator with two DOFs and seven tendons: the dashed arrow indicates the gravity (equal for all postures), the solid arrows represent forces corresponding to a lowest solution and the dotted arrows show a highest solution.

The sets  $\mathcal{P}_{\text{low}}$  and  $\mathcal{P}_{\text{high}}$  are convex (Def. A.12, p. 127) and the set of acceptable solutions is the intersection of both, hence it is convex, too (although possibly empty). We summarize these considerations in a definition and a proposition.

<sup>4</sup>According to Def. A.3, p. 124, the notation «min» implicitly tells an element  $\underline{f}$  of such norm really exists. This will be proven in Theorem 4.4.

<sup>5</sup>For the homogeneous case with  $\underline{w} = 0$ , it can be shown that an «optimal» solution  $\underline{f}_{\text{opt}}$  is

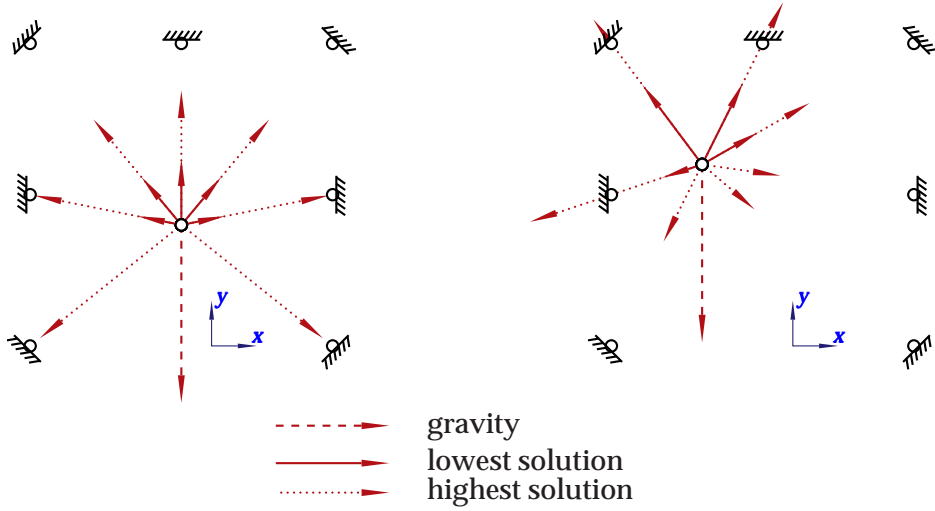


Figure 4.5: Force ranges of two postures for a redundant 2T example

**4.1 Definition (lowest/highest/optimal solution)** An element  $\underline{f}_{\text{low}} \in \mathcal{P}_{\text{low}}$  is called lowest solution if

$$(4.12) \quad \|\underline{f}_{\text{low}}\|_{\infty} = \min_{\underline{f} \in \mathcal{P}_{\text{low}}} \|\underline{f}\|_{\infty}.$$

An element  $\underline{f}_{\text{high}} \in \mathcal{P}_{\text{high}}$  is called highest solution if

$$(4.13) \quad \|\underline{f}_{\text{max}} \underline{1} - \underline{f}_{\text{high}}\|_{\infty} = \min_{\underline{f} \in \mathcal{P}_{\text{high}}} \|\underline{f}_{\text{max}} \underline{1} - \underline{f}\|_{\infty}.$$

An element  $\underline{f}(\sigma) \in \mathbb{R}^m$  (Fig. 4.5) is called optimal solution if it can be written as

$$(4.14) \quad \underline{f}(\sigma) = \sigma \underline{f}_{\text{high}} + (1 - \sigma) \underline{f}_{\text{low}} \quad \text{with} \quad \sigma \in [0, 1] . \diamond$$

**4.2 Proposition (acceptability of solutions)** The following statements are equivalent for a given posture:

- a) Acceptable solutions exist.
- b) All lowest solutions are acceptable.
- c) There is an acceptable lowest solution.
- d) All highest solutions are acceptable.
- e) There is an acceptable highest solution.
- f) All optimal solutions are acceptable.

indeed optimal in the following sense: if there is another solution  $\underline{f}$  with  $\min_{\mu} f_{\mu} = \min_{\mu} f_{\text{opt},\mu}$ , then we have  $\max_{\mu} f_{\mu} \geq \max_{\mu} f_{\text{opt},\mu}$ . In other words, when fixing a minimal force and trying to minimize the maximum component value, there is nothing better than a corresponding optimal solution in the above sense. The same result holds for maximizing the minimum component with a fixed maximum force. For  $\underline{w} \neq 0$  there is no comparable result. So in general the term «optimal» is a convention rather than a fact.

g) *There is an acceptable optimal solution.*  $\diamond$

**Proof.** The proposition results from the following implications:

$$(4.15) \quad \begin{aligned} a &\Rightarrow b \Rightarrow c \Rightarrow a \\ a &\Rightarrow d \Rightarrow e \Rightarrow a \\ b \wedge d &\Rightarrow f \Rightarrow g \Rightarrow a \end{aligned}$$

where « $a \Rightarrow b$ » and « $a \Rightarrow d$ » follow from the above considerations, while « $b \wedge d \Rightarrow f$ » holds because the set of acceptable solutions is convex. The implications « $b \Rightarrow c$ », « $d \Rightarrow e$ » and « $f \Rightarrow g$ » follow from Theorem 4.4 below (the nontrivial point is that lowest/highest/optimal solutions really exist). The rest is obvious.  $\square$

Now we shall state that lowest/highest solutions always exist and that they are found in a very particular region of their respective polyhedra, namely in the convex hull (Def. A.12, p. 127) of their vertices. **This fact is irrelevant for the actual computation because computation of all vertices is far more expensive than computation of the solutions themselves**, as explained in Section 4.7. However, it gives some additional theoretic insight and we shall use it in the following section for the construction of examples.

The unbounded sets  $\mathcal{P}_{\text{low}}$  and  $\mathcal{P}_{\text{high}}$  are polyhedra in the sense of Def. A.12, p. 127 because they are the sets of those  $\underline{f}$  which satisfy

$$(4.16) \quad \begin{pmatrix} \underline{A}^T \\ -\underline{A}^T \\ -\underline{I}_m \end{pmatrix} \underline{f} \leq \begin{pmatrix} \underline{0} \\ \underline{0} \\ -f_{\min} \underline{1} \end{pmatrix} \quad \text{for } \mathcal{P}_{\text{low}},$$

$$(4.17) \quad \begin{pmatrix} \underline{A}^T \\ -\underline{A}^T \\ \underline{I}_m \end{pmatrix} \underline{f} \leq \begin{pmatrix} \underline{0} \\ \underline{0} \\ f_{\max} \underline{1} \end{pmatrix} \quad \text{for } \mathcal{P}_{\text{high}}.$$

These polyhedra have a zero-dimensional lineality space (Def. A.14, p. 129); they extend towards infinity only in positive directions for  $\mathcal{P}_{\text{low}}$  and only in negative ones for  $\mathcal{P}_{\text{high}}$ :

**4.3 Lemma** *The polyhedra  $\mathcal{P}_{\text{low}}$ ,  $\mathcal{P}_{\text{high}}$  are pointed and they fulfill<sup>6</sup>*

$$(4.18) \quad \text{char.cone } \mathcal{P}_{\text{low}} \subset \mathbb{R}_{+0}^m \quad \text{and} \quad \text{char.cone } \mathcal{P}_{\text{high}} \subset \mathbb{R}_{-0}^m . \diamond$$

**Proof.** Eq. (4.18) follows directly from Eq. (4.16), (4.17) by setting the right hand side to zero according to Eq. (A.17), p. 129. Then the lineality space is contained in  $\mathbb{R}_{+0} \cap -\mathbb{R}_{+0} = \{\underline{0}\}$  for  $\mathcal{P}_{\text{low}}$  and  $\mathbb{R}_{-0} \cap -\mathbb{R}_{-0} = \{\underline{0}\}$  for  $\mathcal{P}_{\text{high}}$ , so both polyhedra are pointed.  $\square$

Now Theorem A.15, p. 130 enables us to prove that lowest (highest) solutions always exist (this was not yet shown so far) and that they are found in the convex hull of the vertices of  $\mathcal{P}_{\text{low}}$  ( $\mathcal{P}_{\text{high}}$ ). This can also be observed in Fig. 4.4a; it is not visible in Fig. 4.4b because there, a second vertex with  $f_3 = f_{\min}$  lies on the left hand side outside the drawing region.

<sup>6</sup>see Def. A.14, p. 129 for the definition of the characteristic cone and of the term «pointed»

**4.4 Theorem (solutions between vertices)** Let  $\mathcal{Q}_{\text{low}}$  and  $\mathcal{Q}_{\text{high}}$  be the convex hulls of the vertices of  $\mathcal{P}_{\text{low}}$  and  $\mathcal{P}_{\text{high}}$ . Whenever  $\mathcal{P}_{\text{low}}$  ( $\mathcal{P}_{\text{high}}$ ) is nonempty, then so is  $\mathcal{Q}_{\text{low}}$  ( $\mathcal{Q}_{\text{high}}$ ) and we have

$$(4.19) \quad \inf_{\underline{f} \in \mathcal{Q}_{\text{low}}} \|\underline{f}\|_{\infty} = \inf_{\underline{f} \in \mathcal{P}_{\text{low}}} \|\underline{f}\|_{\infty} \quad \text{and}$$

$$(4.20) \quad \inf_{\underline{f} \in \mathcal{Q}_{\text{high}}} \|\underline{f}_{\max} \underline{1} - \underline{f}\|_{\infty} = \inf_{\underline{f} \in \mathcal{P}_{\text{high}}} \|\underline{f}_{\max} \underline{1} - \underline{f}\|_{\infty}.$$

Furthermore lowest (highest) solutions exist and lie all in  $\mathcal{Q}_{\text{low}}$  ( $\mathcal{Q}_{\text{high}}$ ).  $\diamond$

**Proof.** We show the theorem for lowest solutions, the proof for highest ones is similar.

a) If the pointed polyhedron  $\mathcal{P}_{\text{low}}$  is nonempty, then it has a nonempty set of vertices by Theorem A.15, p. 130.

b) With Theorem A.15, p. 130, we can write

$$(4.21) \quad \begin{aligned} \inf \{ \|\underline{f}\|_{\infty} : \underline{f} \in \mathcal{P}_{\text{low}} \} &= \inf \{ \|\underline{f} + \underline{f}_1\|_{\infty} : \underline{f} \in \mathcal{Q}_{\text{low}} \wedge \underline{f}_1 \in \text{char.cone } \mathcal{P} \} \\ &= \inf \{ \|\underline{f}\|_{\infty} : \underline{f} \in \mathcal{Q}_{\text{low}} \} \end{aligned}$$

because the additional  $\underline{f}_1$  has nonnegative components by Lemma 4.3.

c) This implies that, if lowest solutions exist, then they lie in  $\mathcal{Q}_{\text{low}}$ , which is compact by Lemma A.19, p. 132. Now, the infinity norm is continuous, so it takes a minimum on this compact set by Prop. A.26, p. 133.  $\square$

## 4.4. Discontinuity of Optimal Solutions

When performing a trajectory, Prop. 4.2 implies that one can choose  $\sigma \in [0, 1]$  a priori and then compute  $\underline{f}(\sigma)$  at each point of the trajectory. Either the result is acceptable at each point or there is no acceptable force path. In any case, one does not need to reconsider  $\sigma$  during the motion. Now an interesting question is whether the result is continuous or not. By their definition, optimal solutions  $\underline{f}(\sigma)$  with  $0 < \sigma < 1$  are continuous if and only if both lowest and highest solutions are continuous. But these can fail to be continuous, as we will show in the following examples. We will give an example for the nonsingular as well as for the singular case, because the latter turns out to be a more general problem. Both examples are treated quite in detail because this also provides a practical illustration how the results obtained so far can be applied.

### 4.4.1. Nonsingular Case

We consider the manipulator shown in Fig. 4.6, where a point  $\underline{p}$  is attached to five tendons and moved in the plane. The system has two end-effector-DOFs and five actuators, hence there are three degrees of force redundancy. We look at postures which satisfy the angular conditions

$$(4.22) \quad \begin{aligned} -\delta < \alpha < \delta & \quad \text{with } \delta \text{ such that} & -\epsilon < \sin \alpha < \epsilon \\ 0 < \beta < \delta' & \quad \text{with } \delta' \text{ such that} & 0 < \sin \beta < \zeta - \epsilon \end{aligned}$$

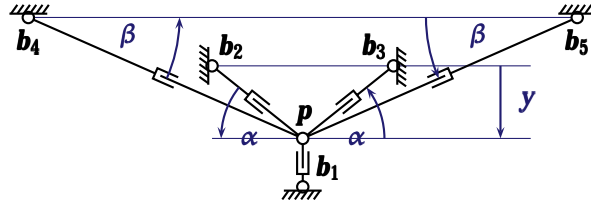


Figure 4.6: Example of discontinuity

with some  $0 < \epsilon < \frac{1}{2}$  and  $\epsilon < \zeta \leq \frac{1}{2}$ .

With Eq. (2.35), p. 32, the figure supplies directly

$$(4.23) \quad \underline{A}^T = \begin{pmatrix} 0 & -\cos \alpha & \cos \alpha & -\cos \beta & \cos \beta \\ -1 & \sin \alpha & \sin \alpha & \sin \beta & \sin \beta \end{pmatrix}$$

and one can easily imagine three independent force distributions in the kernel of  $\underline{A}^T$ , such that we obtain a representation  $\ker \underline{A}^T = \langle \underline{H} \rangle$  with

$$(4.24) \quad \underline{H} = \begin{pmatrix} 2 \sin \alpha & 2 \sin \beta & 0 \\ 1 & 0 & \cos \beta \\ 1 & 0 & -\cos \beta \\ 0 & 1 & -\cos \alpha \\ 0 & 1 & \cos \alpha \end{pmatrix}.$$

The first column represents a situation where tendons 1, 2 and 3 balance each other, while the others are inactive. The second one is the same with tendons 1, 4 and 5. The third one shows how tendons 2, 3, 4 and 5 create a force equilibrium while the first tendon is inactive. *None of these vectors is a positive solution of the tension problem because they contain zero and even negative entries*, but they generate the kernel of  $\underline{A}^T$ . So in the homogeneous case  $\underline{w} = \underline{0}$  (i. e. the only forces in the system are tendon forces), any solution  $\underline{f}$  has the form

$$(4.25) \quad \underline{f} = \underline{H} \underline{\lambda} \quad \text{with some} \quad \underline{\lambda} \in \mathbb{R}^3.$$

We assume  $f_{\min} = 1$ . Due to the symmetry of the mechanism, it is clear that solutions with minimal force will have

$$(4.26) \quad \lambda_3 = 0.$$

Therefore it is sufficient to work with a matrix  $\underline{H}'$  consisting of the first two columns of  $\underline{H}$  and with the corresponding polyhedra  $\mathcal{P}'_{\text{low}}$  and  $\mathcal{Q}'_{\text{low}}$ . Any element of  $\mathcal{P}'_{\text{low}}$  then has the form

$$(4.27) \quad \underline{f} = (2\lambda_1 \sin \alpha + 2\lambda_2 \sin \beta \quad \lambda_1 \quad \lambda_1 \quad \lambda_2 \quad \lambda_2)^T.$$

Now we have to compute the vertices of  $\mathcal{Q}'_{\text{low}}$ . As  $\mathcal{P}'_{\text{low}}$  is two-dimensional, vertices are given by those elements  $\underline{f}$  which have the form of Eq. (4.27) and two components equal to 1 in one of the following cases:

a) For  $f_2 = f_4 = 1$ , Eq. (4.22) implies  $f_1 < 1$ , so such a point is not contained in  $\mathcal{P}'_{\text{low}}$  and hence not a vertex of it.

b) For  $f_1 = f_2 = 1$ , we obtain

$$(4.28) \quad \lambda_1 = 1 \wedge \sin \alpha + 2\lambda_2 \sin \beta = 1 \quad \text{and therefore}$$

$$(4.29) \quad \|\underline{f}\|_\infty = \lambda_2 = \frac{\overbrace{1 - 2 \sin \alpha}^{\in ]1-2\epsilon, 1+2\epsilon[}}{\underbrace{2 \sin \beta}_{\in ]0, 2\zeta - 2\epsilon[ \subset ]0, 1-2\epsilon[}} \in [1, \infty[$$

and for the ranges of Eq. (4.22), this is always a vertex of  $\mathcal{Q}'_{\text{low}}$ .

c) Analogously, for  $f_1 = f_4 = 1$ , we have

$$(4.30) \quad \|\underline{f}\|_\infty = \lambda_1 = \frac{\overbrace{1 - 2 \sin \beta}^{\in ]1-2\zeta+2\epsilon, 1[}}{\underbrace{2 \sin \alpha}_{\in ]-2\epsilon, 2\epsilon[}} \in [1, \infty[ \quad \text{only for } \alpha > 0$$

which is in  $\mathcal{P}'_{\text{low}}$  only for  $\alpha > 0$ .

**Case a)** For  $\alpha < 0$  there is only one vertex in  $\mathcal{Q}'_{\text{low}}$ , hence  $\mathcal{Q}'_{\text{low}}$  consists in this vertex. By Theorem 4.4, this vertex is then the only lowest solution. It has the form

$$(4.31) \quad \underline{f}_{\text{low}} = \left( 1 \quad 1 \quad 1 \quad \frac{1 - 2 \sin \alpha}{2 \sin \beta} \quad \frac{1 - 2 \sin \alpha}{2 \sin \beta} \right)^T.$$

For that case, the end-effector is above the level of  $\mathbf{b}_2, \mathbf{b}_3$  (i. e.  $y > 0$ ): then the last two tendons need much more tension to apply a force in  $y$  direction than the first one does, thus it is optimal to tend the first three with minimum tension and the last two with the necessary tension to balance this.

**Case b)** For  $\alpha > 0$  (i. e.  $y < 0$ ) all tendons except tendon 1 need much tension to apply a force in  $y$  direction. So it is best to have minimum tension in the first tendon; but then the tension in the pairs of tendon 2–3 and 4–5 can be distributed in various ways. Candidates for minimal solutions are found in the segment between the two solutions, i. e. they have the form

$$(4.32) \quad \underline{f}(\tau) := \begin{pmatrix} 1 \\ \tau \frac{1-2 \sin \beta}{2 \sin \alpha} + (1 - \tau) \\ \tau \frac{1-2 \sin \beta}{2 \sin \alpha} + (1 - \tau) \\ \tau + (1 - \tau) \frac{1-2 \sin \alpha}{2 \sin \beta} \\ \tau + (1 - \tau) \frac{1-2 \sin \alpha}{2 \sin \beta} \end{pmatrix} \quad \text{with } \tau \in [0, 1].$$

A lowest solution is obtained at  $\tau_\infty$  when the tensions in tendons 4–5 are equal, i. e.

$$(4.33) \quad \tau_\infty \frac{1 - 2 \sin \beta}{2 \sin \alpha} + (1 - \tau_\infty) = \tau_\infty + (1 - \tau_\infty) \frac{1 - 2 \sin \alpha}{2 \sin \beta},$$



provided that this happens for  $\tau \in [0, 1]$ . This is in fact the case, and the result is

$$(4.34) \quad \tau_\infty = \frac{\sin \alpha}{\sin \alpha + \sin \beta}$$

$$(4.35) \quad \underline{f}(\tau_\infty) = \left( 1 \quad \frac{1}{2(\sin \alpha + \sin \beta)} \quad \cdots \quad \frac{1}{2(\sin \alpha + \sin \beta)} \right)^T$$

$$(4.36) \quad \|\underline{f}(\tau_\infty)\|_\infty = \frac{1}{2(\sin \alpha + \sin \beta)}.$$

Taking Eq. (4.31) and Eq. (4.35) together, we find that for  $\zeta < \frac{1}{2}$ , the lowest solutions are discontinuous at  $\alpha = 0$ :

$$(4.37) \quad \underline{f}_{\text{low}} \xrightarrow{\alpha \nearrow 0} \left( 1 \quad 1 \quad 1 \quad \frac{1}{2 \sin \beta} \quad \frac{1}{2 \sin \beta} \right)^T$$

$$(4.38) \quad \underline{f}_{\text{low}} \xrightarrow{\alpha \searrow 0} \left( 1 \quad \frac{1}{2 \sin \beta} \quad \frac{1}{2 \sin \beta} \quad \frac{1}{2 \sin \beta} \quad \frac{1}{2 \sin \beta} \right)^T.$$

A closer look at the result shows us that these two different limits are the vertices of a segment of lowest solutions at  $\alpha = 0$ . In fact, Theorem 4.4 only states that *there are* lowest solutions in  $\mathcal{Q}'_{\text{low}}$ , not that they are *unique*.

The example shows that the algorithm for finding optimal solutions has a serious drawback: the result may be discontinuous. We will prove later that it can be discontinuous only if the lowest (or highest) solution is not unique. Informally speaking, this happens in our example because at a certain point quite in the central region of workspace, the force contribution of a group of tendons (no. 2 and 3) changes sign for a certain direction (the y axis) and at the point of change, tension of this group is decoupled from the other tensions: they pull in x direction, the others in y direction. This is a phenomenon that is likely to happen for many manipulator geometries near the center of workspace, so the problem has a practical relevance.

#### 4.4.2. Singular Case

Now we will show that any reasonable choice of tensions may fail to be continuous if the manipulator crosses a singularity. We briefly illustrate this with a simple example (Fig. 4.7): three tendons are attached to a single point of the platform and two other ones are connected to points on opposite ends, such that the former tendons only control translation, while the latter control rotation. The construction is asymmetric and rather useless in practice, but it is good to illustrate the problem. From the figure we derive with Eq. (2.36), p. 32:

$$(4.39) \quad \underline{A}^T = \begin{pmatrix} 0 & -\cos \alpha & \cos \alpha & -\cos \beta & \cos \beta \\ -1 & \sin \alpha & \sin \alpha & \sin \beta & \sin \beta \\ 0 & 0 & 0 & -d \sin \beta & 2d \sin \beta \end{pmatrix}$$

and again it is easy to find two independent solutions in the kernel of  $\underline{A}^T$ . First, the tendons 1, 2 and 3 form a subsystem that can be in equilibrium if the other two

tendons are without tension. If instead tendon no. 5 has a positive tension, then tendon no. 4 must have the double amount of tension to balance this. This results in a negative force in x direction, which can be counteracted by forces in tendon no. 2 and no. 3. Then the overall result is a positive force in y direction, so tendon no. 1 must bear this force. As the kernel of  $\underline{A}^T$  is known to be 2-dimensional, any solution is a superposition of these two:

$$(4.40) \quad \ker \underline{A}^T = \left\langle \begin{pmatrix} 2 \sin \alpha & 3 (\cos \alpha \sin \beta + \sin \alpha \cos \beta) \\ 1 & \cos \beta \\ 1 & 2 \cos \beta \\ 0 & 2 \cos \alpha \\ 0 & \cos \alpha \end{pmatrix} \right\rangle.$$

As before, we consider the homogeneous case  $\underline{w} = \underline{0}$  with a normalized minimum tension  $f_{\min} = 1$ . Now if all sines and cosines are positive, the only lowest solution is obtained from the second column in Eq. (4.40), because the first column just adds more tension to the first three tendons without taking it away from the last two ones. If in addition  $\beta$  is small we have  $\beta < \alpha$  and the result is

$$(4.41) \quad \underline{f}_{\text{low}} = \begin{pmatrix} 3 (\tan \alpha \cos \beta + \sin \beta) & \frac{\cos \beta}{\cos \alpha} & 2 \frac{\cos \beta}{\cos \alpha} & 2 & 1 \end{pmatrix}^T.$$

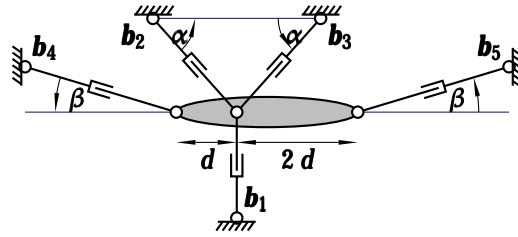


Figure 4.7: Example of discontinuity (singular for  $\beta = 0$ )

Now the geometry was chosen such that  $\alpha = 60^\circ$  when  $\beta = 0$ , i. e. when the tendons 4 and 5 are parallel. Thus, as  $\beta$  approaches zero, we get

$$(4.42) \quad \|\underline{f}_{\text{low}}\|_\infty = 3 (\tan \alpha \cos \beta + \sin \beta) \xrightarrow{\beta \rightarrow 0} 3\sqrt{3},$$

but in the point  $\beta = 0$  itself, we have a singularity because rotation cannot be controlled there<sup>7</sup> and Eq. (4.39)–(4.41) become

$$(4.43) \quad \underline{A}^T = \begin{pmatrix} 0 & -\frac{1}{2}\sqrt{3} & \frac{1}{2}\sqrt{3} & -1 & 1 \\ -1 & \frac{1}{2} & \frac{1}{2} & 0 & 0 \\ 0 & 0 & 0 & 0 & 0 \end{pmatrix}$$

$$(4.44) \quad \ker \underline{A}^T = \left\langle \begin{pmatrix} 1 & 3 & 0 \\ 1 & 2 & 0 \\ 1 & 4 & 0 \\ 0 & 2\sqrt{3} & 1 \\ 0 & \sqrt{3} & 1 \end{pmatrix} \right\rangle$$

<sup>7</sup>This implies that this posture does not belong to the controllable workspace in the sense of Def. 3.1, p. 36, but there may be tasks where a short-time loss of controllability in rotation does not harm [159], so it is worthwhile to check what happens.

$$(4.45) \quad \underline{f}_{\text{low}} = (1 \ 1 \ 1 \ 1 \ 1)^T$$

$$(4.46) \quad \|\underline{f}_{\text{low}}\|_{\infty} = 1.$$

In fact, the continuous extension of the previous solution still exists, but as the kernel of  $\underline{A}^T$  has passed from a 2- to a 3-dimensional space, the range of possible solutions has become much larger and the lowest one is not the extension of the lowest one for positive  $\beta$ . Thus, there is a discontinuity for both  $\underline{f}_{\text{low}}$  and its infinity norm in the point  $\beta = 0$ :

**4.5 Proposition (discontinuity in singularities)** *Singularities, in addition to the loss of controllability, can also break the continuity of optimal tension configurations.*  $\diamond$

It is easy to see that any approach based on minimizing a «reasonable» norm leads to this solution: if we have to respect a lower bound on tensions, if we want to minimize tensions by some norm and if the norm gives the same weight to all tendons, then there cannot be any solution better than that having all tensions equal. This phenomenon is a problem particular to singularities in *tendon-based* parallel systems: it has no equivalent for classical systems with rigid links.

## 4.5. Approximation of Optimal Solutions

As already mentioned in Section 4.4.1, the discontinuity of optimal solutions in certain postures has to do with their non-uniqueness. The lack of uniqueness results from the fact that neither the sets  $\mathcal{P}_{\text{low}}, \mathcal{P}_{\text{high}}$  nor the sets  $\{\underline{f} \in \mathbb{R}^m : \|\underline{f}\|_{\infty} \leq c\}$  are strictly convex. This can be overcome by replacing the infinity norm with some strict  $p$ -norm as defined in Def. A.17, p. 130. These norms are known to approximate the infinity norm as  $p \rightarrow \infty$ . We shall prove in Section 4.6 that for  $p > 1$ , the « $p$ -lowest» and « $p$ -highest» solutions  $\underline{f}_{\text{low},p}, \underline{f}_{\text{high},p}$  obtained that way are *always unique and continuous* except in singularities.

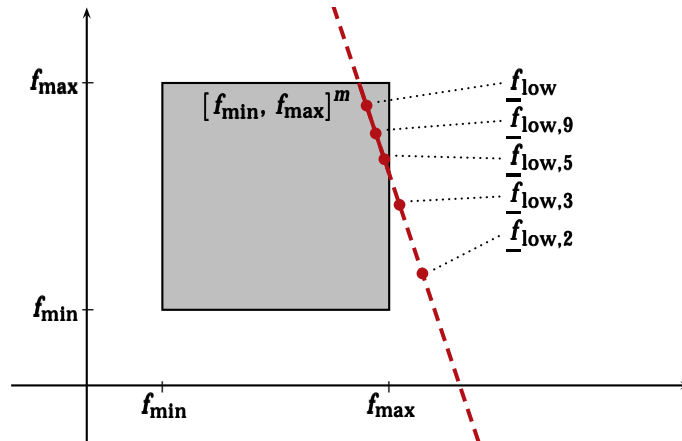


Figure 4.8: Approximation of  $\underline{f}_{\text{low}}$  with  $\underline{f}_{\text{low},p}$

Clearly, the drawback is that such solutions may be not really optimal. In particular, Prop. 4.2 cannot be applied to solutions of that kind, i. e. one might fail to

find acceptable solutions although they exist. For instance, Fig. 4.8 shows a simple example where acceptable lowest solutions exist and the  $p$ -lowest solutions for  $p \geq 5$  are indeed acceptable, but for  $p \leq 3$  they are not.

For illustration, let us continue the example of Section 4.4.1. The proof of Theorem 4.4 can be generalized to show that all  $p$ -norms take a minimum for  $\mathcal{P}_{\text{low}}$  in  $\mathcal{Q}_{\text{low}}$  – in this example,  $\mathcal{Q}'_{\text{low}}$  –. So for  $\alpha < 0$  the point  $f_{\text{low}}$  of Eq. (4.31) is optimal for any  $p$ . In the case of  $\alpha > 0$ , we have to compute the respective  $p$ -norms of the points in  $\mathcal{Q}'_{\text{low}}$ :

$$(4.47) \quad \|\underline{f}(\tau)\|_p = \sqrt[p]{1 + 2 \left( \tau \frac{1-2\sin\beta}{2\sin\alpha} + (1-\tau) \right)^p + 2 \left( \tau + (1-\tau) \frac{1-2\sin\alpha}{2\sin\beta} \right)^p}.$$

As this is a differentiable function, the minimum is taken exactly at that point where the derivative vanishes, provided that this happens inside  $[0, 1]$ . Otherwise it is 0 or 1, whichever is closer to the point found. This leads to the condition

$$(4.48) \quad \tau_p \frac{1-2\sin\beta}{2\sin\alpha} + (1-\tau_p) = \sqrt[p-1]{\frac{\sin\alpha}{\sin\beta}} \left( \tau_p + (1-\tau_p) \frac{1-2\sin\alpha}{2\sin\beta} \right)$$

which looks quite similar to Eq. (4.33). Indeed, both equations coincide when setting  $p = \infty$ . The results are

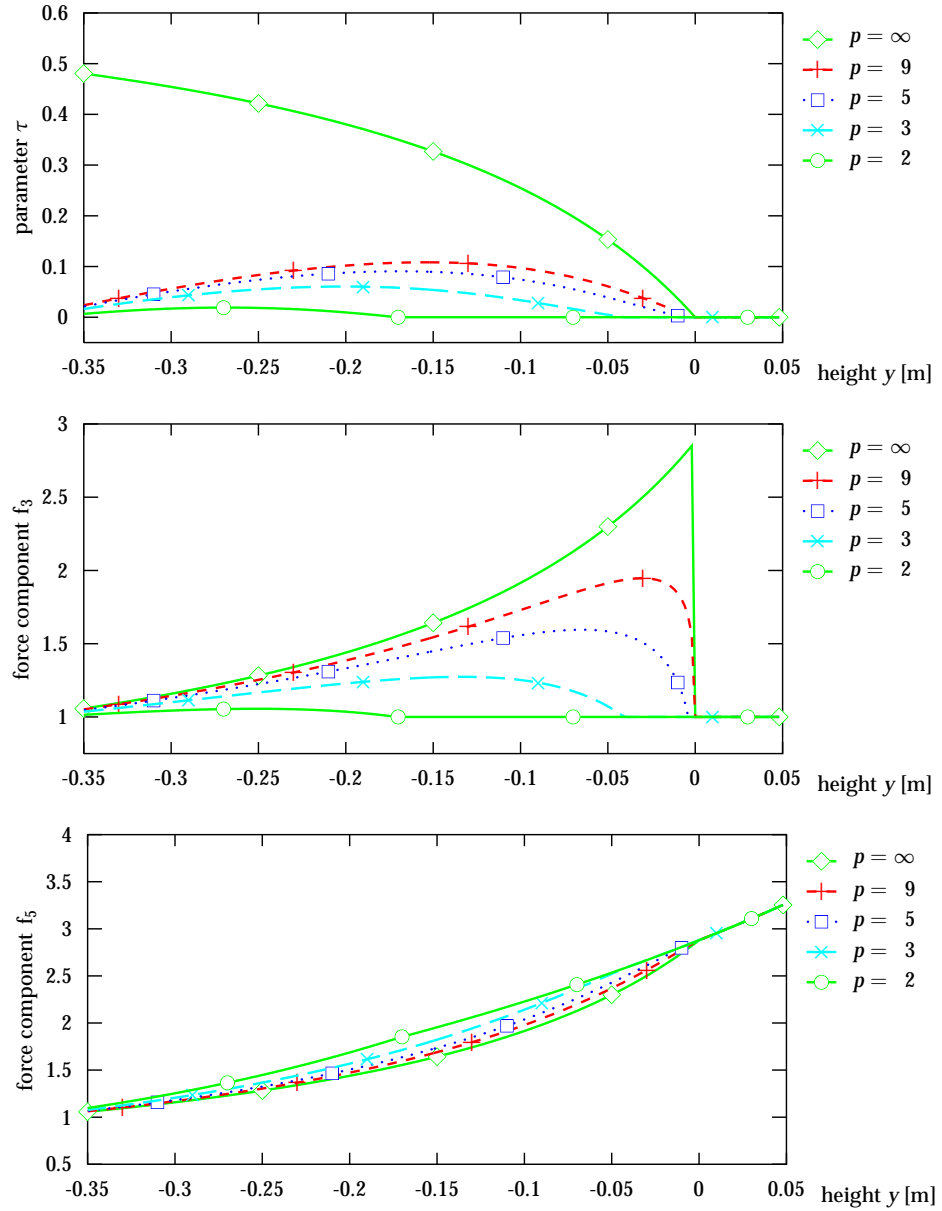
$$(4.49) \quad \tau_p = \max \left\{ \frac{\sin^{\frac{p}{p-1}}\alpha - 2\sin\alpha \left( \sin^{\frac{p}{p-1}}\alpha + \sin^{\frac{p}{p-1}}\beta \right)}{(1-2\sin\alpha - 2\sin\beta) \left( \sin^{\frac{p}{p-1}}\alpha + \sin^{\frac{p}{p-1}}\beta \right)}, 0 \right\}$$

$$(4.50) \quad \underline{f}(\tau_p) = \begin{pmatrix} \frac{1}{\sin^{\frac{1}{p-1}}\alpha} \\ \frac{\sin^{\frac{1}{p-1}}\alpha}{2 \left( \sin^{\frac{p}{p-1}}\alpha + \sin^{\frac{p}{p-1}}\beta \right)} \\ \frac{\sin^{\frac{1}{p-1}}\alpha}{2 \left( \sin^{\frac{p}{p-1}}\alpha + \sin^{\frac{p}{p-1}}\beta \right)} \\ \frac{\sin^{\frac{1}{p-1}}\beta}{2 \left( \sin^{\frac{p}{p-1}}\alpha + \sin^{\frac{p}{p-1}}\beta \right)} \\ \frac{\sin^{\frac{1}{p-1}}\beta}{2 \left( \sin^{\frac{p}{p-1}}\alpha + \sin^{\frac{p}{p-1}}\beta \right)} \end{pmatrix} \quad \text{or} \quad \underline{f}(\tau_p) = \underline{f}(0)$$

$$(4.51) \quad \|\underline{f}_{\text{low},p}\|_{\infty} = \frac{\max \left\{ \sin^{\frac{1}{p-1}}\alpha, \sin^{\frac{1}{p-1}}\beta \right\}}{2 \left( \sin^{\frac{p}{p-1}}\alpha + \sin^{\frac{p}{p-1}}\beta \right)} \quad \text{or} \quad \frac{1-2\sin\alpha}{2\sin\beta}$$

where the second alternative in Eq. (4.50), (4.51) applies if  $\tau_p$  is zero. For  $p = \infty$ , this coincides with the results obtained in Section 4.4.1.

Fig. 4.9 shows the results for some postures according to Fig. 4.6. It can be seen clearly that  $f_3$  has a discontinuity at  $y = 0$  for  $p = \infty$  and that the  $p$ -solutions

Figure 4.9: Comparison of  $p$ -solutions

provide a more or less smooth approximation at that point. An interesting detail is the fact that for  $p = 2$ , we have  $\tau_2 = 0$  already for all  $y \geq -0.2$ : this means that the vertex of case a) is chosen as the best solution. The diagram with the  $f_5$ -values (which coincide with the infinity norms) shows that for this example, it does not harm to choose  $p = 2$  instead of  $p = \infty$  because the maximum component of  $f_{\text{low},p}$  changes just by a very small amount. Here it is maybe the best choice to take  $p = 2$ , considering that the corresponding  $f_3$ -curve is very smooth. The influence of the choice of  $p$  will be examined more in detail in Section 6.2, p. 101 ff.

## 4.6. Proof of Continuity

Now we will show that  $p$ -optimal solutions as defined in the preceding section are unique and continuous along any trajectory  $(\mathbf{r}, \mathbf{R})(t)$  that lies inside the controllable workspace (which implies that it does not cross singularities) provided that the other wrenches  $\underline{w}(t)$  acting on the platform are continuous while performing that trajectory. More precisely, we shall prove:

- For any norm  $\|\cdot\|$ , in particular for any  $p$ -norm with  $p \in [1, \infty]$  (including one and infinity), the minimum *value* of  $\|\underline{f}\|$  on  $\mathcal{P}_{\text{low}}(t)$  is continuous in  $t$ . The same applies to  $\|\underline{f}_{\text{max}} \underline{1} - \underline{f}\|$  on  $\mathcal{P}_{\text{high}}(t)$ .
- In the domain where the minimum-norm solution is *unique*, this *solution* is continuous in  $t$  as well. This is the case for any  $p$ -norm  $p \in ]1, \infty[$  (not including neither one nor infinity).

We prove only the statements about lowest solutions because proofs for the highest ones can be worked out the same way. Without loss of generality, we can assume a normalized minimum force  $f_{\text{min}} = 1$ .

In this section, we need tools from a branch of mathematics called «parametric optimization». It deals with the question of what happens to results of optimization problems if the constraints and/or the objective function changes. There is extensive literature for problems with special kinds of constraints, e. g. fixed constraints, constraint inequalities where only the right hand side depends on parameters, or constraints expressed by a single inequality with a (twice) continuously differentiable function and a (twice) continuously differentiable objective function. But the tension optimization problem is just at the other end of the spectrum: the objective function is fixed, but the constraints are inequalities representing a polyhedron, so they cannot be replaced by a single equation with differentiable terms; and both sides of the inequalities depend on parameters. In addition, we would like to obtain certain results also for the infinity norm, which is a non-differentiable objective function. Therefore, we need a more general theory, as presented by Bank et al. [18]. For convenience of the reader, all the definitions and theorems taken from that book are briefly presented in Section A.5, p. 134 ff. in a form suitable for this dissertation. (This means not only that the notation was adapted to our writing conventions, but also that the propositions were substantially simplified because the tension problem is still a very special case when compared to the whole range of that theory.)

We start by defining some mappings that map a structure matrix  $\underline{A}^T$  and a platform wrench  $\underline{w}$  to the corresponding polyhedron  $\mathcal{P}_{\text{low}}$  or parts of it. Then we show that these point-to-set mappings have certain useful properties. In the following we write  $\|\cdot\|$  to denote an arbitrary norm when the result holds for any norm (including  $\|\cdot\|_p$ ,  $p \in [1, \infty]$ ).

**4.6 Lemma** For  $c \in [1, \infty]$ , define a point-to-set mapping:<sup>8</sup>

$$(4.52) \quad \Gamma^{(c)} : \mathbb{R}^{n \times m} \times \mathbb{R}^n \rightarrow 2^{\mathbb{R}^m},$$

$$\left( \underline{A}^T, \underline{w} \right) \mapsto \left\{ \underline{f} \in \mathbb{R}^m : \underline{A}^T \underline{f} + \underline{w} = \underline{0} \wedge \underline{f} \in [1, c]^m \right\}.$$

---

<sup>8</sup>  $2^{\mathbb{R}^m}$  is the set of all subsets of  $\mathbb{R}^m$ , see Section A.1, p. 123 ff.

We will use  $\Gamma$  as a shorthand for  $\Gamma^{(\infty)}$ .

a) Then the mappings  $\Gamma^{(c)}$ ,  $c \in [1, \infty]$  are closed in the sense of Def. A.28, p. 134.

b) Define the set of those matrices  $\underline{A}^T$  that correspond to postures in the controllable workspace<sup>9</sup> and which have maximal dimension of the polyhedron  $\Gamma^{(c)}(\underline{A}^T, \underline{w})$ :

$$(4.53) \quad \Lambda^{(c)} := \left\{ \left( \underline{A}^T, \underline{w} \right) \in \mathbb{R}^{n \times m} \times \mathbb{R}^n : \begin{aligned} &\text{rank } \underline{A}^T = n \\ &\wedge \ker \underline{A}^T \cap \mathbb{R}_+^m \neq \emptyset \\ &\wedge \dim \Gamma^{(c)}(\underline{A}^T, \underline{w}) = m - n \end{aligned} \right\}.$$

We will use  $\Lambda$  as a shorthand for  $\Lambda^{(\infty)}$ . Then the restricted mapping  $\Gamma^{(c)}|_{\Lambda^{(c)}}$  is lower semicontinuous according to Berge (l. s. c.-B) in the sense of Def. A.28, p. 134.

c) For  $c = \infty$ , the maximum dimension of the polyhedron follows from the other conditions and hence does not depend on  $\underline{w}$ . Thus, the set  $\Lambda$  is simply the set of structure matrices corresponding to postures in the controllable workspace, together with arbitrary wrenches:

$$(4.54) \quad \Lambda = \left\{ \underline{A}^T \in \mathbb{R}^{n \times m} : \text{rank } \underline{A}^T = n \wedge \ker \underline{A}^T \cap \mathbb{R}_+^m \neq \emptyset \right\} \times \mathbb{R}^n.$$

d) Given  $c < \infty$  and a pair  $(\underline{A}_0^T, \underline{w}_0) \in \Lambda^{(c)}$ , we can observe that matrices/vectors close to that pair are contained in a slightly larger parameter set  $\Lambda^{(c+\epsilon)}$ :

$$(4.55) \quad \forall_{\epsilon > 0} \quad \exists_{\delta > 0} \quad \forall_{(\underline{A}^T, \underline{w}) \in \mathbb{R}^{n \times m} \times \mathbb{R}^n} \quad \left( \underline{A}^T, \underline{w} \right) \in \Lambda^{(c+\epsilon)} \quad \diamond \\ \|\underline{A}^T - \underline{A}_0^T\| < \delta \wedge \|\underline{w} - \underline{w}_0\| < \delta$$

**Proof.** a) For  $c < \infty$ , we can write

$$(4.56) \quad \Gamma^{(c)}(\underline{A}^T, \underline{w}) = \left\{ \underline{f} \in \mathbb{R}^m : \begin{pmatrix} -\underline{A}^T \\ \underline{I}_m \\ -\underline{I}_m \end{pmatrix} \underline{f} - \begin{pmatrix} -\underline{w} \\ \underline{w} \\ c \underline{1} \\ -\underline{1} \end{pmatrix} \leq \underline{0} \right\}$$

and thus, the mapping  $\Gamma^{(c)}$  is closed by Theorem A.30, p. 135. Similarly,  $\Gamma^{(\infty)}$  is closed (because the definition of  $\Gamma$  can be written in much the same way, just leaving out the third row in the above inequality).

b) The characteristic index set (Def. A.29, p. 135) for the representation Eq. (4.56) includes the first  $2n$  indexes. As  $\dim \Gamma^{(c)}(\underline{A}^T, \underline{w}) = m - n$ , any other elements of the characteristic index set denote equations which are linearly dependent on

<sup>9</sup>To be precise: postures in the controllable workspace have such matrices, but there may be such matrices that do not correspond to any postures because they cannot be written in the form of Eq. (2.23), p. 26.



the first  $2n$  ones. Thus, the region of  $\mathbb{R}^m$  where the inequalities belonging to the characteristic index set are fulfilled is the solution set of the equation

$$(4.57) \quad \underline{A}^T \underline{f} + \underline{w} = \underline{0}.$$

This is a (by assumption of maximum dimension) nonempty affine subspace of  $\mathbb{R}^m$  and hence equal to its own lineality space. The dimension of this space is  $m - \text{rank } \underline{A}^T$  and therefore, by definition of the mapping restriction, it does not change within  $\Lambda^{(c)}$ . Now Theorem A.30, p. 135 implies that the mapping is l. s. c.-B.

c) Assume that  $\text{rank } \underline{A}^T = n \wedge \ker \underline{A}^T \cap \mathbb{R}_+^m \neq \emptyset$ . Then the idea is similar to the proof of Prop. 3.2, p. 36: as  $\underline{A}^T$  is of full rank, it has a Moore-Penrose pseudo inverse and a particular (maybe not positive) solution of the tension problem is

$$(4.58) \quad \underline{f}_0 := -\underline{A}^{+T} \underline{w}.$$

Now, by the above assumption  $\ker \underline{A}^T \cap \mathbb{R}_+^m \neq \emptyset$ , there is an element  $\underline{h} \in \ker \underline{A}^T \cap \mathbb{R}_+^m$  and this allows to find a solution of the tension problem that lies in the set  $]1, \infty[^m$ :

$$(4.59) \quad \underline{f}_0 + 2 \left( \max_{1 \leq \mu \leq m} \frac{1 - f_{0,\mu}}{h_\mu} \right) \underline{h} \in ]1, \infty[^m.$$

As the set  $]1, \infty[^m$  is open (Def. A.18, p. 131), its intersection with the affine space of solutions of Eq. (4.57) has the same dimension as that affine space itself according to Lemma A.21, p. 132. Now  $\Gamma(\underline{A}^T, \underline{w})$  contains this intersection, hence  $\Gamma(\underline{A}^T, \underline{w})$  has maximum dimension.

d) The assumptions include that  $\Gamma^{(c)}(\underline{A}_0^T, \underline{w}_0)$  is  $(m - n)$ -dimensional and convex. Then by Lemma A.21, p. 132, its relative interior (Def. A.20, p. 132) is  $(m - n)$ -dimensional, too. This means that we can find  $m - n + 1$  affinely independent points  $\underline{f}_{0,0}, \dots, \underline{f}_{0,m-n}$  (Def. A.12, p. 127) in its interior, hence for sufficiently small  $\epsilon$ , we have

$$(4.60) \quad \underline{A}_0^T \underline{f}_{0,\mu} + \underline{w}_0 = \underline{0} \wedge \underline{f}_{0,\mu} \in [1 + \epsilon, c]^m.$$

Then it is possible to find matrices  $\underline{B}_\mu \in \mathbb{R}^{(m-n) \times m}$  and vectors  $\underline{b}_\mu \in \mathbb{R}^{(m-n)}$  such that for each  $\mu \in \{0, \dots, m - n\}$  the matrix  $\begin{pmatrix} \underline{A}_0^T & \underline{B}_\mu^T \end{pmatrix}$  has rank  $m$  and  $\underline{f}_{0,\mu}$  is the unique solution of

$$(4.61) \quad \begin{pmatrix} \underline{A}_0^T \\ \underline{B}_\mu^T \end{pmatrix} \underline{f}_{0,\mu} = \begin{pmatrix} -\underline{w}_0 \\ \underline{b}_\mu \end{pmatrix}.$$

If a matrix has full rank, any other matrix sufficiently close to it has full rank, too; and the solution of a full-rank system of linear equations depends continuously on both the coefficient matrix and the right-hand side. Both facts imply

$$(4.62) \quad \begin{aligned} & \exists_{\delta > 0} \quad \forall_{(\underline{A}^T, \underline{w}) \in \mathbb{R}^{n \times m} \times \mathbb{R}^n} \quad \text{rank} \begin{pmatrix} \underline{A}^T \\ \underline{B}_\mu \end{pmatrix} = m \\ & \quad \|\underline{A}^T - \underline{A}_0^T\| < \delta \wedge \|\underline{w} - \underline{w}_0\| < \delta \quad \wedge \quad \left\| \underbrace{\begin{pmatrix} \underline{A}^T \\ \underline{B}_\mu \end{pmatrix}^{-1} \begin{pmatrix} \underline{w} \\ \underline{b}_\mu \end{pmatrix}}_{=: \underline{f}_\mu} - \underline{f}_{0,\mu} \right\|_\infty < \epsilon; \end{aligned}$$

this supplies  $(m - n + 1)$  affinely independent points  $\underline{f}_\mu$  for sufficiently small  $\delta$ . In addition, we have

$$(4.63) \quad \underline{f}_\mu \in [1, c + \epsilon]^m \quad \text{and thus} \quad \underline{f}_\mu \in \Gamma^{(c+\epsilon)}(\underline{A}^T, \underline{w}) .$$

Thus, the set  $\Gamma^{(c+\epsilon)}(\underline{A}^T, \underline{w})$  contains  $(m - n + 1)$  affinely independent points. Similarly, it can be shown that for sufficiently small  $\epsilon$ , we also have  $\ker \underline{A}^T \cap \mathbb{R}_+^m \neq \emptyset$ . All this implies then  $(\underline{A}^T, \underline{w}) \in \Lambda^{(c+\epsilon)}$ .  $\square$

The next theorem states that the minimum *value* of any norm (including  $p$ -norms with  $p \in [1, \infty]$ ) on  $\mathcal{P}_{\text{low}}$  depends continuously on the structure matrix and the platform wrench, as long as the manipulator moves inside the controllable workspace. Furthermore there is always a tension distribution *reaching* this minimum value.

**4.7 Theorem** For any norm  $\|\cdot\|$  on  $\mathbb{R}^m$ , let

$$(4.64) \quad \Phi : \Lambda \rightarrow [1, \infty[ ,$$

$$(4.65) \quad (\underline{A}^T, \underline{w}) \mapsto \inf \left\{ \|\underline{f}\| : \underline{f} \in \Gamma(\underline{A}^T, \underline{w}) \right\} .$$

a) This mapping is continuous.

b) For each  $(\underline{A}^T, \underline{w})$ , there is an  $\underline{f} \in \Gamma(\underline{A}^T, \underline{w})$  with

$$(4.66) \quad \|\underline{f}\| = \Phi(\underline{A}^T, \underline{w}) . \diamond$$

**Proof.** We prove continuity in each single point  $(\underline{A}_0^T, \underline{w}_0) \in \Lambda$ . Due to the equivalence of all norms on  $\mathbb{R}^m$  (Theorem A.22, p. 132), there is a factor  $c_1 \geq 1$  such that

$$(4.67) \quad \forall_{\underline{f} \in \mathbb{R}^m} \|\underline{f}\|_\infty \leq c_1 \|\underline{f}\| .$$

By definition of  $\Phi$ , for each  $\epsilon > 0$  there is an  $\underline{f} \in \Gamma(\underline{A}_0^T, \underline{w}_0)$  with

$$(4.68) \quad \|\underline{f}\|_\infty \leq c_1 \|\underline{f}\| < c_1 \left( \Phi(\underline{A}_0^T, \underline{w}_0) + \epsilon \right)$$

and therefore  $\Gamma(\underline{A}_0^T, \underline{w}_0) \cap ]0, c_1 \Phi(\underline{A}_0^T, \underline{w}_0) + c_1 \epsilon]^m$  is the nonempty intersection of the convex  $(m - n)$ -dimensional  $\Gamma(\underline{A}_0^T, \underline{w}_0)$  with an open set, thus  $(m - n)$ -dimensional itself (Lemma A.21, p. 132). It follows

$$(4.69) \quad (\underline{A}_0^T, \underline{w}_0) \in \Lambda^{(c_1 \Phi(\underline{A}_0^T, \underline{w}_0) + c_1 \epsilon)} .$$

If we set

$$(4.70) \quad c := c_1 \Phi(\underline{A}_0^T, \underline{w}_0) + 2 c_1 \epsilon ,$$

then by Lemma 4.6d, we can find a small  $\delta > 0$  such that

$$(4.71) \quad \mathcal{U}_\delta(\underline{A}_0^T, \underline{w}_0) \subset \Lambda^{(c)}$$

where

$$(4.72) \quad U_\delta(\underline{A}_0^T, \underline{w}_0) := \left\{ (\underline{A}^T, \underline{w}) \in \mathbb{R}^{n \times m} \times \mathbb{R}^n : \begin{array}{l} \|\underline{A}^T - \underline{A}_0^T\| < \delta \\ \wedge \quad \|\underline{w} - \underline{w}_0\| < \delta \end{array} \right\}.$$

This is an open environment of  $(\underline{A}_0^T, \underline{w}_0)$  and it is sufficient to show continuity of the restricted mapping  $\Phi|_{U_\delta(\underline{A}_0^T, \underline{w}_0)}$  (Def. A.1, p. 124). Now, Eq. (4.71) implies that for all  $(\underline{A}^T, \underline{w}) \in U_\delta(\underline{A}_0^T, \underline{w}_0)$ , we have

$$(4.73) \quad \Phi(\underline{A}^T, \underline{w}) = \inf \left\{ \|\underline{f}\| : \underline{f} \in \Gamma^{(c)}(\underline{A}^T, \underline{w}) \right\}.$$

By Lemma 4.6a,  $\Gamma^{(c)}$  is closed and then the restricted mapping  $\Gamma^{(c)}|_{U_\delta(\underline{A}_0^T, \underline{w}_0)}$  is still closed. We set

$$(4.74) \quad \mathcal{K} := [1, c]^m;$$

this is compact and for each  $(\underline{A}^T, \underline{w}) \in U_\delta(\underline{A}_0^T, \underline{w}_0)$ , we find that

$$(4.75) \quad \Gamma^{(c)}(\underline{A}^T, \underline{w}) \cap \mathcal{K} = \Gamma^{(c)}(\underline{A}^T, \underline{w}) \neq \emptyset \quad \text{is compact.}$$

As all norms on  $\mathbb{R}^n$  are equivalent, the  $\|\cdot\|$ -norm is continuous, so it takes a minimum on this compact set for each  $\underline{A}^T$ . This proves b).

Then Theorem A.31b, p. 136 implies that the mapping  $\Phi|_{U_\delta(\underline{A}_0^T, \underline{w}_0)}$  is *lower* semicontinuous (Def. A.27, p. 133) in  $(\underline{A}_0^T, \underline{w}_0)$ . On the other hand, Lemma 4.6b implies that  $\Gamma^{(c)}$  is l.s.c.-B in  $(\underline{A}_0^T, \underline{w}_0)$ ; now Theorem A.31a, p. 136 tells us that the mapping in  $\Phi|_{U_\delta(\underline{A}_0^T, \underline{w}_0)}$  is also *upper* semicontinuous in  $(\underline{A}_0^T, \underline{w}_0)$ . And this means that it is continuous in  $(\underline{A}_0^T, \underline{w}_0)$ .  $\square$

Next, we consider the set of minimum-norm points in the polyhedron  $\Gamma(\underline{A}^T, \underline{w})$ , which in general may contain more than one point. We show that, if the set contains a unique point, then the application that maps  $(\underline{A}^T, \underline{w})$  to this point is continuous.

**4.8 Lemma** *Define the mapping*

$$(4.76) \quad \Theta : \Lambda \rightarrow 2^{\mathbb{R}^m}, \quad (\underline{A}^T, \underline{w}) \mapsto \left\{ \underline{f} \in \mathbb{R}^m : \|\underline{f}\| \leq \Phi(\underline{A}^T, \underline{w}) \right\}.$$

a) *Then the mapping  $\Theta \cap \Gamma$  (defined according to Def. A.28, p. 134) is closed.*

b) *Furthermore  $\Theta \cap \Gamma$  is u. s. c.-B (Def. A.28b, p. 134).*

c) *Define the set where this mapping yields unique points:*

$$(4.77) \quad \Lambda_1 := \left\{ (\underline{A}^T, \underline{w}) \in \Lambda : |(\Theta \cap \Gamma)(\underline{A}^T, \underline{w})| = 1 \right\}$$

*For  $(\underline{A}^T, \underline{w}) \in \Lambda_1$ , let  $\underline{f}_{\text{low}}$  be the unique point in  $(\Theta \cap \Gamma)(\underline{A}^T, \underline{w})$ . Then the mapping*

$$(4.78) \quad \Psi : \Lambda_1 \rightarrow \mathbb{R}^m, \quad (\underline{A}^T, \underline{w}) \mapsto \underline{f}_{\text{low}}$$

*is continuous.*  $\diamond$

**Proof.** a) As the  $\|\cdot\|$  norm is convex and continuous, the mapping  $\Theta \cap \Gamma$  fulfills all the conditions of Theorem A.30a, p. 135 (cf. proof of Lemma 4.6a).

b)  $\Gamma|_{\Lambda}$  is closed and l. s. c.-B due to Lemma 4.6 and the image sets of  $\Gamma$  are convex;  $\Phi$  is continuous by Theorem 4.7; the sets  $(\Theta \cap \Gamma)(\underline{A}^T, \underline{w})$  are nonempty by Theorem 4.7 and bounded. Theorem A.30c, p. 135 then implies that this mapping is u. s. c.-B.

c) The definition of «u. s. c.-B» implies that, if a point-to-set mapping is u. s. c.-B and the image sets consist in single points, then the mapping to these points is continuous.  $\square$

Finally, we remark that strict norms on  $\mathbb{R}^m$  always lead to unique minimal points. This includes the  $p$ -norms with  $1 < p < \infty$  and implies the desired result that for these norms, the mapping from  $(\underline{A}^T, \underline{w})$  to the lowest point is continuous.

**4.9 Corollary** a) Let  $\|\cdot\|$  be a strict norm. Then we have  $\Lambda_1 = \Lambda$ .

b) For  $p \in ]1, \infty[$ , there is always a unique point  $\underline{f}_{\text{low},p}$  and the mapping  $\underline{A}^T \mapsto \underline{f}_{\text{low},p}$  is continuous.  $\diamond$

**Proof.** We just have to prove that points of minimal norm over a convex set are unique with strict norms. Now, if there were two distinct points of minimal norm, then there would be a convex combination of them with a strictly smaller norm, which is impossible.  $\square$

## 4.7. Practical Computation

To compute optimal solutions, one has to resolve a nonlinear optimization problem. This could be done with standard software packages, but there are some reasons why it is appropriate to implement a tailor-made solution:

- As the objective function is not linear, derivatives of the simplex algorithm cannot be used; as the constraints cannot be expressed in a single twice differentiable function, the most common second-order methods cannot be applied, either. So the problem is too general for many packages.
- On the other hand, the constraints are of quite special nature (intersection of an affine space with some axis-parallel halfspaces). One can make use of this to minimize computation time, but this is hardly possible with standard software.
- The objective function may involve high powers (if  $p$  is large). Such computation is likely to become a source of numerical problems unless it is implemented quite carefully.

Therefore, a proprietary implementation in C++ was prepared. We shall describe the computation of  $\underline{f}_{\text{low}}$ ; the method for  $\underline{f}_{\text{high}}$  is similar. Some details will be given in footnotes: they are not necessary to understand the algorithm as such,

though they are needed to make the implementation work properly. (These details also show how problem-specific tricky solutions can – and sometimes must – be used here.)

Immediately one might think that a good way to start could be the computation of the polyhedron  $\mathcal{Q}_{\text{low}}$ , i. e. of the vertices of  $\mathcal{P}_{\text{low}}$ . This provides a compact set which contains the optimal solution and compact sets are always fine in numerics. It also gives a good overview on the entire set of acceptable solutions: the vertices of  $\mathcal{P}_{\text{low}}$  are those points in  $\mathcal{P}_{\text{low}}$  which have  $(m - n)$  components equal to  $f_{\min}$ , and all elements of  $\mathcal{Q}_{\text{low}}$  are convex combinations of these vertices. This knowledge may be useful in some applications for sophisticated fine-tuning of tensions. However, computation of the vertices of a polyhedron is extremely time-consuming, because basically one has to compute *all* the intersections of

$$(4.79) \quad \mathcal{A} := \left\{ \underline{f} \in \mathbb{R}^m : \underline{A}^T \underline{f} + \underline{w} = \underline{0} \right\}$$

with  $(m - n)$  out of  $m$  axis-parallel planes and then to check which of the intersection points are contained in  $\mathcal{P}_{\text{low}}$ . The total number of points to check is therefore  $\binom{m}{m-n}$ . For instance, a spatial manipulator with 6 DOFs actuated by 12 tendons would lead to 1848 points (for  $\mathcal{Q}_{\text{low}}$  and  $\mathcal{Q}_{\text{high}}$  together). This is certainly not appropriate, at least for real-time applications.

For that reason, the chosen implementation does not compute any vertices. But without knowledge of vertices, it is not even trivial to find an element of  $\mathcal{P}_{\text{low}}$  at all (a so-called *feasible point*), also because  $\mathcal{P}_{\text{low}}$  may be empty, in which case no solution exists. Or  $\mathcal{P}_{\text{low}}$  may be very small and then it is hard to find elements of it. Therefore, the algorithm consists of three major steps:

1. Obtain an initial guess for  $\underline{f}_{\text{low}}$ , possibly such that in many cases it is contained in  $\mathcal{P}_{\text{low}}$ .
2. If the initial guess is not yet in  $\mathcal{P}_{\text{low}}$ , move towards  $\mathcal{P}_{\text{low}}$  until a feasible point is found.
3. Move along the negative gradient of the chosen objective function until some termination criterion applies. There are several termination criteria.

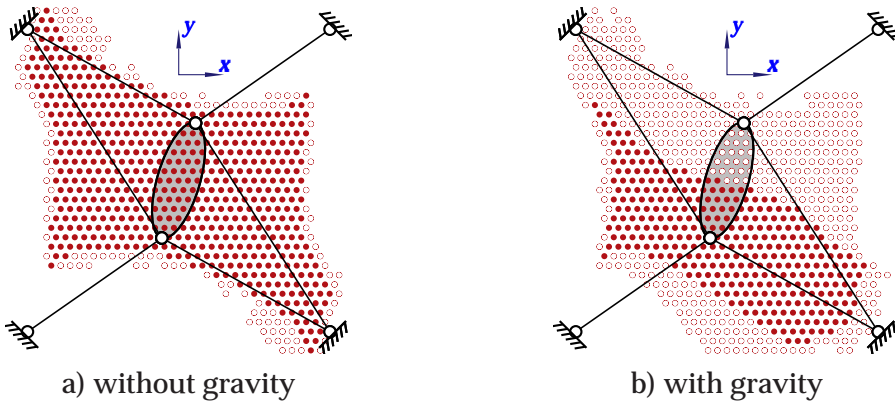


Figure 4.10: Region of acceptable solutions of a 1R2T system

The initial guess is computed as the orthogonal projection of the vector  $\underline{1}$  onto the kernel of  $\underline{A}^T$ , as explained in the context of Prop. 3.3, p. 38. The initial guess itself is not always a positive solution, as illustrated in Fig. 4.10a: the solid circles represent positions of the origin of  $\mathcal{K}_P$  where this is the case, while the empty ones show positions where only the subsequent iterations supply a positive solution.

In the homogeneous case ( $\underline{w} = \underline{0}$ ), appropriate scaling then provides a feasible point. For the inhomogeneous case, one can use the same approach by transforming the problem to a homogeneous one (similar to Eq. (2.31), p. 29):

$$(4.80) \quad \underbrace{\begin{pmatrix} \underline{A}^T & \underline{w} \end{pmatrix}}_{=: \underline{A}'^T} \underbrace{\begin{pmatrix} \underline{f} \\ \underline{f}_{m+1} \end{pmatrix}}_{=: \underline{f}'} = \underline{0}.$$

A positive solution to this equation exists if and only if a positive solution to the original inhomogeneous one exists. Again, we project the vector  $\underline{1}$  (which is now  $(m+1)$ -dimensional rather than  $m$ -dimensional) onto  $\ker \underline{A}'^T$ . Then the result has to be scaled such that  $\underline{f}_{m+1} = 1$  and the resulting  $\underline{f}$  is a (hopefully feasible) solution to the inhomogeneous problem. Fig. 4.10b represents the result for an example with gravity.

The big advantage of this initial guess method is that it can be calculated in closed form without iteration, so it is very fast. Fig. 4.10 shows that often the initial guess is already acceptable, so for very time-critical applications where tension optimization is secondary, this may even be sufficient if the trajectory performed is not too close to the border of the controllable workspace. The figures also show that this works better in the homogeneous case (without gravity) than in the inhomogeneous one (which is not surprising, considering that in the first case we can obtain  $\underline{f} \geq \underline{f}_{\min}$  by appropriate scaling, while in the second, the scaling factor is fixed by the requirement  $\underline{f}_{m+1} = 1$ ).

Computation of the initial guess is represented by item n° 1 in the flowchart Fig. 4.11. We will now roughly present the algorithm following the flowcharts, but the explanation does not perfectly fit them because the implementation requires sometimes a certain order of operations, while a different order is easier to explain.

The second major step starts with item n° 2 in Fig. 4.11, by calculating the gradient of the distance from the current approximation  $\underline{f}$  to the polyhedron  $\mathcal{P}_{\text{low}}$ , where distance is measured with the squared 2-norm. This is the notion of distance whose gradient is most easy to compute and tests have shown that use of other distance functions does not decrease the number of required iterations. If  $\underline{d}$  is zero,  $\underline{f}$  is feasible and we can proceed with the actual optimization (see below and Fig. 4.12).

Otherwise we start the outermost loop in the figure (shown with dark background), trying to enter  $\mathcal{P}_{\text{low}}$  with item n° 5. As the current  $\underline{f}$  is contained in  $\mathcal{A}$ , we remain inside  $\mathcal{A}$  if and only if any vectors we add to  $\underline{f}$  are contained in  $\ker \underline{A}^T$ . Thus, we project the vector  $\underline{d}$  orthogonally into  $\ker \underline{A}^T$ . This provides a descent direction (in the terminology of [21, Sec. 2.2.1]). Now we have to find a good step size. We compute the minimum scaling factor  $s_{\min}$  of the direction

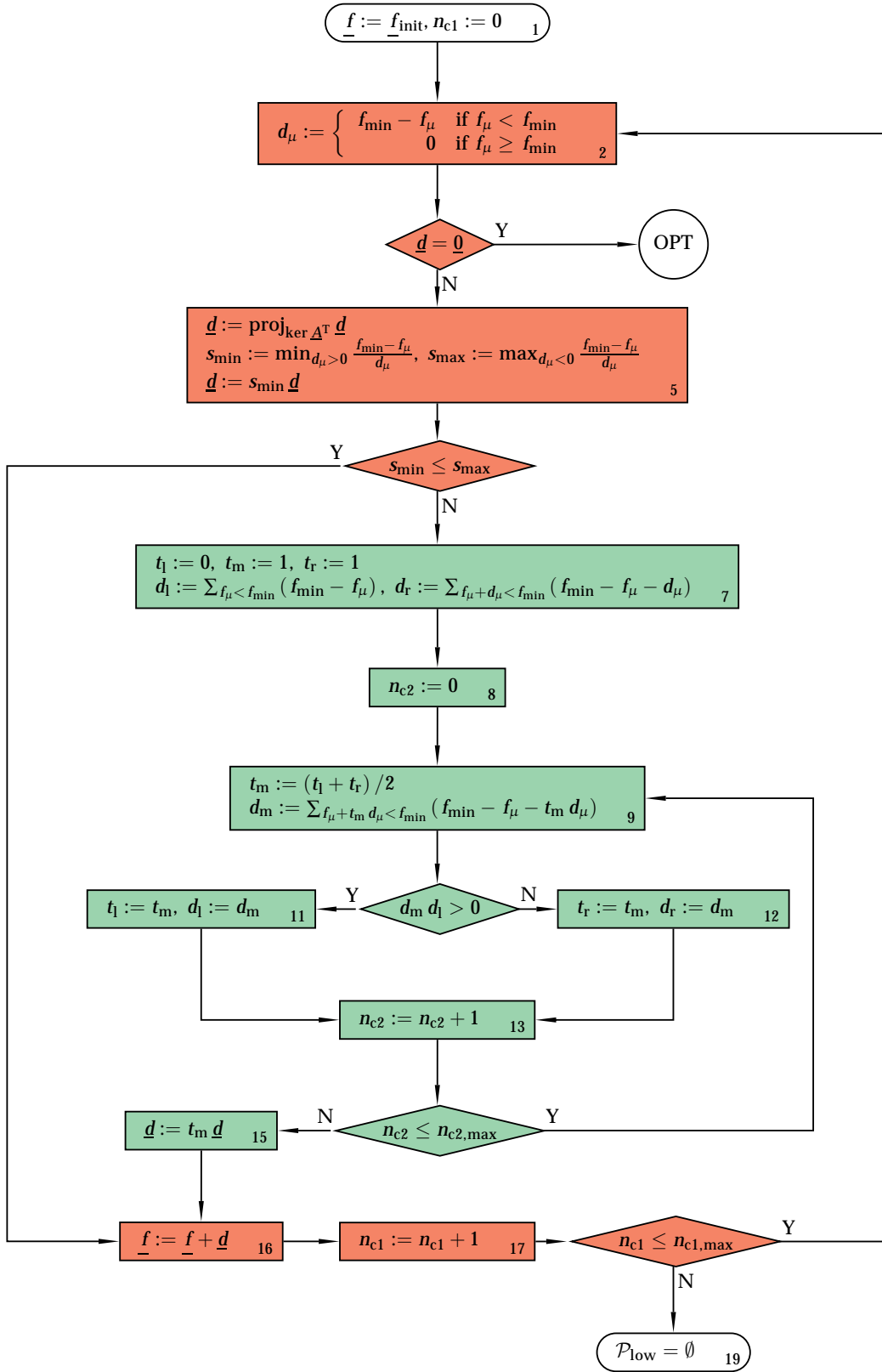


Figure 4.11: Tension computation algorithm, part 1



that we need to *enter* the set  $[f_{\min}, \infty[^m$  and the maximum factor  $s_{\max}$  we can use without *leaving* it (because if the step size is too large, we might step over  $\mathcal{P}_{\text{low}}$  and leave it again on the opposite side). If the minimum step size is less than or equal to the maximum, then we apply it<sup>10</sup> (item n° 16) and start the next loop unless the maximum number of iterations is reached. If we exceed the maximum number of iterations,  $\mathcal{P}_{\text{low}}$  is empty or at least so small that no feasible point could be found.

If the minimum step size found in item n° 3 is greater than the maximum one, we cannot enter  $\mathcal{P}_{\text{low}}$  in this step, we can only try to get as close as possible. Therefore, we compute that step size (between zero and the computed minimum) where the distance to  $\mathcal{P}_{\text{low}}$  becomes minimal (this step size strategy is called limited minimization rule [21, Eq. (2.8)]), where distance again is measured in the squared 2-norm. This is a compact one-dimensional optimization problem with a differentiable function known to have at most one minimum in the given interval. We solve it by finding the zero of the derivative using bisection (the innermost loop in the figure, shown with light background). Bisection methods may be slower than Newton methods, but they have the advantage of providing a result of known precision after a known number of steps.<sup>11</sup> This is particularly important in real-time applications where safety is an issue (e.g. when transporting injured persons in rescue applications).

The third major step minimizes the value of the objective function inside  $\mathcal{P}_{\text{low}}$ , once a feasible point is found. For the objective function we have chosen the  $p$ th

---

<sup>10</sup>The actual implementation is more complicated: tests have shown that in unfavorable conditions, such a step size may be extremely large and it can lead so far away that we would not approach the optimal solution with a reasonable number of iterations. Therefore, the step size is limited to a value that equals  $f_{\min}$  in the first loop and may increase up to  $f_{\max}$  in subsequent iterations. In other words, at the beginning we try to enter the feasible region with caution in small steps and we become more daring if this does not help.

On the other hand, the initial guess may be extremely far away in the negative quadrant and such a strict step size limitation can inhibit from entering the feasible region. Therefore, if the current value of  $f$  still has negative components, the step size limit is relaxed such that positive values can be reached within a single step.

<sup>11</sup>As the bisection steps involve only vector operations, they are much cheaper than the steps in the outer loop which have matrix operations. Hence, it is a good idea to compute the bisection result with a very high precision, as the number of iterations increases only logarithmically with the precision and this may save steps in the outer loop. In addition, if the bisection precision is only in the order of magnitude of the requested result precision, the algorithm may arrive at an infinite oscillation between two solutions. The precision used in the current implementation is about 100 times the machine precision.

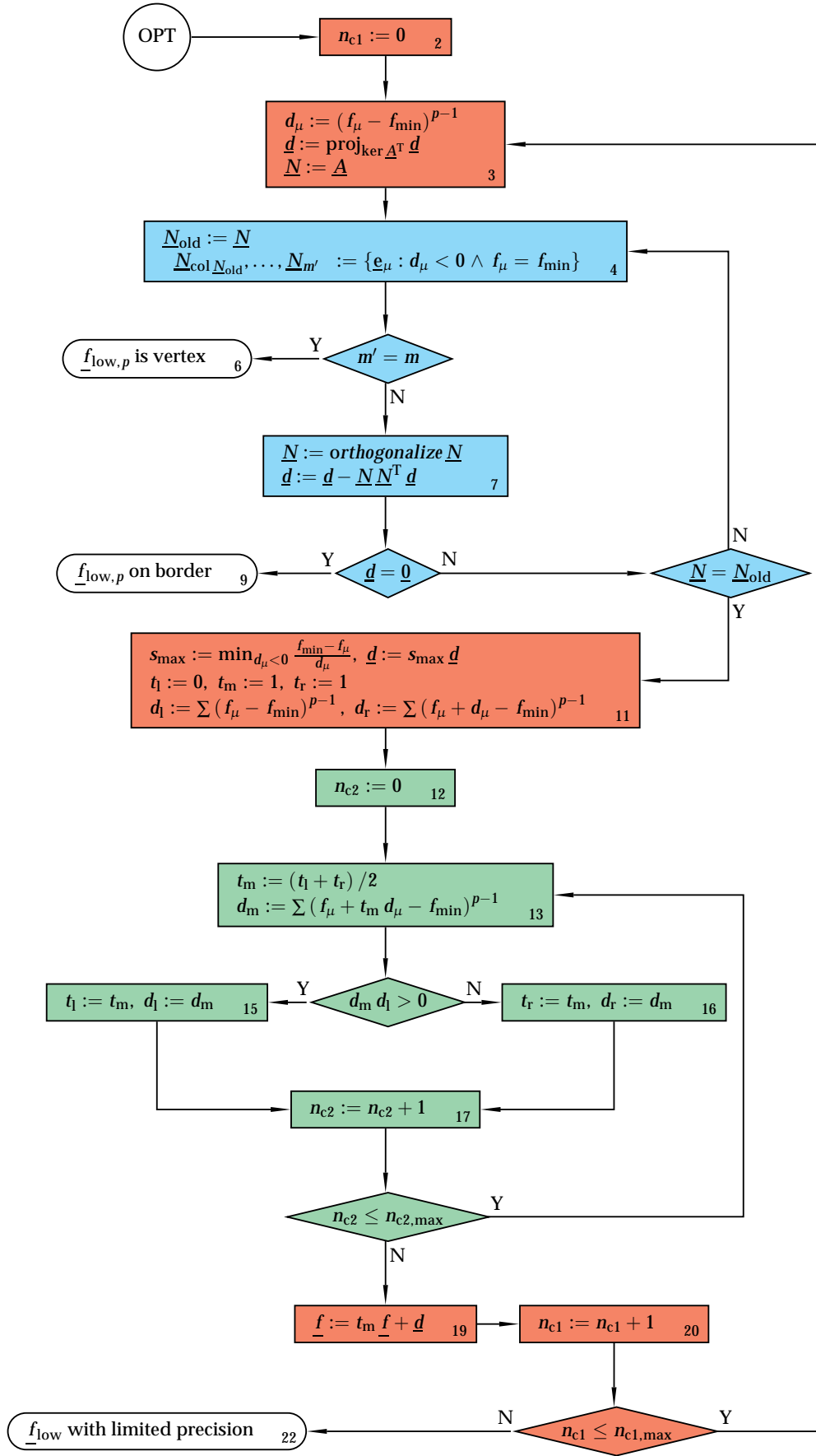


Figure 4.12: Tension computation algorithm, part 2

power of some  $p$ -norm<sup>12</sup> with  $p < \infty$ . The infinity norm is necessarily excluded because it is not differentiable, so gradient methods cannot be applied directly.<sup>13</sup>

In item n° 3 (Fig. 4.12), we compute the gradient of the objective function<sup>14</sup> and project it onto  $\ker \underline{A}^T$  as before. But unlike the second major step, this is not sufficient because not only we have to stay inside  $\mathcal{A}$  but even inside  $\mathcal{P}_{\text{low}} \subset \mathcal{A}$ . Therefore we check if the current  $\underline{f}$  lies on the border<sup>15</sup> of  $\mathcal{P}_{\text{low}}$ . If so, we project the current  $\underline{d}$  onto this border. This is done in the first inner loop in the figure: in item n° 4, we collect all the indices  $\mu \in \{1, \dots, m\}$  where  $f_\mu$  is on the border and  $d_\mu$  points out of  $\mathcal{P}_{\text{low}}$ . If these are  $(m - n)$  indices, this means that we have found the optimum in a vertex and the algorithm terminates successfully.

Otherwise, we set up a matrix  $\underline{N}$  whose columns are those of matrix  $\underline{A}$  plus the canonical unit vectors belonging to the collected indices. Then (item n° 7) we project  $\underline{d}$  onto the orthogonal complement of this matrix.<sup>16</sup>

If the result is zero, this means that the gradient of the objective function is orthogonal to the border of  $\mathcal{P}_{\text{low}}$  and again the iteration terminates successfully. Otherwise, we may have to repeat the whole procedure because the projection might have modified  $\underline{d}$  such that it now points out of  $\mathcal{P}_{\text{low}}$  in some other coordinate. Therefore we loop through this part until the number of collected indices is constant.

When this loop is done, we compute the maximum step size that allows us to remain inside  $\mathcal{P}_{\text{low}}$  (item n° 11). Now, in the second inner loop in the figure,

---

<sup>12</sup>Actually, the objective function is not  $\|\cdot\|_p^p$  which has been used so far in the theoretical discussion, but  $\|\cdot - f_{\min} \underline{1}\|_p^p$  because this is more symmetric to the objective function  $\|f_{\max} \underline{1} - \cdot\|_p^p$  used for  $\mathcal{P}_{\text{high}}$ . The results of the preceding sections apply to this as well and the optima found are almost the same.

Furthermore high values of  $p$  suffer from the fact that their gradients are almost axis-parallel in large regions. This often leads to very small step sizes. Therefore, the current implementation always starts with  $p = 2$  and then increases  $p$  in each iteration step up to the requested value. Thus, the first large steps towards smaller  $\underline{f}$  can be done fast and then the final fine-tuning is done with the actually desired norm.

<sup>13</sup>One could still figure out similar methods, considering that the behavior of  $\|\cdot\|_\infty$  in the non-differentiable points is not that complicated. But after all, the added value in practice does not seem to justify such extra effort.

<sup>14</sup>If  $p$  is large, the powers with exponent  $(p - 1)$  can have large errors or even exceed the numerical range on the machine (either towards zero or towards infinity). But at this point, only the direction of  $\underline{d}$  is important while the scale does not matter. So before computing powers, the vector is rescaled such that the logarithms of the absolute values of the single components are distributed evenly around zero. Then the powers are computed: if the result is infinite, the vector  $\underline{d}$  is rescaled to half of its length until the result is finite. This exploits to the best the numerical range at disposition.

<sup>15</sup>The decision whether  $f_\mu = f_{\min}$ , is a very critical aspect of the entire algorithm. If we admit equality with a large tolerance, we find points distant from the real border of  $\mathcal{P}_{\text{low}}$  and if  $\mathcal{Q}_{\text{low}}$  is small, we may fail to find acceptable solutions. On the other hand, if we ask for equality too strictly, we may make a lot of extremely small steps towards the border which do not take us much closer to the optimal solution. As a compromise, the implementation uses a border tolerance which is the geometric mean between the requested result precision and the machine precision.

<sup>16</sup>Actually, the implementation does not orthogonalize  $\underline{N}$  at this point. Instead, an orthogonalized version of  $\underline{A}$  is computed before the entire iteration. The matrix  $\underline{N}$  starts with this and then it is re-orthogonalized each time a vector  $\underline{e}_\mu$  is added. It is a bit tricky to implement this in an optimal way because the number of columns deriving from  $\underline{A}$  may decrease if the projections of two columns become linearly dependent.

we find a step size (between zero and the maximum step size) via limited minimization rule as in the first major step above,<sup>17</sup> and we apply it (item n° 11). The whole (outer) loop is repeated until it terminates in one of the above mentioned cases, or the absolute value of the last step is less than the requested precision,<sup>18</sup> or the maximum number of iterations is reached. In the latter case, the algorithm supplies a result which is inside  $\mathcal{P}_{\text{low}}$  and close to the optimum, but maybe not perfectly optimal. Tests have shown that it is necessary to limit the number of iterations (in both the second and the third major step) because in some (quite rare) situations, the steps resulting from iteration can be extremely small.

The actual implementation is substantially more complicated than the flow-charts because the limited machine precision requires many steps where vectors are normalized and/or compared to zero.

There is yet another interesting aspect of powers. In the algorithm, we often have to compute powers with exponent  $p - 1$  as part of the gradients. Now, if  $p - 1$  is a power of two, this can be done very fast (and with potentially better precision) by repeated squaring instead of using the general-purpose floating-point power function. As the precise value of  $p$  does not really matter, we are free to choose such  $p$  without any problems. The current implementation chooses  $p$  appropriately, thus saving some percent of computation time, especially if  $p$  is small.

---

<sup>17</sup>Again, the maximum step size is limited by a bound that increases as iteration goes on, as in the second major step (see footnote 10). And again, we have to make an exception from this limitation: if the current value  $f$  has components larger than  $f_{\text{max}}$ , then the step size limit is relaxed such that  $f \leq f_{\text{max}}$  can be obtained in a single step.

<sup>18</sup>More precisely, if more than  $m$  consecutive steps are smaller than this: a single step may be very small because it projects  $f$  onto a near border and the next step may be much larger because then also the direction  $\underline{d}$  is projected onto that border *before* computing the step size. Up to  $m$  such projections may happen consecutively, one for each dimension.

# Chapter 5

## Workspace Optimization

*Section 5.1 explains the difficulty of workspace optimization. Section 5.2 introduces a measure for the quality of workspace, which is used in the following sections to analyze designs of the various DOF classes. The considerations lead to a collection of rules of thumb, obtained with a mixture of analysis, intuition and experience.*

### 5.1. Introduction

While the preceding chapters aim at the *analysis* of the workspace of tendon-based Stewart platforms, we will now provide some results on *synthesis* of such manipulators, focusing on workspace maximization. This requires a description of the workspace as a whole, which one could seek in various ways:

- Using the closed-form description of Theorem 3.4, p. 40. But, as already pointed out (Table 3.1, p. 41), this description leads to extremely complex expressions especially for spatial redundant systems. Thus, attempts to perform workspace optimization on this basis [45] were limited to a small number of special planar cases up to now.
- Applying universal methods to explore the workspace boundaries [53, 153] which do not make any use of particular properties of the mechanism. But this is time-consuming and for nonconvex, disconnected workspaces it may be difficult to obtain the workspace volume from the boundary description.
- Stepping through a grid of points in posture space and counting the number of grid points which belong to the workspace. However, this summarizes the workspace size in a single figure which is difficult to interpret because it tells nothing about the shape of the workspace.
- Printing 2-dimensional slices of the workspace for some choices of values for the other (up to four) posture coordinates [161]. This is a quite useful approach for systems with a low number of end-effector-DOFs and it will be adopted in this chapter for 1R2T systems. But it remains difficult to get an overview of the shape of a six-dimensional workspace with this method.

- For each orientation, write down a convex polyhedron in space known to contain the workspace. As shown in 2000 [173], such a superset can be obtained by looking at the force equilibrium only, but the real workspace may be just a small subset of this.

The present thesis follows a different approach, in particular for 2R3T and 3R3T systems. In Section 5.2, we shall define a measure for workspace quality in a given posture, which reaches 1 in the workspace center and 0 on its boundary. Thus, this measure gives an indication about the distance of a posture from the workspace border. Then we step through a very rough grid in posture space and look at the workspace quality in each grid point. The result will be shown in a table, where the workspace quality in each posture is represented graphically. This allows to check at a glance in which DOFs the workspace is large and in which ones it is small. It also makes it easy to compare designs.

Once chosen a way to describe the workspace of a given design, the second problem is then how to obtain good designs. Classical gradient methods are difficult to apply due to the huge number of design parameters: for each tendon, there are 3 coordinates for the winch position and other 3 for the platform connection point. For instance, a 3R3T manipulator with 8 tendons is thus defined by about 31 parameters.<sup>1</sup> And things get much more complex when the number of tendons itself becomes a variable subject to optimization.

A more promising approach is offered by nonclassical methods [32, 88, 144] like genetic algorithms or simulated annealing, in particular when considering some recent discoveries. Indeed, during optimization, most of the CPU time will be spend to approximately compute the workspace size (with any of the above methods), and the result will still have a considerable degree of uncertainty. Now, Ball et al. have shown [17] that this uncertainty can be used as a randomizer for simulated annealing, so that the cooling schedule in simulated annealing corresponds to an increasing precision in workspace computation. A similiar but faster algorithm has recently been proposed by Meisel [116]. In practice, this means that the optimization has basically the same computation cost as repeatedly computing a workspace size with increasing precision. Similar recent results exist for genetic algorithms [30].

However, the set of solutions can be limited in advance, so that nonclassical optimization like genetic algorithms or simulated annealing can then be applied to a smaller set of feasible solutions.<sup>2</sup> As pointed out in Section 3.5, p. 54 ff., there is a number of advantages when connecting several tendons to the same winch or connection point. Furthermore for most applications in engineering (except those dedicated to one single task), it is good to have some symmetry. Finally, it

---

<sup>1</sup>Considering that the absolute position and orientation of platform and basis in space does not matter and neither the absolute scale, one has  $48 - 6 - 6 - 1$  parameters. One could also think of introducing one plane of symmetry in both platform and basis: then the number of point coordinates reduces to its half. Then one can still subtract 3 parameters for absolute posture of basis and platform, respectively and one for absolute scale, thus arriving at 17 remaining parameters.

<sup>2</sup>For certain classes of discrete problems, it is known that the number of iterations needed at each temperature for guaranteed convergence towards a global optimum, is proportional to the square of the size of the set of feasible solutions [1]. Therefore, any further limitation of this set would be a substantial enhancement.



is clear that an extremely high number of tendons implies disadvantages, at least in terms of cost.

The objective of this chapter is to state some rules of thumb, with a mixture of analysis, intuition and experience. Such rules can be used to define the basic structure of a system; then any known algorithms may be applied to fine-optimize the design parameters. Such an approach has already proven to be efficient within limited sets of designs [91, 93, 94, 161].

## 5.2. Measuring Workspace Quality

The results obtained so far enable us to tell whether a posture does or does not belong to the workspace for a given platform wrench. But often one also needs to know when a posture is close to the border of the workspace. To express this, we will develop a dimensionless «quality measure» which equals 1 in «optimal» conditions,<sup>3</sup> reaches 0 precisely on the border of the workspace and is continuous over the workspace. These are standard requirements for quality measures which also appear in the context of isotropy/dexterity [5, 15, 39, 50, 154].

We approach the border of the workspace if one of the tensions reaches either the lower bound  $f_{\min}$  or the upper bound  $f_{\max}$ . Hence, for a given solution  $\underline{f}$ , we can consider the value

$$(5.1) \quad \frac{2}{f_{\max} - f_{\min}} \min \left\{ \min_{1 \leq \mu \leq m} (f_{\mu} - f_{\min}), \min_{1 \leq \mu \leq m} (f_{\max} - f_{\mu}) \right\},$$

which lies in the interval  $[0, 1]$ . If we express this in terms of  $\|\cdot\|_{\infty}$ -distance from the center of the cube  $[f_{\min}, f_{\max}]^m$  and take the minimum over all the optimal solutions,<sup>4</sup> we arrive at the quality criterion<sup>5</sup>

$$(5.2) \quad d_{\partial} := 1 - \frac{2}{f_{\max} - f_{\min}} \min_{\sigma \in [0,1]} \left\| \underline{f}_{\sigma} - \frac{f_{\min} + f_{\max}}{2} \underline{1} \right\|_{\infty}.$$

This vanishes if the entire set of solutions computed from  $\underline{f}_{\text{low},p}$ ,  $\underline{f}_{\text{high},p}$  lies on the border of the cube  $[f_{\min}, f_{\max}]^m$ , it equals 1 if and only if all the tensions are equal to  $\frac{f_{\min} + f_{\max}}{2}$  for some  $\sigma$  and it continuously depends on  $\underline{f}_{\text{low}}$  and  $\underline{f}_{\text{high}}$ . It is easy to compute with the following lemma.

**5.1 Lemma** *Let  $\mathcal{S} \subset \mathbb{R}^m$  be a line and  $m \geq 2$ . Define  $\mathcal{C} := \mathcal{S} \cap [-1, 1]^m$ . If  $\mathcal{C} \neq \emptyset$  then there is an element of  $\mathcal{C}$  with minimal infinity norm having two coordinates*

<sup>3</sup>In the sense of «optimal solutions» in Def. 4.1, p. 62. In applications like wind-tunnels [93] where some tendons are more important than others, this might not be appropriate, but the measure can be adapted to that. Also note that in general, the proposed measure *only* evaluates the possibility to achieve desired force distributions in the tendons, while it does not provide any information about vicinity to singularities.

<sup>4</sup>We could easily compute the minimum over the entire set  $\mathcal{P}$  because in such a minimum, a number of coordinates would have the same absolute value. However, what we are interested in is not the real distance of  $\mathcal{P}$  from the center of the cube, but rather the distance of the solutions we actually compute with a given  $p$ -norm.

<sup>5</sup>The letter  $d$  stands for «distance» and the symbol  $\partial$  is used in mathematics to denote, among others, the border of a set.



of equal absolute values:

$$(5.3) \quad \exists_{\underline{f}_0 \in \mathcal{C}} \exists_{1 \leq \mu_1 < \mu_2 \leq m} \|\underline{f}_0\|_\infty = \min_{\underline{f} \in \mathcal{C}} \|\underline{f}\|_\infty \wedge |f_{0,\mu_1}| = |f_{0,\mu_2}|. \diamond$$

**Proof.** a) A minimum exists by Prop. A.26, p. 133 because the infinity norm is continuous and  $\mathcal{C}$  is compact.

b) Let  $f_0 \in \mathcal{C}$  minimize the infinity norm on  $\mathcal{C}$ . If it does not satisfy the second part of Eq. (5.3), we assume without loss of generality

$$(5.4) \quad \forall_{1 \leq \mu < m} |f_{0,m}| > |f_{0,\mu}|.$$

Now let  $\mathcal{V}$  be the difference space (Def. A.12, p. 127) of  $\mathcal{S}$ . If there is a  $\underline{v}_0 \in \mathcal{V}$  with  $v_{0,m} > 0$ , then Eq. (5.4) implies

$$(5.5) \quad \exists_{\epsilon > 0} \underline{f}_0 - \epsilon \underline{v}_0 \in \mathcal{C} \wedge \|\underline{f}_0 - \epsilon \underline{v}_0\|_\infty < \|\underline{f}_0\|_\infty$$

which is impossible by assumption. Therefore  $\mathcal{S}$  lies in the plane  $\mathbb{R}^{m-1} \times \{f_{0,m}\}$ . Eq. (5.4) further implies that  $\mathcal{S}$  intersects the set  $] -f_{0,m}, f_{0,m}[^{m-1} \times \{f_{0,m}\}$  which lies in that plane. It follows that  $\mathcal{S}$  also intersects the border of that set, and each point  $f$  on that border has the property that there is  $1 \leq \mu_0 < m$  with  $|f_{\mu_0}| = |f_{0,m}|$ .  $\square$

Hence we can find such a minimum just by considering the finite set of all points on the segment where two coordinates are equal.

It should be emphasized that the border distance measure  $d_\partial$  does not have anything to do with isotropy or dexterity. It does not measure efficiency of force or motion transmission and has nothing to do with vicinity to singularities (in the sense of Section 2.1, p. 17 ff.). For instance, the *nonsingular* posture in Fig. 3.12, p. 47 is on the border of the workspace and therefore has  $d_\partial = 0$  and the *singular* posture in Fig. 3.8, p. 45 has  $d_\partial = 1$  because all the tensions are equal. Indeed, as pointed out in Section 2.1.1, p. 17 ff., workspace boundary has nothing to do with kinematic singularity when dealing with tendon-based parallel robots.

### 5.3. Class 2T

For purely translational systems, we limit ourselves to the planar case because it is easier to illustrate and spatial systems with pure translation do not provide substantially different situations.

We consider some manipulators which cover a large spectrum of redundancy (Fig. 5.1), ranging from a CRPM with the minimum number of tendons up to an RRPM with as many as thirteen extra tendons. This allows us to study in particular the effect of high redundancy. The overall size of the CRPM (design a) was chosen somewhat larger, so that the largest square fitting into the polygon formed by the winches, is about the same for all the manipulators.

Fig. 5.1 shows the workspace quality of each manipulator: the size of the small squares is proportional to the value of  $d_\partial$  in the center of the square; it is 1 if two

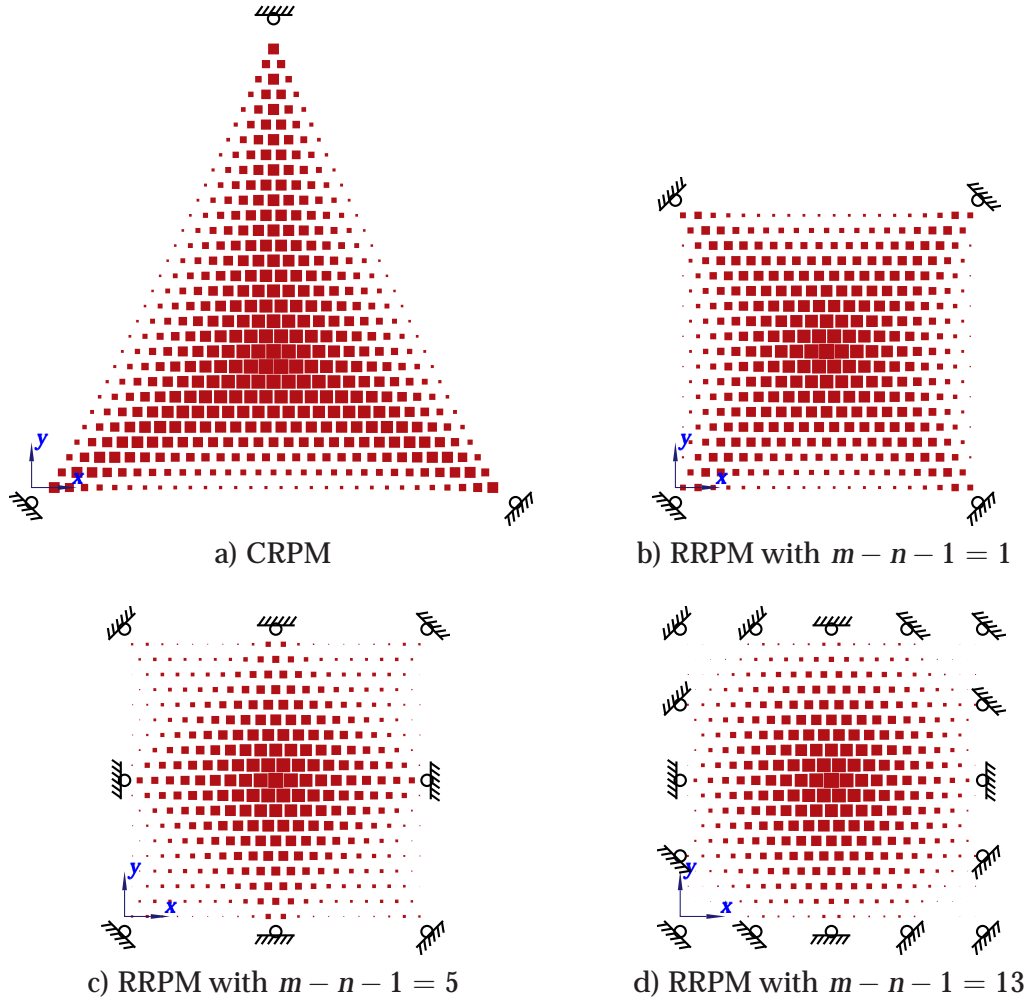


Figure 5.1: Workspace of 2T sample designs

( $f_{\min} = 0.010$  kN,  $f_{\max} = 1.000$  kN)

adjacent squares touch each other, while it is 0 if the square vanishes. Here the computation does not take into account any platform wrenches other than tendon forces. The most obvious result is that the RRPM b provides a larger square-shaped workspace than the CRPM a, with a smaller overall manipulator size. Then the workspace region with  $d_0 \approx 1$  shrinks as redundancy increases. This is because close to a winch, the corresponding tendon has to balance at least the minimum tension in all the other tendons. So this requires more tension if the number of tendons increases. Experience with several geometries has shown that this is a general phenomenon:

**5.2 Rule of Thumb** *If no external wrenches are involved, then extra redundant tendons are useful to improve the shape of the workspace, but not its quality.  $\diamond$*

Next (Fig. 5.2), we consider almost the same designs, taking gravity into account (with a quite large load). Some winches were removed which seem unnecessary if gravity is present. As expected, now a higher number of tendons allows for a better distribution of the load, so that design c is preferable to b.

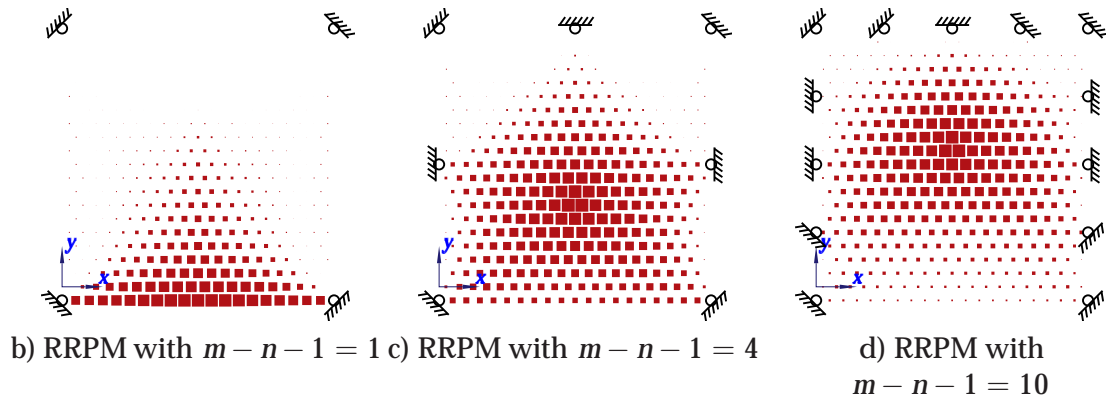


Figure 5.2: Workspace of 2T sample designs with gravity  
 ( $f_{\min} = 0.010$  kN,  $f_{\max} = 1.000$  kN,  $m_p = 100.0$  kg)

**5.3 Rule of Thumb** *If large external wrenches<sup>6</sup> need to be supported, it may be a good idea to add a higher number of redundant tendons.* ◇

## 5.4. Class 1R2T

Even though 1R2T systems are fairly simple, there is already a vast variety of possible design ideas. We will not try to give a survey here, but just consider examples which illustrate some important rules. Fig. 5.3 shows these designs and their workspace quality for two rotation angles, without external wrenches.

Designs a and b illustrate the already mentioned fact that workspace is larger the more connection points coincide: both are CRPMs, but b has a higher degree of connection coincidence and it turns out that b has a much larger workspace for large rotations.

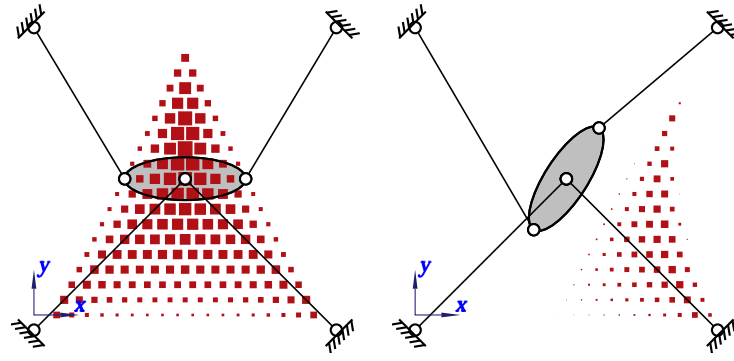
**5.4 Rule of Thumb** *Connection points should be put together as often as possible. This usually increases substantially the rotational workspace.* ◇

It is easy to see that the workspace of design b is always the entire triangle area, for any angle between  $-90^\circ$  and  $90^\circ$ . And the figure shows that even the quality remains at a rather high level. Applying the method of Prop. 3.6, p. 45, we find that there are singularities only when the two upper tendons are parallel. Then the rotational DOF is uncontrolled. The only drawback of the design is that tendons often intersect with each other (but this is the case in design a as well). To the author's knowledge, there is no planar 3-DOF CRPM superior to this.

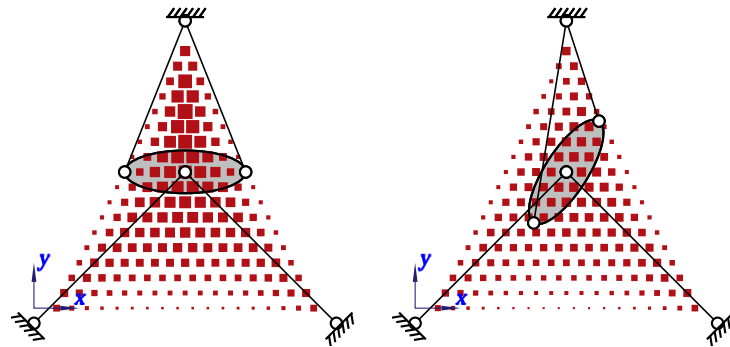
**5.5 Rule of Thumb** *In terms of rotational workspace, the design in Fig. 5.3b is presumably an optimal CRPM within the 1R2T class.* ◇

A disadvantage of this design is that the workspace is triangle-shaped rather than square-shaped. A possible solution is to add tendons obtained by mirroring the existing ones on a horizontal axis. This would lead to a platform with three connection points such that the central one bears four tendons in all directions

<sup>6</sup>This may also apply for inertia forces, gravity is just an example.



a) poor CRPM



b) excellent CRPM

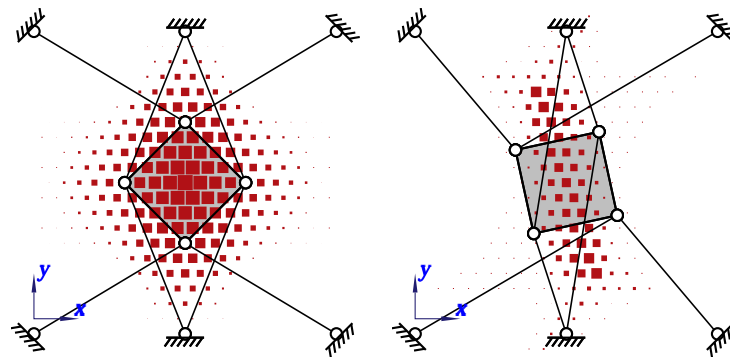
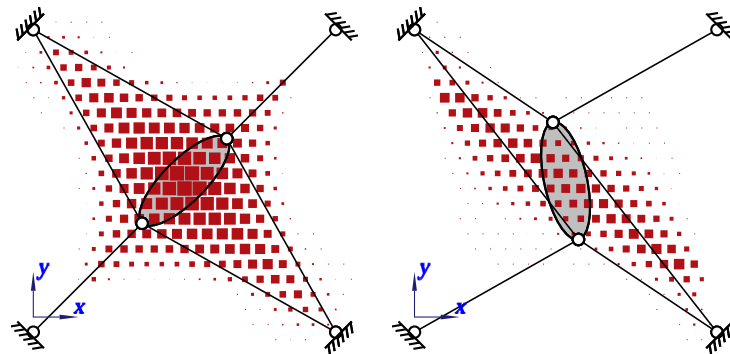
c) RRPM with  $m = n + 5$ d) RRPM with  $m = 2n$ 

Figure 5.3: Workspace of 1R2T sample designs  
 ( $f_{\min} = 0.010$  kN,  $f_{\max} = 1.000$  kN)

and it would be difficult to append a load anywhere. So design c was derived from this by splitting this point into two. Fig. 5.3 shows that the workspace is good, but tendons intersect *always* with each other. Again, singularities appear only for extreme rotations.

Design d is obtained from another idea. It is a known result for tendon-driven serial systems that  $n$  DOFs can be controlled quite well with  $2n$  tendons [137, 139]. In the ideal case, for each DOF there are two tendons, controlling this one exclusively and pulling with opposite signs. To a certain degree, this is the case at home position of d: we have

$$(5.6) \quad \underline{A}^T = \begin{pmatrix} -0.707 & 0.872 & 0.490 & 0.707 & -0.872 & -0.490 \\ -0.707 & -0.490 & -0.872 & 0.707 & 0.490 & 0.872 \\ 0.000 & 1.907 & -1.907 & 0.000 & 1.907 & -1.907 \end{pmatrix}$$

$$(5.7) \quad \frac{1}{k'} \underline{K} = \begin{pmatrix} 0.469 & -0.036 & -0.000 \\ -0.036 & 0.469 & 0.000 \\ -0.000 & 0.000 & 0.505 \end{pmatrix}.$$

This means that the force along one diagonal is controlled exclusively by tendons 1 and 4. The force along the other diagonal is obtained by antagonistic operation of no. 2 and 3 against 5 and 6, having equal tension in 2 and 3 (as well as 5 and 6). Similarly, pure torque is given by antagonistic operation of no. 2 and 5 against 3 and 6, having equal tension in 2 and 5 (3 and 6). As a consequence, the rotational stiffness is decoupled from the translational one and the two eigenvector directions of the translational stiffness are the diagonals of the system.

Hence, this design has good decoupling properties at home posture. In addition, Fig. 5.3 shows that its workspace is larger than that of c. As two platform points are always controlled in respectively two DOFs, the design has no singularities at all. Tendon collisions occur, but much less than in case c.

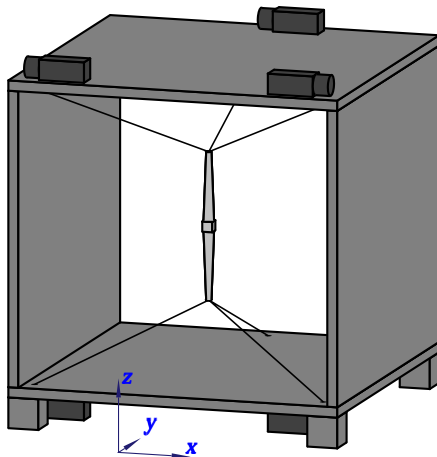
**5.6 Rule of Thumb** *Manipulators with  $m = 2n$  tendons can be designed to have good decoupling properties at home posture. They offer a good workspace also for large rotations. This can be considered a reasonable limit on the maximum number of tendons to employ.*  $\diamond$

## 5.5. Class 2R3T

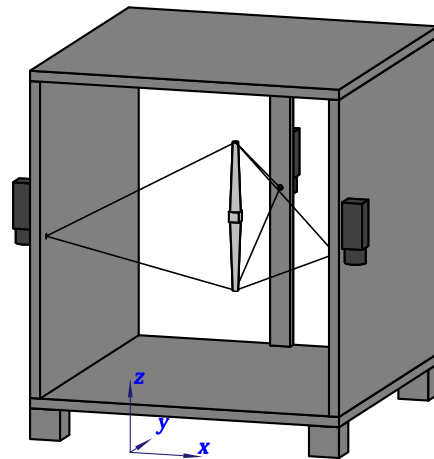
Fig. 5.4 presents a number of 2R3T designs, which are all singularity-free and autocollision-free. Table 5.1 illustrates the quality of their workspaces for a grid of postures.<sup>7</sup> Roll denotes rotation about the x axis and pitch rotation about the y axis as usual.<sup>8</sup> As the designs are all symmetric in x direction but not all in y and z, the grid covers only half an x range but a full y and z range. In each cell, the lengths of the bars indicate the values of  $d_0$  for designs a–f.

<sup>7</sup>Coordinates are given in meters; the supporting frame is a cube of size 10 m.

<sup>8</sup>However, the postures are not defined by performing two consecutive rotations because then, the roles of both angles would not be symmetric. Instead, for a roll  $\varphi$  and a pitch  $\vartheta$ , the direction



a) simple CRPM



b) excellent CRPM

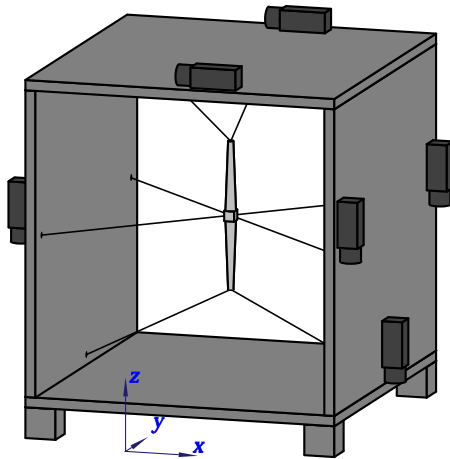
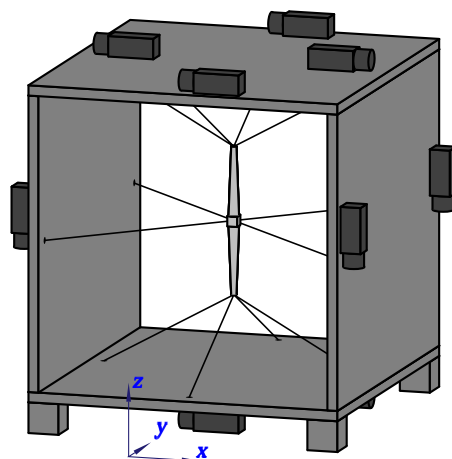
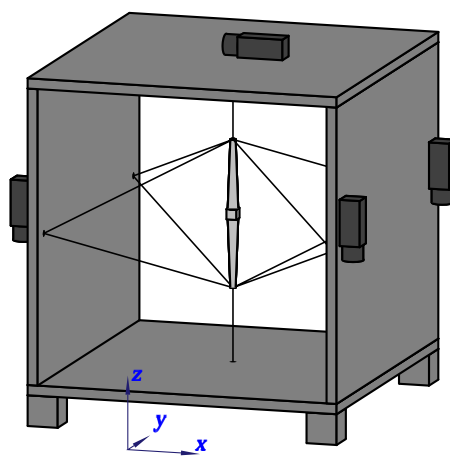
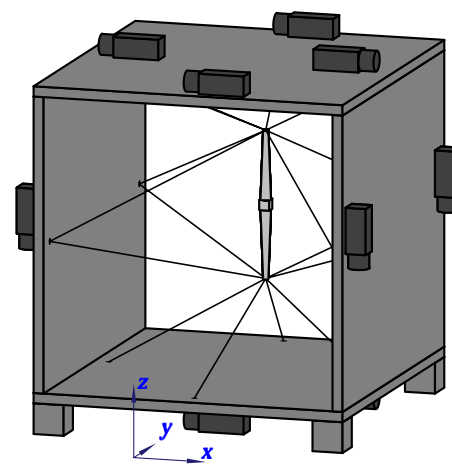
c) RRPM with  $m - n - 1 = 2$ d) RRPM with  $m - n - 1 = 6$ e) RRPM with  $m = 2n$ f) RRPM with  $m - n - 1 = 10$ 

Figure 5.4: 2R3T sample designs

			roll				0				30				60				90			
			pitch				0	30	60	90	0	30	60	90	0	30	60	90	0	30	60	90
$x$	$y$	$z$																				
5.0	2.0	5.0																				
5.0	2.0	5.5																				
5.0	2.0	6.0																				
5.0	5.0	5.0																				
5.0	5.0	5.5																				
5.0	5.0	6.0																				
5.0	8.0	5.0																				
5.0	8.0	5.5																				
5.0	8.0	6.0																				
6.5	2.0	5.0																				
6.5	2.0	5.5																				
6.5	2.0	6.0																				
6.5	5.0	5.0																				
6.5	5.0	5.5																				
6.5	5.0	6.0																				
6.5	8.0	5.0																				
6.5	8.0	5.5																				
6.5	8.0	6.0																				
8.0	2.0	5.0																				
8.0	2.0	5.5																				
8.0	2.0	6.0																				
8.0	5.0	5.0																				
8.0	5.0	5.5																				
8.0	5.0	6.0																				
8.0	8.0	5.0																				
8.0	8.0	5.5																				
8.0	8.0	6.0																				

Table 5.1: Workspace quality of 2R3T sample designs



Rule 5.4 implies that optimal designs of class 2R3T have exactly two distinct platform connection points. Then the simplest idea is design a, but Rule 5.4 can be applied once more and yields design b. Table 5.1 shows that indeed, b has a much better rotational workspace than a.<sup>9</sup> This is a maximal application of Rule 5.4 because there must be at least 3 distinct winch positions in order to get a non-planar system. Intuitively, it appears difficult to design something better with 6 tendons and 5 DOFs.

**5.7 Rule of Thumb** *In terms of workspace, the design in Fig. 5.4b is presumably an optimal CRPM within the 2R3T class.* ◇

Design c implements the idea of subdividing DOFs between tendons: at home posture, the central ones control translation in the xy plane, the lower (upper) ones rotation about the y (x) axis and lower and upper ones together translation in z direction. However, Table 5.1 shows a very poor workspace and even addition of 4 extra tendons (thus obtaining much more symmetry) in design d does not improve the workspace significantly. This confirms Rule 5.4.

Design e is a trial to apply Rule 5.6. Indeed, the result has a good translational workspace (better than a), although the range of rotations is smaller than that of a. Again, a design like f with much more tendons does not have a larger workspace, but rather a smaller one. This confirms the limit statement in Rule 5.6 (and also Rule 5.2).

## 5.6. Class 3R3T

Manipulators with 6 DOFs are the most important ones from an application point of view, but as they have the largest number of design variables, they are also most difficult to optimize. Thus, several designs were proposed, but little has been written about their optimization (except for Tadokoro et al. [161]). Here we compare just a small number of designs (Fig. 5.5) mostly taken from existing publications.

The CRPM a implements the idea of separating translation control from rotation control with a small number of connection points, but Table 5.2<sup>10</sup> shows that it has a very poor workspace. Design b is the CRPM presented by Kawamura et al. [80] for a tennis simulator: it turns out to be quite good in rotation, while the translational range is rather limited. The RRPMS c and d were proposed by Tadokoro et al. [161]. Table 5.2 confirms the conclusion of that paper: the «Nishioka» type is capable of quite large rotations, while the «Kawamura» type is somewhat better in translation.

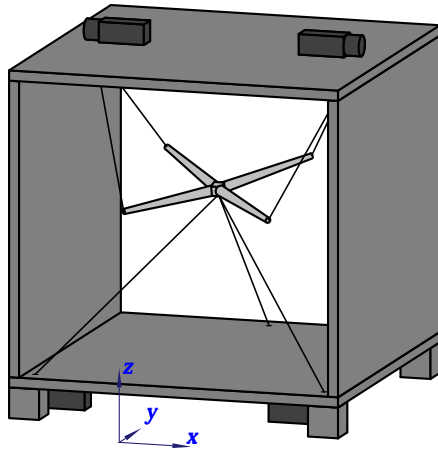
Design e is a trial to apply Rule 5.6 but reveals a very poor workspace. A

---

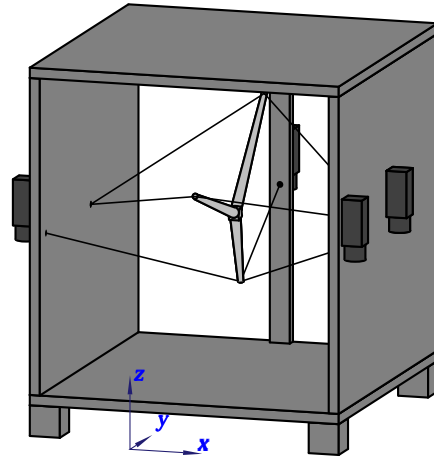
of  $(\cos \varphi \sin \vartheta, -\sin \varphi \cos \vartheta, \cos \varphi \cos \vartheta)^T$  was taken. This mapping is singularity-free in each hemisphere, treats both angles in a symmetric manner and is almost isometric for small angles.

<sup>9</sup>Note that the excellent performance of b for a pitch of  $90^\circ$  is referred only to the question of distribution of forces – at the same time, the manipulator is singular, but this is not reflected in the quality measure.

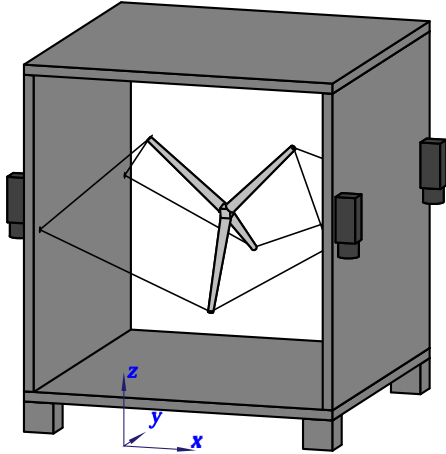
<sup>10</sup>Again, the supporting frames of all proposed manipulators are cubes of 10 m size.



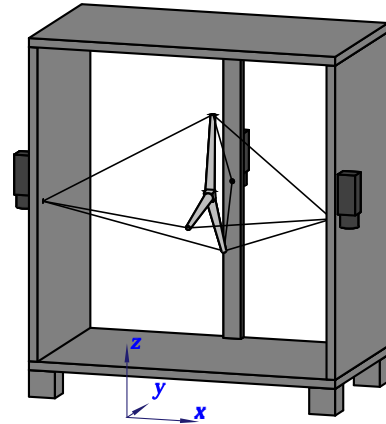
a) CRPM



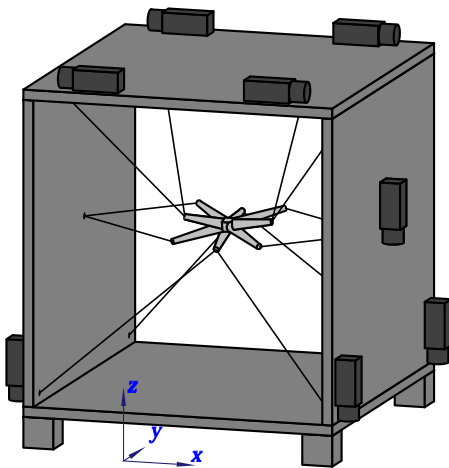
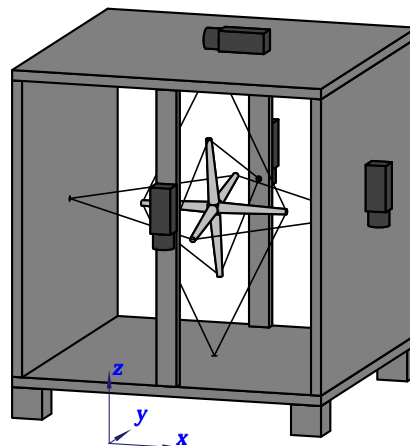
b) «Virtual Tennis» CRPM



c) «Kawamura» RRPM



d) «Nishioka» RRPM

e) RRPM with  $m = 2n$ 

f) «French-German» RRPM

Figure 5.5: 3R3T sample designs



more successful application is the «French-German» manipulator f [95],<sup>11</sup> which at home posture implements a complete decoupling of DOFs from each other. It shows rotational capabilities like the «Nishioka» design, but with a somewhat larger translational workspace in the domain of small  $y$  values.

All these designs are singularity-free except for extreme rotations. While a–d are almost free of tendon collisions (for c and d this was also stated by Tadokoro et al. [161]), such collisions present a serious problem in manipulators e and f when performing large rotations. This was not investigated here because in addition to collisions among tendons, also collisions between tendons and load – which depend on the shape of the load and therefore cannot be discussed in general – are likely to occur often.

The 3R3T class is different from the other ones in that autocollisions play a central role; thus, the question of optimal manipulators in this class is still open.

---

<sup>11</sup>This design was invented by Pascal Lafourcade and the author during Pascal's visit at Duisburg in January 2003, as a contribution to celebrate the 40th anniversary of the Ellysée treatise.

# Chapter 6

## Motion Simulation Results

*All the results of the preceding chapters are combined and used for simulation of motions. In Section 6.1 we state some general results on tendon velocity and acceleration. Later on, the influence of several parameters is examined in detail for manipulators moving a point in the plane (Section 6.2). Finally, a complex 6-DOF motion is simulated for some relatively good designs (Section 6.3).*

### 6.1. Characteristics of Tendon Motion

For the design of tendon-based Stewart platforms it is important to know the velocities, accelerations and forces that will occur in the tendons, and the required actuator power. While in Chapter 4, we examined the forces much in detail, in this chapter we will state results on velocity, acceleration and power.

Given an end-effector twist  $\underline{t} = (\underline{v}^T, \underline{\omega}^T)^T$ , the vector of tendon velocities is obtained from Eq. (2.21), p. 26, by the principle of D'Alembert:<sup>1</sup>

$$(6.1) \quad \underline{\dot{l}} = -\underline{A} \underline{t}.$$

We obtain more insight into the structure of  $\underline{\dot{l}}$  when looking at a single tendon. In the general 6-DOF case (Eq. (2.41), p. 34), we find

$$(6.2) \quad \dot{l}_\mu = - \left( \underline{u}_\mu^T \quad (\underline{p}_\mu \times \underline{u}_\mu)^T \right) \begin{pmatrix} \underline{v} \\ \underline{\omega} \end{pmatrix}$$

$$(6.3) \quad = -\underline{u}_\mu^T (\underline{v} + \underline{\omega} \times \underline{p}_\mu)$$

$$(6.4) \quad = -\underline{u}_\mu^T \underline{\dot{p}}_{B,\mu} \quad \text{and therefore}$$

$$(6.5) \quad |\dot{l}_\mu| \leq |\dot{p}_{B,\mu}|, \quad \text{considering that } \underline{u}_\mu \text{ is a unit vector.}$$

This means that the velocity of a tendon equals the velocity of the respective platform attachment point, projected onto the tendon direction. This is always less than or equal the velocity of the attachment point; it is equal if the attachment point moves straight away (or towards) the winch.

<sup>1</sup>The wrench in Eq. (2.21) is the external wrench *balanced* by the platform; the wrench *exerted*

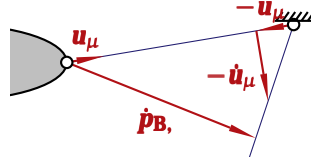


Figure 6.1: Second term of acceleration

The acceleration is more complicated because it involves also the change of the structure matrix in time. Derivation of Eq. (6.1) yields

$$(6.6) \quad \ddot{\underline{l}} = -\underline{A} \dot{\underline{l}} - \dot{\underline{A}} \underline{l},$$

and proceeding the same way as above, we find for a single tendon:

$$(6.7) \quad \ddot{l}_\mu = -\underline{u}_\mu^T \ddot{\underline{p}}_{B,\mu} - \dot{\underline{u}}_\mu^T \dot{\underline{p}}_{B,\mu} \quad \text{and therefore}$$

$$(6.8) \quad |\ddot{l}_\mu| \leq |\ddot{\underline{p}}_{B,\mu}| + |\dot{\underline{u}}_\mu| |\dot{\underline{p}}_{B,\mu}|.$$

This tendon acceleration is the sum of two terms, one of which is at most the attachment point acceleration (similar to the above result on velocity), while the other one is the scalar product of the attachment point velocity and the change rate of the direction of the tendon. As the tendon direction follows the attachment point, the angle between  $-\dot{\underline{u}}_\mu$  and  $\dot{\underline{p}}_{B,\mu}$  is never more than a right angle (Fig. 6.1). Therefore, *the second term of acceleration is always nonnegative*. It follows that a (signed) tendon acceleration is always greater than or equal to the projection of the respective attachment point acceleration on the tendon direction. This «acceleration shift» is large if the attachment point is close to the winch and if it moves almost perpendicularly to the tendon.

The mechanical power  $P_\mu$  generated by the  $\mu$ th actuator is the product of tendon force and velocity.<sup>2</sup> Defining a power as positive if the motor puts energy into the mechanical system, we obtain

$$(6.9) \quad P_\mu = -f_\mu \dot{l}_\mu.$$

A negative power means that the motor is used as a brake and in theory energy can be gained back. Disregarding friction and other (e. g. electromagnetic) losses, the overall power consumption at a point of time is then the sum  $P_\Sigma$  of the signed powers of the single actuators. It depends on the design of the actuators up to which degree this is true. In the worst case when nothing can be regained, the overall power consumption is the sum  $P_+$  of all the positive powers (again disregarding friction and other losses). Then we have two sums

$$(6.10) \quad P_\Sigma = \sum_{\mu=1}^m P_\mu = -\underline{f}^T \dot{\underline{l}},$$

$$(6.11) \quad P_+ = \sum_{\mu=1}^m \max \{P_\mu, 0\}.$$

---

has the opposite sign. On the other hand, by convention the vector  $\underline{l}_\mu$  points *towards* the winches, such that pulling forces are positive. Therefore a positive change of  $\underline{l}_\mu$  in this direction means that the tendon is *shortened*, i. e.  $\dot{l}_\mu = \frac{d}{dt} |\underline{l}_\mu|$  is *negative*. This explains for the minus sign in Eq. (6.1).

<sup>2</sup>Again one has to pay attention to the sign: a positive tendon force points towards the winch, while a positive change in tendon length corresponds to a vector  $\underline{l}_\mu$  pointing away from the winch.

Due to the conservation of energy, the time integral of the first sum vanishes for an entire cycle (i. e. a motion where end-effector position and velocity at time  $t_2$  are the same as at time  $t_1$ ). The time integral of the second sum is the overall mechanical energy  $W$  needed to perform the cycle in worst case:

$$(6.12) \quad \int_{t_1}^{t_2} P_{\Sigma} dt = 0$$

$$(6.13) \quad \int_{t_1}^{t_2} P_{+} dt = W.$$

In the following sections, we will have a look at  $W$  in order to get a rough idea of energy consumption.

Clearly, this is only the mechanical power as output by the motors; it does not take into account many other factors depending on the actuator concept. For instance, electrical actuators require energy also to *hold* a tension even when the velocity is zero. The amount of power depends on the motor type: it may be proportional to the tension, to its square, or follow more complicated laws. Furthermore motors with winches (and eventually gears) have their own inertia which may contribute significantly to the overall power consumption. This is somewhat different when using electrical direct drives (which require power to hold tension, but do not have so much inertia). And it is completely different when using hydraulic actuators which can hold a tension almost without employing energy. As the present discussion aims at an overall picture independent of the actuator concept, the only quantities discussed in the following sections are mechanical power and energy.

## 6.2. Planar Translational Systems

Fig. 6.2a is taken from a simulation of a manipulator (time  $t$  indicated in the lower right corner) performing an  $\infty$ -shaped trajectory. The dashed arrow (pointing out of the drawing region) indicates the inertia force at the end-effector, while the solid ones represent the tendon forces at that point of time. Axis-parallel squares at the winches indicate that a motor puts energy into the mechanical system, while a rotated square means that a motor acts as a brake, taking energy out of the mechanical system. In both cases, the area of the square is proportional to the mechanical actuator power at that point of time. The trajectory can be described as

$$(6.14) \quad \underline{r}(\xi) = (d_1 \sin \xi, d_2 \sin 2\xi)^T, \quad \xi \in [0, 2\pi]$$

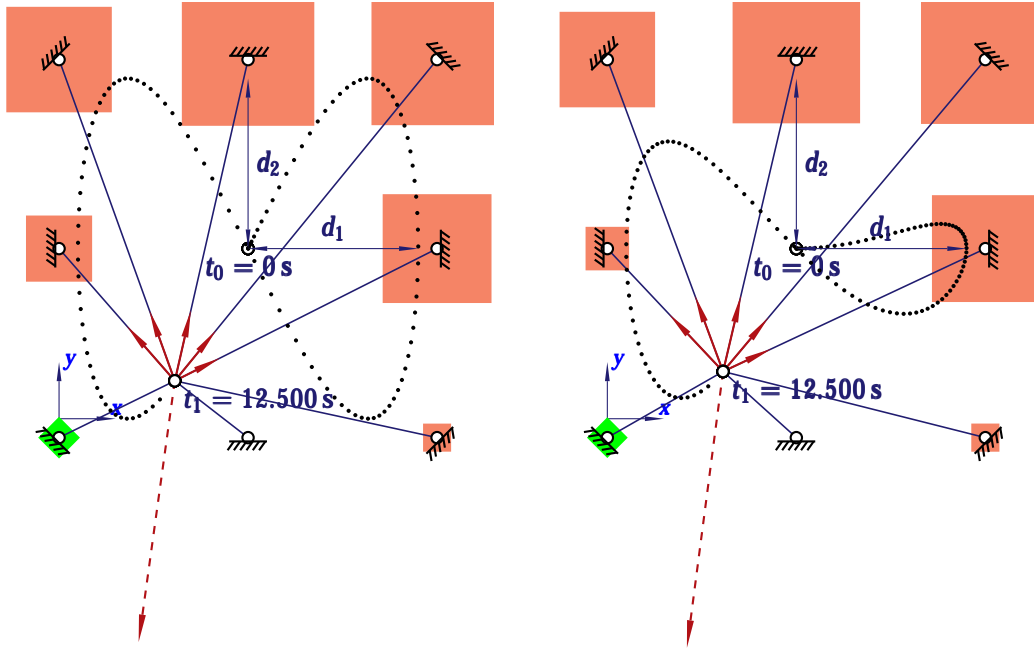
where  $d_1, d_2$  are lengths specifying the geometrical extension of the trajectory. Such a trajectory covers a wide variety of velocity/acceleration situations in different regions of the workspace. So it provides a good overall impression of manipulator capability.

If we express the parameter<sup>3</sup>  $\xi$  as a function of time  $t$ , we find

$$(6.15) \quad \dot{\underline{r}} = \dot{\xi} (d_1 \cos \xi, 2 d_2 \cos 2\xi)^T$$

<sup>3</sup>Unfortunately, it is not possible to parameterize the curve by arc length. Indeed, the arc length as a function of  $\xi$  can be expressed in closed form, but its inverse function cannot.



a)  $\infty$ -shaped trajectory

b) Modified trajectory

Figure 6.2: Test trajectories for 2T

$$(6.16) \quad \ddot{\mathbf{r}} = \ddot{\xi} (d_1 \cos \xi, 2 d_2 \cos 2\xi)^T - \dot{\xi}^2 (d_1 \sin \xi, 4 d_2 \sin 2\xi)^T$$

$$(6.17) \quad \dddot{\mathbf{r}} = \dddot{\xi} (d_1 \cos \xi, 2 d_2 \cos 2\xi)^T - 3 \ddot{\xi} \dot{\xi} (d_1 \sin \xi, 4 d_2 \sin 2\xi)^T - \dot{\xi}^3 (d_1 \cos \xi, 8 d_2 \cos 2\xi)^T.$$

For  $\xi(t)$ , we use a point-to-point-motion from 0 to  $2\pi$  with finite jerk, i. e. a three times differentiable<sup>4</sup> time-optimal motion such that velocity and acceleration are zero at the beginning and the end and velocity, acceleration and jerk (the derivate of acceleration) are limited to prescribed values  $\dot{\xi}_{\max}$ ,  $\ddot{\xi}_{\max}$  and  $\ddot{\xi}_{\max}$ . Then we have the estimates:<sup>5</sup>

$$(6.18) \quad |\dot{\mathbf{r}}| \leq c_1 |\dot{\xi}|, \quad c_1 := \sqrt{d_1^2 + 4 d_2^2}$$

$$(6.19) \quad |\ddot{\mathbf{r}}| \leq c_1 |\ddot{\xi}| + c_2 |\dot{\xi}|^2, \quad c_2 := \frac{d_1^2 + 64 d_2^2}{16 d_2}$$

$$(6.20) \quad |\dddot{\mathbf{r}}| \leq c_1 |\dddot{\xi}| + 3 c_2 |\ddot{\xi}| |\dot{\xi}| + c_3 |\dot{\xi}|^3, \quad c_3 := \sqrt{d_1^2 + 64 d_2^2}.$$

There are several ways to choose  $\dot{\xi}_{\max}$ ,  $\ddot{\xi}_{\max}$ ,  $\ddot{\xi}_{\max}$  such that given bounds  $v_{\max}$ ,  $a_{\max}$ ,  $j_{\max}$  for the velocity  $\dot{\mathbf{r}}$ , acceleration  $\ddot{\mathbf{r}}$  and jerk  $\dddot{\mathbf{r}}$  are not exceeded, but it is difficult to find a choice such that the bounds are actually reached. A very conservative approach could be to limit each term in Eq. (6.19) to  $\frac{1}{2} a_{\max}$

<sup>4</sup>more precisely, two times continuously differentiable and three times differentiable everywhere except for a finite number of points.

<sup>5</sup> $c_2$  is found by computing the maximum of  $|(d_1 \sin \xi, 4 d_2 \sin 2\xi)|^2$ ;  $c_1, c_3$  are obvious.

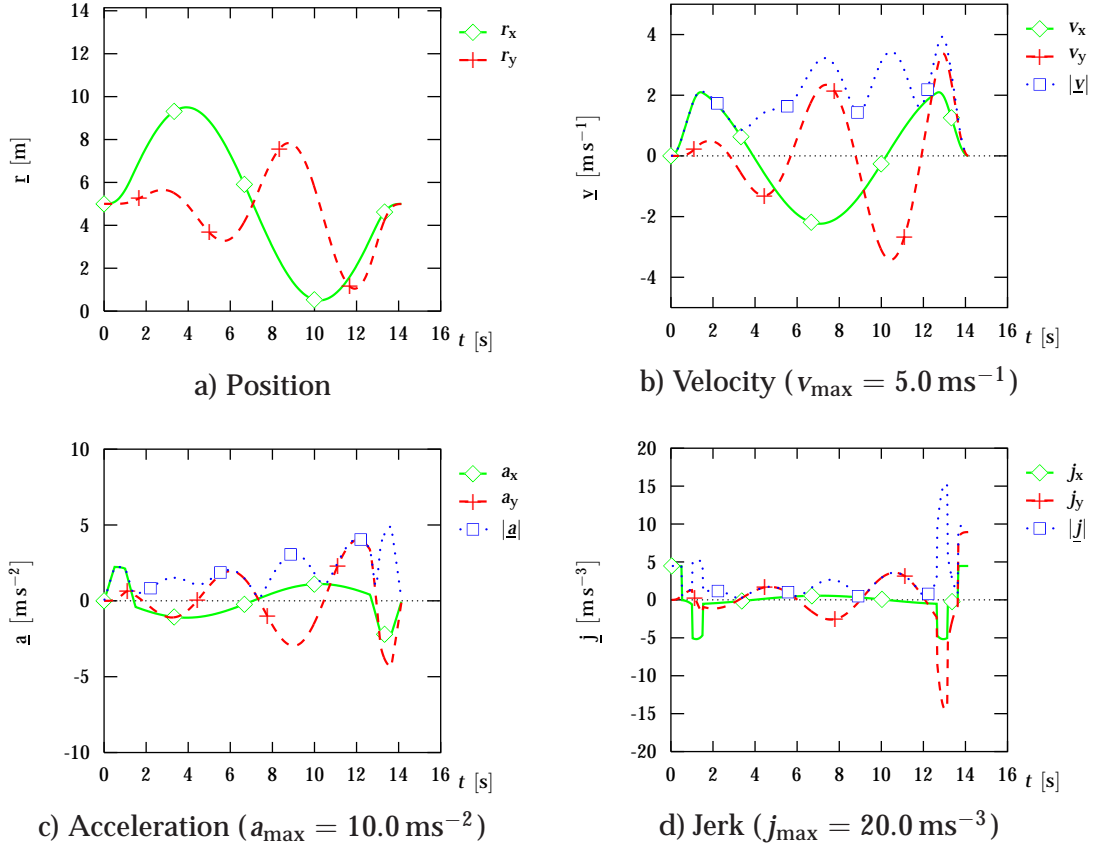


Figure 6.3: End-effector motion for 2T trajectory

and each term in Eq. (6.20) to  $\frac{1}{3} j_{\max}$ . Then the resulting velocities, accelerations and jerks are certainly inside the limits, but far away from them. Now, velocity and acceleration of point-to-point-motions are never maximal at the same time and experience shows that the limits are therefore still respected when neglecting the mixed term in Eq. (6.20). This leads to

$$(6.21) \quad \dot{\xi}_{\max} := \min \left\{ \frac{v_{\max}}{c_1}, \sqrt{\frac{a_{\max}}{2 c_2}}, \sqrt[3]{\frac{j_{\max}}{2 c_3}} \right\}$$

$$(6.22) \quad \ddot{\xi}_{\max} := \frac{a_{\max}}{2 c_1}$$

$$(6.23) \quad \dddot{\xi}_{\max} := \frac{j_{\max}}{2 c_1}.$$

The trajectory just presented has two axes of symmetry, so it would lead to four basically equal tendon force paths (provided that the arrangement of winches has two axes of symmetry, too). In order to get a more general example, we consider a slightly different curve where the second radius  $d_2$  starts from zero and increases linearly up to its maximum value (Fig. 6.2b). This leads to a nonsymmetric trajectory described by

$$(6.24) \quad \underline{r} = \left( d_1 \sin \xi, \frac{d_2}{2\pi} \xi \sin 2\xi \right)^T$$

$$(6.25) \quad \dot{\underline{r}} = \dot{\xi} \left( d_1 \cos \xi, \frac{d_2}{2\pi} \sin 2\xi + \frac{d_2}{\pi} \xi \cos 2\xi \right)^T$$

$$(6.26) \quad \ddot{\mathbf{r}} = \ddot{\xi} \left( d_1 \cos \xi, \frac{d_2}{2\pi} \sin 2\xi + \frac{d_2}{\pi} \xi \cos 2\xi \right)^T - \dot{\xi}^2 \left( d_1 \sin \xi, -\frac{2d_2}{\pi} \cos 2\xi + \frac{2d_2}{\pi} \xi \sin 2\xi \right)^T.$$

We see that the y component of velocity and acceleration consists now of two terms, where the second one is less than or equal to the result for constant  $d_2$  (because it contains the factor  $\frac{\xi}{2\pi}$  which varies from 0 to 1). For the sake of simplicity, we assume that the first term is not that large and that the estimates Eq. (6.18), (6.19) and (6.20) still hold. Then we can still use Eq. (6.21), (6.22) and (6.23) to guess appropriate parameters for the point-to-point motion in  $\xi$ . Experience has shown that this works: Fig. 6.3 shows position, velocity, acceleration and jerk for the example of Fig. 6.2b.

Now we perform this trajectory with the manipulators presented in Section 5.3, p. 88 ff. (Fig. 6.4) and solve the inverse kinematics (which is trivial) and the inverse dynamics (with the algorithm presented in Section 4.7, p. 77 ff).

Fig. 6.5 shows the tendon velocities for designs a and b. As explained in Section 6.1, the tendon velocity is always less than or equal to the end-effector velocity. Comparison of Fig. 6.5 with Fig. 6.3b shows that this bound is in fact reached, i. e. often some tendon moves almost as fast as the end-effector. Similar results can be found for the other two designs.

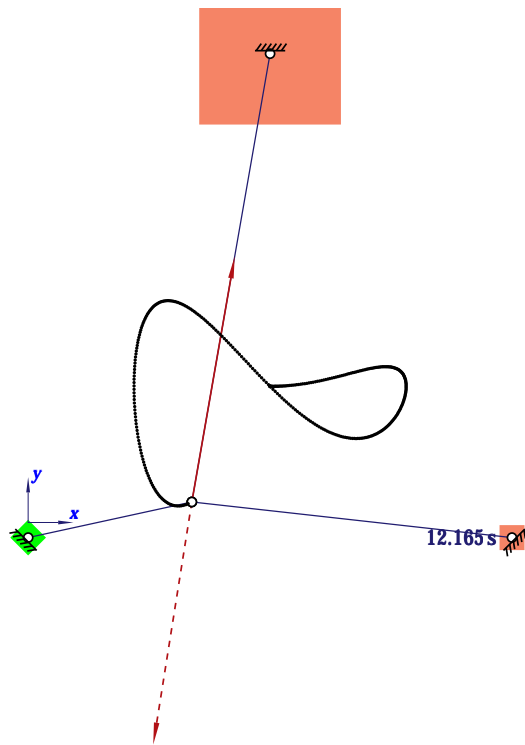
When looking at the accelerations as illustrated in Fig. 6.5, we find that the acceleration shift explained in Section 6.1 is almost invisible in design b and most of the time also in c. But for a short period of less than a second, it leads to very high peaks in c: this is when the end-effector comes very close to winch n° 8 (on the left border of the system). The same can be observed for design a which behaves like b and for d which resembles c. We can conclude that most of the time during a task, tendon acceleration is in the order of magnitude of end-effector acceleration, but near actuators, high acceleration peaks can come up very suddenly. The control hardware and software must be aware of such sudden events. For the software this should not be difficult, as the peaks can be foreseen easily. If this is not possible, trajectories should be planned such that they avoid vicinity of winches.<sup>6</sup>

		a)	b)	c)	d)	where
$\overline{k_{e1}}$	$[\text{kN m}^{-1}]$	0.955	2.053	5.972	14.079	$K = 10.0 \text{ kN}$
$\min_t k_{e1}$	$[\text{kN m}^{-1}]$	0.622	1.493	4.447	10.495	

Table 6.1: Stiffness for 2T trajectory

Next, we take a look at the stiffness eigenvalues, as plotted in Fig. 6.7. As pointed out in the context of Eq. (3.31), p. 50, the value of the smaller one measures vicinity to singularities: it vanishes if a singular posture is reached. It was

<sup>6</sup>Note that there is a difference between «vicinity of winches» and «vicinity of the border of the workspace»: for instance, in case a, the trajectory comes very close to the border of the workspace (cf. Fig. 6.4a), but it is always quite far away from the winches.



a) CRPM

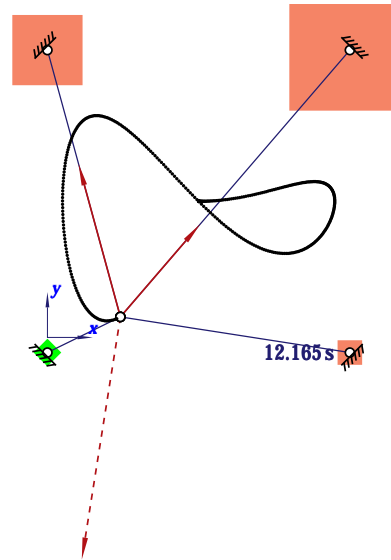
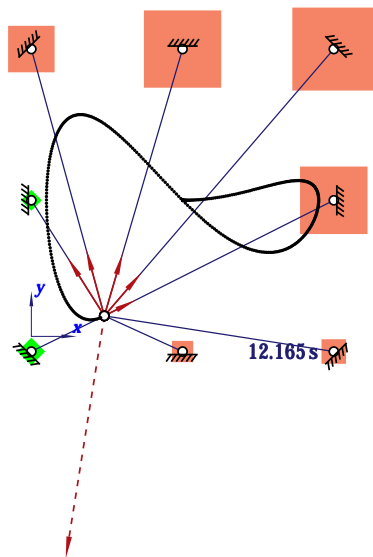
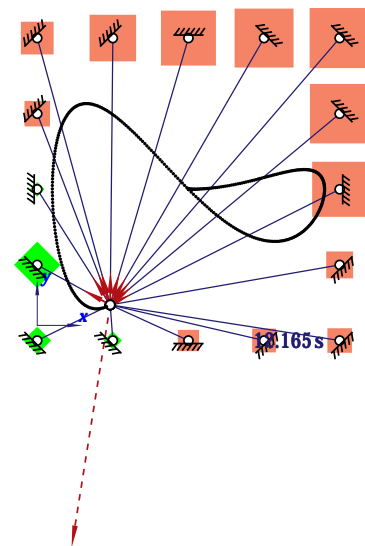
b) RRPM with  $m - n - 1 = 1$ c) RRPM with  $m - n - 1 = 5$ d) RRPM with  $m - n - 1 = 13$ 

Figure 6.4: 2T sample designs

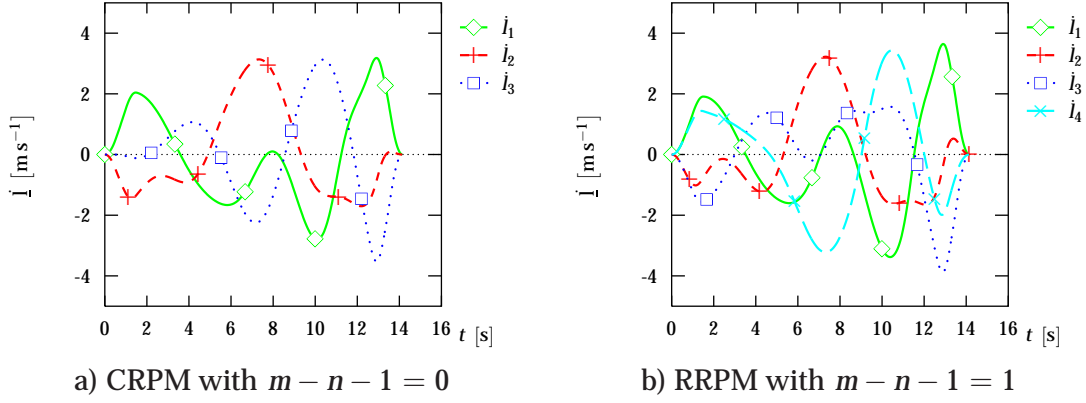


Figure 6.5: Tendon velocity for 2T trajectory

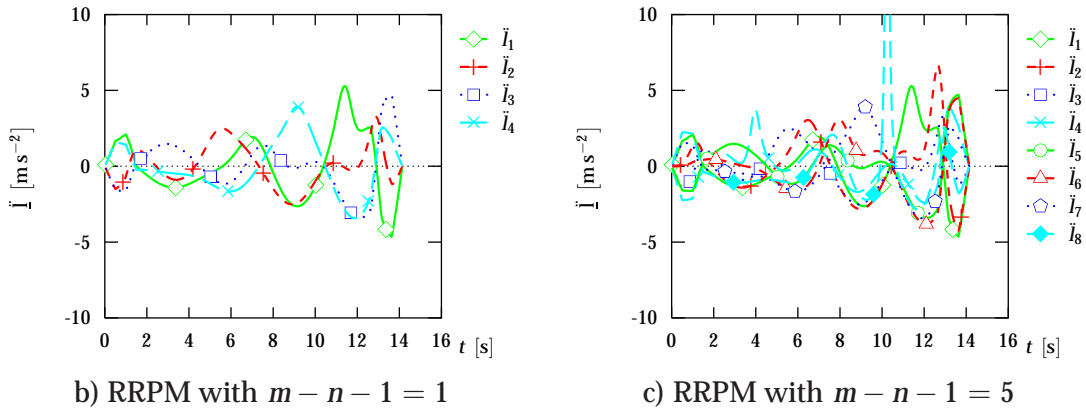
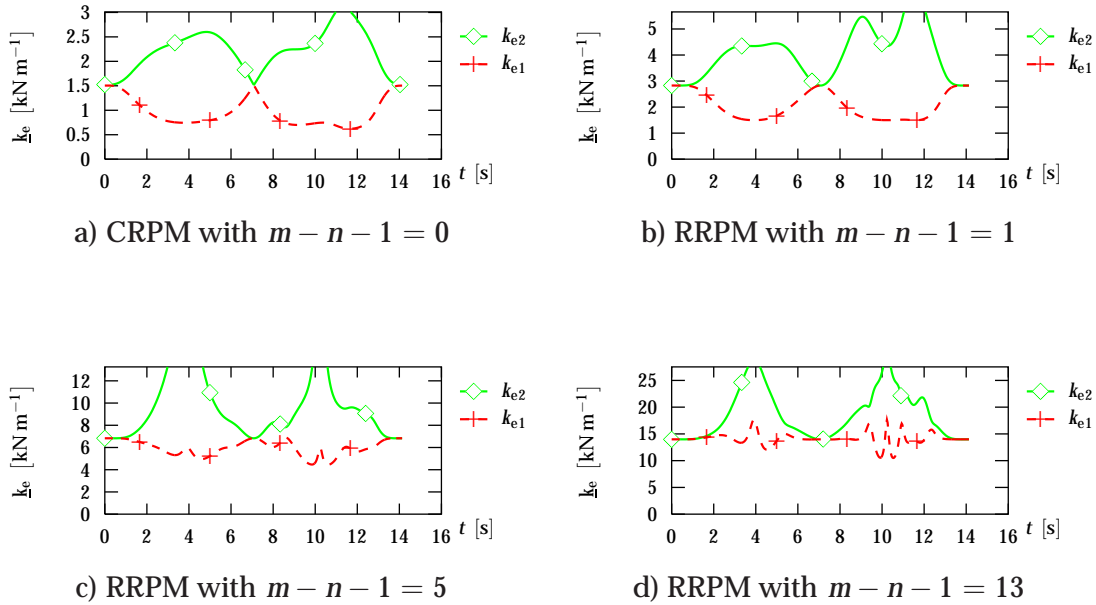


Figure 6.6: Tendon acceleration for 2T trajectory

Figure 6.7: Stiffness for 2T trajectory  
(with  $k' = 10.0$  kN)

shown in Section 3.3, p. 43 ff. that purely translational systems are singularity-free and in fact, the eigenvalues are far away from zero in all designs. The overall level of stiffness is higher if more tendons are employed,<sup>7</sup> as shown also in Table 6.1.

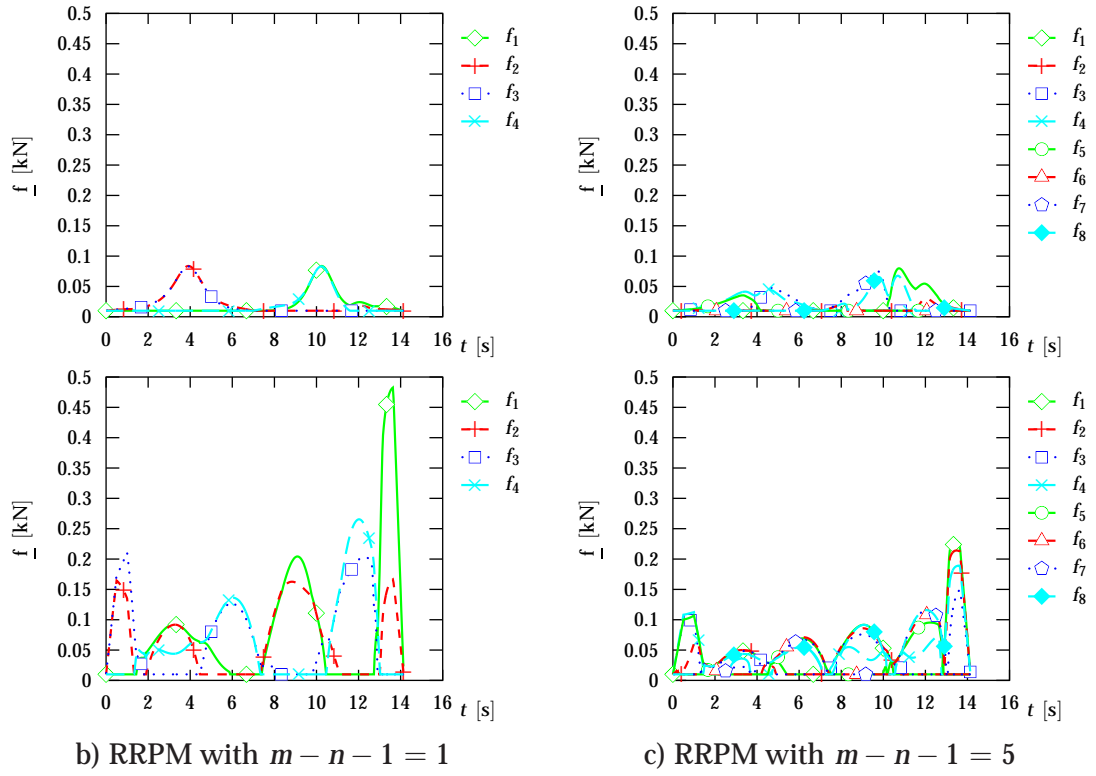


Figure 6.8: Tendon forces for 2T trajectory

( $f_{\min} = 0.010$  kN,  $f_{\max} = 1.000$  kN;

for each design, forces computed with the  $\|\cdot\|_5$ -norm,

$m_P = 1.0$  kg in the first plot,  $m_P = 100.0$  kg in the second one)

	a)	b)	c)	d)	where
$\max_t \ \underline{f}(t)\ _\infty$ [kN]	0.159	0.084	0.080	0.083	$m_P = 1.0$ kg
$\max_t \ \underline{f}(t)\ _\infty$ [kN]	0.565	0.483	0.224	0.120	$m_P = 100.0$ kg
$\max_t \ \underline{\dot{f}}(t)\ _\infty$ [kN s <sup>-1</sup> ]	0.226	0.081	0.292	0.315	$m_P = 1.0$ kg
$\max_t \ \underline{\dot{f}}(t)\ _\infty$ [kN s <sup>-1</sup> ]	2.087	1.577	2.030	1.203	$m_P = 100.0$ kg

Table 6.2: Maximum forces / force change rates for 2T trajectory

Fig. 6.8 shows some tendon forces, computed to  $\underline{f}_{\text{low},5}$  as described in Section 4.5, p. 69 ff. The trajectory is performed once with a platform mass of  $m_P = 1.0$  kg, and another time with  $m_P = 100.0$  kg in each design. Thus, the first version is an almost quasistatic motion in the sense that tendon forces are required only to balance each other, while in the second version they also have to balance platform inertia.<sup>8</sup> Both simulations do not contain gravity, i. e. we as-

<sup>7</sup>Note that the y axes are scaled individually for each design, such that the point where both eigenvalues are equal is always in the middle of the axis range.

<sup>8</sup>The forces shown in Fig. 6.4 refer to the second case.

sume that the motion takes place in a horizontal plane. The maximum forces (i. e. the maximum of the tensions among all tendons in all points of time) are summarized in Table 6.2. As expected, the peak force decreases with the number of tendons and this especially if the load is high. Intuitively speaking, a larger number of tendons then shares the same load and in fact, the maxima for the heavy load are roughly proportional to  $\frac{1}{m}$ .

There is a general tendency that only some tendons are «active» with a tension  $f_\mu > f_{\min}$  while the others just hold the minimum force  $f_{\min}$ , so that at certain points, some tendons are «switched on», while others are «switched off». However, the force paths are continuous, as proven in Section 4.6, p. 72 ff. In this context it is interesting to have a look at the time derivatives  $\dot{f}$  of the forces<sup>9</sup> (Table 6.2). It does not seem that there is a systematic dependency on the number of tendons,<sup>10</sup> but it can be observed that the force derivatives have larger values for the higher mass. This is mainly due to the changes in acceleration direction which are negligible only if the mass is small.

	a)	b)	c)	d)	where
$\overline{d_\partial}$	0.637	0.583	0.502	0.484	$m_P = 1.0 \text{ kg} \quad \ \cdot\ _p = \ \cdot\ _5$
$\overline{d_\partial}$	0.718	0.620	0.537	0.501	$m_P = 100.0 \text{ kg}$
$\min_t d_\partial(t)$	0.080	0.177	0.114	0.105	$m_P = 1.0 \text{ kg} \quad \ \cdot\ _p = \ \cdot\ _5$
$\min_t d_\partial(t)$	0.438	0.261	0.177	0.158	$m_P = 100.0 \text{ kg}$

Table 6.3: Distance from border for 2T trajectory

The quality index developed in Section 5.2, p. 87 ff. is shown in Fig. 6.9 and Table 6.3. Both its average and minimum value over the trajectory tends to decrease because in peripheral regions, more force may be required to balance the other tendons, as explained in the context of Rule 5.2, p. 89.

Our next topic is mechanical power consumption (Fig. 6.10 and Table 6.4). For the large mass, the maximum power occurring in a single actuator is very roughly proportional to  $\frac{1}{m}$ . The power peak of the entire system does not vary that much with the number of actuators, while the overall energy consumption increases with  $m$ , but much less than proportionally.

Finally, we discuss the computation time in these examples. Fig. 6.11 shows the CPU<sup>11</sup> time needed to compute the force distribution in each single point of the trajectory and Table 6.5 summarizes the average time for each trajectory. As expected, CPU time increases dramatically with the degree of redundancy. Computation requires more time if large additional forces (in this case, inertia) appear.

<sup>9</sup>The force paths are differentiable not everywhere, but almost. Hence, a numerical derivate can always be computed: in non-differentiable points, it lies somewhere between limes inferior and limes superior of the quotient of differences, and this is still a meaningful result.

<sup>10</sup>Actually, the most interesting point of these figures is that they help to validate the force optimization algorithm. If the implementation is correct, then the resulting force paths are continuous and their derivatives bounded. While developing the current implementation, many bugs were found and fixed by investigating extreme peaks in the  $\dot{f}$ -plots.

<sup>11</sup>on a 1.1 MHz Pentium™ III



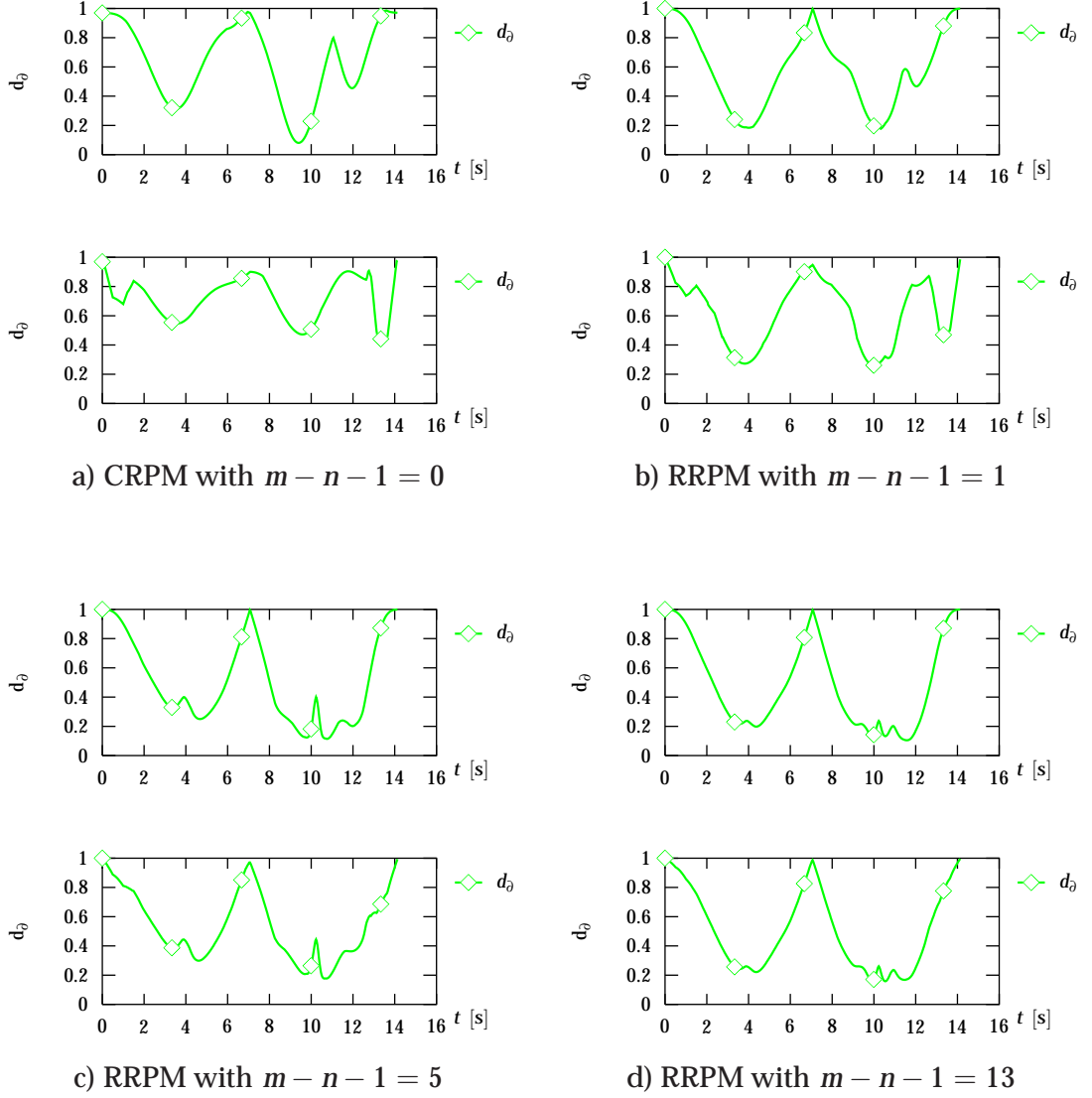


Figure 6.9: Distance from border for 2T trajectory

	a)	b)	c)	d)	where
$\max_t \ \underline{P}(t)\ _\infty$ [kW]	0.334	0.280	0.252	0.243	$m_P = 1.0$ kg
$\max_t \ \underline{P}(t)\ _\infty$ [kW]	1.049	0.670	0.319	0.178	$m_P = 100.0$ kg
$\max_t P_+(t)$ [kW]	0.338	0.296	0.293	0.574	$m_P = 1.0$ kg
$\max_t P_+(t)$ [kW]	1.063	1.066	1.075	1.174	$m_P = 100.0$ kg
$W$ [kJ]	0.645	0.823	1.210	2.401	$m_P = 1.0$ kg
$W$ [kJ]	2.428	2.503	2.815	3.382	$m_P = 100.0$ kg

Table 6.4: Energy consumption for 2T trajectory

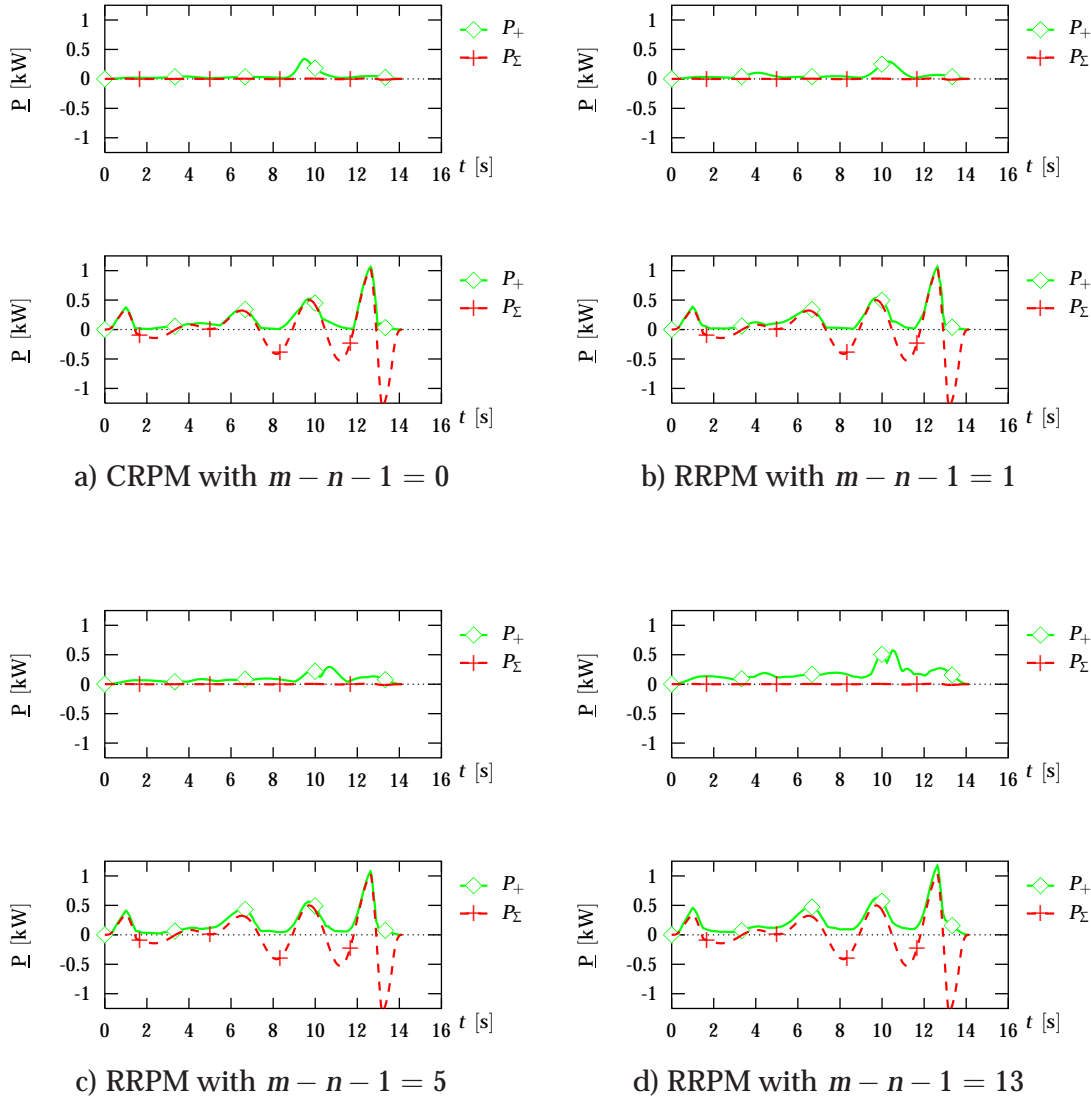


Figure 6.10: Power consumption for 2T trajectory

After this general discussion about geometry and mass, we examine the influence of some other parameters, with a mass of  $m_p = 10.0$  kg as a kind of average situation. Table 6.6 shows force, workspace quality, energy and CPU time characteristics for several values of the approximation parameter  $p$  (introduced in Section 4.5, p. 69 ff.):

$$(6.27) \quad p = 2^k + 1, \quad k = 0, \dots, 5;$$

such values allow fast computation of powers (see Section 4.7, p. 77 ff.). As expected from theory, the maximum forces are lower for higher  $p$ , although this phenomenon is remarkable only for high redundancy, while the force change rate increases with  $p$  in an irregular manner and the workspace quality increases significantly with  $p$ .

The dashes in the energy row for design b indicate that no overall energy consumption could be computed because the trajectory could not be performed under these conditions. The reader might be surprised because the only change with respect to Table 6.4 was the platform mass. But the chosen trajectory comes

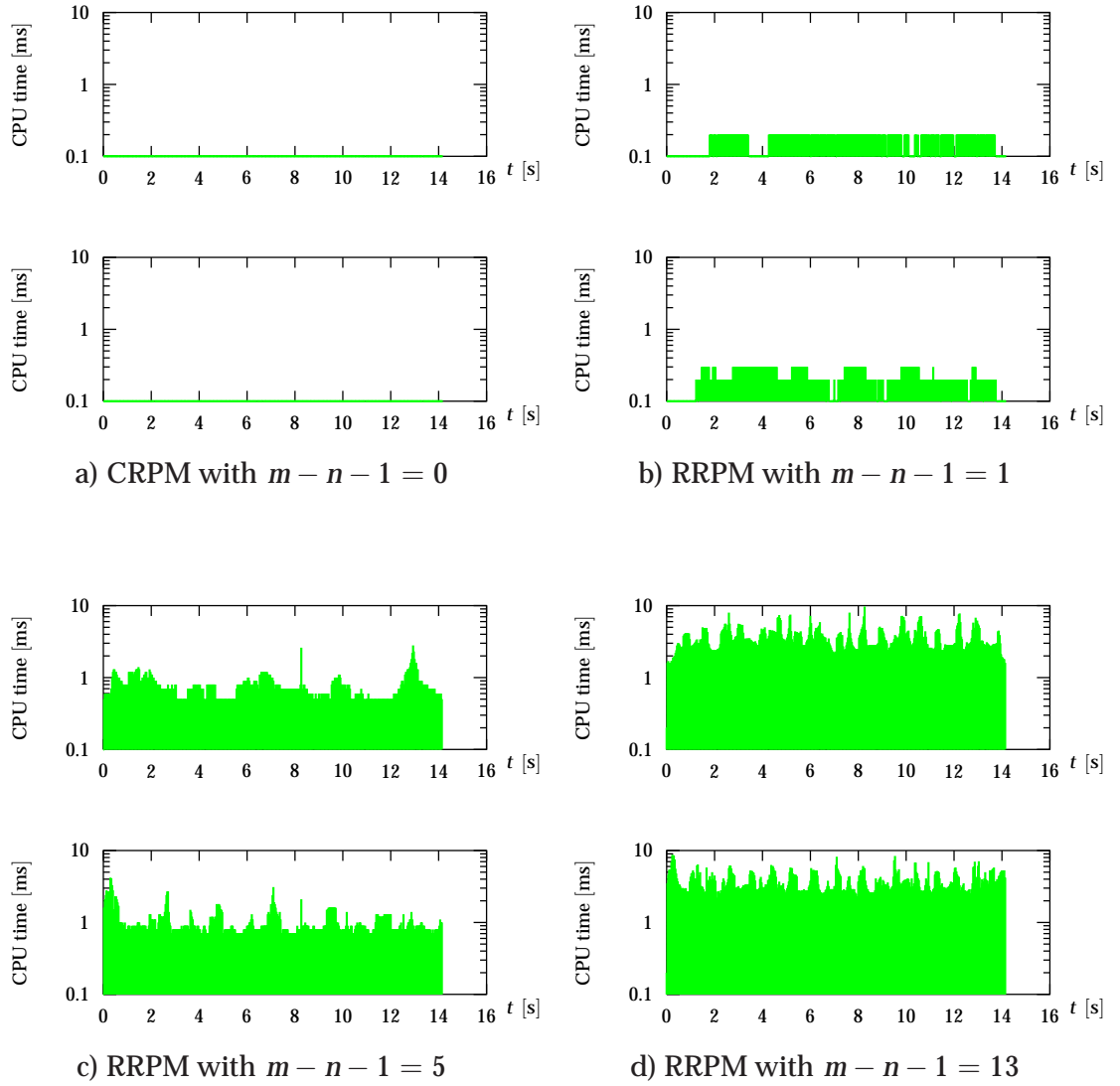


Figure 6.11: CPU time usage for 2T trajectory  
(computing optima up to a precision of about  $10^{-3}$ )

	a)	b)	c)	d)	where
$\overline{t_{\text{CPU}}} \text{ [ms]}$	0.000	0.172	0.777	3.683	$m_{\text{P}} = 1.0 \text{ kg}$ precision $10^{-3}$
$\overline{t_{\text{CPU}}} \text{ [ms]}$	0.017	0.216	1.040	3.838	$m_{\text{P}} = 100.0 \text{ kg}$

Table 6.5: Average computation time for 2T trajectory

$p$		2	3	5	9	17	33
$\max_t \ \underline{f}(t)\ _\infty$ [kN]	a)	0.065	0.065	0.065	0.065	0.065	0.065
	b)	0.058	0.058	0.058	0.058	0.058	0.058
	c)	0.056	0.056	0.056	0.056	0.056	0.056
	d)	0.081	0.074	0.070	0.067	0.066	0.066
$\max_{t,\mu} \dot{f}_\mu$ [kN s <sup>-1</sup> ]	a)	0.198	0.198	0.198	0.198	0.198	0.198
	b)	0.149	0.149	0.149	0.149	0.149	0.149
	c)	0.148	0.148	0.148	0.148	0.391	0.813
	d)	0.202	0.170	0.191	0.194	0.201	0.539
$\overline{d_\partial}$	a)	0.650	0.650	0.650	0.650	0.650	0.650
	b)	—	—	—	—	—	—
	c)	0.405	0.458	0.506	0.529	0.540	0.545
	d)	0.374	0.436	0.487	0.512	0.524	0.530
$\min_t d_\partial(t)$	a)	0.117	0.117	0.117	0.117	0.117	0.117
	b)	—	—	—	—	—	—
	c)	0.001	0.024	0.121	0.164	0.186	0.197
	d)	0.000	0.002	0.111	0.161	0.185	0.197
$\max_t \ \underline{P}(t)\ _\infty$ [kW]	a)	0.118	0.118	0.118	0.118	0.118	0.118
	b)	0.126	0.126	0.126	0.126	0.126	0.126
	c)	0.180	0.180	0.180	0.180	0.180	0.180
	d)	0.229	0.218	0.213	0.210	0.216	0.219
$\max_t P_+(t)$ [kW]	a)	0.133	0.133	0.133	0.133	0.133	0.133
	b)	0.142	0.142	0.142	0.142	0.143	0.145
	c)	0.221	0.221	0.221	0.221	0.221	0.221
	d)	0.462	0.499	0.514	0.522	0.527	0.528
$W$ [kJ]	a)	0.447	0.447	0.447	0.447	0.447	0.447
	b)	—	—	—	—	—	—
	c)	1.092	1.101	1.108	1.113	1.115	1.117
	d)	2.123	2.210	2.272	2.306	2.324	2.333
$\overline{t_{\text{CPU}}}$ [ms]	a)	0.004	0.004	0.004	0.005	0.003	0.003
	b)	0.106	0.115	0.179	0.189	0.292	0.499
	c)	0.600	0.696	0.874	1.139	1.504	2.304
	d)	2.057	2.569	3.397	4.637	5.406	7.002

Table 6.6: Influence of the parameter  $p$  for 2T trajectory

very near to the border of the workspace and hence feasibility of some pieces of the curve depends very much on the other forces involved. Further investigations have shown that *the set of «feasible platform masses» for this trajectory is indeed disconnected: masses up to 2 kg or above 15 kg can be used, while masses between 3 and 10 kg cannot.*

There is no clear relationship between the parameter  $p$  and the energy consumption. Indeed, this would be minimized by using a weighted  $\|\cdot\|_1$ -norm which uses the tendon velocities  $\dot{l}_\mu$  as weighting factors.<sup>12</sup> If velocities are not taken into account, higher values of  $p$  tend to slightly increase power consumption.

Computation time increases considerably with higher  $p$ . This is clear if we think that sets of solutions with equal  $\|\cdot\|_\infty$ -norm (so-called «level sets») are axis-parallel boxes, level sets for the  $\|\cdot\|_2$ -norm are balls and other  $\|\cdot\|_p$ -norms lead to intermediate shapes. Now the boundary conditions  $\bar{f} \in [f_{\min}, f_{\max}]^m$  correspond to another axis-parallel box. Therefore, the higher  $\bar{p}$ , the more the level-sets are box-shaped and hence the objective function gradients tend to be almost perpendicular to the boundary. This leads to smaller steps and therefore to higher computation times.

Thus, workspace quality requires larger values of  $p$  and computation speed suggests to choose  $p$  not too high, while the other criteria do not provide substantial recommendations. We propose  $p = 5$  as a compromise and shall continue using it throughout this section.

precision		$10^{-1}$	$10^{-2}$	$10^{-3}$	$10^{-4}$	$10^{-5}$	$10^{-6}$
$\overline{d_0}$	a)	0.650	0.650	0.650	0.650	0.650	0.650
	b)	—	—	—	—	—	—
	c)	0.506	0.506	0.506	0.506	0.506	0.506
	d)	0.487	0.487	0.487	0.487	0.487	0.487
$\min_t d_0(t)$	a)	0.116	0.117	0.117	0.117	0.117	0.117
	b)	—	—	—	—	—	—
	c)	0.121	0.121	0.121	0.121	0.121	0.121
	d)	0.110	0.111	0.111	0.111	0.111	0.111
$\overline{t_{\text{CPU}}}$ [ms]	a)	0.006	0.004	0.001	0.003	0.004	0.004
	b)	0.113	0.142	0.178	0.182	0.177	0.185
	c)	0.551	0.698	0.873	1.079	1.288	1.515
	d)	1.884	2.580	3.444	4.440	5.403	6.314

Table 6.7: Influence of the computation precision for a 2T trajectory

Another interesting parameter is the requested *precision* we try to achieve when computing the optimal force distribution, as explained in Section 4.7, p. 77 ff. Table 6.7 shows a comparison for various values of precision. It turns

<sup>12</sup>However, the  $\|\cdot\|_1$ -norm might lead to discontinuous force paths the same way as the  $\|\cdot\|_\infty$ -norm does.

out that we may lose a little bit of workspace quality when computing very rough solutions, while we waste much computation time when requesting too high precision. Apparently,  $10^{-3}$  is more than sufficient for this type of systems.

To conclude this section, we simulate the test trajectory with gravity, using the modified designs of Fig. 5.2, p. 90 where some winches pulling downwards (regarded as superfluous) were removed.

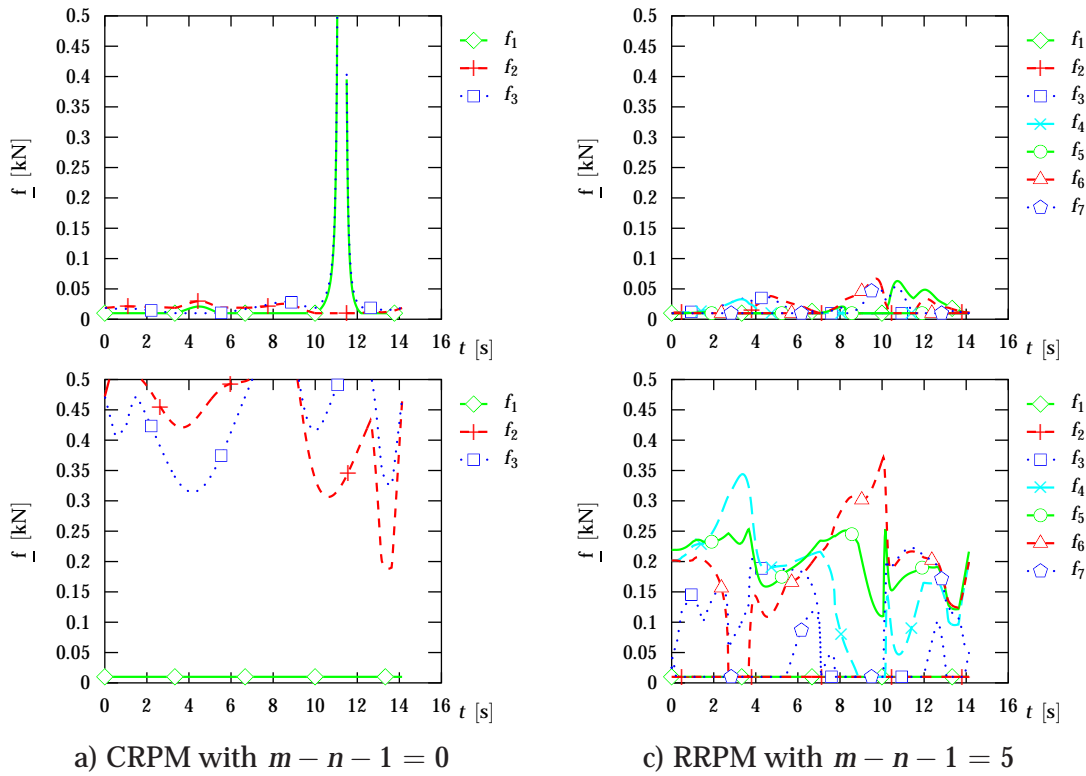


Figure 6.12: Tendon forces for a 2T trajectory with gravity  
(for each design,  $m_P = 1.0$  kg in the first plot,  
 $m_P = 50.0$  kg in the second one)

Again, we compare two masses; but in this case, the second mass was chosen smaller than before, because otherwise the CRPM and the RRPM with  $m - n - 1 = 1$  would not have been able to handle it. They're not able to handle the light mass, either; but this was left unchanged, to show again that small masses can be a problem as well as large ones. Fig. 6.12 shows forces for two designs (with the same force limits as in the previous simulations). Clearly, in this case the forces for the large mass tend to be much higher than those for the small one. The summary in Table 6.8 confirms all the general remarks made above on the examples without gravity. Some other trajectories, which are not discussed here, were also simulated and give similar results.

	a)	b)	c)	d)	where
$\max_t \  \underline{f}(t) \ _\infty$ [kN]	0.616	0.086	0.067	0.125	$m_p = 1.0$ kg
$\max_t \  \underline{f}(t) \ _\infty$ [kN]	0.608	0.547	0.372	0.195	$m_p = 50.0$ kg
$\overline{d_\partial}$	—	—	0.463	0.393	$m_p = 1.0$ kg
$\overline{d_\partial}$	0.510	0.430	0.541	0.463	$m_p = 50.0$ kg
$\min_t d_\partial(t)$	—	—	0.169	0.020	$m_p = 1.0$ kg
$\min_t d_\partial(t)$	0.293	0.145	0.098	0.189	$m_p = 50.0$ kg
$\max_t \  \underline{P}(t) \ _\infty$ [kW]	1.730	0.260	0.200	0.190	$m_p = 1.0$ kg
$\max_t \  \underline{P}(t) \ _\infty$ [kW]	1.651	1.299	0.794	0.378	$m_p = 50.0$ kg
$W$ [kJ]	—	—	1.033	2.040	$m_p = 1.0$ kg
$W$ [kJ]	8.443	6.552	6.595	7.055	$m_p = 50.0$ kg
$\overline{t_{\text{CPU}}}$ [ms]	0.006	0.170	0.703	2.579	$m_p = 1.0$ kg
$\overline{t_{\text{CPU}}}$ [ms]	0.033	0.195	0.875	2.724	$m_p = 50.0$ kg

Table 6.8: Summary for a 2T trajectory with gravity

### 6.3. Spatial Systems with six DOFs

Now, we will simulate a spatial trajectory similar to that in the preceding section, by adding a z component which also varies in time:

$$(6.28) \quad \underline{r} = \left( d_1 \sin \xi, \frac{d_2}{2\pi} \xi \sin 2\xi, d_3 \sin \frac{1}{2}\xi \right)^T, \quad \xi \in [0, 2\pi]$$

$$(6.29) \quad \underline{\dot{r}} = \dot{\xi} \left( d_1 \cos \xi, \frac{d_2}{2\pi} \sin 2\xi + \frac{d_2}{\pi} \xi \cos 2\xi, \frac{d_3}{2} \cos \frac{1}{2}\xi \right)^T$$

$$(6.30) \quad \underline{\ddot{r}} = \ddot{\xi} \left( d_1 \cos \xi, \frac{d_2}{2\pi} \sin 2\xi + \frac{d_2}{\pi} \xi \cos 2\xi, \frac{d_3}{4} \sin \frac{1}{2}\xi \right)^T \\ - \dot{\xi}^2 \left( d_1 \sin \xi, -\frac{2 d_2}{\pi} \cos 2\xi + \frac{2 d_2}{\pi} \xi \sin 2\xi, \frac{d_3}{4} \sin \frac{1}{2}\xi \right)^T.$$

Fig. 6.13 shows one posture in the trajectory as well as an overview of the entire trajectory with some postures of the platform coordinate frame.

With the same approximation as in Eq. (6.18), (6.19) and (6.20) and neglecting the contribution of the z component to the absolute value of acceleration and jerk, we obtain the estimates

$$(6.31) \quad |\underline{\dot{r}}| \leq c_1 |\dot{\xi}|, \quad c_1 := \sqrt{d_1^2 + 4 d_2^2 + \frac{1}{4} d_3^2}$$

$$(6.32) \quad |\underline{\ddot{r}}| \leq c_1 |\ddot{\xi}| + c_2 |\dot{\xi}|^2, \quad c_2 := \frac{d_1^2 + 64 d_2^2}{16 d_2}$$

$$(6.33) \quad |\underline{\dddot{r}}| \leq c_1 |\dddot{\xi}| + 3 c_2 |\ddot{\xi}| |\dot{\xi}| + c_3 |\dot{\xi}|^3, \quad c_3 := \sqrt{d_1^2 + 64 d_2^2}.$$

Then we can use the same guesses for  $\dot{\xi}_{\max}$ ,  $\ddot{\xi}_{\max}$ ,  $\dddot{\xi}_{\max}$  as in Eq. (6.21), (6.22) and (6.23).



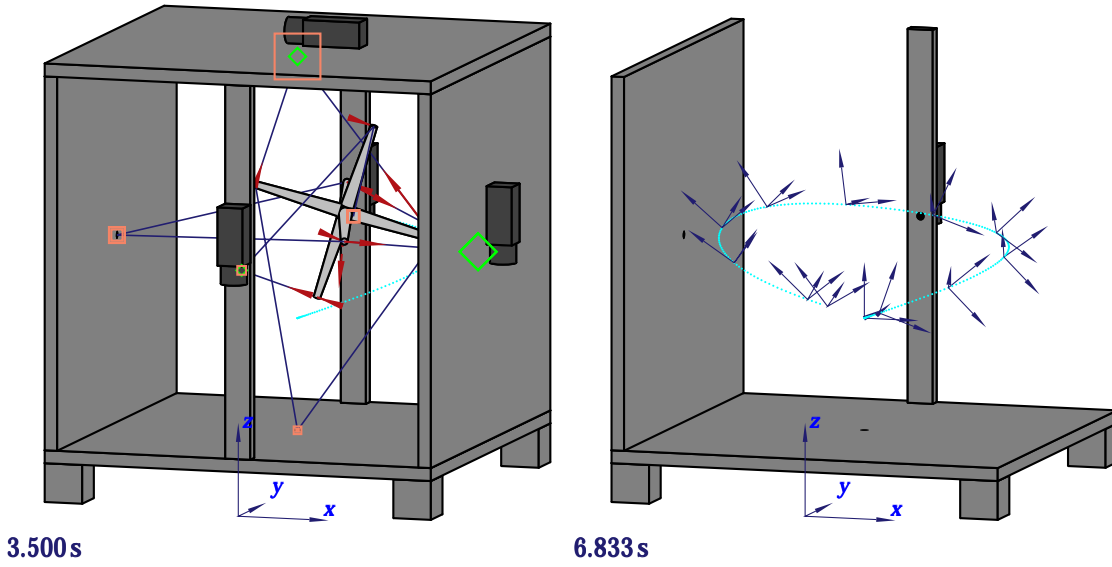


Figure 6.13: Test trajectory for 3R3T systems

For the orientation of the platform, we require that the negative  $z$  axis of  $\mathcal{K}_P$  should always be oriented towards a point below the start position and that the projection of the  $x$  axis of  $\mathcal{K}_P$  on the  $xy$  plane of  $\mathcal{K}_B$  should be a multiple of  $(1, \sin \xi, 0)^T$ , i.e. it performs a cyclic motion within the limits  $\pm 45^\circ$ . This way, the third column of the rotation matrix  $\underline{R}$  can be written down directly, the first one can be computed by an appropriate vector product and the second one is the vector product of the other two:

$$(6.34) \quad \underline{R}_3 = \frac{\underline{r} + (0, 0, 1)}{|\underline{r} + (0, 0, 1)|}$$

$$(6.35) \quad \underline{R}_1 = \frac{\underline{R}_3 \times (\sin \xi, -1, 0)}{|\underline{R}_3 \times (\sin \xi, -1, 0)|}$$

$$(6.36) \quad \underline{R}_2 = \underline{R}_3 \times \underline{R}_1.$$

The corresponding end-effector posture and velocity are plotted in Fig. 6.14.

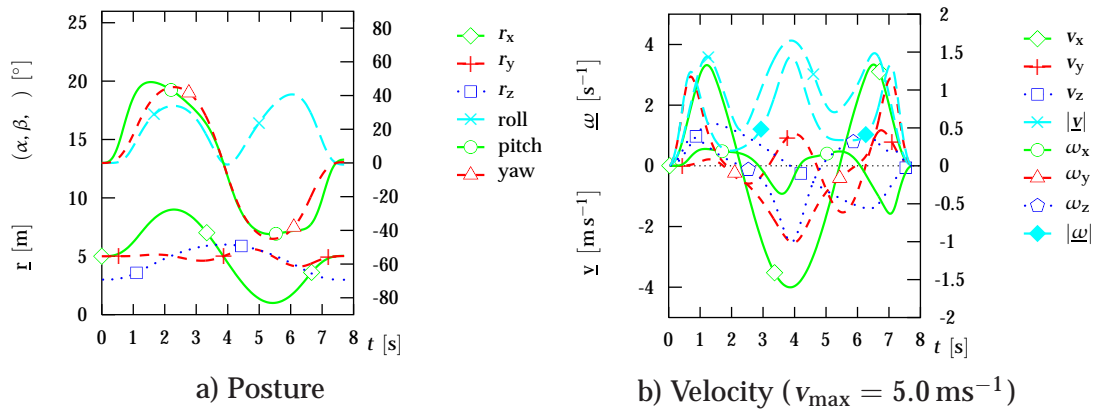


Figure 6.14: End-effector motion for a 3T3T trajectory

$p$		2	3	5	9	17	33
$\overline{d_\theta}$	b)	—	—	—	—	—	—
	d)	0.121	0.139	0.155	0.166	0.175	0.181
	f)	0.110	0.173	0.223	0.263	0.285	0.298
$\min_t d_\theta(t)$	b)	—	—	—	—	—	—
	d)	0.000	0.000	0.000	0.000	0.000	0.000
	f)	0.000	0.000	0.000	0.000	0.012	0.042
$\overline{t_{\text{CPU}}}$ [ms]	b)	1.110	1.105	1.100	1.099	1.105	1.095
	d)	0.545	0.606	0.664	0.831	1.223	1.987
	f)	1.622	1.894	2.274	2.879	3.709	5.327

Table 6.9: Influence of the parameter  $p$  for a 3R3T trajectory

Table 5.2, p. 97 suggests that it is worthwhile to take into consideration the following designs of Fig. 5.5, p. 96 which offer a relatively large workspace:

- The «Virtual Tennis» design b),
- the «Nishioka» design d),
- the «French-German» design f).

Simulations have shown that the higher number of end-effector-DOFs (and tendons) when compared to 2T systems, require higher values for the parameter  $p$  to find acceptable solutions (Table 6.9).

	b)	d)	f)	where
$\overline{k_{e1}}$ [kN m <sup>-1</sup> ]	0.345	0.714	2.016	$k' = 10.0$ kN
$\min_t k_{e1}$ [kN m <sup>-1</sup> ]	0.057	0.243	0.976	
$\max_t \ f(t)\ _\infty$ [kN]	0.390	0.388	0.438	$m_p = 10.0$ kg
$\overline{d_\theta}$	—	0.175	0.285	$\ \cdot\ _p = \ \cdot\ _{17}$
$\min_t d_\theta(t)$	—	0.000	0.012	
$\max_t \ \underline{P}(t)\ _\infty$ [kW]	0.324	0.550	0.695	
$\max_t P_+(t)$ [kW]	0.562	0.973	0.793	
$W$ [kJ]	—	2.572	3.098	
$\overline{t_{\text{CPU}}}$ [ms]	1.082	1.225	3.665	precision $10^{-3}$

Table 6.10: Summary for a 3R3T trajectory

Summarizing the results for reasonable choices, Table 6.10 provides a good overview of the dilemma typical for the design of tendon-based Stewart platforms, which was seen already in the previous section but is much more striking for 3R3T systems:

- Independently of any simulation results, one would try to use as few actuators as possible for reasons of cost.
- But workspace can be improved a lot by adding more tendons, as already seen in Table 5.2, p. 97.
- If stiffness is important, it is useful to use as many tendons as possible. In the examples presented, stiffness increases much more than proportionally with the number of tendons if tendons of equal stiffness are employed.
- Maximum forces tend to increase with the number of tendons because more forces need to be balanced. This somewhat counterintuitive phenomenon was already observed for 2T systems and might discourage the use of a large number of tendons.
- Workspace size, shape and quality improve a lot if additional tendons are arranged in an intelligent way. In this example, the chosen test trajectory cannot be performed by the CRPM. On the other hand, tests have shown that the French-German design is able to perform larger trajectories of that shape which are partly outside the workspace of the Nishioka design.
- The relationship between number of tendons and energy consumption does not give a clear picture.
- Computation time increases much more than linearly with the degree of redundancy.

In few simple words, large workspaces of high quality can be obtained with large numbers of tendons, but one has to pay a price for this in terms of actuator cost, force requirements and computation time.

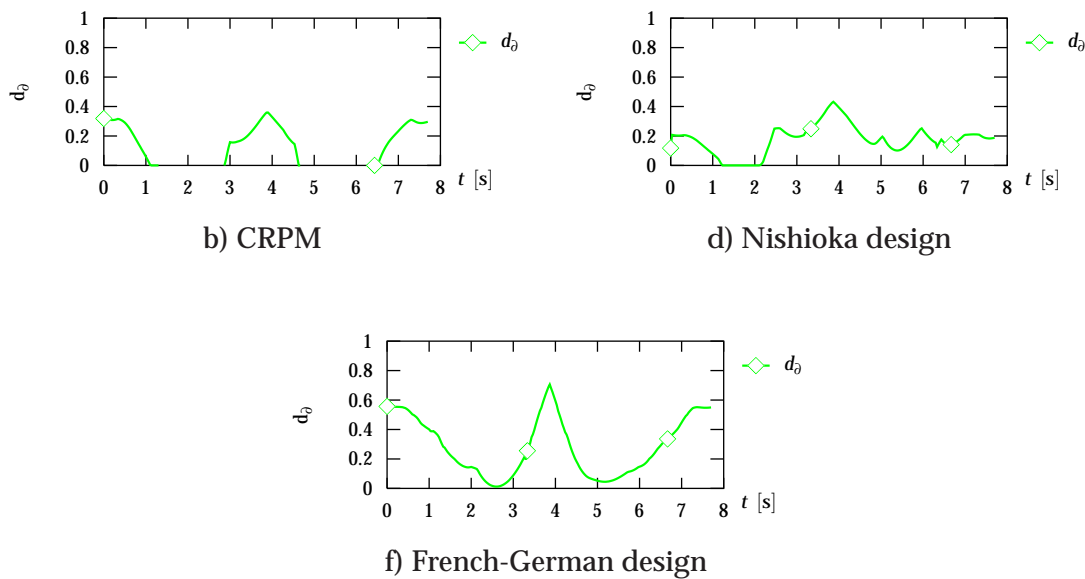


Figure 6.15: Distance from border for a 3R3T trajectory  
(with  $\|\cdot\|_p = \|\cdot\|_{17}$ )

The plots for  $d_{\theta}$  are shown in Fig. 6.15. These plots have proven to be a most useful tool when looking for a test trajectory which should fit at least into the workspaces of the Niskioka and the French-German design, because they show clearly which parts of the trajectory approach the border and therefore need to be modified. Without the concept of workspace quality index, such an analysis would require knowledge of the 6-dimensional workspace shape around the current posture, which is most difficult to obtain (as already stated several times).

**6.1 Rule of Thumb** *While it is almost impossible to get an overview of the shape of the workspace of a 3R3T system, the workspace quality index often allows to do without such knowledge.  $\diamond$*



# Chapter 7

## Conclusions and Outlook

### 7.1. Workspace Basics

The first part of this thesis gave an introduction to tendon-based Stewart platforms. While many of the cited facts were already known, to the author's knowledge this is the first time that they were collected and presented in a coherent manner and in rather mathematical terms.

An important negative result was the proof that an intuitive way to compute tensions does not always guarantee a positive solution (Prop. 3.3, p. 38). A completely new result, obtained with theory of convex sets, was that it is possible to write down the controllable workspace in closed form (Theorem 3.4, p. 40), but this is useless from a practical point of view. Another interesting fact, which to the author's knowledge was not yet stated elsewhere, is the possibility to build (almost) singularity-free manipulators in an easy constructive way (Prop. 3.6, p. 45).

### 7.2. Optimal Tension Distribution

One of the main topics in this thesis was the development of an algorithm to find acceptable tension distributions. Key points include:

1. The theory of convex sets proved again to be a powerful tool.
2. An algorithm was developed which provides solutions with lowest (or highest) possible tensions (Section 4.3, p. 60 ff.).
3. It was proven that a slightly modified algorithm (Section 4.5, p. 69 ff.) provides solutions which form a continuous path in time (Section 4.6, p. 72 ff.) when the platform moves.
4. The algorithm was implemented in C++ (Section 4.7, p. 77 ff.).

### 7.3. Workspace Optimization

There is currently no sound theory on optimization of the workspace of tendon-based Stewart platforms (see Section 5.1, p. 85 ff.) and the present the-

sis did not provide it, either. General results are of negative type: a closed-form representation exists but is useless. Therefore, the chapter on workspace optimization presented a collection of rules of thumb (several of them were already known) which can be used as a first guideline in structural synthesis.

The main achievement in this context was the development of a quality index (Section 5.2, p. 87 ff.) which tells us for a given posture how far it is from the workspace boundary, *without any knowledge of the workspace shape*. Even though it is a measure computed in force space, which cannot be mapped to a distance in meters, it has proven very useful to roughly compare the workspace of designs.

Motions along test trajectories were simulated for planar 2-DOF (Section 6.2, p. 101 ff.) and spatial 6-DOF (Section 6.3, p. 115 ff.) designs and the influence of some design and computation parameters were studied. Here, the new quality index was a quite useful tool to fit trajectories into workspaces.

## 7.4. Outlook

The idea of tendon-based Stewart platforms was pioneered about fifteen years ago and only the last five to ten years have seen an increasing worldwide interest for this concept. The current state of research is characterized by a rapidly increasing number of prototypes and a rather small collection of theory-oriented articles spread over various journals mainly in the USA and Japan. One of the objectives of the present thesis was to provide a first consolidation of the theory known so far, collecting material from a number of sources.

Investigation of workspace has lead to some negative results, like the closed form representation which exists but is useless. From the author's point of view, the question of an adequate description of workspace, as well as the problem of optimizing the manipulator geometry in terms of workspace, is an open issue. Some facts known from intuition and/or experience are summarized in the present work.

The main result of this thesis was the development of the theory of tension distribution and of an algorithm to compute optimal tensions. The algorithm was implemented in C++. It could be developed further: for instance, the conditions for acceptable forces could be modified to obtain smooth boundaries, such that force paths become not only continuous, but also differentiable.

A local workspace quality measure was developed and proven useful for analysis of workspaces and trajectories. In tendon-based Stewart platforms, the problem of tensions is more critical than the classical problems of kinematic performance and singularity avoidance. So such a measure may be important for future work.

The mathematical theory of convex sets has proven quite useful for all of these results. It is likely to offer still a lot of opportunities in the context of tendon-based robots, which are worthwhile to investigate further.



# Appendix A

## Mathematical Background

*This appendix explains the mathematical notation used and summarizes the main facts needed in the preceding chapters. In the first sections, we recall some basic concepts, mainly in order to clarify the terminology. Then we proceed to more specific arguments, probably known to people specialized in certain fields of robotics. We end up with rather sophisticated tools of parametric optimization, which most readers may never have heard of. We will not define all the concepts used in the entire thesis, but rather restrict ourselves to the notions needed in definitions, propositions and proofs. The exposition is intended as a quick reference, rather than an exhaustive introduction to the subjects; however, occasionally we will give explanations in order to convey an intuitive idea of the concepts.*

### A.1. Set Theory

Sets of any kind (including sets of sets) are written with calligraphic letters such as  $\mathcal{X}, \mathcal{Y}$ . The symbol  $\emptyset$  denotes the empty set. The character  $\mathbb{N}$  stands for the set of natural numbers (i. e.  $\{1, 2, \dots\}$ ),  $\mathbb{N}_0$  for the nonnegative integers (i. e.  $\{0, 1, 2, \dots\}$ ) and  $\mathbb{R}$  for the real numbers. Real intervals are written as follows:

$$\begin{array}{ll} [a, b] & := \{x \in \mathbb{R} : a \leq x \leq b\} \\ ]a, b] & := \{x \in \mathbb{R} : a < x \leq b\} \\ [a, b[ & := \{x \in \mathbb{R} : a \leq x < b\} \\ ]a, b[ & := \{x \in \mathbb{R} : a < x < b\} \end{array} \quad \text{and} \quad \begin{array}{ll} \mathbb{R}_+ & := ]0, \infty[ \\ \mathbb{R}_{+0} & := [0, \infty[ \\ \mathbb{R}_- & := ]-\infty, 0[ \\ \mathbb{R}_{-0} & := ]-\infty, 0] \end{array}.$$

The notation  $\mathcal{X} \subset \mathcal{Y}$  means that  $\mathcal{X}$  is a subset of  $\mathcal{Y}$ ; this applies also if both sets are equal. The intersection of two sets is written  $\mathcal{X} \cap \mathcal{Y}$  and their union is  $\mathcal{X} \cup \mathcal{Y}$ . With  $2^{\mathcal{X}}$  we write the power set of  $\mathcal{X}$ , i. e. the set of all the sets  $\mathcal{Y}$  with  $\mathcal{Y} \subset \mathcal{X}$ . (For instance, we have  $\emptyset \in 2^{\mathcal{X}}$  and  $\mathcal{X} \in 2^{\mathcal{X}}$ .)

The Cartesian product  $\mathcal{X} \times \mathcal{Y}$  denotes the set of all the pairs  $(x, y)$  with  $x \in \mathcal{X}$  and  $y \in \mathcal{Y}$ . The term  $\mathcal{X}^m$  denotes the set of all  $m$ -tuples of elements of  $\mathcal{X}$ ; for instance,  $\mathbb{R}_+^3$  is a shorthand for  $\mathbb{R}_+ \times \mathbb{R}_+ \times \mathbb{R}_+$  (all triples of positive real numbers). With  $(x_v) \in \mathcal{X}^{\mathbb{N}}$  we express that  $x_1, x_2, \dots \in \mathcal{X}$  is a sequence of elements of  $\mathcal{X}$ .

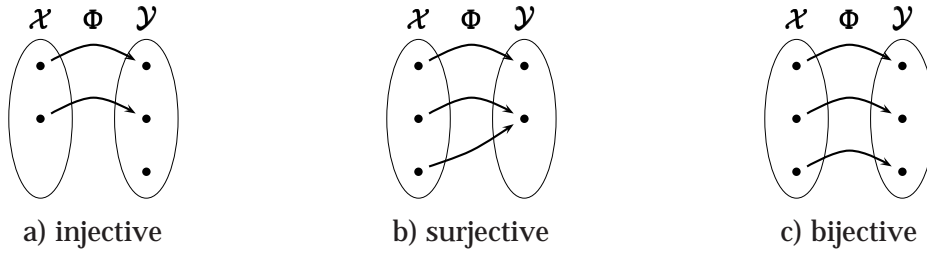


Figure A.1: Examples of mappings

The number of elements in a set  $\mathcal{X}$  is written as  $|\mathcal{X}|$ .

**A.1 Definition (mapping, restriction)** a) Let  $\mathcal{X}, \mathcal{Y}$  be sets of any kind. A mapping that maps an element  $x \in \mathcal{X}$  to  $\Phi(x) \in \mathcal{Y}$  is written as

$$\Phi : \mathcal{X} \rightarrow \mathcal{Y}, x \mapsto \Phi(x) .$$

b) If  $\mathcal{X}_1 \subset \mathcal{X}$ , then the mapping

$$\Phi|_{\mathcal{X}_1} : \mathcal{X}_1 \rightarrow \mathcal{Y}, x \mapsto \Phi(x) .$$

which is identical to  $\Phi$  except that it is defined on a smaller set, is called restriction of  $\Phi$  to  $\mathcal{X}_1$ .  $\diamond$

**A.2 Definition (injective, surjective, bijective)** A mapping  $\Phi : \mathcal{X} \rightarrow \mathcal{Y}$  is called

a) one-to-one or injective (Fig. A.1a) if for each  $y \in \mathcal{Y}$ , there is at most one  $x \in \mathcal{X}$  such that  $x \mapsto y$ ,

b) onto or surjective (Fig. A.1b) if for each  $y \in \mathcal{Y}$ , there is at least one  $x \in \mathcal{X}$  such that  $x \mapsto y$ ,

c) bijective (Fig. A.1c) if for each  $y \in \mathcal{Y}$ , there is exactly one  $x \in \mathcal{X}$  such that  $x \mapsto y$ .  $\diamond$

**A.3 Definition (infimum/supremum, minimum/maximum)** a) Given a (possibly empty) set  $\mathcal{X} \subset [-\infty, \infty]$ , its infimum  $\inf \mathcal{X}$  is the largest element of  $[-\infty, \infty]$  satisfying

$$\forall_{x \in \mathcal{X}} \inf \mathcal{X} \leq x .$$

Similarly, the supremum  $\sup \mathcal{X}$  is the smallest number with

$$\forall_{x \in \mathcal{X}} \sup \mathcal{X} \geq x .$$

These definitions imply

$$\inf \emptyset = \infty \quad \text{and} \quad \sup \emptyset = -\infty .$$

b) The infimum is called minimum if  $\inf \mathcal{X} \in \mathcal{X}$  and the supremum is called maximum if  $\sup \mathcal{X} \in \mathcal{X}$ .  $\diamond$

This way, the infimum and supremum of any set  $\mathcal{X} \subset [-\infty, \infty]$  is always defined, while minimum and maximum may not exist; e. g. the set  $]0, 1[$  has infimum zero and supremum one, but neither minimum nor maximum. Therefore, the expressions «minimum» and «maximum» must be used with care; actually we can talk about them only after they have been proven to exist.

## A.2. Vector Spaces and Linear Mappings

A (real) vector space is a set  $\mathcal{V}$  where the sum of two vectors and the product of a real number with a vector are defined and obey certain rules (that we will not list here). Any book about mechanics actually deals with two different kinds of vector spaces, which in this thesis are also written in distinct ways. «Physical» vectors are physical observables such as velocities, forces etc.; they are written with bold lowercase letters like  $\mathbf{v}$ ,  $\mathbf{f}$ .

«Mathematical» vectors are tuples of real numbers, i.e. elements of vector spaces like  $\mathbb{R}^n$ ; we write them with underlined lowercase letters such as  $\underline{v}$ ,  $\underline{f}$ . Mathematical vectors are obtained from physical ones when measuring the latter with respect to a coordinate frame. Throughout this thesis, it does not matter which coordinate frame is used. So  $\underline{v}$  denotes a coordinate representation of  $\mathbf{v}$  in an arbitrary coordinate frame. We refer to its components using indexes, such as

$$\underline{v} = (v_1, \dots, v_n)^T \in \mathbb{R}^n$$

(where the terms  $v_v$  denote scalars and therefore are not underlined).<sup>1</sup> The example illustrates that elements of  $\mathbb{R}^n$  are considered to be column vectors; when row vectors are needed (often for convenience in writing, as in this case), they are explicitly transposed. The symbols  $\underline{0}$  and  $\underline{1}$  denote vectors having each component equal to 0 (to 1).

**A.4 Definition (independency, dimension)** *a) A family of vectors  $\mathbf{v}_1, \dots, \mathbf{v}_m$  is called linearly independent if the equation*

$$\sum_{\mu=1}^m \alpha_{\mu} \mathbf{v}_{\mu} = \mathbf{0} \quad \text{with} \quad \alpha_1, \dots, \alpha_m \in \mathbb{R}$$

*implies  $\alpha_1, \dots, \alpha_m = 0$ .*

*b) The maximum number of linearly independent vectors that can be found in a vector space is called the dimension of that space.  $\diamond$*

**A.5 Definition (linear mapping)** *Given vector spaces  $\mathcal{V}$  and  $\mathcal{W}$ , a mapping  $A : \mathcal{V} \rightarrow \mathcal{W}$  is called linear if it satisfies for all vectors  $\mathbf{v}_1, \mathbf{v}_2 \in \mathcal{V}$  and all scalars  $\alpha \in \mathbb{R}$*

$$(A.1) \quad A(\mathbf{v}_1 + \mathbf{v}_2) = A\mathbf{v}_1 + A\mathbf{v}_2$$

$$(A.2) \quad \alpha A\mathbf{v}_1 = A(\alpha \mathbf{v}_1) . \diamond$$

We write such mappings with bold uppercase letters. If the vectors in  $\mathcal{V}$  and  $\mathcal{W}$  are represented by tuples  $\underline{v}$ ,  $\underline{w}$  of  $m$  and  $n$  scalars respectively, then each linear mapping  $A$  can be represented by exactly one matrix  $\underline{A} \in \mathbb{R}^{n \times m}$  (a matrix with  $n$  rows and  $m$  columns) such that

$$\underline{w} = \underline{A} \underline{v} .$$

---

<sup>1</sup>Note the difference to expressions like  $\underline{v}_1, \dots, \underline{v}_m$  which represent families of vectors.

The following definitions and propositions are formulated in terms of matrices (because this is what mostly appears in this thesis), but they can be applied to linear mappings as well. The term  $\underline{I}_n$  denotes the  $n \times n$  unit matrix (having ones in the main diagonal and zeros in all other positions); we may write just  $\underline{I}$  if the dimension is clear from context.

**A.6 Definition (span, image, rank, kernel)** a) Given vectors  $\underline{v}_1, \dots, \underline{v}_m \in \mathbb{R}^n$ , the span of these vectors (or the vector space they generate) is

$$(A.3) \quad \langle \underline{v}_1, \dots, \underline{v}_m \rangle := \left\{ \sum_{\mu=1}^m \alpha_{\mu} \underline{v}_{\mu} : \alpha_1, \dots, \alpha_m \in \mathbb{R} \right\} \subset \mathbb{R}^n.$$

b) If  $\underline{A} \in \mathbb{R}^{n \times m}$  is a matrix, then the term  $\langle \underline{A} \rangle$  denotes the span of the columns of  $\underline{A}$  and is called image of  $\underline{A}$ .

c) The dimension of the span of a matrix is called rank of the matrix.

d) The kernel of the matrix  $\underline{A}$  is the vector space

$$(A.4) \quad \ker \underline{A} := \{ \underline{v} \in \mathbb{R}^m : \underline{A} \underline{v} = \underline{0} \} . \diamond$$

**A.7 Proposition (dimension formula)** Any matrix  $\underline{A} \in \mathbb{R}^{n \times m}$  satisfies

$$(A.5) \quad \dim \langle \underline{A} \rangle + \dim \ker \underline{A} = m . \diamond$$

**A.8 Proposition (pseudo inverse)** a) If  $\underline{A} \in \mathbb{R}^{n \times m}$  and  $\text{rank } \underline{A} = n < m$ , then the so-called Moore-Penrose pseudo inverse

$$(A.6) \quad \underline{A}^+ := \underline{A}^T (\underline{A} \underline{A}^T)^{-1} \quad \text{satisfies} \quad \underline{A} \underline{A}^+ = \underline{I}_n .$$

b) Analogously, if  $\text{rank } \underline{A} = m < n$ , then

$$(A.7) \quad \underline{A}^+ := (\underline{A}^T \underline{A})^{-1} \underline{A}^T \quad \text{satisfies} \quad \underline{A}^+ \underline{A} = \underline{I}_m . \diamond$$

We use the shorthands  $\underline{A}^{-T}$  and  $\underline{A}^{+T}$  to denote  $(\underline{A}^{-1})^T$  and  $(\underline{A}^+)^T$ .

**A.9 Definition (eigenvector, eigenvalue)** If  $\underline{A}$  is a square matrix,  $\underline{v} \neq \underline{0}$  a nonzero vector and  $\lambda$  a scalar such that

$$\underline{A} \underline{v} = \lambda \underline{v} ,$$

then  $\underline{v}$  is called eigenvector and  $\lambda$  eigenvalue of  $\underline{A}$ . The set of eigenvectors to an eigenvalue, together with the zero vector, forms a vector space, the so-called eigenspace. The dimension of an eigenspace is called multiplicity of the corresponding eigenvalue.  $\diamond$

**A.10 Proposition (zero eigenvalues, trace, estimate)** a) A matrix  $\underline{A} \in \mathbb{R}^{n \times n}$  has the eigenvalue zero if and only if  $\text{rank } \underline{A} < n$ .

b) The sum of all eigenvalues of a matrix (taking multiplicity into account) equals the sum of its diagonal entries, called trace  $\underline{A}$ .

c) If  $\underline{A} = \underline{A}^T$  with nonnegative eigenvalues  $\lambda_1, \dots, \lambda_n \geq 0$ , then

$$(A.8) \quad \forall_{\underline{v} \in \mathbb{R}^n \setminus \{0\}} \min_{1 \leq \nu \leq n} \lambda_\nu \leq \frac{|\underline{A} \underline{v}|}{|\underline{v}|} \leq \max_{1 \leq \nu \leq n} \lambda_\nu$$

where  $|\underline{v}| := \sqrt{\sum_{\nu=1}^n v_\nu^2}$  denotes the Euclidean norm of a vector.  $\diamond$

**A.11 Definition (particular sets)** a) The  $n$ -dimensional sphere is the set

$$(A.9) \quad S^n := \left\{ \underline{d} \in \mathbb{R}^{n+1} : |\underline{d}| = 1 \right\} .$$

b) The set of three-dimensional rotation matrices is

$$(A.10) \quad \text{SO}_3 := \left\{ \underline{R} \in \mathbb{R}^{3 \times 3} : \underline{R} \underline{R}^T = \underline{I} \wedge \det \underline{R} = 1 \right\} . \diamond$$

### A.3. Convex Sets and Polyhedra

Most of the material in this section is taken from [147, part I, chapters 7–8]. We adopt the terminology used there but use sometimes different letters, to be coherent with the use of letters in other parts of this thesis.

**A.12 Definition (convexity, cone, polyhedron)** a) A set  $\mathcal{Q} \subset \mathbb{R}^m$  is called convex [147, p. 6] if

$$(A.11) \quad \forall_{\underline{y}_1, \underline{y}_2 \in \mathcal{Q}} \quad \forall_{\substack{\alpha_1, \alpha_2 \geq 0 \\ \alpha_1 + \alpha_2 = 1}} \quad \alpha_1 \underline{y}_1 + \alpha_2 \underline{y}_2 \in \mathcal{Q} .$$

If  $\mathcal{X} \subset \mathbb{R}^m$  is any set, then the intersection of all of its convex supersets

$$\text{conv } \mathcal{X} := \bigcap \{ \mathcal{Q} \subset \mathbb{R}^m : \mathcal{X} \subset \mathcal{Q} \wedge \mathcal{Q} \text{ is convex} \}$$

is called convex hull of  $\mathcal{X}$ .

b) A set  $\mathcal{C} \subset \mathbb{R}^m$  is called a cone [147, p. 87] if

$$(A.12) \quad \forall_{\underline{y}_1, \underline{y}_2 \in \mathcal{C}} \quad \forall_{\alpha_1, \alpha_2 \geq 0} \quad \alpha_1 \underline{y}_1 + \alpha_2 \underline{y}_2 \in \mathcal{C} .$$

If  $\mathcal{X} \subset \mathbb{R}^m$  is any set, then the intersection of all of the cones containing  $\mathcal{X}$

$$\text{cone } \mathcal{X} := \bigcap \{ \mathcal{C} \subset \mathbb{R}^m : \mathcal{X} \subset \mathcal{C} \wedge \mathcal{C} \text{ is a cone} \}$$

is called the cone generated by  $\mathcal{X}$ .

c) A set  $\mathcal{A} \subset \mathbb{R}^m$  is called an affine subspace of  $\mathbb{R}^m$  if

$$(A.13) \quad \forall_{\underline{y}_1, \underline{y}_2 \in \mathcal{A}} \quad \forall_{\alpha_1 + \alpha_2 = 1} \quad \alpha_1 \underline{y}_1 + \alpha_2 \underline{y}_2 \in \mathcal{A} .$$

The dimension of an affine space is the dimension of the vector space of differences (the so-called difference space) of elements of  $\mathcal{A}$

$$(A.14) \quad \dim \mathcal{A} := \dim \{ \underline{a}_1 - \underline{a}_2 : \underline{a}_1, \underline{a}_2 \in \mathcal{A} \} .$$

A family of points  $\underline{a}_0, \dots, \underline{a}_n$  is called affinely independent if the vectors  $\underline{a}_1 - \underline{a}_0, \dots, \underline{a}_n - \underline{a}_0$  are linearly independent. If  $\mathcal{X} \subset \mathbb{R}^m$  is any set, then the set

$$\text{aff.hull } \mathcal{X} := \bigcap \{ \mathcal{A} \subset \mathbb{R}^m : \mathcal{X} \subset \mathcal{A} \wedge \mathcal{A} \text{ is an affine space} \}$$

is called affine hull of  $\mathcal{X}$ .

d) The dimension of any set is the dimension of its affine hull.

e) A set  $\mathcal{P} \subset \mathbb{R}^m$  is called a polyhedron [147, p. 87] if there are a matrix  $\underline{B} \in \mathbb{R}^{n \times m}$  and a vector  $\underline{b} \in \mathbb{R}^n$  such that

$$(A.15) \quad \mathcal{P} = \{ \underline{v}_1 \in \mathbb{R}^m : \underline{B} \underline{v}_1 \leq \underline{b} \} ,$$

where the inequality means that each component of the left hand side is less or equal the corresponding one on the right hand side.  $\diamond$

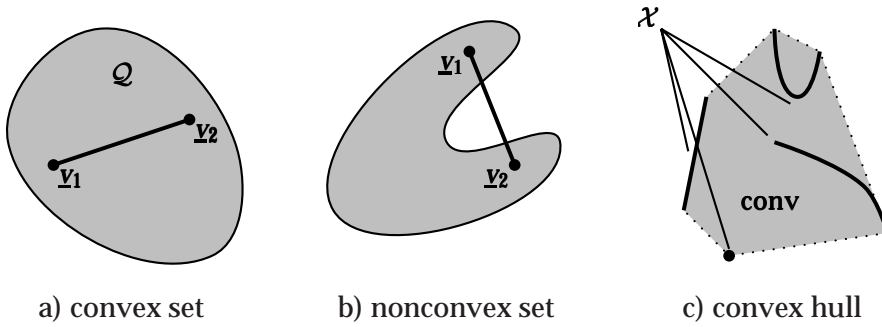


Figure A.2: Convexity examples

This means that a set is convex if the segment joining any two of its points is completely contained in it and the convex hull of a set is the smallest convex superset (Fig. A.2). A cone is a convex set of points that contains all nonnegative multiples of itself (see Fig. A.3a). Simple examples of cones are  $\mathbb{R}_{+0}^m$  and, obviously,  $\mathbb{R}^m$ . Affine subspaces are points, lines and planes (and similar objects in higher-dimensional spaces); the definition implies that a set is  $n$ -dimensional if and only if it contains  $(n + 1)$  affinely independent points. Eq. (A.11), (A.12) and (A.13) show that the definitions of cones and affine spaces are obtained by strengthening the condition for convexity in two different ways; in particular, all cones and all affine spaces are convex.

A polyhedron is a geometric object delimited by hyperplanes (i. e.  $(m - 1)$ -dimensional affine subspaces of  $\mathbb{R}^m$ ); the « $\leq$ »-sign in Eq. (A.15) implies that the row vectors of  $\underline{B}$  are normals to these hyperplanes pointing out of  $\mathcal{P}$ , as shown in Fig. A.3b. A polyhedron is always convex because it is defined as the intersection of halfspaces, which are convex. Polyhedra can be unbounded, as in Fig. A.3b; they can also be empty. In particular, each affine subspace is a polyhedron.

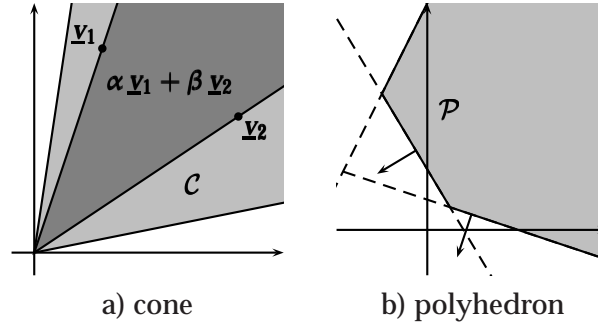


Figure A.3: Cone and polyhedron examples

**A.13 Theorem (Carathéodory)** *If  $\mathcal{X} \subset \mathbb{R}^n$  and  $\underline{v} \in \text{cone } \mathcal{X}$ , then [147, p. 94] there are linearly independent vectors  $\underline{v}_1, \dots, \underline{v}_d \in \mathcal{X}$  such that*

$$(A.16) \quad \underline{v} \in \text{cone } \{\underline{v}_1, \dots, \underline{v}_d\} . \diamond$$

In other words, any element of a cone can be expressed as a nonnegative linear combination of finitely many linear independent generators of that cone. In the case of full-dimensional cones generated by a finite set  $\mathcal{X}$ , the theorem allows to test if an arbitrary vector  $\underline{v}$  belongs to the cone: one can take all the subsets of  $\mathcal{X}$  which contain exactly  $n$  linear independent elements and check whether  $\underline{x}$  can be expressed as a nonnegative linear combination of the vectors in such a subset (due to the linear independency such a representation is unique). By the theorem,  $\underline{x}$  belongs to the cone only if such a representation exists (and obviously, the converse is true as well).

**A.14 Definition (char.cone, lin.space, vertex)** *a) For a polyhedron  $\mathcal{P} \subset \mathbb{R}^m$  given by Eq. (A.15), the set*

$$(A.17) \quad \text{char.cone } \mathcal{P} := \left\{ \underline{v}_2 \in \mathbb{R}^m : \forall_{\underline{v}_1 \in \mathcal{P}} \underline{v}_1 + \underline{v}_2 \in \mathcal{P} \right\} = \{ \underline{v}_2 \in \mathbb{R}^m : \underline{B} \underline{v}_2 \leq \underline{0} \}$$

*is called characteristic cone of  $\mathcal{P}$  [147, p. 100].*

*b) The intersection of a characteristic cone with the opposite copy of itself*

$$(A.18) \quad \text{lin.space } \mathcal{P} := \text{char.cone } \mathcal{P} \cap -\text{char.cone } \mathcal{P} = \{ \underline{v}_2 \in \mathbb{R}^m : \underline{B} \underline{v}_2 = \underline{0} \}$$

*is called lineality space of  $\mathcal{P}$ . A polyhedron having lineality space  $\{\underline{0}\}$  is called pointed [147, p. 100].*

*c) A point  $\underline{v} \in \mathcal{P}$  is called vertex [147, p. 104] of  $\mathcal{P}$  if there is a matrix  $\underline{B}' \in \mathbb{R}^{m \times m}$  consisting of  $m$  linear independent rows of  $\underline{B}$  and a vector  $\underline{b}'$  of the corresponding components of  $\underline{b}$  such that  $\underline{v}$  is the solution (which is then unique) of*

$$\underline{B}' \underline{v} = \underline{b}' . \diamond$$

The characteristic cone is therefore the largest cone that always stays inside  $\mathcal{P}$  when translated to any point in  $\mathcal{P}$  (Fig. A.4a). The lineality space is the vector space belonging to the largest affine subspace contained in  $\mathcal{P}$  (Fig. A.4b). A



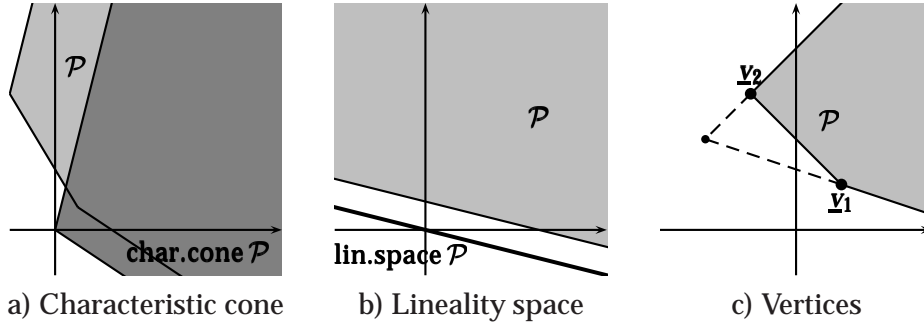


Figure A.4: Examples for structure of polyhedra

vertex is a point of  $\mathcal{P}$  which is given by the intersection of (at least)  $m$  delimiting hyperplanes. Note that the condition that the point belongs to  $\mathcal{P}$  is essential because there may be choices of  $m$  planes that intersect outside of  $\mathcal{P}$  (Fig. A.4c). A polyhedron does not need to have any vertices at all, e. g. there are no vertices in  $\mathbb{R}^m$  (neither in the polyhedron of Fig. A.4b). The polyhedron  $\mathbb{R}_{+0}^m$  has the only vertex  $\underline{0}$ .

**A.15 Theorem** Let  $\mathcal{P} \subset \mathbb{R}^m$  be a pointed polyhedron and  $\mathcal{Q}$  the convex hull of its vertices. Then [147, p. 106]

$$(A.19) \quad \mathcal{P} = \mathcal{Q} + \text{char.cone } \mathcal{P} . \diamond$$

For example, the corresponding convex hull  $\mathcal{Q}$  for the polyhedron  $\mathcal{P}$  shown in Fig. A.4c consists in the two vertices  $\underline{v}_1, \underline{v}_2$  and the segment joining them. The theorem implies that any nonempty pointed polyhedron has at least one vertex.

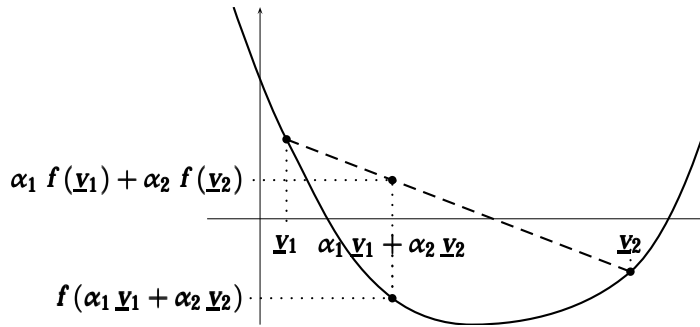


Figure A.5: Convex function

**A.16 Definition (convex function)** A real-valued function  $\Phi$  on a convex subset of  $\mathbb{R}^m$  is called convex (Fig. A.5) if

$$(A.20) \quad \forall_{\underline{v}_1, \underline{v}_2 \in \mathbb{R}^m} \quad \forall_{\substack{\alpha_1, \alpha_2 \geq 0 \\ \alpha_1 + \alpha_2 = 1}} \quad \Phi(\alpha_1 \underline{v}_1 + \alpha_2 \underline{v}_2) \leq \alpha_1 \Phi(\underline{v}_1) + \alpha_2 \Phi(\underline{v}_2) . \diamond$$

## A.4. Normed Vector Spaces and Topology

**A.17 Definition (norm)** a) A norm on  $\mathbb{R}^m$  is a mapping

$$\|\cdot\| : \mathbb{R}^m \rightarrow \mathbb{R}_{+0}$$

with the following properties for all  $\underline{y}, \underline{y}_1, \underline{y}_2 \in \mathbb{R}^m$  and  $\alpha \in \mathbb{R}$ :

$$(A.21) \quad \|\underline{y}\| = 0 \Leftrightarrow \underline{y} = \underline{0},$$

$$(A.22) \quad \|\alpha \underline{y}_1\| = |\alpha| \|\underline{y}_1\|,$$

$$(A.23) \quad \|\underline{y}_1 + \underline{y}_2\| \leq \|\underline{y}_1\| + \|\underline{y}_2\|.$$

b) A norm is called *strict* if

$$(A.24) \quad \forall_{\underline{y}_1, \underline{y}_2 \in \mathbb{R}^m} \quad \forall_{\substack{\alpha_1, \alpha_2 > 0 \\ \alpha_1 + \alpha_2 = 1}} \quad \|\alpha_1 \underline{y}_1 + \alpha_2 \underline{y}_2\| < \alpha_1 \|\underline{y}_1\| + \alpha_2 \|\underline{y}_2\|.$$

c) For  $p \in [1, \infty[$ , the  $p$ -norms are defined by

$$(A.25) \quad \|\underline{y}\|_p := \sqrt[p]{\sum_{\mu=1}^m v_{\mu}^p}.$$

For  $p \in ]1, \infty[$ , these norms are *strict*.

d) The *infinity norm* is defined as

$$(A.26) \quad \|\underline{y}\|_{\infty} := \max_{1 \leq \mu \leq m} |v_{\mu}|. \diamond$$

Finite dimensional vector spaces with norms are a special kind of topological spaces, i. e. spaces where concepts such as open or closed sets and continuity are defined. In the following, we define some topological ideas in terms of norms. Such formulations make use of the very special topological properties of  $\mathbb{R}^m$ . So they are quite appropriate for the needs of this dissertation, although they do not convey an idea of these concepts in general topological spaces.

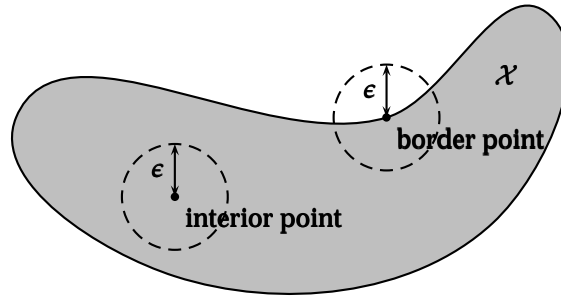


Figure A.6: Interior and border points

**A.18 Definition (open, closed etc.)** Let  $\mathcal{X} \subset \mathbb{R}^m$  be a set and  $\underline{y} \in \mathbb{R}^m$  a point. For  $\epsilon > 0$  define the  $\epsilon$ -environment

$$(A.27) \quad U_{\epsilon}(\underline{y}) := \{\underline{y}_1 \in \mathbb{R}^m : \|\underline{y}_1 - \underline{y}\| < \epsilon\}.$$

a)  $\underline{y}$  is said to belong to the interior (Fig. A.6) of  $\mathcal{X}$  if

$$(A.28) \quad \exists_{\epsilon > 0} \quad U_{\epsilon}(\underline{y}) \subset \mathcal{X}.$$

b)  $\underline{y}$  is said to belong to the closure of  $\mathcal{X}$  if

$$(A.29) \quad \forall_{\epsilon > 0} \quad U_{\epsilon}(\underline{y}) \cap \mathcal{X} \neq \emptyset.$$

c) The set of points that belong to the closure but not to the interior is called border of  $\mathcal{X}$  (Fig. A.6).

d) A set equal to its interior is called open and a set equal to its closure is called closed.

e)  $\mathcal{X}$  is called bounded if there is  $c > 0$  with

$$(A.30) \quad \mathcal{X} \subset U_c(\underline{0}).$$

A closed bounded set is called compact.  $\diamond$

**A.19 Lemma (convex hulls of vertices are compact)** If  $\mathcal{P}$  is a polyhedron and  $\mathcal{Q}$  the convex hull of its vertices, then  $\mathcal{Q}$  is compact.  $\diamond$

Sometimes we need the set of points of a polyhedron which are «not on its border» in an intuitive sense. The intuitive idea does not always fit the above definition because a polyhedron in  $\mathbb{R}^n$  with dimension smaller than  $n$  consists entirely in its border in the above sense. This is because the definition considers it as part of the entire  $\mathbb{R}^n$ . Instead, what we need here is to consider the polyhedron just in the context of its affine hull.

**A.20 Definition (relative interior)** Given a set  $\mathcal{X} \subset \mathbb{R}^m$ , a point  $\underline{y} \in \mathcal{X}$  is said to belong to the relative interior of  $\mathcal{X}$  if

$$(A.31) \quad \exists_{\epsilon > 0} \quad U_{\epsilon}(\underline{y}) \cap \text{aff.hull } \mathcal{X} \subset \mathcal{X}. \quad \diamond$$

The following lemma can be proven in a straightforward way just employing the definitions involved. It appears quite useful in Chapter 4.

**A.21 Lemma (dimension in open sets)** a) If  $\mathcal{Q} \subset \mathbb{R}^m$  is a convex set,  $\mathcal{O} \subset \mathbb{R}^m$  is open, then

$$(A.32) \quad \mathcal{Q} \cap \mathcal{O} \neq \emptyset \quad \Rightarrow \quad \dim(\mathcal{Q} \cap \mathcal{O}) = \dim \mathcal{Q}.$$

b) The relative interior of a convex set has the same dimension as the set itself.  $\diamond$

The following theorem states that all norms on  $\mathbb{R}^m$  lead to the same topology, i. e. the notions of openness, closedness, compactness etc. do not depend on the particular chosen norm.

**A.22 Theorem (norm equivalence)** All norms on  $\mathbb{R}^m$  are topologically equivalent. This means that for any two norms  $\|\cdot\|, \|\cdot\|'$ , there is a  $c > 0$  such that

$$(A.33) \quad \forall_{\underline{y} \in \mathbb{R}^m} \quad \|\underline{y}\|' \leq c \|\underline{y}\|. \quad \diamond$$

The next two definitions generalize the ideas of convergence and continuity known for real numbers.

**A.23 Definition (convergence)** A sequence  $(\underline{y}_n) \in (\mathbb{R}^m)^\mathbb{N}$  is said to converge to an element  $\underline{y}_0 \in \mathbb{R}^m$  if

$$(A.34) \quad \forall_{\epsilon > 0} \quad \exists_{n_0 \in \mathbb{N}} \quad \forall_{n \geq n_0} \quad \|\underline{y}_n - \underline{y}_0\| < \epsilon.$$

We then write  $(\underline{y}_n) \rightarrow \underline{y}_0$ .  $\diamond$

**A.24 Definition (continuity)** Given an open set  $\mathcal{O} \subset \mathbb{R}^m$ , a mapping  $\Phi : \mathcal{O} \rightarrow \mathbb{R}^n$  is called continuous in a point  $\underline{y} \in \mathcal{O}$  if

$$(A.35) \quad \forall_{\epsilon > 0} \quad \exists_{\delta > 0} \quad \forall_{\substack{\underline{y}_1 \in \mathcal{O} \\ \|\underline{y}_1 - \underline{y}\| < \delta}} \quad \|\Phi(\underline{y}_1) - \Phi(\underline{y})\| < \epsilon. \quad \diamond$$

Theorem A.22 implies that also the notion of continuity is independent of the choice of a norm. Thus all norms on  $\mathbb{R}^m$  (as mappings to the vector space  $\mathbb{R}$ ) are continuous in every point.

A mapping which is continuous in every point is simply called *continuous*. In general, when we define a property of a mapping in a point, then we may say «the mapping has this property» to express that the mapping has this property in any point. We will not mention this any more in the following (e. g. in Def. A.27). The following corollary states that continuous mappings map a convergent sequence to a convergent sequence, such that the latter converges to the image of the limit.

**A.25 Corollary** A mapping  $\Phi : \mathcal{O} \rightarrow \mathbb{R}^n$  on an open set  $\mathcal{O} \subset \mathbb{R}^m$  is continuous in  $\underline{y}_0 \in \mathcal{O}$  if and only if

$$(A.36) \quad \forall_{\substack{(\underline{y}_\nu) \in \mathcal{O}^\mathbb{N} \\ (\underline{y}_\nu) \rightarrow \underline{y}_0}} \quad (\Phi(\underline{y}_\nu)) \rightarrow \Phi(\underline{y}_0). \quad \diamond$$

**A.26 Proposition (continuous function on compact set)** A real-valued continuous function on a compact set takes a minimum and a maximum.  $\diamond$

In Section A.5, we will need to split up the idea of continuity into two parts, which are called upper and lower semicontinuity (Fig. A.7). Then a mapping is continuous in a point if and only if it is both upper and lower semicontinuous in that point. This concept requires the image space to lie in  $[-\infty, \infty]$  rather than  $\mathbb{R}^n$ .

**A.27 Definition (semicontinuity)** Let  $\Phi : \mathbb{R}^m \rightarrow [-\infty, \infty]$  be a mapping.

a)  $\Phi$  is said to be upper semicontinuous in  $\underline{y} \in \mathbb{R}^m$  if

$$(A.37) \quad \forall_{\epsilon > 0} \quad \exists_{\delta > 0} \quad \forall_{\substack{\underline{y}_1 \in \mathbb{R}^m \\ \|\underline{y}_1 - \underline{y}\| < \delta}} \quad \Phi(\underline{y}_1) < \Phi(\underline{y}) + \epsilon.$$

b)  $\Phi$  is said to be lower semicontinuous in  $\underline{y} \in \mathbb{R}^m$  if

$$(A.38) \quad \forall_{\epsilon > 0} \quad \exists_{\delta > 0} \quad \forall_{\substack{\underline{y}_1 \in \mathbb{R}^m \\ \|\underline{y}_1 - \underline{y}\| < \delta}} \quad \Phi(\underline{y}_1) > \Phi(\underline{y}) - \epsilon. \quad \diamond$$

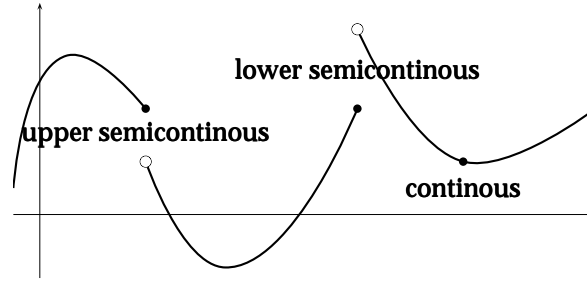


Figure A.7: Semicontinuity and continuity

## A.5. Parametric Optimization

The material in this section is taken completely from [18]. For this dissertation we need only a small slice out of the broad theory presented in that book and often we do not even need the results in their full generality because the problem treated in Chapter 4, p. 57 ff. is just a special case. Therefore, definitions and propositions presented in the following are adapted to the writing conventions of this document and sometimes restricted to the special situation that we need.<sup>2</sup>

First, let us take a look at the point-to-set mappings like those which provide the constraints for the optimization problem in Chapter 4, p. 57 ff. We define some properties, each of which generalizes some aspect of the idea of continuity known from point-to-point mappings. It turns out that there are several ways to do it (we choose only three out of the five provided in the book [18, p. 25]); in other words, the property of continuity splits up into a couple of different properties that are quite independent of each other.

### A.28 Definition (point-to-set mapping, closedness, semicontinuity)

Let  $\Lambda \subset \mathbb{R}^l$ . A point-to-set mapping of  $\Lambda$  into  $\mathbb{R}^m$  is a mapping

$$(A.39) \quad \Gamma: \Lambda \rightarrow 2^{\mathbb{R}^m}$$

assigning to every  $\underline{\lambda} \in \Lambda$  a (possibly empty) subset of  $\mathbb{R}^m$ . Given two such point-to-set mappings  $\Gamma, \Theta$ , the point-to-set mapping  $\Gamma \cap \Theta$  is defined as

$$(A.40) \quad \Gamma \cap \Theta: \Lambda \rightarrow 2^{\mathbb{R}^m}, \underline{\lambda} \mapsto \Gamma(\underline{\lambda}) \cap \Theta(\underline{\lambda}).$$

a)  $\Gamma$  is called closed at  $\underline{\lambda}_0 \in \Lambda$  if for each pair of sequences  $(\underline{\lambda}_v) \in \Lambda^{\mathbb{N}}$ ,  $(\underline{y}_v) \in (\mathbb{R}^m)^{\mathbb{N}}$  and each point  $\underline{y}_0 \in \mathbb{R}^m$  with

$$(A.41) \quad (\underline{\lambda}_v) \rightarrow \underline{\lambda}_0 \quad \text{and} \quad (\underline{y}_v) \rightarrow \underline{y}_0 \quad \text{and} \quad \forall_{v \in \mathbb{N}} \underline{y}_v \in \Gamma(\underline{\lambda}_v)$$

it follows that  $\underline{y}_0 \in \Gamma(\underline{\lambda}_0)$ .

b)  $\Gamma$  is called upper semicontinuous according to Berge (u. s. c. -B) at  $\underline{\lambda}_0 \in \Lambda$  if

$$(A.42) \quad \forall_{\substack{\text{open set } \mathcal{O} \subset \mathbb{R}^m \\ \Gamma(\underline{\lambda}_0) \subset \mathcal{O}}} \exists_{\delta > 0} \forall_{\underline{\lambda} \in U_{\delta}(\underline{\lambda}_0)} \Gamma(\underline{\lambda}) \subset \mathcal{O}.$$

<sup>2</sup>For instance, the condition «metric space» (a term which is not defined in this appendix) was replaced by «subset of  $\mathbb{R}^m$ », which is a very special case of a metric space.

c)  $\Gamma$  is called lower semicontinuous according to Berge (l. s. c.-B) at  $\underline{\lambda}_0 \in \Lambda$  if

$$(A.43) \quad \forall_{\substack{\text{open set } \mathcal{O} \subset \mathbb{R}^m \\ \Gamma(\underline{\lambda}_0) \cap \mathcal{O} \neq \emptyset}} \exists_{\delta > 0} \forall_{\underline{\lambda} \in U_\delta(\underline{\lambda}_0)} \Gamma(\underline{\lambda}) \cap \mathcal{O} \neq \emptyset. \diamond$$

Now we define a special class of point-to-set mappings, where a parameter  $\underline{\lambda}$  is mapped to the solution set of a system of inequalities with convex constraint mappings depending on  $\underline{\lambda}$ . The definition and the following proposition are substantially simplified with respect to the formulation in [18] because for the applications we need we can assume much stronger conditions.

**A.29 Definition (characteristic index set)** Let  $g_1, \dots, g_n : \mathbb{R}^m \times \Lambda \rightarrow \mathbb{R}$  be a family of continuous mappings such that

$$(A.44) \quad \forall_{1 \leq v \leq n} \forall_{\underline{\lambda} \in \Lambda} g_v(\cdot, \underline{\lambda}) : \mathbb{R}^m \rightarrow \mathbb{R}, \underline{y} \mapsto g_v(\underline{y}, \underline{\lambda}) \text{ is convex.}$$

Then define a point-to-set mapping  $\Gamma$  by

$$(A.45) \quad \Gamma : \Lambda \rightarrow 2^{\mathbb{R}^m}, \underline{\lambda} \mapsto \left\{ \underline{y} \in \mathbb{R}^m : \forall_{1 \leq v \leq n} g_v(\underline{y}, \underline{\lambda}) \leq 0 \right\}.$$

Similarly, for  $\mathcal{I} \subset \{1, \dots, n\}$ , let

$$(A.46) \quad \Gamma^{(\mathcal{I})} : \Lambda \rightarrow 2^{\mathbb{R}^m}, \underline{\lambda} \mapsto \left\{ \underline{y} \in \mathbb{R}^m : \forall_{v \in \mathcal{I}} g_v(\underline{y}, \underline{\lambda}) \leq 0 \right\}.$$

For  $\underline{\lambda} \in \Lambda$ , the set

$$(A.47) \quad \text{ch.ind } \Gamma(\underline{\lambda}) := \left\{ v \in \{1, \dots, n\} : \forall_{\underline{y} \in \Gamma(\underline{\lambda})} g_v(\underline{y}, \underline{\lambda}) = 0 \right\}$$

is called characteristic index set of  $\Gamma(\underline{\lambda})$  [18, p. 43].  $\diamond$

The definition implies that all the sets  $\Gamma(\underline{\lambda})$  and  $\Gamma^{(\mathcal{I})}(\underline{\lambda})$  are convex and closed. The next proposition supplies conditions under which such mappings have some of the properties defined in Def. A.28.

**A.30 Theorem (closedness, semicontinuity)** We assume the conditions of Def. A.29.

a) Then  $\Gamma$  is closed [18, Theorem 3.2.1 (1), p. 44].

b) Let  $\underline{\lambda}_0 \in \Lambda$  and  $\mathcal{I} = \text{ch.ind } \Gamma(\underline{\lambda}_0)$  satisfy the following conditions:

$$(A.48) \quad \forall_{\underline{\lambda} \in \Lambda} \Gamma^{(\mathcal{I})}(\underline{\lambda}) \text{ is a nonempty affine space}$$

$$(A.49) \quad \forall_{\underline{\lambda} \in \Lambda} \dim \text{lin.space } \Gamma^{(\mathcal{I})}(\underline{\lambda}) = \dim \text{lin.space } \Gamma^{(\mathcal{I})}(\underline{\lambda}_0).$$

Then  $\Gamma, \Gamma^{(\mathcal{I})}$  are l. s. c.-B at  $\underline{\lambda}_0$  [18, Theorem 3.2.2, p. 45].

c) Let  $\Theta$  be another point-to-set mapping with the conditions of Def. A.29. If  $\Gamma$  is l. s. c.-B at  $\underline{\lambda}_0$  and the set  $(\Gamma \cap \Theta)(\underline{\lambda}_0)$  is nonempty and bounded, then  $\Gamma \cap \Theta$  is u. s. c.-B at  $\underline{\lambda}_0$  [18, Theorem 3.1.3, p. 37].  $\diamond$

Now we come to the optimization problem itself, providing some results on stability. Again our formulation is much simpler than in [18] because we maintain the much stronger conditions of Def. A.29.

**A.31 Theorem** Given a point-to-set mapping  $\Gamma: \Lambda \rightarrow 2^{\mathbb{R}^m}$  and a continuous function  $f: \mathbb{R}^m \times \Lambda \rightarrow \mathbb{R}$ , we define the extreme value function

$$(A.50) \quad \Phi: \Lambda \rightarrow [-\infty, +\infty], \underline{\lambda} \mapsto \inf \{ f(\underline{v}, \underline{\lambda}) : \underline{v} \in \Gamma(\underline{\lambda}) \}$$

and the optimal set mapping

$$(A.51) \quad \Psi: \Lambda \rightarrow 2^{\mathbb{R}^m}, \underline{\lambda} \mapsto \{ \underline{v} \in \Gamma(\underline{\lambda}) : f(\underline{v}, \underline{\lambda}) = \Phi(\underline{\lambda}) \} .$$

a) If  $\Gamma$  is l. s. c.-B at  $\underline{\lambda}_0 \in \Lambda$ , then  $\Phi$  is upper semicontinuous at  $\underline{\lambda}_0$  [18, Theorem 4.2.2 (1), p. 61].

b) If there is a compact subset  $\mathcal{K} \subset \mathbb{R}^m$  such that

$$(A.52) \quad \forall_{\underline{\lambda} \in \Lambda} \Psi(\underline{\lambda}) \cap \mathcal{K} \neq \emptyset ,$$

then  $\Phi$  is lower semicontinuous [18, Theorem 4.2.1 (1), p. 61].  $\diamond$

If both conditions a and b can be satisfied, this theorem allows to conclude that an objective function is continuous. Concerning the optimal set mapping, we do not need further theorems in this dissertation because the only case we are interested in is where optimal points are unique. In that case, both lower and upper semicontinuity according to Berge are equivalent to continuity in the usual sense.



# Appendix B

## List of Figures

1.1. Skywash manipulator . . . . .	2
1.2. Manipulator concepts . . . . .	3
1.3. Boom crane . . . . .	3
1.4. Container crane . . . . .	4
1.5. Hexabot <sup>TM</sup> 5-axis CNC machine . . . . .	5
1.6. Tendon-based Stewart platform . . . . .	5
1.7. C-MISPP prototype . . . . .	6
1.8. Skycam <sup>TM</sup> tendon-suspended camera . . . . .	7
1.9. Cablev prototype at Rostock . . . . .	11
1.10. SEGESTA prototype at Duisburg . . . . .	12
1.11. Tethered aerostat . . . . .	13
1.12. Winch design in the SEGESTA prototype . . . . .	14
1.13. Winch design in the Cablev prototype . . . . .	15
2.1. Examples of serial and parallel manipulators . . . . .	18
2.2. Constraint as a relation between actuator and end-effector . . . . .	19
2.3. Redundancy and singularity in serial systems . . . . .	21
2.4. Redundancy and singularity in parallel systems . . . . .	23
2.5. Symbols used to describe tendon-based Stewart platforms . . . . .	25
2.6. Incompletely / completely restrained positioning mechanism . . . . .	27
2.7. Redundantly restrained positioning mechanism . . . . .	28
2.8. The classes of Theorem 2.1 . . . . .	31
3.1. The proof of Prop. 3.2 . . . . .	37
3.2. The manipulator corresponding to Fig. 3.1 . . . . .	37
3.3. Counterexample for the projection of $\underline{1}$ onto $\ker \underline{A}^T$ . . . . .	37
3.4. Example CRPMs . . . . .	38
3.5. Acceptably controllable workspace of a 2T manipulator . . . . .	42
3.6. Acceptably controllable workspace of a 1R2T manipulator . . . . .	42
3.7. Acceptably controllable workspace with gravity . . . . .	44

3.8. Singularities in 1R2T systems . . . . .	45
3.9. Almost singularity-free 1R2T systems . . . . .	45
3.10. Singularities in 2R3T systems . . . . .	46
3.11. Singularities in 3R3T systems . . . . .	47
3.12. Nonsingular posture with singular submatrix . . . . .	47
3.13. Stiffness of some 2T systems . . . . .	51
3.14. Techniques to avoid autocollisions . . . . .	54
4.1. Fixing some forces does not always yield acceptable solutions . . .	58
4.2. In CRPMs, acceptable solutions form a line segment . . . . .	59
4.3. Optimal solutions as a range: basic idea . . . . .	60
4.4. Polyhedra of solutions . . . . .	61
4.5. Force ranges of two postures for a redundant 2T example . . . . .	62
4.6. Example of discontinuity . . . . .	65
4.7. Example of discontinuity (singular for $\beta = 0$ ) . . . . .	68
4.8. Approximation of $\underline{f}_{\text{low}}$ with $\underline{f}_{\text{low},p}$ . . . . .	69
4.9. Comparison of $p$ -solutions . . . . .	71
4.10. Region of acceptable solutions of a 1R2T system . . . . .	78
4.11. Tension computation algorithm, part 1 . . . . .	80
4.12. Tension computation algorithm, part 2 . . . . .	82
5.1. Workspace of 2T sample designs . . . . .	89
5.2. Workspace of 2T sample designs with gravity . . . . .	90
5.3. Workspace of 1R2T sample designs . . . . .	91
5.4. 2R3T sample designs . . . . .	93
5.5. 3R3T sample designs . . . . .	96
6.1. Second term of acceleration . . . . .	100
6.2. Test trajectories for 2T . . . . .	102
6.3. End-effector motion for 2T trajectory . . . . .	103
6.4. 2T sample designs . . . . .	105
6.5. Tendon velocity for 2T trajectory . . . . .	106
6.6. Tendon acceleration for 2T trajectory . . . . .	106
6.7. Stiffness for 2T trajectory . . . . .	106
6.8. Tendon forces for 2T trajectory . . . . .	107
6.9. Distance from border for 2T trajectory . . . . .	109
6.10. Power consumption for 2T trajectory . . . . .	110
6.11. CPU time usage for 2T trajectory . . . . .	111
6.12. Tendon forces for a 2T trajectory with gravity . . . . .	114
6.13. Test trajectory for 3R3T systems . . . . .	116
6.14. End-effector motion for a 3T3T trajectory . . . . .	116
6.15. Distance from border for a 3R3T trajectory . . . . .	118

A.1. Examples of mappings . . . . .	124
A.2. Convexity examples . . . . .	128
A.3. Cone and polyhedron examples . . . . .	129
A.4. Examples for structure of polyhedra . . . . .	130
A.5. Convex function . . . . .	130
A.6. Interior and border points . . . . .	131
A.7. Semicontinuity and continuity . . . . .	134



# Appendix C

## List of Tables

2.1. Possible DOF classes . . . . .	30
3.1. Size of the closed-form expression for workspace . . . . .	41
3.2. Stiffness in some postures of a 1R2T manipulator . . . . .	53
5.1. Workspace quality of 2R3T sample designs . . . . .	94
5.2. Workspace quality of 3R3T sample designs . . . . .	97
6.1. Stiffness for 2T trajectory . . . . .	104
6.2. Maximum forces / force change rates for 2T trajectory . . . . .	107
6.3. Distance from border for 2T trajectory . . . . .	108
6.4. Energy consumption for 2T trajectory . . . . .	109
6.5. Average computation time for 2T trajectory . . . . .	111
6.6. Influence of the parameter $p$ for 2T trajectory . . . . .	112
6.7. Influence of the computation precision for a 2T trajectory . . . . .	113
6.8. Summary for a 2T trajectory with gravity . . . . .	115
6.9. Influence of the parameter $p$ for a 3R3T trajectory . . . . .	117
6.10. Summary for a 3R3T trajectory . . . . .	117



# Appendix D

## Bibliography

- [1] Aarts, E. H. L. and Laarhoven, P. J. M. van. Statistical cooling: A general approach to combinatorial optimization problems. *Philips Journal of Research*, 40:193–226, 1985.
- [2] Albus, James S., Bostelman, Roger V., and Dagalakis, Nicholas G. The NIST ROBOCRANE. *Journal of Research of the NIST*, 97(3):373–385, May 1992.
- [3] Albus, James S., Bostelman, Roger V., and Dagalakis, Nicholas G. The NIST ROBOCRANE. *Journal of Robotic Systems*, 10(5):709–724, 1993.
- [4] Alizade, Rasim I., Tagiyev, Nazim R., and Duffy, Joseph. A forward and reverse displacement analysis of a 6-DOF in-parallel manipulator. *Mechanism and Machine Theory*, 29(1):115–124, 1994.
- [5] Angeles, Jorge. The design of isotropic manipulator architectures in the presence of redundancies. *Int. Journal of Robotics Research*, 11(3):196–201, June 1992.
- [6] Angeles, Jorge and Chablat, Damien. On isotropic sets of points in the plane. application to the design of robot architectures. In Lenarčič and Stanišić [12], pages 73–82.
- [7] Angeles, Jorge, Kovac, Peter, and Hommel, Günter. *Computational Kinematics*. Kluwer Academic Publishers, Dordrecht, Netherlands, 1993.
- [8] Arai, Tamio and Osumi, Hisashi. Three wire suspension robot. *The Industrial Robot*, 19(4):17–22, 1992.
- [9] Arcara, Paolo. Control of haptic and robotic telemanipulation systems. Ph. D. thesis, Università di Bologna, Bologna, Italy, 2001.
- [10] Arcara, Paolo, Di Stefano, Luigi, Mattoccia, Stefano, Melchiorri, Claudio, and Vassura, Gabriele. Perception of depth information by means of wire-actuated haptic interface. In *Proc. 2000 IEEE Int. Conf. on Robotics and Automation*, pages 3443–3448, San Francisco, USA, April 2000. IEEE.
- [11] *Proc. 6th Int. Symposium on Advances in Robot Kinematics*, Strobl/Salzburg, Austria, June 1998. Lenarčič, Jadran and Husty, Manfred L., editors, Kluwer Academic Publishers.



- [12] *Proc. 7th Int. Symposium on Advances in Robot Kinematics*, Portorož, Slovenia, June 2000. Lenarčič, Jadran and Stanišić, Michael M., editors, Kluwer Academic Publishers.
- [13] *Proc. 8th Int. Symposium on Advances in Robot Kinematics*, Caldes de Malavella, Spain, June 2002. Lenarčič, Jadran and Thomas, Frederico, editors, Kluwer Academic Publishers.
- [14] Armstrong, M. A. A. *Basic Topology*. Springer Verlag, Berlin, Heidelberg, New York, 1990.
- [15] Asada, Haruhiko and Cro Granito, Jose A. Kinematic and static characterization of wrist joints and their optimal design. In *Proc. 1985 IEEE Int. Conf. on Robotics and Automation*, pages 244–250, St. Louis, MO, USA, 1985. IEEE.
- [16] *Proc. 26th ASME Biennial Mechanisms Conf.*, Baltimore, USA, September 2000.
- [17] Ball, Robin C., Fink, Thomas M. A., and Bowler, Neill E. Stochastic annealing. *Physical Review Letters*, 91(1), January 2003.
- [18] Bank, Bernd, Guddat, Jürgen, and Klatte, Diethard. *Non-linear parametric optimization*. Birkhäuser Verlag, Basel, Switzerland, 1983.
- [19] Barrette, Guillaume and Gosselin, Clément M. Kinematic analysis and design of planar parallel mechanisms actuated with cables. In ASME-BMC. [16].
- [20] Bergamasco, Massimo, Frisoli, Antonio, and Salsedo, Fabio. Design of a new tendon driven haptic interface with six degrees of freedom. In *ROMAN '99, 8th IEEE Intl. Workshop on Robot and Human Interaction*, pages 303–308. IEEE, 1999.
- [21] Bertsekas, Dimitri P. *Nonlinear programming*. Athena Scientific, Belmont, MA, USA, 1995.
- [22] Bhattacharya, Soumya, Hatwal, Himangshu, and Ghosh, Amitabha. Comparison of an exact and an approximate method of singularity avoidance in platform type parallel manipulators. *Mechanism and Machine Theory*, 33(7):965–974, 1998.
- [23] Bonev, Ilian. Parallelemic – the parallel mechanisms information center. <http://www.parallelemic.org>, 2003.
- [24] Bostelman, Roger V. and Albus, James S. Stability of an underwater work platform suspended from an unstable reference. In *Proc. Oceans '93, Engineering in Harmony with the Ocean*, pages II 321–325, Victoria, British Columbia, Canada, October 1993. IEEE.
- [25] Bostelman, Roger V., Albus, James S., Dagalakis, Nicholas G., Jacoff, Adam, and Gross, John. Applications of the NIST ROBOCRANE. In *Proc. 5th Int. Symp. on Robotics and Manufacturing: Research, Education, and Applications*, pages 403–410, Maui, HI, USA, August 1994. ASME.

- [26] Bostelman, Roger V., Albus, James S., Dagalakis, Nicholas G., and Jacoff, Adam. Robocrane project: An advanced concept for large scale manufacturing. In *Proc. Association for Unmanned Vehicles Systems Int.*, Orlando, FL, USA, July 1996.
- [27] Bostelman, Roger V., Albus, James S., Murphy, Karl, Tsai, Tsung-Ming, and Amatucci, Ed. A Stewart platform lunar rover. In *Proc. Engineering Construction and Operations in Space IV*, Albuquerque, MN, USA, February 1994.
- [28] Bostelman, Roger V., Dagalakis, Nicholas G., and Albus, James S. A robotic crane system utilizing the Stewart platform configuration. In *Proc. 4th Int. Symp. on Robotics and Manufacturing: Research, Education and Applications*, Santa Fe, NM, USA, November 1992. ASME.
- [29] Bostelman, Roger V., Jacoff, Adam, Dagalakis, Nicholas G., and Albus, James S. RCS-based robocrane integration. In *Proc. Int. Conf. on Intelligent Systems: A Semiotic Perspective*, Gaithersburg, MD, USA, October 1996.
- [30] Branke, Jürgen and Schmidt, Christian. Selection in the presence of noise. *GECCO*, pages 766–777, 2003.
- [31] Clavel, Reymond. Dispositif pour le déplacement et le positionnement d'un élément dans l'espace. Brevet Suisse 672089 A5, Switzerland, 1985.
- [32] Koza, John R. *New Ideas in Optimization*. McGraw-Hill, New York, USA, 1992.
- [33] Dagalakis, Nicholas G., Albus, James S., Wang, Ben-Li, Unger, Joseph, and Lee, James D. Stiffness study of a parallel link robot crane for shipbuilding applications. *ASME Journal of Offshore Mechanics and Arctic Engineering*, 111(3):183–193, August 1989.
- [34] Dasgupta, Bhaskar and Mruthyunjaya, T. S. Singularity-free path planning for the Stewart platform manipulator. *Mechanism and Machine Theory*, 33(6):711–725, 1998.
- [35] Dasgupta, Bhaskar and Mruthyunjaya, T. S. Force redundancy in parallel manipulators: theoretical and practical issues. *Mechanism and Machine Theory*, 33(6):727–742, 1998.
- [36] Dasgupta, Bhaskar and Mruthyunjaya, T. S. The Stewart platform manipulator: a review. *Mechanism and Machine Theory*, 35(1):15–40, 2000.
- [37] *ASME Design Eng. Tech. Conf.*, Pittsburgh, USA, September 2001.
- [38] *ASME Design Eng. Tech. Conf.*, Montreal, Canada, September 2002.
- [39] Di Gregorio, R. and Parenti-Castelli, Vincenzo. Dynamic performance indices for 3-DOF parallel manipulators. In Lenarčič and Thomas [13], pages 11–20.
- [40] Dietmaier, Peter. The Stewart-Gough platform of general geometry can have 40 real postures. In Lenarčič and Husty [11], pages 7–16.

- [41] Dietmaier, Peter. Can the Stewart-Gough platform with planar base and planar platform also have 40 real configurations? Presentation held on the 7th. Intl. Symp. on Advances in Robot Kinematics, Portoroz, Slovenia, 2000, June 2000.
- [42] Dougherty, Ed. Advanced robotic crane for container handling. [http://www.august-design.com/html/projects/prj\\_aacts.htm](http://www.august-design.com/html/projects/prj_aacts.htm), November 1999.
- [43] Ebert-Uphoff, Imme and Chirikjian, Gregory S. Efficient workspace generation for binary manipulators with many actuators. *Journal of Robotic Systems*, 12(6):383–400, 1995.
- [44] Fang, Shiqing, Mielczarek, Sonja, Verhoeven, Richard, and Hiller, Manfred. Seilgetriebene Stewart-Plattformen in Theorie und Anwendung (SEGESTA). Abschlussbericht zum DFG-Vorhaben HI 370/18-1,2, Lehrstuhl für Mechatronik, Universität Duisburg – Essen, Duisburg, Germany, August 2003.
- [45] Fattah, Abbas and Agrawal, Sunil Kumar. Workspace and design analysis of cable-suspended planar parallel robots. In DETC. [38].
- [46] Fattah, Abbas and Agrawal, Sunil Kumar. Design of cable-suspended planar parallel robots for an optimal workspace. In Gosselin and Ebert-Uphoff [140], pages 195–202.
- [47] Faugère, J. C. and Lazard, Daniel. Combinatorial classes of parallel manipulators. *Mechanism and Machine Theory*, 30(6):765–776, 1995.
- [48] Franitza, Daniel, Fang, Shiqing, Haß, Carsten, and Hiller, Manfred. Analyse und Anwendung seilgetriebener Stewart-Plattformen. In *Proc. 4th German-Polish Mechatronic Workshop*, Suhl, Germany, 2003.
- [49] Gallina, Paolo, Rossi, Aldo, and Williams, Robert L. Planar cable-direct-driven robots, part II: Dynamics and control. In DETC. [37].
- [50] Gosselin, Clément M. and Angeles, Jorge. A global performance index for the kinematic optimization of robotic manipulators. *ASME Journal of Mechanical Design*, 113(3):220–226, 1991.
- [51] Gosselin, Clément M. and Merlet, Jean-Pierre. The direct kinematics of planar parallel manipulators: Special architectures and number of solutions. *Mechanism and Machine Theory*, 29(8):1083–1097, 1994.
- [52] Gough, V. E. Contribution to discussion of papers on research in auto stability and control and in true performance by cornell staff. *Proc. Institute of Mechanical Engineering*, pages 392–403, 1956.
- [53] Hay, Alexander Morrison. Optimal dimensional synthesis of planar parallel manipulators with respect to workspaces. Ph. D. thesis, University of Pretoria, Pretoria, South Africa, 2003.

- [54] Hayward, Vincent and Kurtz, Ronald. Modeling of a parallel wrist mechanism with actuator redundancy. In Stifter, S. and Lenarčič, Jadran, editors, *Proc. 2nd Int. Workshop on Advances in Robot Kinematics*, page 444, Linz, Austria, September 1990. Springer Verlag.
- [55] Heyden, Thomas, Maier, Thomas, and Woernle, Christoph. Trajectory tracking control for a cable suspension manipulator. In Lenarčič and Thomas [13], pages 125–134.
- [56] Higuchi, Toshiro, Ming, Aiguo, and Jiang-yu, J. Application of multi-dimensional wire cranes in construction. In *Proc. 5th Int. Symp. on Robotics in Construction*, pages 661–668, 1988.
- [57] Hiller, Manfred, Fang, Shiqing, Mielczarek, Sonja, Verhoeven, Richard, and Tadokoro, Satoshi. Design, analysis and realization of tendon-based parallel manipulators. In *Proc. of the 10th German-Japanese Seminar on Nonlinear Problems in Dynamical Systems – Theory and Applications*, Hakui, Ishikawa, Japan, October 2002.
- [58] Hiller, Manfred, Krupp, Thorsten, and Tilders, Jörg. Kinetostatische Analyse einer Stewart-Plattform. Institutsbericht 96-2, Fachgebiet Mechatronik, Gerhard-Mercator-Universität Duisburg, Duisburg, Germany, 1996.
- [59] Hirose, Shigeo and Ma, Shugen. Coupled tendon-driven multijoint manipulator. In *Proc. 1991 IEEE Int. Conf. on Robotics and Automation*, pages 1268–1275, Sacramento, CA, USA, 1991. IEEE.
- [60] Homma, Keiko and Arai, Tamio. Upper limb motion assist system with parallel mechanisms. In JFM. [74], pages 388–391.
- [61] Homma, Keiko and Arai, Tamio. Static model for upper limb motion assist system. In *Proc. 7th Int. Conf. on Advanced Robotics*, pages 945–950. IEEE, 1995.
- [62] Homma, Keiko, Hashino, Satoshi, and Arai, Tamio. An upper limb motion assist system: Experiments with arm models. In *Proc. 1998 IEEE / RSJ Int. Conf. on Intelligent Robots and Systems*, pages 758–763, Victoria, Canada, October 1998. IEEE.
- [63] Honegger, Marcel, Codourey, A., and Burdet, E. Adaptive control of the hexaglide, a 6 dof parallel manipulator. In *Proc. 1997 IEEE Int. Conf. on Robotics and Automation*, Albuquerque, USA, April 1997. IEEE.
- [64] Husty, Manfred L. An algorithm for solving the direct kinematic of Stewart-Gough-type platforms. *Mechanism and Machine Theory*, 31(4):365–380, 1996.
- [65] Husty, Manfred L., Mielczarek, Sonja, and Hiller, Manfred. Constructing an overconstrained planar 4RPR manipulator with maximal forward kinematics solution set. In *Proc. 10th Intl. Workshop on Robotics in the Alpe-Adria-Danube Region*, Vienna, Austria, May 2001.

- [66] Husty, Manfred L., Mielczarek, Sonja, and Hiller, Manfred. A redundant spatial Stewart-Gough platform with a maximal forward kinematics solution set. In Lenarčič and Thomas [13], pages 147–154.
- [67] Hyodo, Kazuhito, Kobayashi, Hiroaki, Ogane, Daisuke, and Yamamoto, Keiji. On stiffness control of tendon-driven robotic mechanism with redundant tendons. *Journal of the Robotics Soc. of Japan*, 17(4):37–46, 1999.
- [68] *Proc. 1999 IEEE Int. Conf. on Robotics and Automation*, Detroit, USA, May 1999.
- [69] Innocenti, Carlo and Parenti-Castelli, Vincenzo. Direct position analysis of the Stewart platform mechanism. *Mechanism and Machine Theory*, 25(6):611–621, 1990.
- [70] Innocenti, Carlo and Parenti-Castelli, Vincenzo. Direct kinematics in analytical form of a general geometry 5-4 fully parallel manipulator. In *Computational Kinematics* [7], pages 141–152.
- [71] Innocenti, Carlo and Parenti-Castelli, Vincenzo. Echelon form solution of direct kinematics for the general fully-parallel spherical wrist. *Mechanism and Machine Theory*, 28(4):553–561, 1993.
- [72] Innocenti, Carlo and Parenti-Castelli, Vincenzo. Closed-form direct position analysis of a 5-5 parallel mechanism. *ASME Journal of Mechanical Design*, 115(3):515–521, 1993.
- [73] Jacobsen, S. C., Wood, J. E., Knutti, D. F., and Biggers, K. B. The Utah/MIT dextrous hand: Work in progress. *Int. Journal of Robotics Research*, 4(4):21–49, 1984.
- [74] *Proc. 2nd Japanese-French Cong. of Mechatronics*, Takamatsu, Japan, November 1994.
- [75] *Proc. 1996 Japan-U.S.A. Symposium on Flexible Automation*, Boston, MA, USA, July 1996. Stelson, K. and Oba, F., editors.
- [76] Karger, Adolf. Architecture singular parallel manipulators. In Lenarčič and Husty [11], pages 445–454.
- [77] Karger, Adolf. Singularities and self-motions of a special type of platforms. In Lenarčič and Thomas [13], pages 155–164.
- [78] Karger, Adolf and Husty, Manfred L. On self-motions of a class of parallel manipulators. In Lenarčič and Parenti-Castelli [103], pages 339–348.
- [79] Kawamura, Sadao, Choe, W., Tanaka, S., and Pandian, S.R. Development of an ultrahigh speed robot FALCON using wire drive system. In *Proc. 1995 IEEE Int. Conf. on Robotics and Automation*, pages 215–220, Nagoya, Japan, 1995. IEEE.



- [80] Kawamura, Sadao, Ida, M., Wada, T., and Wu, J. L. Development of a virtual sports machine using a wire drive system – A trial of virtual tennis. In *Proc. 1995 IEEE / RSJ Int. Conf. on Intelligent Robots and Systems*, pages 111–116. IEEE, 1995.
- [81] Kawamura, Sadao, Kino, Hitoshi, and Won, Choe. High speed manipulation by using parallel wire driven robots. *Robotica*, 18:13–21, 2000.
- [82] Kino, Hitoshi, Miyazono, Hiroyuki, Choe, W., and Kawamura, Sadao. Realization of large work space using parallel wire drive robots. In *Proc. 2nd Asian Control Conf.*, pages 591–594, Seoul, Korea, July 1997.
- [83] Kino, Hitoshi, Yabe, Sigeru, Shimamoto, Takeshi, and Kawamura, Sadao. Stiffness increase method of wire driven systems using interference of wire tension with mechanical constraint directions. In *Proc. Intl. Conf. on Machine Automation*, pages 63–68, Osaka, Japan, September 2000.
- [84] Kobayashi, Hiroaki, Hyodo, Kazuhito, and Ogane, Daisuke. On tendon-driven robotic mechanisms with redundant tendons. *Int. Journal of Robotics Research*, 17(5):561–571, May 1998.
- [85] Komainda, Artur and Hiller, Manfred. Motion control of redundant large-scale manipulators in a changing environment. In *Proc. 10th World Cong. on Theory of Machines and Mechanisms*, pages 1033–1038, Oulu, Finland, 1999. IFToMM.
- [86] Kossowski, Craig. Novel wire driven parallel robot: Design, analysis and simulation of the CAT4. M. Sc. thesis, Dept. of Mech. Engineering, Queen's University, Kingston, ON. Canada, 2001.
- [87] Kossowski, Craig and Notash, Leila. CAT4 (cable actuated truss – 4 degrees of freedom): A novel 4 DOF cable actuated parallel manipulator. *Journal of Robotic Systems*, 19(12):605–615, 2002.
- [88] Koza, John R. *Genetic Programming*. MIT Press, Cambridge, MA, USA, 1992.
- [89] Kurtz, Ronald. Kinematic and optimization of a parallel robotic wrist with redundancy. Ph. D. thesis, McGill University, Montréal, Québec, Canada, January 1990.
- [90] Kurtz, Ronald and Hayward, Vincent. Multiple-goal kinematic optimization of a parallel spherical mechanism with actuator redundancy. *IEEE Transactions on Robotics and Automation*, 8(5):644–651, October 1992.
- [91] Lafourcade, Pascal. Contribution à l'étude des manipulateurs à câbles: application à la conception d'une suspension active pour soufflerie; Définition des premiers concepts. Rapport d'activité 3/05663, DCSD, ONERA, Toulouse, France, December 2001.
- [92] Lafourcade, Pascal. Contribution à l'étude des manipulateurs à câbles: application à la conception d'une suspension active pour soufflerie. Rapport technique 1/06751, DCSD, ONERA, Toulouse, France, December 2002.

- [93] Lafourcade, Pascal, Llibre, Michel, and Reboulet, Claude. Design of a parallel wire-driven manipulator for wind tunnels. In Gosselin and Ebert-Uphoff [140].
- [94] Lafourcade, Pascal, Llibre, Michel, and Reboulet, Claude. Le manipulateur parallèle à câbles SACSO. In *Conférence Internationale Francophone d'Automatique*, Nantes, France, July 2002.
- [95] Lafourcade, Pascal and Verhoeven, Richard. Une nouvelle architecture, fortement redondante, pour un manipulateur câbles au volume de travail étendu. In *16ème Congrès Français de Mécanique*, Nice, France, September 2003.
- [96] Lafourcade, Pascal, Zheng, Ya-Qing, and Liu, Xiong-Wie. Stiffness analysis of wire-driven parallel kinematic manipulators. In *Proc. 11th World Cong. on Theory of Machines and Mechanisms*, Tianjin, China, August 2003. IFToMM.
- [97] Landsberger, Samuel Ernest. Design and construction of a cable-controlled parallel link manipulator. Master's thesis, Dept. of Mech. Eng., MIT, Cambridge, MA, USA, September 1984.
- [98] Landsberger, Samuel Ernest and Sheridan, Thomas B. Parallel link manipulators. U. S. patent 4,666,362, USA, May 1987.
- [99] Landsberger, Samuel Ernest and Sheridan, Thomas B. A minimal, minimal linkage: the tension-compression parallel link manipulator. In Takamori, Toshi and Tsuchiya, K., editors, *Robotics, Mechatronics and Manufacturing Systems*, pages 81–88. Elsevier, New York, USA, 1993.
- [100] Lazard, Daniel. On the representation of rigid-body motions and its application to generalized platform manipulators. In *Computational Kinematics* [7], pages 175–181.
- [101] Lee, Young-Tae, Choi, Hyoun-Ryeol, Chung, Wan-Kyun, and Youm, Youngil. Stiffness control of a coupled tendon-driven robot hand. *IEEE Control Systems Magazine*, 14(5):10–19, October 1994.
- [102] Lees, David S. and Chirikjian, Gregory S. An efficient method for computing the forward kinematics of binary manipulators. In *Proc. 1996 IEEE Int. Conf. on Robotics and Automation*, pages 1012–1017, Minneapolis, USA, 1996. IEEE.
- [103] Lenarčič, Jadran and Parenti-Castelli, Vincenzo, editors. *Recent Advances in Robot Kinematics*. Kluwer Academic Publishers, Dordrecht, Netherlands, 1996.
- [104] Li, Hongyou. Ein Verfahren zur vollständigen Lösung der Rückwärtstransformation für Industrieroboter mit allgemeiner Geometrie. Ph. D. dissertation, Universität Duisburg, Duisburg, Germany, 1990.
- [105] Liu, Qing, Lorenc, Steven J., and Bernold, Leonhard E. Control of an inverted Stewart platform in challenging environments. In *Proc. American Nuclear Soc. Annual Robotics Conf.*, 1999.



- [106] Ma, Shugen, Hirose, Shigeo, and Yoshinada, Hiroshi. Design and experiments for a coupled tendon-driven manipulator. *IEEE Control Systems Magazine*, 13(1):30–36, 1993.
- [107] Maeda, Kiyoshi, Tadokoro, Satoshi, Takamori, Toshi, Hiller, Manfred, and Verhoeven, Richard. On design of a redundant wire-driven parallel robot WARP manipulator. In *IEEE-ICRA*. [68], pages 895–900.
- [108] Maier, Thomas. Bahnsteuerung eines seilgeführten Handhabungssystems – Modellbildung, Simulation und Experiment. Ph. D. thesis, Universität Rostock, Rostock, Germany, May 2003.
- [109] Maier, Thomas and Woernle, Christoph. Kinematic control of cable suspension robots. In *Proc. NATO-ASI Workshop on Computational Methods in Mechanisms*, pages 421–430, Varna, Bulgaria, 1997. NATO.
- [110] Maier, Thomas and Woernle, Christoph. Kinematische Steuerung seilgeführter Handhabungssysteme. *Zeitschrift für angewandte Mathematik und Mechanik*, 1998.
- [111] Maier, Thomas and Woernle, Christoph. Inverse kinematics for an underconstrained cable suspension manipulator. In Lenarčič and Husty [11], pages 97–104.
- [112] Maier, Thomas and Woernle, Christoph. Flatness-based control of underconstrained cable suspension manipulators. In *ASME Design Eng. Tech. Conf.*, Las Vegas, NV, USA, September 1999. ASME.
- [113] Mayer St-Onge, Boris and Gosselin, Clément M. Singularity analysis and representation of spatial six-DOF parallel manipulators. In Lenarčič and Parenti-Castelli [103], pages 389–398.
- [114] McCallion, H., Johnson, G. R., and Pham, D. T. A compliant device for inserting a peg in a hole. *The Industrial Robot*, pages 81–87, June 1979.
- [115] McCallion, H. and Truong, P. D. The analysis of a six-degree-of-freedom work station for mechanised assembly. In *Proc. 5th World Cong. on Theory of Machines and Mechanisms*, pages 611–616, Montreal, Canada, July 1979. IFToMM.
- [116] Meisel, Stephan. Optimierung stochastischer Probleme mit Simulated Annealing. Master’s thesis, Institut für Angewandte Informatik und Formale Beschreibungsverfahren (AIFB), Universität Karlsruhe, Germany, July 2004.
- [117] Melchiorri, Claudio and Vassura, Gabriele. A performance index for defective, multi-wire, haptic interfaces. In *Proc. 1998 IEEE Int. Conf. on Robotics and Automation*, Leuven, Belgium, May 1998. IEEE.
- [118] Melchiorri, Claudio and Vassura, Gabriele. Development and application of wire-actuated haptic interfaces. In *Int. J. of Intell. and Rob. Sys., Special Issue on «Humanoid Robotics and Biorobotics»*. January 2000.

- [119] Melchiorri, Claudio, Vassura, Gabriele, and Arcara, Paolo. What kind of haptic perception can we get with a one-wire interface? In IEEE-ICRA. [68], pages 1620–1625.
- [120] Merlet, Jean-Pierre. Direct kinematics and assembly modes of parallel manipulators. *Int. Journal of Robotics Research*, 11(2):150–162, April 1992.
- [121] Merlet, Jean-Pierre. Determination of the presence of singularities in 6D workspace of a Gough parallel manipulator. In Lenarčič and Husty [11], pages 39–48.
- [122] Mielczarek, Sonja, Husty, Manfred L., and Hiller, Manfred. Designing a redundant Stewart-Gough platform with a maximal forward kinematics solution set. In *Proc. Intl. Symp. on Multibody Systems and Mechatronics*, page M31, Mexico City, Mexico, September 2002.
- [123] Mielczarek, Sonja, Verhoeven, Richard, and Hiller, Manfred. Seilgetriebene Stewart-Plattformen in Theorie und Anwendung (SEGESTA). Zwischenbericht für den Zeitraum 1.1.1999 bis 1.8.2000 im DFG-Vorhaben HI 370/18-1, Fachgebiet Mechatronik, Gerhard-Mercator-Universität, Duisburg, Germany, 2000.
- [124] Miller, Karol and Clavel, Reymond. The Lagrange-based model of DELTA-4 robot dynamics. *Robotersysteme*, 8:49–54, 1992.
- [125] Ming, Aiguo and Higuchi, Toshiro. Study on multiple degree-of-freedom positioning mechanism using wires (part 1) – concept, design and control. *Int. Journal of the Jap. Soc. for Precision Engineering*, 28(2):131–138, June 1994.
- [126] Ming, Aiguo and Higuchi, Toshiro. Study on multiple degree-of-freedom positioning mechanism using wires (part 2) – development of a planar completely restrained positioning mechanism. *Int. Journal of the Jap. Soc. for Precision Engineering*, 28(3):235–242, September 1994.
- [127] Ming, Aiguo, Kajitani, Makoto, and Higuchi, Toshiro. Study on wire parallel mechanism. In JFM. [74], pages 667–670.
- [128] Ming, Aiguo, Kajitani, Makoto, and Higuchi, Toshiro. On the design of wire parallel mechanism. *Int. Journal of the Jap. Soc. for Precision Engineering*, 29(4):337–342, December 1995.
- [129] Morizono, Tetsuya, Kurahashi, Kazuhiro, and Kawamura, Sadao. Analysis and control of a force display system driven by parallel wire mechanism. In Stelson and Oba [75], pages 63–70.
- [130] Nahon, Meyer, Gilardi, Gabriele, and Lambert, Casey. Dynamics/control of a radio telescope receiver supported by a tethered aerostat. *J. of Guidance, Control, and Dynamics*, 25(6):1107–1115, November 2002.
- [131] Nogai, Tooru, Sano, Kazuo, and Sheridan, Thomas B. Interference-drive of a 3DOF joint based on the cable-controlled mechanism. *Journal of the Jap. Soc. for Precision Engineering*, 61(12):1690, 1995.

- [132] Nombrail, Nathalie. Analyse et commande d'une famille de robots manipulateurs à structure parallèle et redondante. Ph. D. Thesis, Supaéro, Toulouse, France, December 1993.
- [133] Ogane, Daisuke, Hyodo, Kazuhito, and Kobayashi, Hiroaki. Mechanism and control of a 7 D.O.F. tendon-driven robotic arm with NST. *Journal of the Robotics Soc. of Japan*, 14(8):68–75, 1996.
- [134] Osumi, Hisashi, Arai, Tamio, and Asama, Hajime. Development of a seven degrees of freedom crane with three wires (1st report) – inverse kinematics of the crane. *Journal of the Jap. Soc. for Precision Engineering*, 59(5):767–772, 1993.
- [135] Osumi, Hisashi, Arai, Tamio, Fujihira, Masanobu, Yamaguchi, Hiroaki, Asama, Hajime, Kaetsu, Hayato, and Urai, Teruo. Development of a seven degrees of freedom crane with three wires (2nd report) – vibration control of a suspended object. *Journal of the Jap. Soc. for Precision Engineering*, 59(12):2061, 1993.
- [136] Osumi, Hisashi, Shen, Yusi, and Arai, Tamio. The manipulability of wire suspension system. *Journal of the Robotics Soc. of Japan*, 12(7):1049–1055, 1994.
- [137] Ou, Yeong-Jeong and Tsai, Lung-Wen. Kinematic synthesis of tendon-driven manipulators with isotropic transmission characteristics. *ASME Journal of Mechanical Design*, 115(4):884–891, December 1993.
- [138] Ou, Yeong-Jeong and Tsai, Lung-Wen. Design of a three-dof tendon-driven manipulator with the characteristics of equal maximum tensions. In Lenarčič, Jadran and Ravani, Bahram, editors, *Advances in Robot Kinematics and Computational Geometry*, pages 369–378. Kluwer Academic Publishers, Dordrecht, Netherlands, 1994.
- [139] Ou, Yeong-Jeong and Tsai, Lung-Wen. Theory of isotropic transmission for tendon-driven manipulators. In *Robotics: Kinematics, Dynamics and Control*, pages 53–61, Minneapolis, USA, 1994. ASME.
- [140] *Proc. Workshop on Fundamental Issues and Future Research Directions for Parallel Mechanisms and Manipulators*, Quebec City, Canada, 2002. Gosselin, Clément M. and Ebert-Uphoff, Imme, editors.
- [141] Raghavan, Madhu. The Stewart platform of general geometry has 40 configurations. *ASME Journal of Mechanical Design*, 115:277–282, June 1993.
- [142] Raghavan, Madhu and Roth, Bernard. Inverse kinematics of the general 6R manipulator and related linkages. *ASME Journal of Mechanical Design*, 115:502–508, 1993.
- [143] Reboulet, Claude and Leguay, Sylvie. The interest of redundancy for the design of a spherical parallel manipulator. In Lenarčič and Parenti-Castelli [103], pages 369–378.

- [144] Reves, Colin. *Modern Heuristic Techniques for Combinatorial Problems*. McGraw-Hill, New York, USA, 1995.
- [145] Richter, Thomas, Lorenc, Steven J., and Bernold, Leonhard E. Cable based robotic work platform for construction. In Poppy, W. and Bock, Th., editors, *Automation and Robotics – Today's Reality in Construction*, pages 137–144, Munich, Germany, March 1998.
- [146] Salisbury, John Kenneth and Craig, J. J. Articulated hands: Force control and kinematic issues. *Int. Journal of Robotics Research*, 1(1):4–17, 1982.
- [147] Schrijver, Alexander. *Theory of linear and integer programming*. Wiley Eastern Ltd., New York, USA, 1999.
- [148] Sciavicco, L. and Siciliano, Bruno. *Modeling and Control of Robotic Manipulators*. McGraw-Hill, New York, USA, 1996.
- [149] Sefrioui, Jaouad and Gosselin, Clément M. Singularity analysis and representation of planar parallel manipulators. *Robotics and Autonomous Systems*, 10(4):209–224, 1992.
- [150] Sefrioui, Jaouad and Gosselin, Clément M. Etude et représentation des lieux de singularité des manipulateurs parallèles sphériques a trois degrés de liberté avec actionneurs prismatiques. *Mechanism and Machine Theory*, 29(4):559–579, 1994.
- [151] Sefrioui, Jaouad and Gosselin, Clément M. On the quadratic nature of the singularity curves of planar three-degree-of-freedom parallel manipulators. *Mechanism and Machine Theory*, 30(4):533–551, 1995.
- [152] Slutski, Leonid. Closed plane mechanisms as a basis of parallel manipulators. In Lenarčič and Parenti-Castelli [103], pages 441–450.
- [153] Snyman, Jan A. and Hay, Alexander Morrison. The chord method for the determination of non-convex workspaces of planar parallel platforms. In Lenarčič and Stanišić [12], pages 285–294.
- [154] Stafetti, Ernesto, Bruyninckx, Hermann, and De Schutter, Joris. On the invariance of manipulability indices. In Lenarčič and Thomas [13], pages 57–66.
- [155] Stewart, D. A platform with six degrees of freedom. *Proc. Institute of Mechanical Engineering*, 180(15):371–386, 1965.
- [156] Study, E. Grundlagen und Ziele der analytischen Kinematik. *Sitzungsberichte der Berliner Math. Gesellschaft*, 104:36–60, December 1912.
- [157] Tadokoro, Satoshi. On a portable parallel manipulator for rescue, 1st report: requirement and conceptual proposal. In *Proc. Robomec 1998*, June 1998.
- [158] Tadokoro, Satoshi. On a portable parallel manipulator for rescue, 2nd report: self position identification of actuator units. In *Proc. RSJ 1998*. RSJ, September 1998.

- [159] Tadokoro, Satoshi, Kimura, Ichiro, and Takamori, Toshi. An evaluation of characteristics of singular points based on a stochastic interpretation of manipulator motion. In *Proc. 1st Int. Symp. on Measurement and Control in Robotics*, pages D.2.2.1–7, Houston, TX, USA, 1990.
- [160] Tadokoro, Satoshi, Murao, Yoshio, Hiller, Manfred, Murata, Rie, Kohkawa, Hideaki, and Matsushima, Toshiyuki. A motion base with 6-DOF by parallel cable drive architecture. *IEEE/ASME Trans. on Mechatronics*, 7(2), 2002.
- [161] Tadokoro, Satoshi, Nishioka, Shinsuke, Kimura, Tetsuya, Hattori, Moto-fumi, Takamori, Toshi, and Maeda, Kiyoshi. On fundamental design of wire configurations of wire-driven parallel manipulators with redundancy. In Stelson and Oba [75], pages 151–158.
- [162] Tadokoro, Satoshi, Verhoeven, Richard, Hiller, Manfred, and Takamori, Toshi. A portable parallel manipulator for search and rescue at large-scale urban earthquakes and an identification algorithm for the installation in unstructured environments. In *Proc. 1999 IEEE / RSJ Int. Conf. on Intelligent Robots and Systems*, pages 1222–1227, Kyonbjju, Korea, October 1999. IEEE.
- [163] Tadokoro, Satoshi, Verhoeven, Richard, Zwiers, Ulrike, Hiller, Manfred, and Takemura, Fumiaki. Kinematic identification method for cable-driven rescue robots in unstructured environments. *J. of Robotics and Mechatronics*, 10(5), 2003.
- [164] Takeda, Yukio and Funabashi, Hiroaki. Kinematic and static characteristics of in-parallel actuated manipulators at singular points and in their neighbourhood. *JSME Int. Journal*, C 39(1):85–93, 1996.
- [165] Takeda, Yukio and Funabashi, Hiroaki. Kinematic synthesis of spatial in-parallel wire-driven mechanism with six degrees of freedom with high force transmissibility. In ASME-BMC. [16].
- [166] Takeda, Yukio and Funabashi, Hiroaki. A transmission index for in-parallel wire-driven mechanisms. *JSME Int. Journal*, C 44(1):180–187, 2001.
- [167] Tanaka, M., Seguchi, Y., and Shimada, S. Kineto-statics of skycam-type wire transport system. In *Proc. USA-Japan Symposium on Flexible Automation, Crossing Bridges: Advances in Flexible Automation and Robotics*, pages 689–694, Minneapolis, Minnesota, 1988. ASME.
- [168] Tsai, Lung-Wen and Lee, Jyh-Jone. Kinematic analysis of tendon-driven robotic mechanisms using graph theory. *ASME Journal of Mechanisms, Transmissions, and Automation Design*, 111(1):59–65, March 1989.
- [169] Tsai, Lung-Wen and Tahmasebi, Farhad. Synthesis and analysis of a new class of six-degree-of-freedom parallel minimanipulators. *Journal of the Robotics Soc. of Japan*, 10(5):561–580, 1993.
- [170] Verhoeven, Richard. Scientific community of tendon-based stewart platforms. <http://www.mechatronik.uni-duisburg.de/robotics/segesta/comunity.html>, December 2002.



- [171] Verhoeven, Richard and Hiller, Manfred. Relationen zur Klassifikation serieller, paralleler und hybrider Manipulatoren. In *Proc. Annual Meeting Gesellschaft für angewandte Mathematik und Mechanik*, Metz, France, April 1999. GAMM.
- [172] Verhoeven, Richard and Hiller, Manfred. Singularität und Redundanz allgemeiner holonomer Manipulatoren. In Heinzl, J., editor, *Kolloquium Getriebetechnik 1999*, pages 19–28, TU München, Germany, September 1999.
- [173] Verhoeven, Richard and Hiller, Manfred. Estimating the controllable workspace of tendon-based Stewart platforms. In Lenarčič and Stanišić [12], pages 277–284.
- [174] Verhoeven, Richard, Hiller, Manfred, and Tadokoro, Satoshi. Workspace, stiffness, singularities and classification of tendon-driven Stewart platforms. In Lenarčič and Husty [11], pages 105–114.
- [175] Waldron, Kenneth J. and Hunt, Kenneth H. Series-parallel dualities in actively coordinated mechanisms. In *Proc. 4th Int. Symp. on Robotics Research*, pages 175–181, Santa Cruz, USA, September 1987.
- [176] Waldron, Kenneth J. and Yang, Po-Hua. Parallel arrays of binary actuators. In Lenarčič and Husty [11], pages 17–26.
- [177] Wang, Qi-Ming, Wang, Jinsong, and Zhang, Hui. Dynamic analysis of a feed fine-tuning test platform for the large radio telescope. In DETC. [38].
- [178] Wenger, Philippe and Chablat, Damien. Workspace and assembly modes in fully-parallel manipulators: a descriptive study. In Lenarčič and Husty [11], pages 117–126.
- [179] Williams, Robert L. Cable-suspended haptic interface. *Int. Journal of Virtual Reality*, 3(3):13–21, 1998.
- [180] Williams, Robert L. and Gallina, Paolo. Planar cable-direct-driven robots, part I: Kinematics and statics. In DETC. [37].
- [181] Woernle, Christoph. Dynamics and control of a cable suspension manipulator. In Braun, Manfred, editor, *Proc. of the 9th German-Japanese Seminar on Nonlinear Problems in Dynamical Systems – Theory and Applications*, University of Duisburg, Germany, 2000.
- [182] Zheng, Ya-Qing. Stiffness mapping of a six-DOF wire-driven parallel kinematic manipulator. internal report, Inst. of Advanced Manufacturing Technology, Huaqiao University, Quanzhou, Fujian, China, February 2003.
- [183] Zheng, Ya-Qing and Liu, Xiong-Wie. Force transmission index based workspace analysis of a six DOF wire-driven parallel manipulator. In DETC. [38].

# Curriculum Vitae

## Personal Data

<b>Name</b>	Richard Verhoeven
<b>Birth</b>	12 Jul 1971 Oberhausen, Germany

## Education

<b>University</b>	Aug 1990 – Jul 1993	Universität Duisburg, Germany
	Oct 1993 – Jul 1994	Università di Bologna, Italy
	Oct 1994 – Jul 1996	Universität Duisburg
<b>Degrees</b>	Aug 1992	Vordiplom in Physics
	Jul 1996	Diplom in Mathematics: thesis in probability theory, supplementary examen in German civil law

## Working Experience

<b>Siemens</b>	Sep 1996 – Aug 1998	Power Generation – Life Cycle Analysis: database development, Mülheim, Germany
<b>WestLB</b>	since Sep 1998	Risk Management – IT Support: integration support, Düsseldorf, Germany
<b>University</b>	Jan 1999 – Dec 2001	Mechatronics Laboratory: webmaster, Universität Duisburg